OCEANOGRAPHY AND PRODUCTIVITY CONDITIONS ON THE IBERIAN MARGIN: A 150 KY FORAMINIFERA RECORD

Dissertation zur Erlangung des

Doktorgrades der Naturwissenschaften

am Fachbereich Geowissenschaften

der Universität Bremen

vorgelegt von

Maria Emília Carvalho Salgueiro

Bremen, Oktober 2006

Tag des Kolloquiums:

30. November 2006

Gutachter:

Herr Prof. Dr. Gerold Wefer

Frau Dr. Fátima Abrantes

Prüfer:

Herr Prof. Dr. Ruediger Stein

Herr Prof. Dr. Jörn Peckmann

TABLE OF CONTENTS

ACKNOWLEDGMENTS

First of all, I would like to express my thanks to Prof. Dr. *Gerold Wefer* for accepting me as a student and giving me the opportunity to learn and work with him and his excellent team at the Geosciences Department of the Bremen University (GeoB). In special with Dr. *Helge Meggers*, who gave me great personal and scientific support, numerous fruitful discussions, reviews and helpful suggestions, which greatly improved this work in various ways.

I am also deeply grateful to Dr. *Fátima Abrantes*, the main responsible for driving me to the mysteries of Paleoceanography when I became part of her team in the Marine Geology Department (DGM) of the Instituto Geológico e Mineiro, actually INETI. Her comments and suggestions greatly improved the quality of the present dissertation. Thanks for the guidance, enthusiasm, friendship and strength that you gave me since the first days.

Special thanks go to Dr. *Antje Voelker*, she was of crucial importance for the development of this work along these years. I am grateful for her useful comments, discussions and permanent availability and friendship, helping me on my work and on my moral.

I gratefully acknowledge Dr. *Uwe Pfluamann* for his patience, teaching me the insights of the SIMMAX 28 transfer function technique, and for the discussions and reviews of first manuscript.

I am also grateful to my remaining co-authors Drs. *Lúcia de Abreu*, *Neven Lončarić* (my first planktonic foraminifera teacher at DGM), *Raquel González-Álvarez*, *Paulo Oliveira*, *Helga Bartels-Jónsdóttir*, and *João Moreno*, for the exchange of data and ideas.

I would like to express my thanks to Dr. *Barbara Donna* for her planktonic foraminifera guidance in the begin of this work, Dr. *Monika Segl* for her help during the isotope measurements, and to Drs. *Stefan Mulitza* and *Tim Freudenthal* for their constructive scientific discussions.

Thanks also to all my friends and colleagues at DGM-INETI and at GeoB for their support and help during this period. A special "*obrigada"* goes to the DGM-INETI "Paleoceanography and Environmental" group for their miscellaneous support throughout these years: from collecting samples, discussing data, reviewing manuscripts, to the

familiar working atmosphere. Also a special "*vielen dank"* to my Ph.D. colleague *Ulrich Alt-Epping*, and Drs. *Holger Kulmann*, *Peer Helmke* and *Jung-Hyun Kim*. They have both helped me scientifically, in my everyday German difficulties, and provided me a wonderful stay at Bremen University and in the City of Bremen. I hope that one day I can return their help. Also, I would like to thank Drs. *Silvia Hess* and *Stefan Rothe* for the warm way they have received me at their home.

I gratefully thank *Apolónia Inês*, *Cremilde Monteiro*, *Ana Margarida Silva*, *M. José Costódio*, *Célia Trindade* and *David Jerónimo* for their assistance with the laboratory work at DGM-INETI. To Dr. *Hipólito Monteiro* a special acknowledgment for his energetic motivation and constant incentive.

Mrs *Adelheid Grimm-Geils* and *Margarida Henriques*, from GeoB and DGM-INETI, respectively, for handling my administrative problems with great patience.

I am deeply grateful to my wonderful parents for their continuing support and encouragement throughout all my life.

I would like to express my thanks to my husband *Vitor Magalhães* for his patience, encouragement and permanent support, mainly when we were living in different countries. "Thanks to Science" for introducing him in my life!

Finally, I would like to thank all my friends and relatives from Carrazedo de Montenegro, Chaves and Lisbon who have always understood my absence and my bad mood during long periods in the last years.

This work has been financially supported by "Fundação para a Ciência e a Tecnologia (FCT)" and "Fundo Social Europeu (FSE) no âmbito do III Quadro Comunitário de Apoio" (ref. SFRH/BD/11743/2003) and by the INGMAR project (PLE/4/98). Two travel grants to Bremen were supported by the Bremen University and the "Fundação Calouste Gulbenkian". The EU PALEOSTUDIES project supported part of the planktonic and benthic foraminifera stable isotope measurements.

ABSTRACT

The main objectives of this thesis were 1) to calibrate the first regional coastal upwelling transfer function for the western Iberian margin and 2) to investigate centennial- to millennial-scale hydrographic and productivity variations along this margin. To improve the knowledge on coastal upwelling areas like the western Iberian margin is of crucial social and economic importance. Upwelling regions act as high accumulation areas allowing high-resolution reconstructions of past climatic changes, and as sinks for CO_2 and thus possible climate regulators.

The Present day record and the past oceanographic and productivity conditions on the Iberian margin were investigated through a multi-proxy study (planktonic and benthic foraminifera abundances and stable isotopes, planktonic foraminifera associations, detrital grain abundance (IRD), grain size analysis, carbonate content) of surface sediments and sediment cores.

The distribution of the most abundant planktonic foraminifera species on surface sediment samples (134) collected along the Iberian margin clearly mirror the specific hydrographic conditions in this area. *Globigerina bulloides* and *Neogloboquadrina pachyderma* (dextral) reflect the seasonal (May to September) coastal upwelling north and south of Lisbon´s latitude, respectively, evidencing the two sources of upwelled water: subpolar Eastern North Atlantic Central Water (ENACW) in the north, and subtropical ENACW in the south. However, *Neogloboquadrina pachyderma* (dextral) in association with *Globorotalia inflata* also seems to mark the descending branch of the North Atlantic Drift (Portugal Current). The tropical-subtropical species *Globigerinoides ruber* (white), *Globigerinoides trilobus trilobus*, and *Globorotalia inflata* are related to the winter-time eastern branch of the Azores Current (Portugal Coastal Countercurrent). This data set and an eighteen year integration of daily satellite SST were used to calibrate and define a regional transfer function, which was then used to compare the results from two commonly different transfer function techniques, Imbrie & Kipp and SIMMAX. The simultaneous application of two different computational approaches allowed the validation of the modern samples and the selection of SIMMAX as the technique to be used to reconstruct sea surface temperature (SST) and export productivity (Pexp) in

sediment cores from this area. This regional data set was also included into the North Atlantic MARGO data set contributing a considerable number of analogs from one upwelling region.

During the Late Holocene, productivity and surface and deep-water hydrography were estimated by studying 6 box/multi-cores recovered along two transects along the southwestern (off Sines, 37° 50´N) and southern (off Albufeira, 8° 15´W) Portuguese margin. Results from productivity proxies show that productivity conditions off Sines were more stable during the major historical warm European North Atlantic periods, i.e. the Roman Warm Period and the Medieval Warm Period, than during the cold ones (Dark Ages and Little Ice Age). The opposite was observed off Albufeira. Alternate intensification of northerly (upwelling along the southwest margin) and westerly winds (upwelling along the south margin) during the summer of warm and cold climatic periods during the last 2500 yr, could explain such results. However, the southwestern transect shows higher productivity than the southern transect through time, which is attributed to the stronger and more persistent upwelling influence on the western Portuguese margin such as today. No major changes between warm and cold climatic periods were observed in both transects for the intermediate and deep bottom currents (Mediterranean Outflow Water and North Atlantic Deep Water).

The impact of millennial-scale climatic variability on the Iberian margin in terms of oceanographic and productivity conditions was investigated back to 150 ky using three deep-sea cores located along a North - South transect (43º12´N - 37º48´N). In all cores, coldest summer SSTs and lowest Pexps are found during the Heinrich events. Only in the southernmost core, the lowest Pexp did not always coincide with these events. At the glacial/interglacial time scale, SST increases from North to South through time, while Pexp shows the opposite trend during interglacials and no significant variation during the glacial periods.

The northernmost core reveals the highest SST amplitude over time, in agreement with the strongest influence of glacial polar front movements. The southermost core shows the highest Pexp amplitude indicating that the Sines upwelling filament was present during most of the studied interval although affected in its intensity by the southward penetration of subpolar to polar water masses.

KURZFASSUNG

Die Hauptziele dieser Dissertation waren 1.) die Kalibration der ersten regionalen Transferfunktion für das küstennahe Auftriebsgebiet entlang des westiberischen Kontinentalhanges und 2.) die Studie von hydrographischen und Produktivitätsänderungen entlang des Hanges in Zeitskalen von Jahrhunderten bis Jahrtausenden. Das bessere Verstehen von Auftriebsgebieten wie dem westiberischen Kontinentalhang ist von sozialer und wirtschaftlicher Bedeutung. Auftriebsgebiete sind Hochakkumulationsgebiete, die zeitlich hochauflösende Rekonstruktionen von Klimaänderungen erlauben, und agieren als CO_2-Senken und damit als mögliche Klimaregulatoren.

Die heutigen und vergangenen ozeanographischen und Produktivitätsbedingungen entlang des iberischen Kontinentalhanges wurden mit Hilfe mehrerer Proxies (Häufigkeiten planktischer und benthischer Foraminiferen, die Verteilung stabiler Isotope in ihren Schalen, Planktonforaminiferenvergesellschaftungen, Konzentration detritischer Körner (IRD), Korngrößenanalyse, Karbonatgehalt) in Oberflächensedimenten und Tiefseekernen untersucht.

Die Verteilung der häufigsten Planktonforaminiferenarten in den Oberflächensedimentproben (134) vom iberischen Kontinentalhang spiegeln deutlich die speziellen hydrographischen Bedingungen in diesem Gebiet wider. *Globigerina bulloides* und *Neogloboquadrina pachyderma* (dextral) reflektieren das jeweilige saisonale (Mai bis September) Auftriebsgeschehen nördlich und südlich des Breitengrades von Lissabon und damit die beiden Ursprungsgebiete des aufgetriebenen Wassers: subpolares nordostatlantisches Zentralwasser (ENACW) im Norden und subtropisches ENACW im Süden. In Verbindung mit *Globorotalia inflata* scheint *Neogloboquadrina pachyderma* (dextral) allerdings auch den absteigenden Ast der Nordatlantikdrift (Portugalstrom) zu markieren. Die tropisch-subtropischen Arten *Globigerinoides ruber* (weiß), *Globigerinoides trilobus trilobus* und *Globorotalia inflata* sind an den winterlichen, östlichen Arm des Azorenstromes (portugiesicher Küstengegenstrom) gebunden. Dieser Datensatz und Satellitenoberflächenwassertemperaturen integriert über 18 Jahre wurden benutzt, um die Ergebnisse zweier häufig benutzter Transferfunktionen zu vergleichen: Imbrie & Kipp und SIMMAX. Die gleichzeitige Anwendung zwei verschiedener

Computerprogramme erlaubte die Bewertung der heutigen Situation und die Wahl von SIMMAX als Technik für die Rekonstruktion von Oberflächenwassertemperaturen (SST) und Exportproduktivität (Pexp) in Sedimentkernen aus dem Studiengebiet. Der regionale Datensatz wurde zudem in den Nordatlantikdatensatz des MARGO Projektes integriert und steuerte eine hohe Anzahl von Analogproben für ein Auftriebsgebiet bei.

Für des Spätholozäns wurden Produktivität und Oberflächen- und Tiefenwasserhydrographie mit Hilfe von 6 Großkastengreifer-/Multikernen rekonstruiert, die entlang zweier Transekte vor dem südwestlichen (vor Sines, 37° 50'N) und südlichen (vor Albufeira, 8° 15'W) portugiesischen Kontinentalhang gezogen wurden. Für die Produktivitätsdaten zeigen die Ergebnisse, daß die Produktivitätsbedingungen vor Sines während der historisch bedeutenden warmen Klimaperioden im europäischen Nordatlantikraum, d.h. während der römischen und der mittelalterlichen Warmzeit, stabiler waren als während der Kälteperioden, d.h. während der dunklen Zeitalter (Frühmittelalter) und der kleinen Eiszeit. Vor Albufeira wurde das genaue Gegenteil beobachtet. Die alternierende Intensivierung der nördlichen (Auftrieb vor des südwestlichen Küste) und westlichen Winde (Auftrieb vor des südlichen Küste) während der Sommer der warmen und kalten Klimaperioden der letzten 2500 Jahre könnte diese Ergebnisse erklären. Allerdings wird entlang des südwestlichen Transektes immer eine höhere Produktivität beobachtet als entlang des südlichen Transektes, was einem stärkeren und konstanterem Auftriebsgeschehen entlang des westlichen portugieschen Kontinentalhanges ähnlich wie heute zugeschrieben wird. Für die Zwischen- und Tiefenwasserströme (Mittelmeerausstrom, Nordatlantisches Tiefenwasser) werden entlang beider Transekte keine nennenswerten Änderungen zwischen den warmen und kalten Klimaperioden beobachtet.

Der Einfluß von tausendjährigen Klimavariationen auf die ozeanographischen und Produktivitätsbedingungen entlang des iberischen Kontinentalhanges während der letzten 150 ky wurde in drei Tiefseekernen entlang eines Nord-Süd-Transektes (43º12´N - 37º48´N) untersucht. In allen Kernen wurden die kältesten Sommeroberflächenwassertemperaturen und die niedrigsten Exportproduktivitäten während der Heinrich-Ereignisse beobachtet. Nur im südlichsten Kern waren die niedrigsten Pexp-Werte nicht immer zeitgleich mit diesen Ereignissen. Auf glazial-interglazial Zeitskalen nehmen die SST von Nord nach Süd zu, während Pexp während der Interglaziale einen gegensätzlichen Trends zeigt und keine signifikanten Änderungen während der Glaziale.

Der nördlichste Kern weist die größte SST-Amplitude über den Zeitraum auf, da er durch Positionsänderungen der Polarfront stärker beeinflußt wird. Der südlichste Kern zeigt die höchste Pexp-Amplitude, was anzeigt, daß das Auftriebsband vor Sines zwar während der meisten Zeit des studierten Zeitintervalles präsent war, seine Intensität aber durch das südwärtige Vordringen von subpolaren und polaren Wassermassen beeinflußt wurde.

CHAPTER 1

1. Introduction

1.1. Motivation and main objectives

Coastal upwelling regions have become areas of great scientific and social interest because they are considered important agents in the global carbon cycle and global climate changes.

Nowadays, coastal upwelling margins occupy about 10% of the oceanic area, but concentrate 80-90% of the new production in the oceans (Hill et al., 1998). Furthermore, recent results of the JGOFS (Joint Global Ocean Flux Study) program highlighted mid latitude coastal upwelling areas as very productive sites characterized by high diatom abundances and the highest carbon export efficiency (Doney et al., 2001; Laws et al., 2000; Moore et al., 2002). In these areas phytoplankton acts as a "biological pump" lowering the partial pressure of CO_2 in surface waters and exporting carbon into the deep ocean (Eppley and Peterson, 1979; Broecker, 1982; Berger and Keir, 1984; Berger et al., 1989; Berger and Wefer, 1990). Thus, productivity fluctuations are important in providing feedback to climatic changes (Berger et al.,1989) and play a role in the control of the greenhouse gas CO_2 concentration in the ocean and atmosphere.

The western Iberian margin (eastern North Atlantic) is characterized by seasonal coastal upwelling (May to September) (Wooster et al., 1976; Fraga, 1981; Fiúza, 1983; 1984) associated with cold waters and high primary productivity which leaves an imprint in the sediments beneath these areas, as shown by Monteiro et al., (1983), Abrantes and Sancetta (1985), and Abrantes (1988).

Since long these areas represent a difficulty for transfer function techniques and samples located there have often been excluded from calibration data sets (Pflaumann et

al., 1996). This decision is mainly based on the possible living planktonic foraminifera response to several environmental variables at the same time, such as temperature and/or food availability. In upwelling regions, in particular, the high primary production could influence the temperature estimates and vice versus (e.g., Ravelo et al., 1990; Andreasen and Ravelo, 1997; Watkins and Mix, 1998).

One of the objectives of this research was to develop a regional transfer function and increase the spatial coverage of modern analogs in the Iberian upwelling margin. These modern analogs were then used in a data base restricted to the Iberian margin and combined with the North Atlantic calibration data set of Kucera et al., (2005) in order to obtain more reliable temperature and productivity reconstructions for this upwelling region through time.

Another important objective was to reconstruct oceanographic and productivity conditions along this upwelling margin at different time intervals. To reach this objective, multi-proxy data including planktonic and benthic foraminifera abundances, planktonic foraminifera associations, stable isotope data, organic carbon abundances and grain size were analyzed in sediment cores recovered along the western and southern Iberian margins. Temperature and export productivity were reconstructed from the planktonic foraminifera assemblage with the SIMMAX transfer function technique (Pflaumann et al., 1996; 2003).

The relationship between actual hydrography/productivity and planktonic foraminifera assemblages preserved in surface sediments is described in Chapter 2. The latest Holocene (2.5 ky to Present) centennial variability is presented as Chapter 3. Chapter 4 exhibits the millennial variability of sea surface temperature and export productivity observed during the last 150 ky BP along the Iberian margin between 43º12´N and 37º48´N.

1.2. Iberian margin climatic and oceanographic settings

Presently, the North Atlantic Oscillation (NAO) is believed to control climate variability across most of the Northern Hemisphere, especially during wintertime. It is characterized by an index calculated as the difference between the atmospheric pressure at sea level between Stykkidhólmur and Lisbon. When the meridional pressure gradient over

the North Atlantic is large due to the enhancement of both pressure centers (the Icelandic low and the Azores high), a positive NAO index phase, atmospheric temperature is warm and strong northerly winds are induced, thereby generating intense upwelling along the western Portuguese margin. In the opposite situation, when both centers are weakened, the negative NAO index phase, there is a reduced gradient and southerly/westerly winds are induced during cold periods, and an increase in precipitation occurs (Hurrell et al., 2001; Trigo and Camara, 2000; Trigo et al., 2004).

The surface ocean circulation along the Iberian margin is characterized by the southward branch of the North Atlantic Drift, the Portugal Current. Close to the coast, however, strong seasonal wind variability causes partial reverse flow patterns with a southward Portugal Coastal Current in summer and a northward subtropical Portugal Coastal Countercurrent (PCC) in winter (Fiúza, 1984; Fiúza et al., 1998; Peliz et al., 2005).

When the seasonal coastal upwelling predominates off Iberia (May to September), the upwelled water forms a cold and nutrient-rich band along the west coast around 50 km wide (Fiúza, 1983), with offshore extensions, filaments and plumes, mainly in the vicinity of the capes (Fraga, 1981; Fiúza, 1983; 1984; Sousa and Bricaud, 1992; Haynes et al., 1993; Álvarez-Salgado et al., 2001). These filaments and plumes may reach distances of more than 200 km from the coast (Sousa and Bricaud, 1992). Thus, the different upwelling patterns off Iberia although largely determined by the bathymetry and coastal morphology, its occurrence depends on local wind conditions (northerly wind along the west coast, westerly wind off the south coast) (Fiúza, 1983).

Eastern North Atlantic Central Water (ENACW), with subtropical (ENACWst) or a subpolar origin (ENACWsp), is the source of the upwelled water and depending on the wind strength either type can be upwelled. North of the latitude of Lisbon, however, the importance of the subtropical branch decreases. The poleward flowing ENACWst, the subsurface component of the PCC, is formed along the Azores front during winter and is lighter, relatively warmer and saltier contains less nutrients than the southward flowing ENACWsp branch. The denser ENACWsp, which flows below the subtropical ENACWst, is formed in the eastern North Atlantic at 46ºN (Fiúza, 1984; Rios et al., 1992; Fiúza et al., 1998).

Mediterranean Outflow Water (MOW) dominates the intermediate depths along the Portuguese margin; it interacts with the ENACW (Ambar & Howe, 1979b) and influences the sedimentary record along the Iberian Margin. This water is characterized by a high

temperature and salinity and flows along the Iberian margin in two main cores: the upper core, around 500-800 m, and the lower core at about 1200 m (Ambar & Howe, 1979a,b; Ambar et al., 2002).

Deeper in the water column, below 2000 m, the prevailing deep-water masses are controlled by the thermohaline equilibrium between the poorly stratified and oxygen-rich North Atlantic Deep Water (NADW), and the carbonate corrosive Antarctic Bottom Water (AABW) (Fiúza, 1984).

1.3. Planktonic foraminifera as a tool for paleoenvironmental reconstructions

Planktonic foraminifera are small unicellular organisms (protozoans) with widespread occurrence over the world oceans. Each species has optimal growing conditions and incorporates into its calcite shell (skeleton) the characteristics of the water mass in which it lives. Besides, different environmental conditions result in distinct compositions (physical and chemical) of the faunal assemblage over the world oceans, indirectly reflecting the characteristics of the various surface water masses (Fig. 1). One example of this is the clear distinction into faunal provinces, which are more or less symmetrical to the equator, a bi-polar latitudinal zonation that mainly reflects the gradient in sea surface temperatures from the cooler waters on the poles to the warm waters in the tropics (Bé and Tolderlund, 1971). The facts that the planktonic foraminifera act as "fingerprints" of pattern changes in these water masses (Imbrie and Kipp, 1971; Kennett, 1982), and that their shells are often preserved on the ocean floor has made this group one of the most commonly used tools in paleoceanography for the reconstruction of past upper ocean conditions (Bé and Tolderlund, 1971; Bé, 1977).

The conjugation of sedimentary studies with sediment traps and culture experiments (e.g., Thunell et al., 1983; Ortiz and Mix, 1992; Thunell and Sautter, 1992; Bijma et al., 1998) have confirmed the importance of this group of organisms mainly as indicators of temperature and nutrient content.

Ever since CLIMAP (CLIMAP, 1976), the most commonly used tool for paleoenvironmental reconstructions with census counts of planktonic foraminifera assemblages involves mathematical analysis, the so-called transfer function approach.

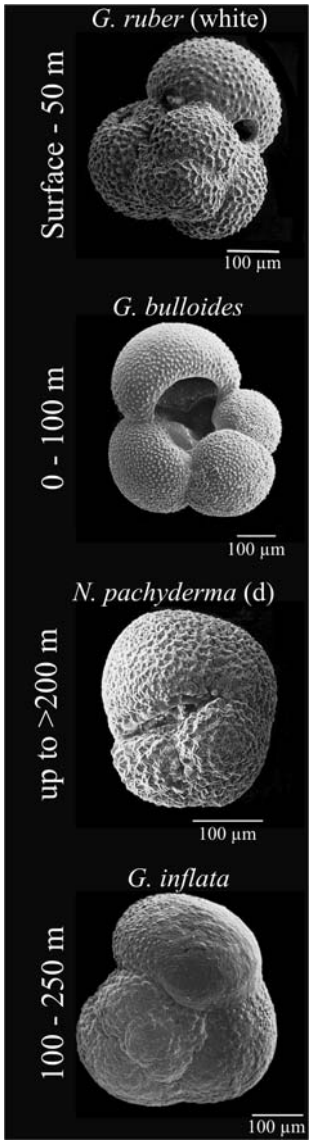

Fig. 1 The most abundant modern planktonic foraminifera species along the Iberian margin with reference to the water-depth in which they live (courtesy of L. de Abreu).

The CLIMAP group used the Imbrie & Kipp method (Imbrie and Kipp, 1971) to reconstruct temperatures for the Last Glacial Maximum. However, in the last three decades several different techniques based mainly on planktonic foraminifera data sets were developed for different environments and regions (e.g., Imbrie and Kipp, 1971; Hutson, 1977; 1980; Mix, 1989; Terbraak and Juggins, 1993; Pflaumann et al., 1996; 2003; Malmgren and Nordlund, 1997; Waelbroeck et al., 1998). Planktonic foraminiferal data sets have also increased and are now available for the world ocean where carbonate is preserved on the sea floor. Optimally, a calibration data set should include samples representing the entire range of the environmental variables as observed today, and, the entire range of ecological and geographical circumstances where the taxonomic units included in the calibration data set occur. However, a calibration data base covering a large area even with a large number of analogs will introduce noise, e.g. from cryptic genetic types or the influence of other environmental gradients, into the reconstructions (Kucera et al., 2005). Le and Shackleton (1994) proposed the use of a regional calibration and a selective number of species with known ecological characteristics to improve the reconstruction of paleoenvironments. Recently, Kucera et al., (2005) also recommended regional over global calibrations, defending that in theory, if these cryptic species have different ecological characteristics, the use of a regional database reduces the probability of having different species that have different ecological preferences within a single morphotype. The advantages of a regional calibration were already reported by Pflaumann and Jian (1999) for the South China Sea.

In this study, the two commonly applied techniques, Imbrie and Kipp (1971) and the SIMMAX modern analog technique of Pflaumann et al., (1996; 2003) will be used. The simultaneous application of two distinct computational approaches to one database, allows us to identify the differences in SST reconstructions that result solely from the use of

different mathematical methods, and find the one that better resolves the SST pattern of the seasonal upwelling along the western Iberian margin.

1.4. Material and Methods

1.4.1. Material

The material studied includes surface, box/multi-core, and piston core samples retrieved from the Iberian margin during several cruises (Fig. 2, Appendix).

For the regional transfer function study (Chapter 2), we used one hundred and thirty four surface sediment samples collected along the Iberian margin by Shipeck grab, Van Veen grab, box-corer, multi-corer, and kasten corer devices, during 19 cruises carried out between 1975 and 2004.

For the Late Holocene paleoceanographic study (Chapter 3), six box/multi-cores recovered along two transects are used. Transect 1 is along 37˚ 50´N, off Sines and spans water depths from 900 to 2331 m (SO83-9GK, PO200/10 6-1, SO83-7GK, SO75-9GK) and Transect 2 is along 8˚ 15´W, off Albufeira on the Algarve coast, between 667 and 1978 m water depth (M39022-1, M39029-6). These cores were recovered during cruises that took place between 1991 and 1997. POSEIDON 200/10 (Mienert, 1993), SONNE 75 (Kudrass, 1993), SONNE 83 (Halbach, 1993), and METEOR 39 (Schott et al., 1999).

In addition, three long cores along a N-S profile on the western Iberian margin were used to reconstruct the climatic variations during the last 150 ky BP (Chapter 4). Piston core SU92-03 off Cape Finisterra was recovered in 1992 during the PALEOCINAT II cruise (Labeyrie and Party, 1990). Core MD95-2040 from the southeastern flank of the Oporto Seamount and core MD95-2042 off Cape Sines were collected during the first International Marine Global Change Study (IMAGES) cruise in 1995 using the CALYPSO giant piston corer (Bassinot and Labeyrie, 1996).

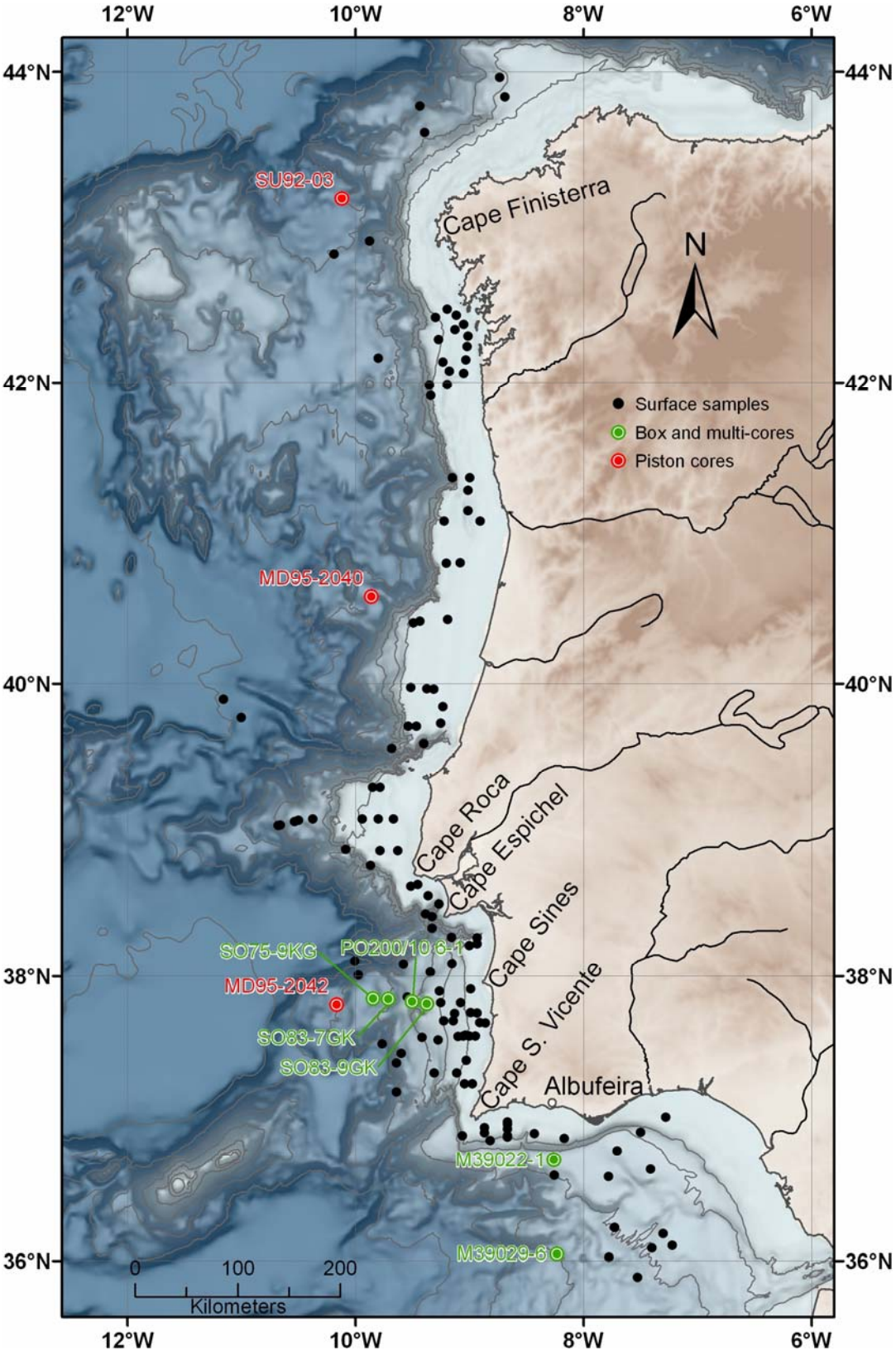

Fig. 2 Geographic distribution of the different samples studied in this dissertation.

1.4.2. Methods

On downcore studies each sediment sample was divided into two subsamples for the different analyses: (1) 2 cc were dried at 40ºC and crushed for the carbonate and carbon content analyses; (2) 8-25 cc were weighted, dried at 40ºC and weighted again to allow dry bulk density calculations. The dried sediment was then dispersed with a 0.005 mol sodium hexametaphosphate solution and washed with distilled water through a sieve stack of 2 mm, 150 μm, and 63 μm mesh-size for foraminifera assemblage, stable isotope and grain size analyses. Surface samples for the planktonic foraminifera assemblage study were prepared following the procedure (2).

Carbon content analyses

Total carbon content was determined in the CHNS-932 LECO Elemental Analyzer of the Marine Geology Laboratory at INETI (former IGM). Two replicates of dried and homogenized sediment (2 mg) were analyzed per level. The same set of samples was later subject to combustion for 8 hours through a predefined stepwise increase in temperature up to 400ºC to remove organic carbon and re-analyzed for inorganic carbon. The organic carbon content (C_{org}) was calculated as the difference between total carbon and inorganic carbon concentration. The relative precision of repeated measurements of both samples and standards was 0.03 wt%. The results are presented as accumulation rate (AR). The component specific AR was calculated for each sample as the product of the fraction of each component and the bulk mass accumulation rate (derived from the dry bulk density and sedimentation rate).

Foraminifera analyses

For quantitative planktonic and benthic foraminifera analyses and planktonic foraminifera assemblage identification, the fraction 150 μm – 2 mm was split to obtain 300-600 planktonic foraminifera specimens that were identified following the taxonomic criteria of Bé and Hamlin (1967), Bé (1977), Kennett and Srinivasan (1983), and Hemleben et al., (1989). In the same split, the number of detrital grains was determined to

trace ice-rafted debris. Quantitative abundances of planktonic and benthic foraminifera were calculated as AR by the product of bulk mass accumulation rate and the number of shells per gram of dry sediment, taking into account the weight of the total sample and the number of times that the >150 μm fraction was split prior to the counting procedure. Quantitative abundances of lithic grains were calculated as numbers per gram of dry sediment.

The % sand is calculated from the weight of the sand fraction from 63 μm to 2 mm and the dry weight of the respective sample.

Stable oxygen and carbon isotopes

Stable isotopes measurements were performed on planktonic (*Globigerina bulloides*, *Globorotalia inflata*, *Globigerinoides ruber* (white)) and benthic (*Cibicidoides* sp., *Uvigerina* sp.) foraminifera species. Samples contained on average 25 planktonic or 6 benthic specimens picked from the fraction >250 μm (mainly between 250 and 350 μm). All samples, except for core PO200/10 6-1, were measured in the Finnigan MAT 252 mass spectrometer of the MARUM at Bremen University. The $^{18}O/^{16}O$ ratio is reported in the δ permil (‰) notation relative to the Vienna Peedee Belemnite (VPDB) standard. Analytical standard deviation is ±0.07 and ±0.05‰ for $\delta^{18}O$ and $\delta^{13}C$, respectively. For core PO200/10 6-1 isotope measurements were performed of the Leibniz laboratory at Kiel University. Duplicate sample analyses give maximal standard deviation of ±0.05‰ for $\delta^{18}O$ and ±0.04‰ for $\delta^{13}C$.

AMS ^{14}C dating

The chronology of each studied core is based on AMS ^{14}C ages measured on mono-specific (*Globigerina bulloides*) planktonic foraminifera samples picked from the fraction 250 μm – 2 mm (mainly between 250 and 350 μm). The ages were measured in three different laboratories: the National Ocean Sciences AMS Facility (NOSAMS), Woods Hole Oceanographic Institution, USA; the AMS ^{14}C Dating Laboratory at University of Aarhus, Denmark; and the Leibniz Labor für Altersbestimmung und Isotopenforschung, Christian Albrechts Universität Kiel, Germany.

Ages were corrected for a marine reservoir-effect of 400 years according to modern values determined in the area (Bard, 1988; Abrantes et al., 2005). The reservoir age was

assumed to be constant through time, since no data exists for the region that could reveal paleo-reservoir age increases due to the southward advance of polar surface waters or the upwelling of aged ENACW. The ^{14}C ages younger than 20 ky were calibrated to calendar years with INTCAL04 (Reimer et al., 2004); for the older ^{14}C age the data of Hughen et al., (2004) was used.

Temperature and productivity reconstructions

In order to calibrate a regional sea surface temperature (SST) transfer function in an upwelling coastal region and minimize the bias associated with the absence of sufficient analogs, a modern analog data base was generated using the abundances of 22 species/group of species of planktonic foraminifera in the 134 surface samples and satellite-derived SST for summer and winter. This modern satellite-derived SST data is based on an integration of daily Pathfinder satellite measurements with a 9 km resolution for the period between 1985 and 2003. Two different transfer techniques: Imbrie & Kipp (Imbrie and Kipp, 1971) and SIMMAX (Pflaumann et al., 1996; 2003), were applied (Chapter 2).

The Imbrie & Kipp tecnique first reduces a matrix of species into a set of statically independent artificial end-member assemblages (factors), using the standard statistical technique of VARIMAX Q-mode factor analysis. After that, a multiple regression analysis is performed to fit an empirical equation between factor loadings (independent variables) and modern SST (dependent variables) by multiple linear regression methods, allowing squared and cross-product terms of the factor loadings to enter the equation to account for moderate nonlinearity in the faunal response to the environment (Mix et al., 1999).

SIMMAX technique differs from the Modern Analog Technique (MAT) (Hutson, 1980) in the way that defines and treats the best analogs. In this technique the scalar product of the normalized assemblage vectors is used as a measure of faunal similarity between a sample with unknown SST and samples from the training set. The estimated temperature is calculated as an average of the temperatures observed for the best analogs (in our case 10) weighted by the similarity coefficient and the inverse of geographical distance between each best analog and the unknown sample. In our calibration both the distance-weighted (dw) and non-distance-weighted (ndw) options were used, so that the option that better performs in this upwelling region could be determined.

These modern analogs were used in a data base restricted to the Iberian margin for the Late Holocene and combined with the North Atlantic data set of Kucera et al., (2005) for the last 150 ky record in order to obtain more reliable temperature and productivity reconstructions for this upwelling area, as well as other upwelling areas, in the near future.

SST reconstructions in the six box/multi-cores from the Portuguese margin during the Late Holocene are derived from planktonic foraminifera census counts and the modern analog technique SIMMAX (dw) applied to regional conditions (Chapter 3). The root-mean square error of prediction (RMSEP) produced for the SIMMAX dw option was 0.4ºC and 0.25ºC, for summer and winter, respectively.

Temperature and productivity reconstructions in the three piston cores back to 150 ky are derived from 27 taxonomic categories of planktonic foraminifera census counts, from the North Atlantic data set (Iberian margin data set included in Kucera et al., (2005) data set), and the SIMMAX (dw) technique (Chapter 4).

Modern SSTs for 10 m water depth were taken from the World Ocean Atlas 1998. Modern oceanic primary productivity (PP) is obtained for each site by averaging 12 monthly primary productivity values, for a 8 year period (1978-1986), and estimated from satellite color data (CZCS) gridded at 0.5º latitude - longitude fields (Antoine et al., 1996). Export Productivity (Pexp) was calculated from the PP values following the empirical relationship *(1)*

(1) $$Pexp=PP^2/400$$

for primary production below 200 $gC/m^2/yr$, and the empiric relationship *(2)*

(2) $$Pexp=PP/2$$

for primary production above 200 $gC/m^2/yr$ (Eppley and Peterson, 1979; Sarnthein and Winn, 1988).

1.5. Overview of the research

The presented thesis contributes: (1) to calibrate a regional transfer function in an upwelling area and increase the number of analogs for the North Atlantic data set; (2) to improve the knowledge of hydrographic and productivity conditions along the Iberian margin, using planktonic foraminifera assemblages compared to other proxies (such as organic carbon and stable isotope data) for the latest Holocene (2.5 ky); and (3) during the

last 150 ky. The main results of this dissertation are presented in three manuscripts, Chapter 2 to Chapter 4, and are briefly summarized here. Conclusions reached by all three studies will be presented in Chapter 5.

Planktonic Foraminifera from Modern Sediments Reflect Upwelling Patterns off Iberia: Insights from a Regional Transfer Function

Emília Salgueiro, Antje Voelker, Fátima Abrantes, Helge Meggers, Uwe Pflaumann, Neven Lončarić, Raquel González-Álvarez, Paulo Oliveira, Helga B. Bartels-Jónsdóttir, João Moreno and Gerold Wefer

(Submitted to Marine Micropaleontology)

Planktonic foraminiferal census data from 134 surface samples collected along the western Iberian margin were used to assess the quality of their spatial record relatively to the present hydrography conditions and to calibrate a regional Sea Surface Temperature (SST) transfer function for this seasonal coastal upwelling region. Species spatial distribution and Q-mode factor analysis derived groups reveal that the most abundant species (Fig. 1) are linked to main superficial water masses: factor 1 is exclusively defined by *Globigerina bulloides*, the most abundant and widespread species, and reflects the modern seasonal (May to September) coastal upwelling areas; factor 2 dominated by *Neogloboquadrina pachyderma* (dextral) and *Globorotalia inflata* appears associated with the descending branch of the North Atlantic Drift (Portugal Current); factor 3 is defined by the tropical–subtropical species *Globigerinoides ruber* (white), *Globigerinoides trilobus trilobus*, and *Globorotalia inflate*, and mirrors the influence of the winter-time Eastern branch of Azores Current (Portugal Coastal Countercurrent). *Neogloboquadrina pachyderma* (dextral), also seems to be related with upwelling along the northwest Iberian margin, evidencing the upwelling of a water mass different than the one revealed by the *G. bulloides* pattern.

This regional planktonic foraminiferal data set was used to calibrate a SST transfer function in conjunction with satellite-derived SST integrated over an 18 year period for summer and winter seasons. Imbrie & Kipp and SIMMAX (dw and ndw) techniques were applied. Derived results from SIMMAX (dw) are more consistent than the ones from the other methods both for the calibration data set as for paleo-SST reconstructions.

Productivity and hydrographic changes off Southwest and South Portugal: Foraminiferal evidence for the Late Holocene

Emília Salgueiro, Antje Voelker, Fátima Abrantes, Neven Lončarić, Helge Meggers, João Moreno, Gerold Wefer

(To be submitted to Quaternary Research)

The paleoceanographic changes off SW and S Portugal were assessed through a multi-proxy study of six box/multi-cores distributed along two transects: an E-W transect off Sines (southwest Portugal); and a N-S transect off Albufeira on the southern coast. As both study regions suffer the influence of the Mediterranean Outflow Water (MOW), which is believed to have been fairly constant in position and intensity throughout the Holocene, it was necessary to distinguish its influence from the productivity signal in the sediment record.

Main results point to more stable productivity conditions off Sines during the major historical warm European North Atlantic periods for the last 2500 yr detected in the region by recent works, i.e. the Roman Warm Period and Medieval Warm Period, than during the cold times, i.e. the Dark Ages and the Little Ice Age. The opposite was observed off Albufeira. No major changes between warm and cold climatic periods were observed in both transects in terms of water masses signal.

Temperature and Productivity Changes off the Western Iberian Margin during the last 150 ky

Emília Salgueiro, Antje Voelker, Lúcia de Abreu, Fátima Abrantes, Helge Meggers, Gerold Wefer

(Submitted to Quaternary Science Reviews)

To better understand the influence of abrupt climate change, in particular of Heinrich events (H), on the North Atlantic's eastern boundary upwelling systems, we have investigated hydrography and productivity variations during the last 150 ky BP in three deep-sea cores located off Iberia along a North - South transect (43º12´N - 37º48´N).

Special attention is given to the northernmost core, more likely to be influenced by polar front movements.

Planktonic foraminifera census counts were used to reconstruct sea surface temperature (SST) and export productivity (Pexp) using the modern analog technique SIMMAX (dw). For this purpose the planktonic foraminifera North Atlantic modern analog database of Kucera et al., (2005) was expanded by the addition of the Iberian margin surface samples leading to a total of 1020 analogs for SST and 999 for Pexp.

The SST increase from North to South is a constant throughout the last 150 ky, while Pexp shows the opposite trend during the interglacial periods but no significant variation during the glacial periods. A boundary between differences in glacial/interglacial productivity appears to be present in the region between 43º12´N and 40º35´N. Coldest SST and lowest Pexp are found during H at all sites. Only at the southernmost site, less influenced by H, the lowest Pexp does not coincide with all of these events.

Appendix:
Detailed information of the different samples studied in this dissertation.

Sample	Longitude (W)	Latitude (N)	Water Depth (m)	Cruise Name	Device
VB033	-9.1500	41.3733	140	VIABOA	shipeck grab
VB057	-9.2233	41.0867	160	VIABOA	shipeck grab
VB060	-8.9050	41.0867	65	VIABOA	shipeck grab
VB073	-9.2033	40.8083	140	VIABOA	shipeck grab
VB075	-9.0817	40.8100	95	VIABOA	shipeck grab
VB094	-9.4917	40.4067	155	VIABOA	shipeck grab
VB095	-9.4333	40.4200	145	VIABOA	shipeck grab
VB098	-9.1917	40.4300	100	VIABOA	shipeck grab
VB106	-9.5150	39.9750	145	VIABOA	shipeck grab
VB108	-9.3150	39.9633	120	VIABOA	shipeck grab
VB133	-9.4667	39.7150	140	VIABOA	shipeck grab
VB135	-9.5367	39.7167	155	VIABOA	shipeck grab
VB136	-9.8500	39.3000	205	VIABOA	shipeck grab
VB138	-9.7833	39.3000	155	VIABOA	shipeck grab
VB156	-9.6650	39.0833	94	VIABOA	shipeck grab
VB161	-9.7983	39.0833	130	VIABOA	shipeck grab
VB164	-9.9417	39.0850	154	VIABOA	shipeck grab
VB165	-10.0833	38.8767	415	VIABOA	shipeck grab
VB172	-9.7833	38.8667	105	VIABOA	shipeck grab
VB176	-9.6300	38.8667	110	VIABOA	shipeck grab
LV010	-7.5000	36.9100	405	LIVRA	Van Veen grab
LV044	-8.1667	36.8667	84	LIVRA	Van Veen grab
LV051	-8.8667	36.9417	100	LIVRA	Van Veen grab
LV053	-8.8667	36.9067	110	LIVRA	Van Veen grab
LV059	-8.4317	36.9000	107	LIVRA	Van Veen grab
LV072	-8.6667	36.9833	74	LIVRA	Van Veen grab
LV073	-8.6667	36.9683	80	LIVRA	Van Veen grab
LV075	-8.6667	36.9333	98	LIVRA	Van Veen grab
LV078	-8.6667	36.8833	105	LIVRA	Van Veen grab
LV079	-8.6667	36.8750	110	LIVRA	Van Veen grab
LV085	-8.9750	37.2500	96	LIVRA	Van Veen grab
LV087	-9.0417	37.2500	122	LIVRA	Van Veen grab
LV099	-9.0633	36.8833	157	LIVRA	Van Veen grab
LV102	-9.0267	37.4150	180	LIVRA	Van Veen grab
LV119	-8.9500	37.5833	145	LIVRA	Van Veen grab
LV122	-9.0000	37.5833	172	LIVRA	Van Veen grab
LV124	-9.0350	37.5883	212	LIVRA	Van Veen grab
LV125	-9.0533	37.5833	245	LIVRA	Van Veen grab
LV126	-9.1000	37.5817	305	LIVRA	Van Veen grab
LV127	-9.1317	37.7417	385	LIVRA	Van Veen grab
LV131	-8.9900	37.7467	152	LIVRA	Van Veen grab
LV134	-8.9333	37.7433	130	LIVRA	Van Veen grab
LV144	-8.9917	37.9142	138	LIVRA	Van Veen grab
LV148	-9.1533	38.0867	335	LIVRA	Van Veen grab
LV171	-9.0000	38.2133	143	LIVRA	Van Veen grab
LV173	-8.9333	38.2250	128	LIVRA	Van Veen grab
SO75 09KG	-9.8467	37.8433	2331	SONNE75	box corer
SO75 13KG	-9.2733	37.5550	636	SONNE75	box corer
SO75 15KG	-9.4150	37.5750	986	SONNE75	box corer
SO75 25KG	-9.5450	37.8550	1300	SONNE75	box corer
SO75 30KG	-9.5983	37.4633	1699	SONNE75	box corer
SO75 33KG	-9.6417	37.3967	1871	SONNE75	box corer
SO83 07GK	-9.7117	37.8400	2010	SONNE83	box corer
SO83 10GK	-9.2533	37.8150	498	SONNE83	box corer
SO83 11GK	-9.0767	37.8150	267	SONNE83	box corer
PO01(2)	-9.1117	37.3267	246	POSEIDON 200-10	box corer
PO03(1)	-9.3100	37.3250	822	POSEIDON 200-10	box corer
PO05(1)	-9.2650	37.8983	550	POSEIDON 200-10	box corer
PO06(1)	-9.5033	37.8217	1085	POSEIDON 200-10	box corer
M39002-3	-7.7750	36.0272	1205	METEOR 39/1	multi corer

Continued

Sample	Longitude (W)	Latitude (N)	Water Depth (m)	Cruise Name	Device
M39003-2	-7.2227	36.1108	800	METEOR 39/1	multi corer
M39004-2	-7.7289	36.2367	967	METEOR 39/1	multi corer
M39016-2	-7.7056	36.7783	580	METEOR 39/1	multi corer
M39017-4	-7.4101	36.6500	532	METEOR 39/1	multi corer
M39021-5	-8.2547	36.6050	900	METEOR 39/1	box corer
M39022-3	-8.2599	36.7117	668	METEOR 39/1	multi corer
M39023-3	-8.2621	36.7350	728	METEOR 39/1	box corer
M39029-6	-8.2333	36.0497	1918	METEOR 39/1	multi corer
M39035-3	-9.5010	37.8217	1082	METEOR 39/1	multi corer
M39058-1	-10.6795	39.0393	1977	METEOR 39/1	box corer
M39059-2	-10.5352	39.0665	1605	METEOR 39/1	box corer
M39070-1	-9.3917	43.6183	1220	METEOR 39/1	box corer
M39072-1	-9.4350	43.7867	2170	METEOR 39/1	box corer
PE151-01A	-9.8668	38.7667	133	IBERIA 2000	box corer
PE151-03B	-8.8203	36.8522	312	IBERIA 2000	box corer
PE151-04A	-7.2792	37.0157	61	IBERIA 2000	box corer
PO287-3-1B	-10.4993	39.0738	1505	PALEO I	box corer
PO287-5-1B	-8.9985	41.3740	87	PALEO I	box corer
PO287-8-1B	-9.0128	41.2910	88	PALEO I	box corer
PO287-13-1B	-9.0125	41.1562	81	PALEO I	box corer
PO287-15-1B	-9.2537	39.7362	111	PALEO I	box corer
PO287-19-1B	-9.2332	39.8480	101	PALEO I	box corer
PO287-21-1B	-9.3753	39.9670	128	PALEO I	box corer
PO287-26-1B	-9.3640	38.5582	96	PALEO I	box corer
PO287-27-1B	-9.4542	38.6340	85	PALEO I	box corer
PO287-28-1B	-9.5145	38.6243	105	PALEO I	box corer
PO287-33-1B	-8.9092	37.6780	119	PALEO I	box corer
PO287-34-1B	-8.8610	37.6758	90	PALEO I	box corer
PO287-40-1B	-9.2242	37.6892	493	PALEO I	box corer
PO287-41-1B	-9.1432	37.6905	380	PALEO I	box corer
PO287-44-1B	-10.6607	39.0425	1866	PALEO I	box corer
PO287-45-1B	-10.3742	39.0833	1216	PALEO I	box corer
PO201/10-702	-8.6900	43.8433	402	POSEIDON 201-10	box corer
PO201/10-703	-8.7367	43.9667	583	POSEIDON 201-11	box corer
ATL-FP1-04B	-9.8750	42.9194	2130	Atalante	multi corer
ATL-FP1-05B	-10.1892	42.8361	2953	Atalante	multi corer
ATL-FP1-08A	-9.3439	38.0306	987	Foram Prox	multi corer
ATL-FP1-09A	-9.7644	37.5283	3124	Foram Prox	multi corer
ATL-FP1-10B	-9.6383	37.1933	1863	Foram Prox	multi corer
64PE218-16	-8.9333	38.2667	430	Canyons 2003	multi corer
64PE218-21	-9.2672	38.4998	498	Canyons 2003	multi corer
64PE218-22	-9.3296	38.4130	1463	Canyons 2003	multi corer
64PE218-36-1	-9.1584	38.2707	1409	Canyons 2003	box corer
64PE225-1-21	-9.5808	38.0833	1742	Canyons 2004	multi corer
64PE225-1-26	-9.4001	39.5990	1118	Canyons 2004	multi corer
64PE225-2-02	-9.3843	38.4330	301	Canyons 2004	multi corer
64PE225-3-03	-9.3266	38.3330	1856	Canyons 2004	multi corer
64PE225-06	-9.9753	38.0080	2945	Canyons 2004	multi corer
64PE225-07	-10.0043	38.1060	4451	Canyons 2004	multi corer
64PE225-25	-10.9999	39.7740	4804	Canyons 2004	multi corer
64PE225-22	-11.1565	39.8980	4975	Canyons 2004	multi corer
64PE225-27	-9.6831	39.5660	1009	Canyons 2004	multi corer
MD04-2811	-10.1647	37.8040	3162	Privilege	kasten corer
MD04-2814	-9.8577	40.5945	2449	Alienor	kasten corer
MD04-2817	-9.7993	42.1618	2365	Alienor	kasten corer
M2004-13	-7.3000	36.1940	742	MOUNDFORCE	box corer
M2004-28	-7.4010	36.0930	815	MOUNDFORCE	box corer
SWIM04-42 SW	-7.5278	35.8855	1172	SWIM 2004	sw corer
GeoB9014-1	-7.7800	36.5970	716	GAP	multi corer
ZS-5	-9.0496	42.0606	125	Investigador	shipeck grab
ZS-9	-9.1953	41.9887	139	Investigador	shipeck grab
ZS-13	-9.3408	41.9170	192	Investigador	shipeck grab
ZS-17	-9.0322	42.1477	122	Investigador	shipeck grab
ZS-21	-9.1747	42.0751	145	Investigador	shipeck grab

Continued

Sample	Longitude (W)	Latitude (N)	Water Depth (m)	Cruise Name	Device
ZS-26	-9.3526	41.9835	244	Investigador	shipeck grab
ZS-30	-9.2323	42.1355	171	Investigador	shipeck grab
ZS-36	-9.0188	42.2358	120	Investigador	shipeck grab
ZS-42	-9.0119	42.3045	104	Investigador	shipeck grab
ZS-51	-9.2715	42.2822	203	Investigador	shipeck grab
ZS-55	-9.1267	42.3481	135	Investigador	shipeck grab
ZS-57	-9.0520	42.3813	105	Investigador	shipeck grab
ZS-63	-9.1153	42.4410	113	Investigador	shipeck grab
ZS-68	-9.2983	42.4268	205	Investigador	shipeck grab
ZS-71	-9.1938	42.4784	123	Investigador	shipeck grab
SO83-9GK	-9.3733	37.8083	900	SONNE83	Box-corer
M39022-1	-8.2599	36.7117	667	METEOR 39/1	Box-corer
SO75-09KG	-9.8467	37.8433	2331	SONNE75	box-corer
SO83-07GK	-9.7117	37.8400	2010	SONNE83	box-corer
PO200/10 6-1	-9.5033	37.8217	1085	POSEIDON 200-10	box-corer
SO83-9GK	-9.3733	37.8083	900	SONNE83	box-corer
M39022-1	-8.2599	36.7117	667	METEOR 39/1	box-corer
M39029-6	-8.2333	36.0497	1918	METEOR 39/1	multi-corer
SU92-03	43º11.75’	10º6.78’	3005	PALEOCINAT II	piston core
MD95-2040	40º34.91’	9º51.67’	2465	IMAGES	calypso giant piston core
MD95-2042	37º47.99’	10º9.99’	3146	IMAGES	calypso giant piston core

References

Abrantes, F. and Sancetta, C., 1985. Diatom assemblages in surface sediments reflect coastal upwelling off Southern Portugal. Oceanologica Acta, 8: 7-12.

Abrantes, F., 1988. Diatom Assemblages as Upwelling Indicators in Surface Sediments Off Portugal. Marine Geology, 85: 15-39.

Abrantes, F. et al., 2005. Shallow-marine sediment cores record climate variability and earthquake activity off Lisbon (Portugal) for the last 2000 years. Quaternary Science Reviews, 24(23-24): 2477-2494.

Álvarez-Salgado, X.A. et al., 2001. Off-shelf fluxes of labile materials by an upwelling filament in the NW Iberian Upwelling System. Progress in Oceanography, 51(2-4): 321-337.

Ambar, I. and Howe, M.R., 1979a. Observations of the Mediterranean Outflow .1. Mixing in the Mediterranean Outflow. Deep-Sea Research Part a-Oceanographic Research Papers, 26(5): 535-554.

Ambar, I. and Howe, M.R., 1979b. Observations of the Mediterranean Outflow .2. Deep Circulation in the Vicinity of the Gulf of Cadiz. Deep-Sea Research Part a-Oceanographic Research Papers, 26 A(5): 555-568.

Ambar, I. et al., 2002. Physical, chemical and sedimentological aspects of the Mediterranean outflow off Iberia. Deep-Sea Research Part Ii-Topical Studies in Oceanography, 49(19): 4163-4177.

Andreasen, D.J. and Ravelo, A.C., 1997. Tropical Pacific Ocean thermocline depth reconstructions for the last glacial maximum. Paleoceanography, 12(3): 395-413.

Antoine, D., Andre, J.M. and Morel, A., 1996. Oceanic primary production .2. Estimation at global scale from satellite (coastal zone color scanner) chlorophyll. Global Biogeochemical Cycles, 10(1): 57-69.

Bard, E., 1988. Correction of accelerator mass spectometry 14C ages measured in planktonic foraminifera: Paleoceanographic implications. Paleoceanography, 3: 635-645.

Bassinot, F. and Labeyrie, L., 1996. IMAGES 101 Report, Institut Français pour la Recherche et la Technologie Polaires, Plouzané.

Bé, A.W.H. and Hamlin, W.H., 1967. Ecology of recent planktonic foraminifera. Part3: Distribution in the North Atlantic during the summer of 1962. Micropaleontology, 13: 87-106.

Bé, A.W.H. and Tolderlund, D.S., 1971. Distribution and ecology of living planktonic foraminifera in surface waters of the Atlantic and Indian Oceans. In: B.M. Funnel, Riedel, W. R. (eds.) (Editor), The Micropaleontology of Oceans. Cambridge University Press, New York, pp. 105–149.

Bé, A.W.H., 1977. An ecological, zoogeographic and taxonomic review of Recent planktonic foraminifera. In: A.T.S. Ramsay (Editor), Oceanic Micropaleontology. Academic, San Diego, California, pp. 1-100.

Berger, W.H. and Keir, R.S., 1984. Glacial-Holocene Changes in Atmospheric CO2 and the Deep-Sea Record. In: M. Ewing (Editor), Climate Processes and Climate Sensitivity. Am. Geophysical Union, pp. 337-351.

Berger, W.H., Smetacek, V.S. and Wefer, G., 1989. Ocean productivicty and paleoproductivity - an overview. In: W.H. Berger, V.S. Smetacek and G. Wefer (Editors), Productivity of the Ocean : Present and Past. John Wiley & Sons, New York, pp. 1-34.

Berger, W.H. and Wefer, G., 1990. Export Production - Seasonality and Intermittency, and Paleoceanographic Implications. Global and Planetary Change, 89(3): 245-254.

Bijma, J., Hemleben, C., Huber, B.T., Erlenkeuser, H. and Kroon, D., 1998. Experimental determination of the ontogenetic stable isotope variability in two morphotypes of Globigerinella siphonifera (d'Orbigny). Marine Micropaleontology, 35(3-4): 141-160.

Broecker, W.S., 1982. Ocean Chemistry During Glacial Time. Geochimica Et Cosmochimica Acta, 46(10): 1689-1705.

CLIMAP, P.M., 1976. The surface of the ice-age Earth. Science, 191: 1131-1137.

Doney, S.C. et al., 2001. Marine Biogeochemical Modeling: Recent Advances and Future Challenges. Oceanography, 14(4): 93-107.

Eppley, R.W. and Peterson, B.J., 1979. Particulate Organic-Matter Flux and Planktonic New Production in the Deep Ocean. Nature, 282(5740): 677-680.

Fiúza, A.F.G., 1983. Upwelling Patterns off Portugal. In: E. Suess and J. Thiede (Editors), Coastal Upwelling its sediment record. Plenum Press, New York, pp. 85-98.

Fiúza, A.F.G., 1984. Hidrologia e Dinamica das Aguas Costeiras de Portugal, Faculdade de Ciências da Universidade de Lisboa, Lisbon, 294 pp.

Fiúza, A.F.G. et al., 1998. Water masses and their circulation off western Iberia during May 1993. Deep Sea Research Part I: Oceanographic Research Papers, 45(7): 1127-1160.

Fraga, F., 1981. Upwelling off the Galician Coast, Northwest Spain. In: F.A. Richards (Editor), Coastal Upwelling. American Geophysical Union, Washington, pp. 176-182.

Halbach, P., 1993. Technischer Fahrtbericht zur SONNE-Fahrt SO83 (MARFLUX 4): Vergleichende marin-geologische und -geochemische Untwesuchungen an Sedimenten, Prazipitaten und Gesteinen von drei submarinen Bergen im NE-Atlantik., Freie Universitat Berlin.

Haynes, R., Barton, E. and Pilling, I., 1993. Development, persistence, and variability of upwelling filaments off the Atlantic coast of the Iberian Peninsula. Journal of Geophysical Research, 98(C12): 22681-22692.

Hemleben, C., Spindler, M. and Anderson, O.R., 1989. Modern Planktonic Foraminifera. Springer-Verlang, Berlin, 363 pp.

Hill, E.A. et al., 1998. Eastern ocean boundaries coastal segment (E). In: A.R. Robinson and K.H. Brink (Editors), The Sea. John Wiley and Sons, New York, pp. 29-67.

Hughen, K. et al., 2004. C-14 activity and global carbon cycle changes over the past 50,000 years. Science, 303(5655): 202-207.

Hurrell, J.W., Kushnir, Y. and Visbeck, M., 2001. Climate - The North Atlantic oscillation. Science, 291(5504): 603-606.

Hutson, W.H., 1977. Transfer-Functions under No-Analog Conditions - Experiments with Indian-Ocean Planktonic Foraminifera. Quaternary Research, 8(3): 355-367.

Hutson, W.H., 1980. The Agulhas Current During the Late Pleistocene - Analysis of Modern Faunal Analogs. Science, 207(4426): 64-66.

Imbrie, J. and Kipp, N.G., 1971. A new micropaleontological method for quantitative paleoclimatology: Application to a late Pleistocene Caribbean core. In: K.K. Turekian, ed. (Editor), The late Cenozoic glacial ages. Yale University Press, New Haven, Conneticut, pp. 71–181.

Kennett, J., 1982. Marine Geology, Marine Geology. Prentice-Hall Inc., Englewood Cliffs, pp. 538-559.

Kennett, J.P. and Srinivasan, M.S., 1983. Neogene planktonic Foraminifera. A phylogenetic atlas. Hutchinson Ross Pulbishing Company, Stroudsburg, 263 pp.

Kucera, M. et al., 2005. Reconstruction of sea-surface temperatures from assemblages of planktonic foraminifera: multi-technique approach based on geographically constrained calibration data sets and its application to glacial Atlantic and Pacific Oceans. Quaternary Science Reviews, 24(7-9): 951-998.

Kudrass, H.R. et al., 1993. Sonne Cruise SO-75-3: Final Report. Mediterranean outflow water at the continental slope of SW Portugal : acoustic facies and benthic foraminifera. Bundesanstalt fur Geowissenschaften und Rohstoffe, Hannover, pp. 65.

Labeyrie, L. and Party, S.S., 1990. Rapport Preliminaire de PALEOCINAT I (Paleocirculation de l´Atlantique nord), IFREMER, INSU.

Laws, E.A., Falkowski, P.G., Smith, W.O., Ducklow, H.W. and McCarthy, J.J., 2000. Temperature effects on export production in the opean ocean. Global Biogeochemical Cycles, 14: 1231-1246.

Le, J. and Shackleton, N.J., 1994. Reconstructing paleoenvironment by transfer function: Model evaluation with simulated data. Marine Micropaleontology, 24(2): 187-199.

Malmgren, B.A. and Nordlund, U., 1997. Application of artificial neural networks to paleoceanographic data. Palaeogeography Palaeoclimatology Palaeoecology, 136: 359-373.

Mienert, J., 1993. European North Atlantic Matgin: sediment pathways, processes and fluxes. RV Poseidon 200/10 Cruise Report, Geomar, Kiel.

Mix, A., 1989. Pleistocene paleoproductivity: Evidence from organic carbon and foraminiferal species. In: V.H. Berger, V.S. Smetacek and G. Wefer (Editors), Productivicty of the Ocean: Present and Past. J Willey & Sons, New York, pp. 313-340.

Mix, A.C., Morey, A.E., Pisias, N.G. and Hostetler, S.W., 1999. Foraminiferal faunal estimates of paleotemperature: Circumventing the no-analog problem yields cool ice age tropics. Paleoceanography, 14(3): 350-359.

Monteiro, J.H., Abrantes, F., Alveirinho-Dias, J.M. and Gaspar, L., 1983. Upwelling records in recent sediments from southern Portugal: a reconnaissance survey. In: E. Suess and J. Thiede (Editors), Coastal Upwelling: Its Sediment Record. Part B; Sedimentary Record of Ancient Coastal Upwelling. NATO Conference Series, Plenum, New York, pp. 145-162.

Moore, T.C., Rea, D.K., Lyle, M. and Liberty, L.M., 2002. Equatorial ocean circulation in an extremely warm climate. Paleoceanography, 17(1): -.

Ortiz, J.D. and Mix, A.C., 1992. The spatial distribution and seasonal succession of planktonic foraminifera in the California Current off Oregon, September 1987 - September 1988. In: C.P. Summerhayes, W.L. Prell and K.C. Emeis (Editors), Upwelling Systems: Evolution Since the Early Miocene. Geological Society Special Publication, London, pp. 197-213.

Peliz, A., Dubert, J., Santos, A.M.P., Oliveira, P.B. and Le Cann, B., 2005. Winter upper ocean circulation in the Western Iberian Basin - Fronts, Eddies and Poleward Flows: an overview. Deep-Sea Research Part I-Oceanographic Research Papers, 52(4): 621-646.

Pflaumann, U., Duprat, J., Pujol, C. and Labeyrie, L.D., 1996. SIMMAX: A modern analog technique to deduce Atlantic sea surface temperatures from planktonic foraminifera in deep-sea sediments. Paleoceanography, 11(1): 15-35.

Pflaumann, U. and Jian, Z., 1999. Modern distribution patterns of planktonic foraminifera in the South China Sea and western Pacific: a new transfer technique to estimate regional sea-surface temperatures. Marine Geology, 156: 41-83.

Pflaumann, U. et al., 2003. Glacial North Atlantic: Sea-surface conditions reconstructed by GLAMAP 2000. Paleoceanography, 18(3): 1065, doi: 10.1029/2002PA000774.

Ravelo, A.C., Fairbanks, R.G. and Philander, S.G.H., 1990. Reconstructing tropical Atlantic hydrography using planktontic foraminifera and an ocean model. Paleoceanography, 5(3): 409-431.

Reimer, P.J. et al., 2004. INTCAL04 Terrestrial Radiocarbon Age calibration, 0–26 cal kyr BP. Radiocarbon, 46: 1029 -1058.

Rios, A.F., Perez, F.F. and Fraga, F., 1992. Water Masses in the Upper and Middle North-Atlantic Ocean East of the Azores. Deep-Sea Research Part a-Oceanographic Research Papers, 39(3-4A): 645-658.

Sarnthein, M. and Winn, K., 1988. Global variations of surface ocean productivity in Low and Mid latitudes: Influence on CO2 reservoirs of the deep ocean and atmosphere during the last 21,000 years. Paleoceanography, 3(3): 361-399.

Schott, F., Koltermann, K.P., Sy, A., Zahn, R. and Zenk, W., 1999. North Atlantic 1997, cruise N. 39, 18 April - 14 September 1997., METEOR-Ber. 99-1.

Sousa, F.M. and Bricaud, A., 1992. Satellite-Derived phytoplankton pigment structures in the Portuguese Upwelling Area. Journal of Geophysical Research, 97(C7): 11,343-11,356.

Terbraak, C.J.F. and Juggins, S., 1993. Weighted Averaging Partial Least-Squares Regression (Wa-Pls) - an Improved Method for Reconstructing Environmental Variables from Species Assemblages. Hydrobiologia, 269: 485-502.

Thunell, R. and Sautter, L.R., 1992. Planktonic foraminiferal faunal and stable isotopic indices of upwelling: a sediment trap study in the San Pedro Basin, Southern California Bight. In: C.P. Summerhayes, W.L. Prell and K.C. Emeis (Editors), Upwelling Systems: Evolution Since the Early Miocene. Geological Society Special Publication, pp. 77-91.

Thunell, R.C., Curry, W.B. and Honjo, S., 1983. Seasonal variation in the flux of planktonic foraminifera: time series sediment trap results from the Panama basin. Earth and Planetary Science Letters, 69: 44-55.

Trigo, R.M. and DaCamara, C.C., 2000. Circulation weather types and their influence on the precipitation regime in Portugal. International Journal of Climatology, 20(13): 1559-1581.

Trigo, R.M. et al., 2004. North Atlantic oscillation influence on precipitation, river flow and water resources in the Iberian peninsula. International Journal of Climatology, 24(8): 925-944.

Waelbroeck, C. et al., 1998. Improving past sea surface temperature estimates based on planktonic fossil faunas. Paleoceanography, 13(3): 272-283.

Watkins, J.M. and Mix, A.C., 1998. Testing the effects of tropical temperature, productivity, and mixed-layer-depth on foraminiferal transfer functions. Paleoceanography, 13(1): 96-105.

Wooster, W., Bakun, A. and McLain, D., 1976. The seasonal upwelling cycle along the eastern boundary of the North Atlantic. Journal of Marine Research, 34(2): 131-141.

CHAPTER 2

Planktonic Foraminifera from Modern Sediments Reflect Upwelling Patterns off Iberia: Insights from a Regional Transfer Function

Emília Salgueiro[a,b], Antje Voelker[a], Fátima Abrantes[a], Helge Meggers[b], Uwe Pflaumann[c], Neven Lončarić[d], Raquel González-Álvarez[e], Paulo Oliveira[f], Helga B. Bartels-Jónsdóttir[a,g], João Moreno[h], Gerold Wefer[b]

[a] Departamento de Geologia Marinha, Instituto Nacional de Engenharia, Tecnologia e Inovação I.P., (INETI-DGM), Estrada da Portela – Zambujal, Apartado 7586, 2721-866 Alfragide, Portugal
[b] Fachbereich Geowissenschaften Universität Bremen, Postfach 33 04 40, D-28359 Bremen, Germany
[c] Institut für Geowissenschaften, Universität Kiel, Olshausenstr. 40, D-24118 Kiel, Germany
[d] Nederlands Instituut voor Onderzoek der Zee (NIOZ), Postbus 59, 1790 AB, Den Burg, Texel, The Nederlands
[e] Departamento de Xeociencias Mariñas e O.T., Facultade de Ciencias do Mar, Universidade de Vigo, 36310 Vigo, Pontevedra, Spain
[f] Instituto Nacional de Investigacão Agrária e das Pescas (INIAP), Av. Brasilia, 1449-006 Lisboa, Portugal
[g] Department of Earth Sciences, University of Aarhus, DK-8000 Aarhus C, Denmark
[h] INETI-DGM former collaborator, Estrada da Portela – Zambujal, Apartado 7586, 2721-866 Alfragide, Portugal

Submitted to Marine Micropaleontology (12 June 2006)

Abstract

Quantitative and qualitative analyses of planktonic foraminiferal assemblages from 134 core-top sediment samples collected along the western Iberian margin were used to assess the latitudinal and longitudinal changes in surface water conditions and to calibrate a Sea Surface Temperature (SST) transfer function for this seasonal coastal upwelling region. Q-mode factor analysis performed on relative abundances yielded three factors that explain 96% of the total variance: factor 1 (50%) is exclusively defined by Globigerina bulloides, the most abundant and widespread species, and reflects the modern seasonal (May to September) coastal upwelling areas; factor 2 (32%) is dominated by Neogloboquadrina pachyderma (dextral) and Globorotalia inflata and seems to be associated with the Portugal Current, the descending branch of the North Atlantic Drift; factor 3 (14%) is defined by the tropical–subtropical species Globigerinoides ruber (white), Globigerinoides trilobus trilobus, and Globorotalia inflata and mirrors the influence of the winter-time Eastern branch of Azores Current. In conjunction with satellite-derived SST for summer and winter seasons integrated over an 18 year period the regional foraminiferal data set is used to calibrate a SST transfer function using Imbrie & Kipp and SIMMAX techniques. SIMMAX (with distance weighting) derived results yield the lowest predicted error (RMSEP), the highest correlation coefficients, and the lowest

residual deviation from SST estimated for the summer and winter seasons. However, all techniques appear to underestimate SST off the southern Portuguese margin, an area mainly occupied by warm waters where upwelling occurs only occasionally, and overestimate SST on the northern part of the west coast of the Portuguese margin, where cold waters are present nearly all year round. The application of the regional calibrations to two cores, one under and the other outside of the direct influence of seasonal upwelling, also suggest that the SIMMAX (with distance weighting) might provide more consistent paleo-SST estimates when applied on a regional scale, and further emphasizes the SST underestimation off the southern Portuguese margin.

Keywords: Planktonic foraminifera; transfer functions; sea surface temperature; upwelling; Iberian margin.

2.1. Introduction

Planktonic foraminifera are one of the most commonly used tools in paleoceanography because they are seen as "fingerprints" of the water masses in which they live, behaving as indicators of temperature, salinity, and nutrient content and making it possible to identify past circulation through the sedimentary record (Imbrie and Kipp, 1971; Kennett, 1982). The use of sediment traps and culture experiments have confirmed the importance of the information that can be derived from the study of these organisms. Sediment trap data from upwelling areas have clearly shown that maximum fluxes of planktonic foraminifera occur when upwelling is most intense (e.g., Thunell et al., 1983; Ortiz and Mix, 1992; Thunell and Sautter, 1992).

Ever since CLIMAP, the abundance patterns of planktonic foraminiferal species in sediments have provided the base for the reconstruction by statistical methods of paleoenvironmental parameters, such as Sea Surface Temperature (SST) (e.g., Imbrie and Kipp, 1971; Hutson, 1977; 1980; Pflaumann et al., 1996; Malmgren and Nordlund, 1997; Waelbroeck et al., 1998; Pflaumann et al., 2003). Such techniques are based on the fundamental assumption that planktonic foraminiferal fauna assemblages at the seafloor are directly or indirectly related to the SST above the respective site (Bé and Tolderlund, 1971). However, planktonic foraminiferal species also respond to other environmental parameters, such as nutrient availability, light intensity, interspecific competition, and salinity, (Bé, 1977; Hemleben et al., 1989). Le and Shackleton (1994), therefore, proposed the use of a regional calibration and of a selective number of species with known ecological characteristics to improve the reconstruction of paleoenvironments. Kucera et al., (2005) also recommend regional over global calibrations to minimize the noise in the data and the error of environmental reconstructions introduced by the large area covered by

the calibration data set. The geographical coverage of calibration data sets has gained additional importance with the discovery of cryptic genetic types within morphologically defined species of planktonic foraminifera (Huber et al., 1997). These genetic types have specific ecological preferences and often restricted geographical ranges (Darling et al., 2000; de Vargas et al., 2001; Darling et al., 2003), suggesting that they represent distinct biological species. Kucera et al., (2005) defend that in theory, if these cryptic species have different ecological characteristics, the use of a regional database reduces the probability of having different species that have different ecological preferences within a single morphotype. For the South China Sea, the advantages of a regional calibration were reported by Pflaumann and Jian (1999).

The Iberian margin (eastern North Atlantic) is characterized by seasonal upwelling (May to October) (Wooster et al., 1976; Fraga, 1981; Fiúza, 1983; 1984) associated with high primary productivity that leaves a sediments imprint beneath these areas, as shown by Monteiro et al., (1983), Abrantes and Sancetta (1985), and Abrantes (1988). In upwelling areas like the western Iberian margin, strong lateral thermal gradients between seasons occur and summer temperatures can be colder than the winter ones. Since long these areas represent a difficulty for transfer function techniques and samples located there have often been excluded from calibration data sets (Pflaumann et al., 1996).

In this study we use the planktonic foraminiferal census data of 134 surface sediment samples from the western Iberian margin and satellite-derived SST, which resolves better the thermal gradient during upwelling in order to: 1) describe the relationships between actual hydrography/productivity and planktonic foraminifera assemblages preserved in surface sediments; 2) calibrate for the first time a regional SST transfer function in an upwelling region by minimizing the bias associated with the absence of sufficient analogs; and 3) reconstruct SST variations during the Late Holocene in two box-cores from the Portuguese margin.

For the regional transfer function we tested two commonly used techniques, Imbrie and Kipp (1971) and Pflaumann et al., (1996; 2003). The simultaneous application of two distinct computational approaches to one database, allows us to identify the differences in SST reconstructions that result solely from the use of different mathematical methods, and find the one that better resolves the SST pattern of the seasonal upwelling along the western Iberian margin.

2.2. Local hydrographic conditions

The surface ocean circulation along the Iberian margin, the Portugal Current (PC) system, is characterized by a broad and slow flow, predominantly with a southward direction. Close to the coast, however, strong seasonal wind variability causes partial reverse flow patterns with a southward current in summer and a northward current in winter (Fiúza, 1984). From May to September, wind-driven coastal upwelling occurs triggered by the northerly Portuguese Trade winds blowing nearly parallel to the coast, and cold nutrient–rich upwelled water is transported southwards by the Portugal Coastal Current (PCC). During the rest of the year, coastal convergence conditions prevail, especially during the winter period and the most relevant transport mechanism is the northward flowing warm undercurrent, the Portugal Coastal Countercurrent (PCCC) (Fiúza, 1984; Fiúza et al., 1998).

The upwelled water is fed by the Eastern North Atlantic Central Water (ENACW) of either subtropical (ENACWst) or subpolar origin (ENACWsp), which form the permanent thermocline at water depths below approximately 100 m. Depending on the wind strength either type can be upwelled. The poleward flowing ENACWst is lighter, relatively warmer and saltier than the southward flowing ENACWsp and contains less nutrients. The ENACWst is formed along the Azores front during winter and then contributes to the PCCC. The ENACWsp, which flows below the subtropical ENACWst, is formed in the eastern North Atlantic at 46ºN (Fiúza, 1984; Ríos et al., 1992; Fiúza et al., 1998).

When the seasonal coastal upwelling predominates off Iberia, the upwelled water forms a cold and nutrient-rich water band along the west coast (Fig. 1) that is generally about 50 km wide, as documented off the coast of Portugal by the analysis of a series of thermal infrared images (Fiúza, 1983). The different upwelling patterns off Iberia are largely determined by the bathymetry, the coastal morphology, and local wind conditions (northerly wind along the west coast, westerly wind off the south coast) (Fiúza, 1983). Modulated by topographic features like submarine ridges and coastal morphologic capes, filaments and plumes of cold water and high pigment concentrations are observed (Fraga, 1981; Fiúza, 1983; 1984; Sousa and Bricaud, 1992; Haynes et al., 1993; Álvarez-Salgado et al., 2001). Such filaments can extend as far as 200 km off Cape Finisterra (43ºN), Porto (41ºN), near 40ºN, and off Lisbon (39ºN; Cape Roca). Plumes, also related to coastal

morphology, are observed south of Capes Espichel and Sines (Fig. 1b). Parallel to the south coast off Cape São (S.) Vicente, upwelled waters along the southern part of the west coast flow around Cape S. Vicente and then continue further to the east over the shelf. Off the Guadiana river (8.6ºW), upwelling plumes can also occasionally occur under favorable westerly wind periods (Sousa and Bricaud, 1992; Relvas and Barton, 2002).

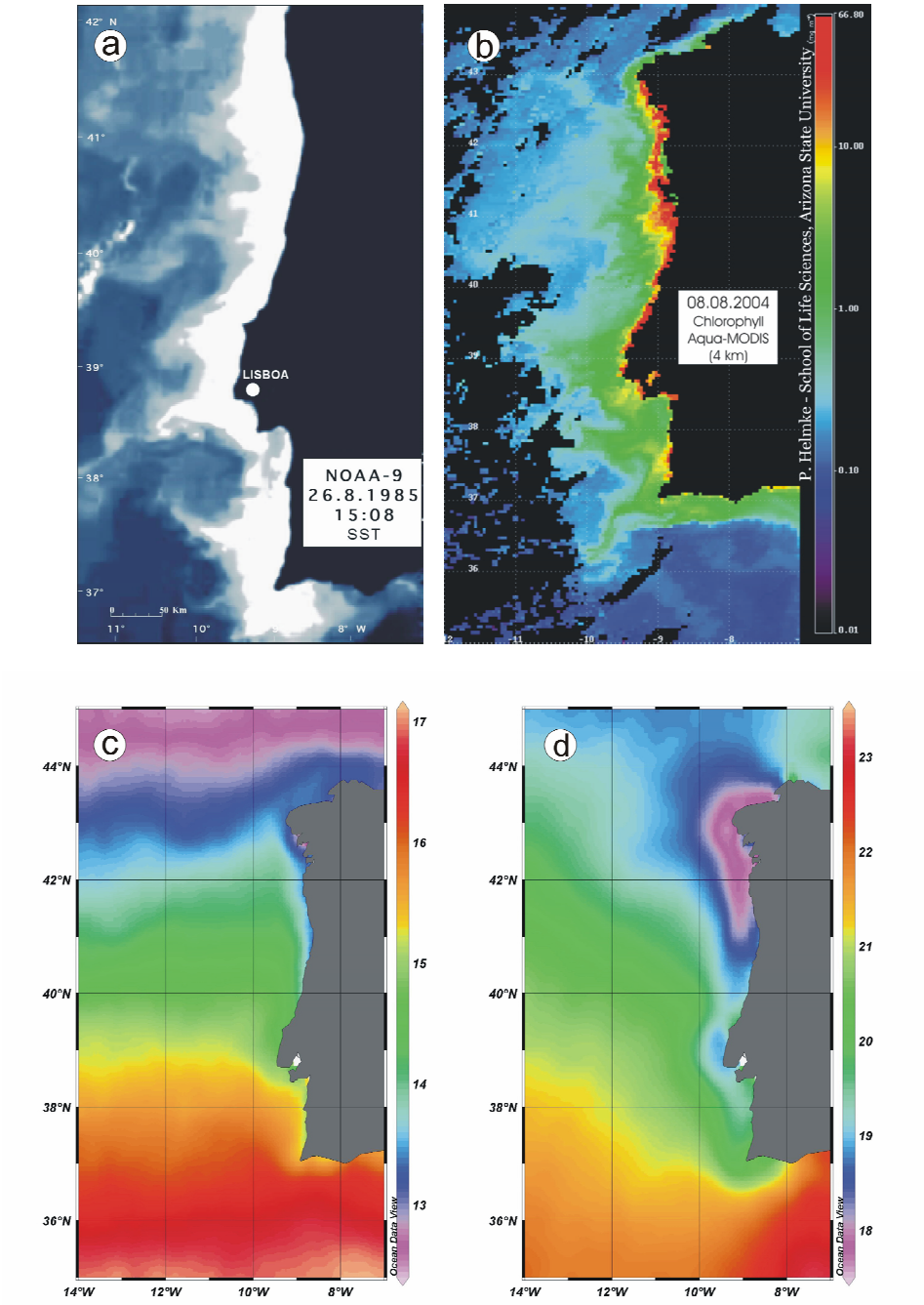

Fig. 1 Sea surface temperatures and chlorophyll concentration along the Iberian margin. a) Satellite image, Tiros – N thermal infrared image, obtained during August 1985 (courtesy of A. Fiúza). Sea surface temperature (SST) values increase from light (coldest waters) to dark grey (warmest waters). b) SeaWiFS chlorophyll data for August 8th, 2002 (SeaWiFS Project, NASA/Goddard Space Flight Center). Mean satellite-derived SST (1985-2003) for winter (c) and summer (d) used in this study. Note the different scales in (c) and (d).

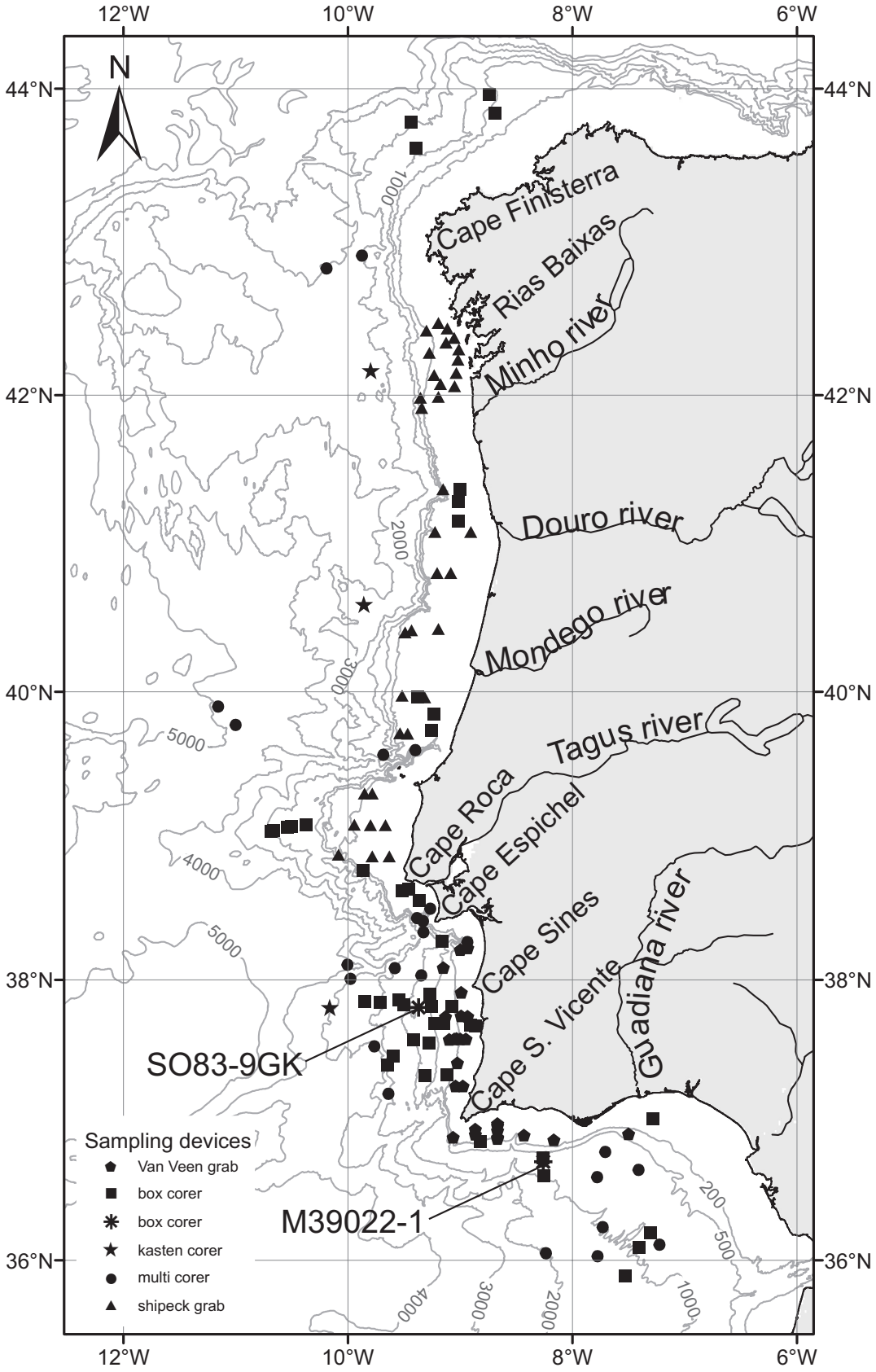

Fig. 2 Geographical distribution of the 134 surface sediment samples and the 2 box-cores (SO83-9GK, M39022-1) used in this study and listed in Appendix 1. Symbols differentiate between the coring device used. Depth contours drawn are 200 and 500 m and then every 1000 m between 1000 and 5000 m. Capes and rivers mentioned in the text are also indicated.

2.3. Material and methods

Calibration data set

This study incorporates census data of planktonic foraminiferal assemblages from 134 surface sediment samples (Fig. 2, Appendix 1). The samples were collected along the Iberian margin by Shipeck grab, Van Veen grab, box-corer, multi-corer, and kasten corer devices during 19 cruises carried out between 1975 and 2004. Most samples are stored at the Departamento de Geologia Marinha, Instituto Nacional de Engenharia, Tecnologia e Inovação I. P. (former Instituto Geológico e Mineiro), while samples Z5 to Z71 (Appendix 1) are archived at the Departamento de Xeociencias Mariñas e O.T., Facultade de Ciencias do Mar, University of Vigo.

Forty six of the surface samples (VB-33 to LV-173; Appendix 1) were prepared and first studied by Levy et al., (1995). The cleaning and washing procedures of these samples for the planktonic foraminifera study was different from the one used for the remaining samples (Appendix 1). Levy et al., (1995) samples for the planktonic and benthic foraminifera study, were preserved in Rose Bengal, weighted, and washed through a sieve of 74 μm mesh size. As the original planktonic foraminifera counts of Levy et al., (1995) were done in the > 74 μm size fraction, they were recounted in the >150 μm fraction, the fraction used in all other samples and in most transfer functions (e.g., Pflaumann et al., 1996).

In all samples, 300–600 planktonic foraminifera specimens were identified following the taxonomic criteria of Bé and Hamlin (1967), Bé (1977), Kennett and Srinivasan (1983), and Hemleben et al., (1989). Difficulties in discriminating between the white and pink varieties of *Globigerinoides ruber* in the samples preserved in Rose Bengal, were overcome by counting these species in the respective non-stained grain size samples. After counting, the relative abundance of each planktonic foraminiferal species was determined.

In this study, the small number of intergrade forms between *Neogloboquadrina dutertrei* and *Neogloboquadrina pachyderma* (dextral) was combined with *Neogloboquadrina pachyderma* (dextral) following Pflaumann et al., (1996). Based on the morphology of the terminal chamber for the species *Globigerinoides trilobus*, we distinguished between morphotypes without (*Globigerinoides trilobus trilobus*) and with

the final sac-like chamber (*Globigerinoides trilobus sacculifer*). Statistical analysis included 22 species/groups of species with relative abundance equal or higher than 2% (rounded; Table 1).

Table 1 Statistical values for the relative abundance of the important planktonic foraminiferal species in the 134 surface sediment samples. Only species with maximum percentages ≥1.8% in the total fauna are shown.

Species	Mean	Minimum	Maximum	Std. dev.
Globigerinella siphonifera	2.7	0.0	8.2	1.8
Globigerina bulloides	34.1	1.9	64.8	14.5
Globigerinella calida	2.2	0.0	8.1	1.9
Neogloboquadrina dutertrei	0.4	0.0	4.6	0.7
Globigerina falconensis	2.8	0.0	11.5	2.2
Globigerinita glutinata	6.0	0.1	16.3	3.6
Globorotalia hirsuta	1.1	0.0	10.2	1.3
Turborotalita humilis	0.4	0.0	4.4	0.9
Globorotalia inflata	11.7	2.4	31.9	5.6
Pulleniatina obliquiloculata	0.1	0.0	1.8	0.3
Neogloboquadrina pachyderma (sinistral)	1.4	0.0	27.4	3.1
Neogloboquadrina pachyderma (dextral)	18.1	0.7	64.0	12.8
Turborotalita quinqueloba	2.4	0.0	19.8	3.3
Globigerinoides ruber (white)	4.6	0.0	30.0	4.9
Globigerinoides ruber (pink)	0.5	0.0	5.6	0.9
Globigerina rubescens	1.7	0.0	9.2	1.9
Globigerinoides trilobus trilobus	2.5	0.0	14.5	3.0
Globigerinoides trilobus sacculifer	0.4	0.0	3.0	0.7
Globorotalia scitula	0.6	0.0	3.8	0.9
Globigerinoides tenellus	0.3	0.0	1.8	0.4
Globorotalia truncatulinoides	2.6	0.0	10.9	2.0
Orbulina s.l.	2.0	0.0	13.3	2.6
Globigerina digitata	0.1	0.0	1.0	0.2
Globigerinoides conglobatus	0.1	0.0	1.0	0.2
Globigerinita uvula	0.0	0.0	0.7	0.1
Turborotalita cristata	0.0	0.0	0.9	0.2
Globigerinita iota	0.0	0.0	0.8	0.1
Globorotalia crassaformis	0.1	0.0	1.2	0.2

Quantitative abundance of planktonic foraminifera was calculated as number per gram of dry sediment taking into account the weight of the original sample and the number of times the 150 μm fraction was split prior to counting.

Even though we are aware that planktonic foraminifera inhabit the upper few hundred meters of the water column (e.g., Hemleben et al., 1989), we used modern (summer and winter) satellite-derived SST data to calibrate the regional transfer function, because the World Ocean Atlas (WOA) 1998 data does not resolve the upwelling features in the study area with enough detail. The SST data is based on an integration of daily

Pathfinder satellite measurements with a 9 km resolution for the period from 1985-2003 (version 4.1; data available at: http://podaac-www.jpl.nasa.gov/sst/). Kearns et al., (2000) found that the average difference between radiometric ship-based (*in situ*) and satellite-based Pathfinder SSTs is 0.07 ±0.31°C from 219 matchups during the low- and midlatitude cruises. The in situ-Pathfinder differences compared favorably with the average midlatitude differences between the *in situ* skin SST and other bulk SST estimates commonly available for these cruises such as the research vessels' thermosalinograph SST (0.12 ±0.17°C) and the weekly National Centers for Environmental Prediction optimally interpolated SST analysis (0.41 ±0.58°C). The satellite temperature seasonality was obtained from the difference between summer and winter temperatures (Appendix 1). The very low correlation (r^2 = 0.14) between annual satellite-derived temperature and the seasonality allows to use the seasonality as another variable.

Calibration techniques

For the regional approach, the relation between the planktonic foraminifera assemblage and the modern SST data was estimated from the two most widely used transfer function techniques for paleoceanography reconstructions: the Imbrie & Kipp (IK) (Imbrie and Kipp, 1971); and the Similarity Maximum 28 (SIMMAX 28) modern analog technique (Pflaumann et al., 2003), an improved version of SIMMAX 24 (Pflaumann et al., 1996).

Some authors (e.g. Prell, 1985; Le, 1992; Pflaumann et al., 1996; Ortiz and Mix, 1997; Waelbroeck et al., 1998; Malmgren et al., 2001; Chen et al., 2005) have compared IK and modern analog techniques in different study areas. In general, both methods estimate SST reliably from the modern planktonic foraminiferal assemblage, but the temperature biases associated with the IK estimate are larger than those generated from the modern analog techniques. According to Le and Shackleton (1994), the IK technique is a robust technique, if used with caution, as demonstrated by its wide usage thanks to the restraints imposed by the regression methodology. Futher, IK options continues to be used (e.g., Malmgren et al., 2001; Chen et al., 2005), given that it provides a good understanding of the way it derives predictors from the calibration data set. In the present study it will be applied for the first time to a coastal upwelling region.

The first two steps of the IK technique, included in the software package of Sieger et al., (1999) and described in detail by Imbrie and Kipp (1971) and Imbrie et al., (1973), were applied in this study. The factor analysis (CABFAC, Imbrie and Kipp, 1971) as the first step, executes a Q-mode factor analysis to identify statistically significant planktonic foraminiferal associations (factors) from a large number of species. The communality obtained shows how well a given combination of species abundances is represented in the calibration data set. The resulting factor scores indicate the weight of each species to the respective Q-mode factor. Factor loadings explain the importance of the individual factors in each sample. The total number of factors was defined by minimizing the remaining "random" variability and by the possibility to relate the factors to modern hydrographic conditions and planktonic foraminiferal ecology.

In a second step, a multiple regression analysis was performed to fit an empirical equation between factor loadings (independent variables) and modern SST (dependent variables) by multiple linear regression methods, allowing squared and cross-product terms of the factor loadings to enter the equation to account for moderate nonlinearity in the faunal response to the environment (Mix et al., 1999). This technique is based on the assumption that relationship between planktonic foraminiferal assemblages and temperature is maintained through time. Ancient assemblages may, however, deviate significantly from the modern fauna and may not be fitted into the modern SST regression model, the so called "no analog sample problem", certainly more important in regionally restricted areas.

SIMMAX is a variant of the Modern Analog Technique (MAT) (Hutson, 1980), which differs from MAT in the way that best analogs are defined and treated. In SIMMAX, a similarity index based on the scalar product of the normalized faunal percentages and a weighting procedure of the best modern assemblage analogs according to their inverse geographical distance from the most similar fossil samples were incorporated. In this technique, similarity coefficients of the best analog can be used, like communality in IK, to express how well a given combination of species abundances is represented in the calibration data set. The inverse distance weighting addresses regional singularities by favoring analogs closer than 100/200 km to the sample site. This implies that more distant samples have less influence, but are not totally ignored (Pflaumann et al., 2003), and that different paleo-SST can be estimated from the same faunal assemblage depending on the geographical position of the studied site. Such approach is advantageous

when estimating a paleoenvironment not too different from the modern one, but may introduce an error in the case of migration of the fossil faunal provinces away from the modern centers (Pflaumann et al., 1996). Parallel with this distance-weighted SIMMAX estimates option (SIMMAX dw), the program also has the non-distance-weighted estimates option (SIMMAX ndw). Although a different similarity coefficient is used to select the best analog samples, SIMMAX ndw is in effect a direct equivalent of the classical MAT technique. Both SIMMAX dw and SIMMAX ndw reconstructions are presented in this study as two different techniques or methods, using the 10 best analogs. This way we can determine which option performs best in the upwelling conditions of the study region, given that in the literature SIMMAX dw is usually used in geographically widely distributed data sets and in areas of lower SST variability.

In this work, a validation of each technique to reconstruct modern SST was assessed by "leave-one-out" cross-validation of the modern data set. This approach generated the predicted values consecutively *n* times (in our case 134) using a training set of size *n*-1 (133). In each of the *n* predictions, one sample is left out in turn and the transfer function based on the *n*-1 sites in the data set is applied to the one sample in the test set and omitted from the data set, giving a predicted value for that sample (Birks, 1995).

To assess the prediction error of both techniques, the root mean square of prediction (RMSEP) was calculated as the square root of the mean of the squared differences between the observed and predicted values for all samples from the test set.

Paleo SST reconstructions

In order to assess the potential differences among the SST estimated by the regional calibrations, we reconstructed SST in two box-cores from the Portuguese margin: SO83-9GK (37.81°N; 9.37°W; 900 m water depth; 38 cm long) retrieved off Cape Sines and under the influence of seasonal upwelling; and M39022-1 (36.71°N; 8.26°W; 667 m water depth; 37 cm long) located off the southern coast and outside of the direct influence of seasonal upwelling (Fig. 2, Appendix 1). Both cores were sampled continuously with a 2 cm resolution, and treated following the surface sample methodology and taxonomic criteria for quantitative foraminiferal identification.

Stable isotope measurements were performed on three planktonic foraminifera species: *Globigerina bulloides*, *Globigerinoides ruber* (white), and *Globorotalia inflata*.

Samples contained on average 25 specimens picked from the 250µm – 2mm fraction and were measured in a Finnigan MAT 252 mass spectrometer of the RCOM at Bremen University. The $^{18}O/^{16}O$ ratio is reported in per mil (‰) relative to the Vienna Peedee Belemnite (VPDB) standard. Analytical standard deviation for $\delta^{18}O$ is ±0.07‰.

All investigated data was mapped with the OceanData View program of Schlitzer (2000).

All data presented in this paper will be stored at the World Data Centre MARE (http://www.wdc-mare.org).

2.4. Results

2.4.1. Planktonic foraminiferal distribution

Planktonic foraminiferal abundance, expressed as the number of specimens per gram of dry sediment ($\#g^{-1}$), along the Iberian margin varies by three orders of magnitude, from 24 to 31 500 $\#g^{-1}$. Values lower than 3 000 $\#g^{-1}$ are observed along the northwestern inner shelf, off the Rias Baixas in Galicia and the major Portuguese rivers (Minho, Douro, Mondego, and Tagus), and in the Iberia abyssal plain (Fig. 3a).

The distribution pattern of total planktonic foraminifera concentrations mirrors (1) productivity of waters along the Iberian margin, with concentrations larger than 8 000 $\#g^{-1}$ below the major upwelling zones; (2) the oligotrophic offshore waters with concentrations lower than 3 000 $\#g^{-1}$; and also (3) the dilution on the northwestern Iberia shelf caused by the presence of a coarse lithic fraction (Monteiro et al., 1980), or by the increased amount of fine fraction from the riverine input off the Rias Baixas and off the major Portuguese rivers.

Twenty eight species/group of species have been identified in the planktonic foraminiferal assemblage of the 134 surface sediment samples (Table 1). Four species dominate the fauna in the study area: *Globigerina bulloides* (2-65%), *Neogloboquadrina pachyderma* (dextral) (1-64%), *Globorotalia inflata* (2-32%), and *Globigerinoides ruber* (white) (0-30%). *G. bulloides* (Fig. 3b), the most abundant and widespread species, is distributed with high relative abundances (>30%) near the coast along the western Iberian

margin. This distribution seems to be related to the cold and productive upwelled waters near the coast during the upwelling season. However, this species also shows the highest percentages (50-65%) off the Douro, Tagus and Guadiana rivers. *N. pachyderma* (dextral) (Fig. 3c), the second most abundant species, dominates (>20%) the assemblage along the coast north of 39ºN, where the water temperature is colder all year round. The highest values (50-64%) are concentrated offshore of the Rias Baixas. *G. inflata* (Fig. 3d) showed the highest relative abundances (>15%) offshore from *G. bulloides* high abundance band, along the western Iberian margin, and seems to be related with oligotrophic waters. *G. ruber* (white), a species characteristic of subtropical waters (Fig. 3e), showed highest abundances (>7.5%) off the southern and southwestern coasts.

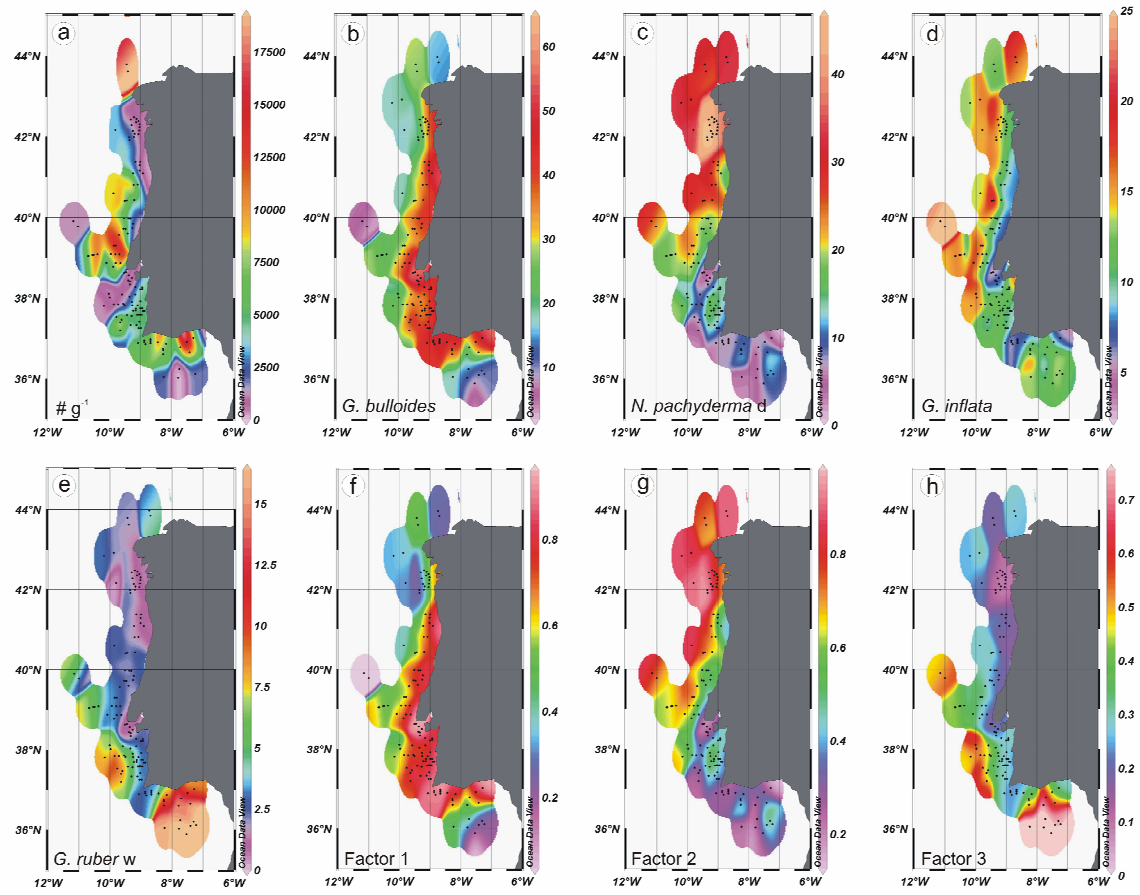

Fig. 3 Spatial distribution patterns of the absolute and relative planktonic foraminifera abundances and the 3 factors resulting from the Q-mode factor analysis along the western Iberian margin. a) number of specimens per gram of dry sediment #g^{-1}. Relative abundances are shown for *G. bulloides* (b), *N. pachyderma* (dextral) (c), *G. inflata* (d), and *G. ruber* (white) (e). Factor 1 (f), the Upwelling factor, explains 49.8% of the variance. Factor 2 (g; 32.2%) is related to the Portugal Current and factor 3 (h; 13.6%) to the Portugal Coastal Countercurrent.

Table 2 Varimax factor score matrix of the 3 factors as determined by the Q-mode factor analyses of the relative abundance of planktonic foraminifera on the western Iberian margin. Relevant species are marked in bold.

Species	Factor 1 Upwelling Factor	Factor 2 Portugal Current Factor	Factor 3 Portugal Coastal Countercurrent Factor
G. siphonifera	0.03	-0.02	0.17
G. bulloides	**0.98**	0.10	0.08
G. calida	0.06	0.02	0.00
N. dutertrei	0.00	0.01	0.01
G. falconensis	0.01	-0.03	0.24
G. glutinata	0.11	0.03	0.16
G. hirsuta	-0.02	0.00	0.13
T. humilis	-0.01	-0.02	0.08
G. inflata	-0.08	**0.31**	**0.52**
P. obliquiloculata	0.00	-0.01	0.03
N. pachyderma (sinistral)	-0.01	0.08	-0.01
N. pachyderma (dextral)	-0.08	**0.93**	-0.13
T. quinqueloba	0.08	-0.02	0.03
G. ruber (white)	-0.07	-0.06	**0.61**
G. ruber (pink)	-0.01	-0.02	0.09
G. rubescens	0.05	0.01	0.02
G. trilobus trilobus	-0.02	-0.06	**0.34**
G. trilobus sacculifer	-0.01	-0.01	0.06
G. scitula	-0.01	0.00	0.06
G. tenellus	0.00	0.00	0.03
G. truncatulinoides	-0.03	0.05	0.17
Orbulina s.l.	-0.06	0.04	0.21
Variance	**49.80**	**32.18**	**13.60**
Cumulative Variance	**49.80**	**81.96**	**95.56**

To assess the planktonic foraminiferal data statistically, Q-mode principal component analysis was performed with the CABFAC factor analysis of the IK technique. On the western Iberian margin, the analysis of 22 species/group of species results (because six of twenty eight are lower than 2%) in three factors that explain 95.6% of the total variance (Table 2). The model provides high communality values (≥0.7) for all samples (Fig. 4a; 5a, b).

Factor 1 (Table 2) explains 49.8% of the total variance and is exclusively defined by *G. bulloides* (score of 0.98). Mirroring the *G. bulloides* distribution pattern (Fig. 3b), the geographic distribution of the high factor loadings (Fig. 3f) also seems to reflect the upwelling close to the coast with the highest values off Capes Roca, Espichel and S. Vicente, where the upwelling plumes first appear under favorable wind conditions (Fiúza, 1983; 1984).

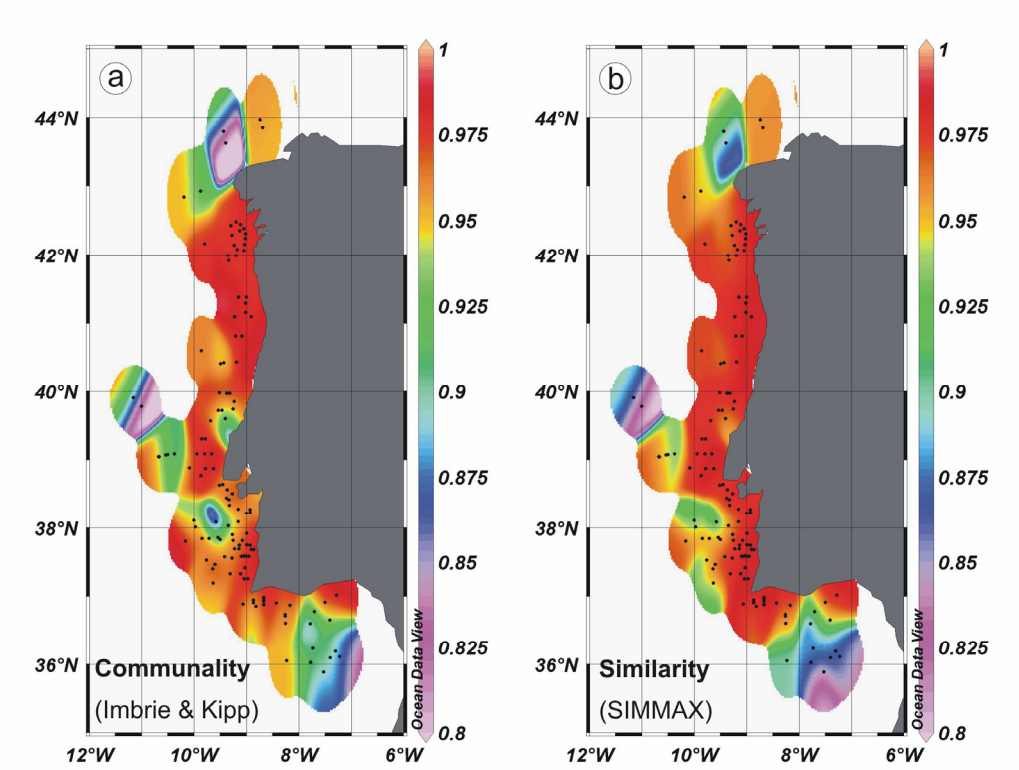

Fig. 4 Spatial distribution of the communality (a) and similarity (b) resulting from the Imbrie & Kipp and SIMMAX technique, respectively.

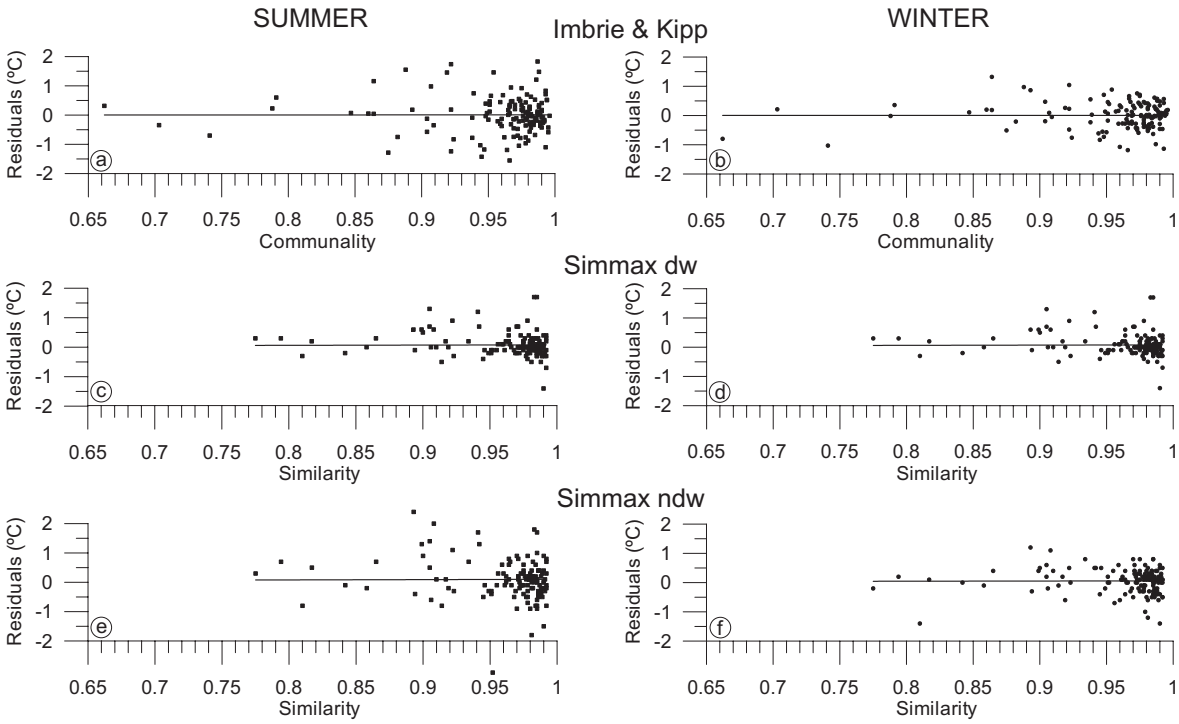

Fig. 5 Scatter plots of the residuals (i.e., observed minus predicted sea surface temperature values) versus communality from the Imbrie & Kipp options for summer (a) and winter (b), and versus similarity for the SIMMAX distance weighting (dw)/ non-distance weighting (ndw) techniques for summer (c/ e) and winter (d/ f).

Factor 2 (Table 2) explains 32.2% of the total variance and is dominated by *N. pachyderma* (dextral) (score of 0.93) and *G. inflata* (score of 0.31). This factor becomes important north of 39°N (Fig. 3g), with high loadings offshore between 39.5 and 41.5°N and offshore and nearshore north of 41.5°N. This factor reflects colder surface waters.

Factor 3 (Table 2) explains 13.6% of the total variance and is defined by the tropical to subtropical species *G. ruber* (white) (score of 0.61), *G. trilobus trilobus* (score of 0.34) and *G. inflata* (score of 0.52). High factor loadings (Fig. 3h) dominate on the southern margin and offshore of the southwestern coast, where warmer surface waters prevail, and reflect the relative abundance patterns of *G. ruber* (white) (Fig. 3e) and *G. trilobus trilobus*.

2.4.2. Modern SST calibrations

We calibrated abundances of 22 species/group of species of planktonic foraminifera in 134 surface samples to summer and winter satellite-derived SST, following different transfer techniques: "Imbrie & Kipp" (Imbrie and Kipp, 1971) and "SIMMAX" (Pflaumann et al., 1996; 2003), using the distance-weighted (dw) and non-distance-weighted (ndw) option.

Imbrie & Kipp technique

After the factor analysis, a multiple regression analysis was run as a nonlinear model of the second degree between the three factors and the summer and winter satellite-derived SST, in order to improve the correlation between the factors and the oceanographic parameters.

The regression equations obtained for our regional transfer function calibration provide (1) SST estimates and (2) residuals (estimated minus observed SST) for the summer and winter season and seasonality for each sample, respectively (Table 3 and Appendix 2).

Table 3 Results of the regression analyses from Imbrie & Kipp technique for summer and winter temperatures.

Winter Season				
Variable number	**Variable name**	**Regression Coefficient**	**Std. Error of reg. Coeff.**	**Computed t-value**
7	F1*F3	9.997	3.934	2.541
6	F1*F2	7.673	4.164	1.843
4	F2SQ	5.311	2.792	1.902
11	F3	-8.654	6.215	-1.392
3	F1SQ	7.158	2.103	3.404
9	F1	-12.647	5.515	-2.293
5	F3SQ	4.883	2.703	1.806
8	F2*F3	8.835	4.464	1.979
10	F2	-12.350	6.512	-1.897
Intercept		21.030		

Summer Season				
Variable number	**Variable name**	**Regression Coefficient**	**Std. Error of reg. Coeff.**	**Computed t-value**
11	F3	-1.095	8.658	-0.126
3	F1SQ	5.257	2.929	1.795
6	F1*F2	4.057	5.800	0.699
4	F2SQ	4.983	3.889	1.281
7	F1*F3	4.320	5.480	0.788
8	F2*F3	6.523	6.218	1.049
10	F2	-9.482	9.070	-1.045
9	F1	-7.415	7.681	-0.965
5	F3SQ	2.459	3.766	0.653
Intercept		22.135		

Low communality values (≤0.95) for all samples (Fig. 4a), were found on the northern coast between 43º and 44ºN, in the Iberia abyssal plain, on the outer Estremadura promontory (~39°N, 10-11°W), in the vicinity of the deeper Lisbon/ Setúbal Canyons, and east of 8°W in the Gulf of Cadiz. The lowest values correspond to samples M39070-1 (0.66), 64PE225-22 (0.74), and M39003-2 (0.79) (Appendix 1), all outside of the direct influence of upwelling, and 64PE225-1-21 (0.70) and 64PE225-1-26 (0.79), located in the Setúbal and Nazaré Canyons, respectively. The distribution of the temperature residuals (summer, winter) versus communality shows no correlation and the low communality values for both seasons do not coincide with high residual values. In general, high communality (0.95-1) coincides with samples with high residuals (Fig. 5a, b), more during the summer than winter season.

Estimated versus satellite-measured SST for summer and winter seasons, ranging from 13º to 23ºC, display a homogeneous scatter with no large deviation and are significantly correlated (p<0.001) with correlation coefficients of 0.85 (summer) and 0.86 (winter) (Fig. 6a). Most of the samples lie within the root-mean square error of prediction

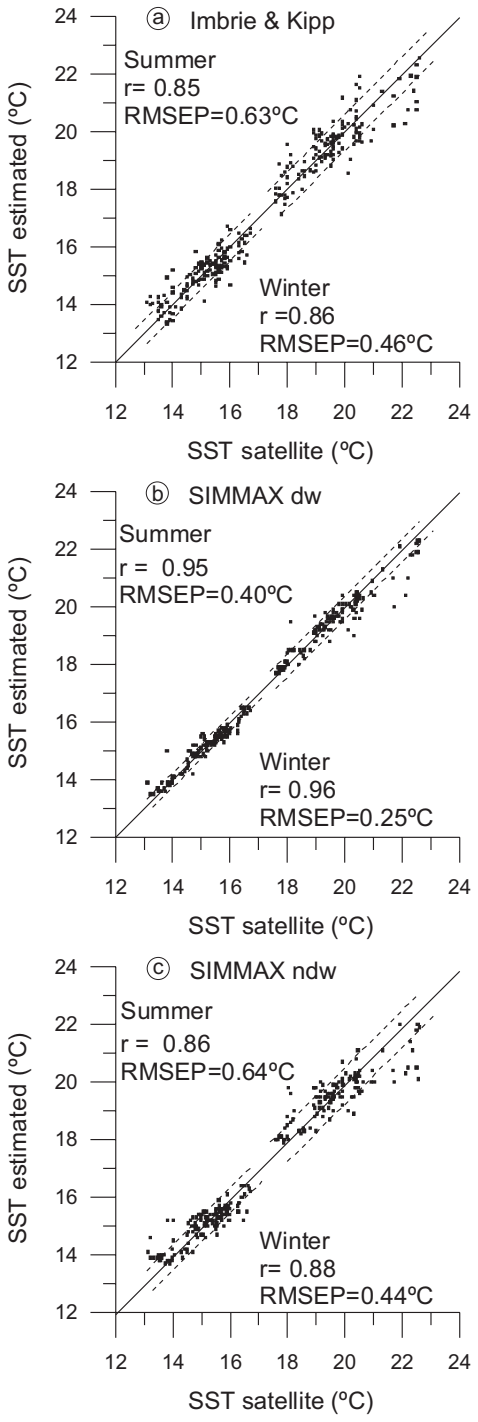

Fig. 6 Comparison between the satellite-derived Sea Surface Temperature (SST; 18 year average) data and the SST estimated with the Imbrie & Kipp (a), and SIMMAX distance weighting (dw; b) and non-distance weighting (ndw; c) techniques for summer and winter. Solid line represents linear regression line and dashed lines the RMSEP confidence interval. "r" is the correlation coefficient.

(RMSEP) for the summer and winter SST, 0.63ºC and 0.46ºC, respectively. However, for observed temperatures above 20.6ºC in summer and 16.2ºC in winter, SST estimates tend to be too low (Fig. 6a). These sites are located mainly at latitudes between 36º-37ºN, with communalities <0.95. On the other hand, for observed temperatures lower than 18.8ºC in summer and 14ºC in winter, SST estimates appear to be too high. These sites are located mainly north of 43ºN, coincident with a low communality area. These problematic zones are clearly evident when the temperature residuals are plotted versus the satellite temperatures for both seasons (Fig. 7a, b).

The relationship among temperature residuals and latitude of the individual sampling sites (Fig. 8a, b) shows a larger deviation from zero in summer (±1.5ºC) than in winter (±1ºC), which could be related to the variability of seasonal coastal upwelling during summer. All samples located on the southern Portuguese margin between 36º-37ºN (Appendix 1), where upwelling occurs only occasionally and where we measured the highest satellite-derived SST, underestimate SST in both seasons by up to 1.1°C, with PE151-04A (37.02ºN, 7.28ºW) being the most underestimated for the summer season and PE151-03B (36.85ºN, 8.82ºW) for the winter season. The most overestimated SST for both seasons is the sample PO287-13-1B (41.16ºN, 9.01ºW) located on the northern shelf, in the region with the lowest modern SST.

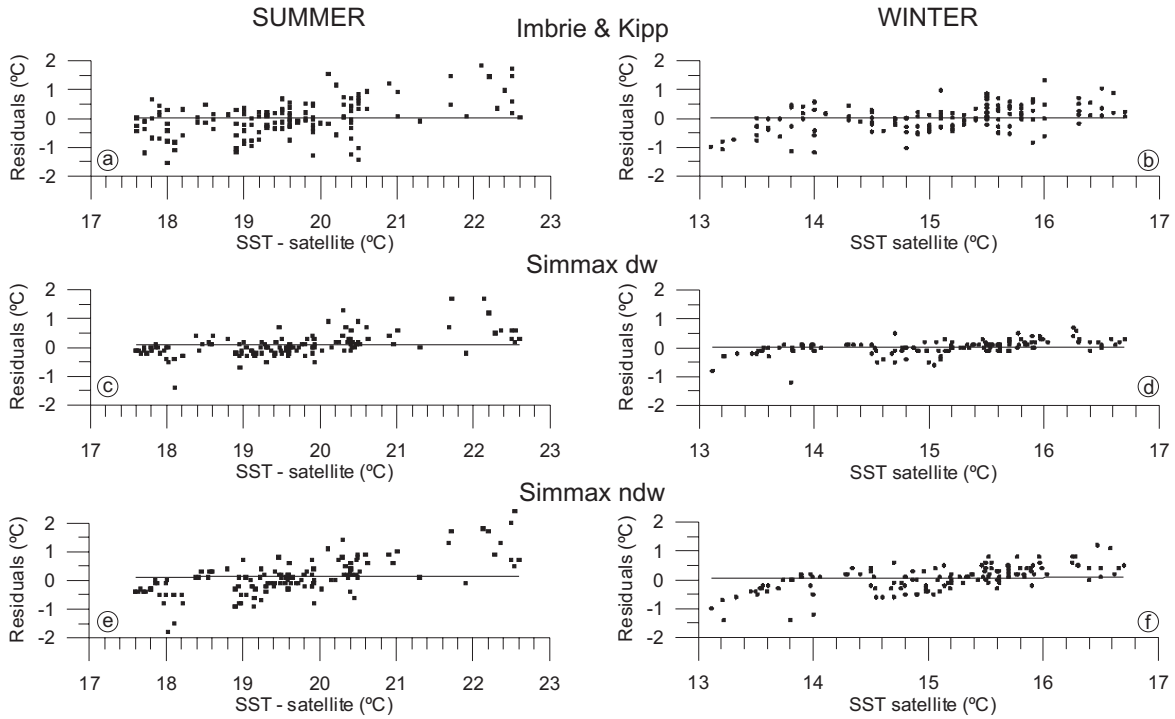

Fig. 7 Relationship between the SST residuals of the Imbrie & Kipp (a, b), and SIMMAX distance weighting (dw – c, d) and without distance weighting (ndw – e, f) techniques versus the satellite-derived SST for summer and winter, respectively.

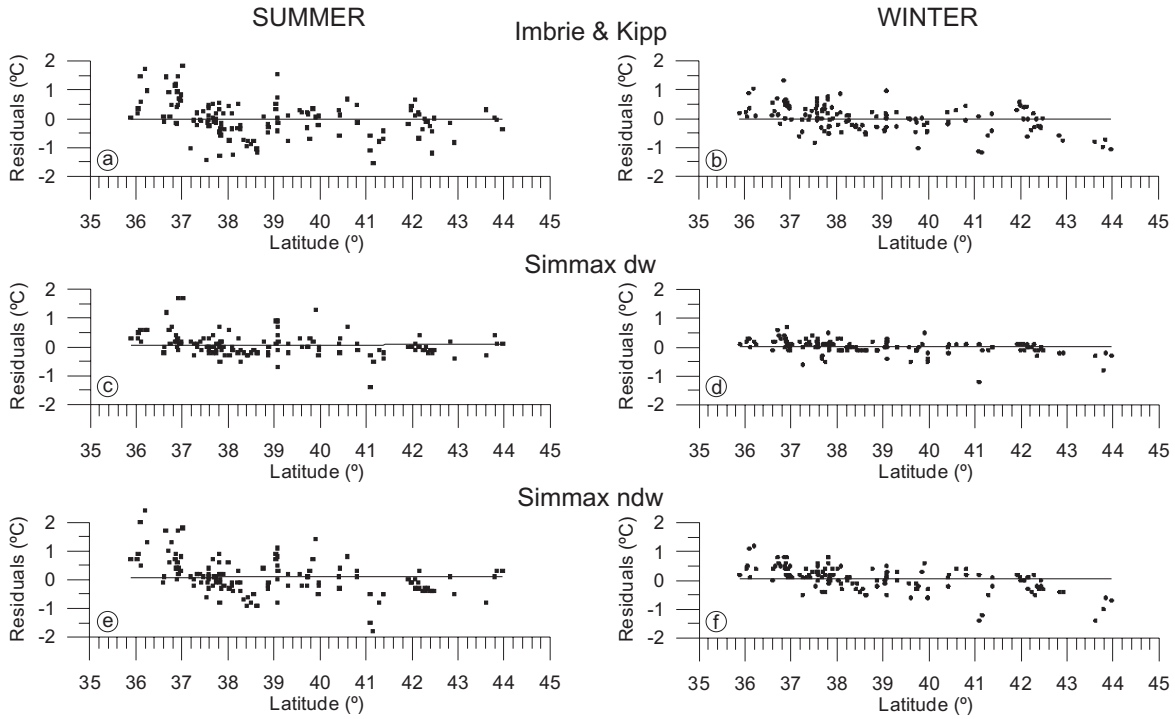

Fig. 8 Latitudinal distribution of summer and winter SST residuals from the Imbrie & Kipp technique (a, b) and the SIMMAX distance weighting (dw; c, d) and without distance weighting (ndw; e, f) methods.

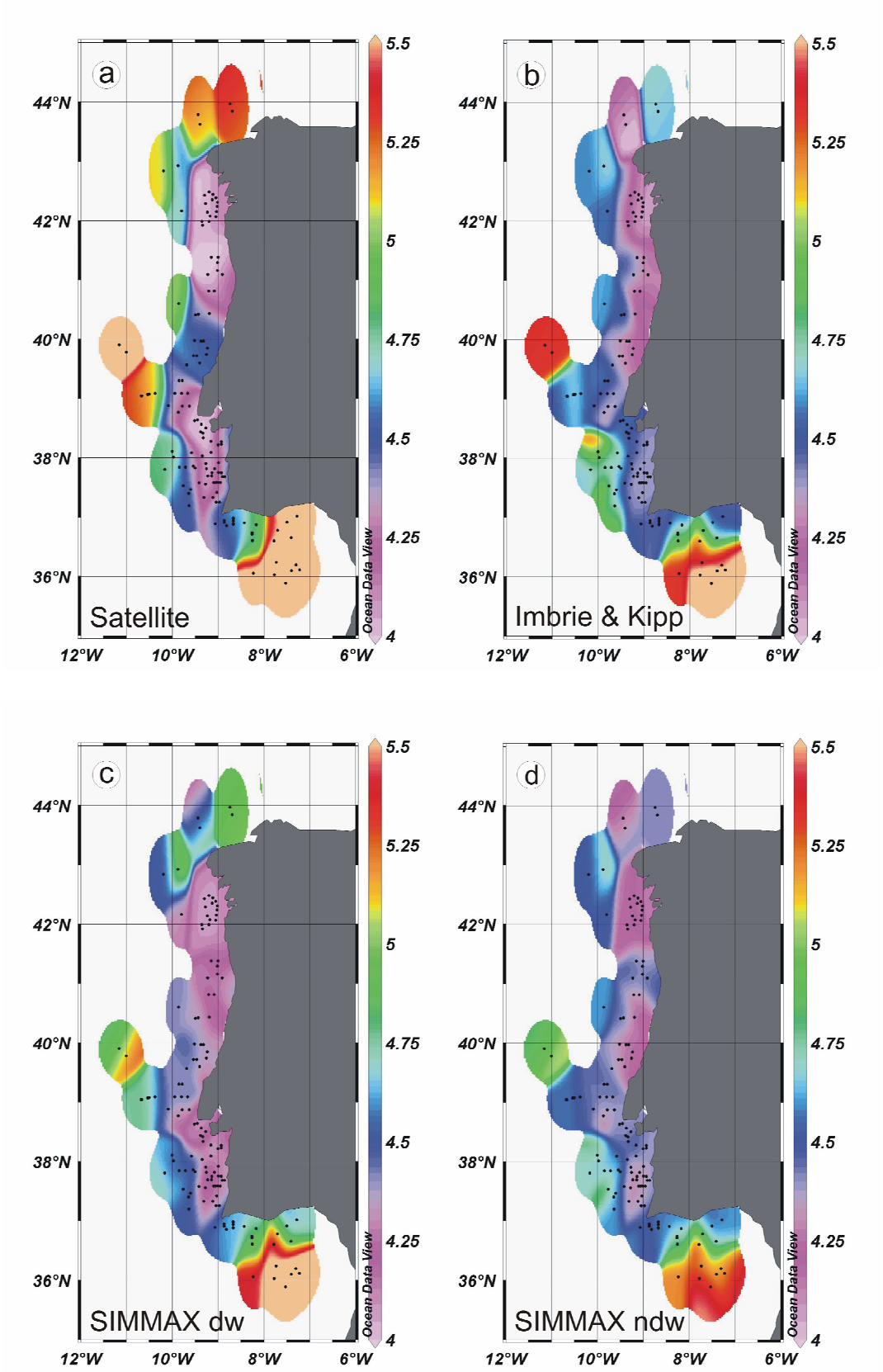

Fig. 9 Spatial distribution of the seasonality (difference between summer and winter SST) along the western Iberian margin. Seasonality calculated from the 18 year average satellite-derived SST is shown in (a), with the Imbrie & Kipp transfer technique in (b), and with the SIMMAX distance weighting (dw) and without distance weighting (ndw) technique in (c) and (d), respectively.

Seasonality, calibrated with this technique as a new variable, gives a temperature range from 4.1ºC to 5.6ºC (Fig. 9b, Table 3), similar to the seasonality values determined by satellite-derived SST (3.9 – 6.3ºC) (Fig. 9a, Appendix 1), and reflects both the cold waters from the upwelling (low values) and the warm waters without influence of the upwelling (high values). However, it does not mirror the cold waters off Capes Roca and Espichel.

SIMMAX modern analog technique

The SIMMAX technique was applied to the same set of samples.

Low similarity coefficients (≤0.90; Fig. 4b; 5c - f) are observed in nearly all the same regions as for the IK communalities (Fig. 4a). The lowest values were found in the samples 64PE225-22 (0.78), SWIM04-42 (0.79), M39003-2 (0.82), and M39070-1 (0.81), (Appendix 1), all outside the direct influence of upwelling. There is no correlation between the temperature residuals of dw and ndw SIMMAX options (summer, winter) and similarity (Fig. 5c – f), and low similarities do not correspond to high residuals.

The scatter diagrams of estimated versus measured SST are significantly correlated (p<0.001) with correlation coefficients of 0.95 (summer) and 0.96 (winter) for dw and 0.86 (summer) and 0.88 (winter) for ndw option (Fig. 6b, c). For the dw SST, the RMSEP is 0.40ºC for summer and 0.25ºC for winter, and for the ndw ones, 0.64ºC for the summer and 0.44ºC for the winter seasons. In general, both SIMMAX options display a homogeneous scatter with no significant deviation. However, dw values show lower deviations than ndw ones for both seasons, with quasi all samples inside the confidence intervals of RMSEP. The largest deviation for both options was found for temperatures above 20.6ºC in summer and below 14ºC in winter (Fig. 7c - f; 8c - f).

The distribution of the temperature residuals versus the latitude of the individual sample site (Fig. 8c – f) for both techniques shows a larger deviation for summer (±1.5ºC) than for winter (±1ºC), conform to IK results. All underestimated SST samples are located on the southern Iberian coast and show occasionally temperature residuals exceeding 1ºC, with LV010 (36.91º N, 7.50º W) and PE151-04A (37.02º N, 7.28ºW) being the most underestimated for summer dw, and M2004-13 (36.19º N, 7.30º W) for summer and winter ndw. The area of most overestimated SST is located in the northern coast: VB060

(41.09ºN, 8.9ºW) for summer and winter dw; PO287-13-1B (41.16ºN, 9.01ºW) for summer ndw, and VB060 and M39070-1 (43.62ºN, 9.39ºW) for winter ndw.

Seasonality was also calibrated with the SIMMAX dw and ndw options. For the dw option, the values range from 4 to 5.8ºC (Fig. 9c, Table 3), slightly lower, but with similar pattern as the seasonality obtained from the satellite-derived SST (3.9 – 6.3ºC) (Fig. 9a, Appendix 1). The ndw option gives values from 4.1 to 5.6ºC (Fig. 9d, Table 3) but differs the most from the satellite data in the geographical distribution of the values (Fig. 9). However, the ndw derived values indicate to some extent the cold waters from the upwelling (low values) and the warm waters without influence from the upwelling (high values). Like IK technique, SIMMAX ndw does not mirror the cold waters off Capes Roca and Espichel, but SIMMAX dw does it.

Similarity for both techniques

Following Kucera et al., (2005), the similarities between the IK and SIMMAX dw and ndw techniques were investigated (Fig. 10). The residuals are significantly correlated (p<0.001) for both technique pairs and in both seasons. SIMMAX dw versus ndw (r^2 = 0.73 for summer; r^2 = 0.66 for winter) and SIMMAX ndw versus IK (r^2 = 0.69 for summer; r^2 = 0.67 for winter) show the highest correlation, suggesting that there two techniques alone do not constitute a sufficiently independent framework. SIMMAX dw and IK are correlated the least (r^2 = 0.47 for summer; r^2 = 0.34 for winter).

Bias associated with upwelling region

To assess the potential bias that planktonic foraminiferal dissolution could have in our calibration, which might yield an inaccurate result, the fragmentation index of planktonic foraminiferal species was investigated in ninety studied samples (67% of total). The fragmentation index is on average 18%, with a minimum value of 6.9% and a maximum of 41.8%, suggesting that mechanical fragmentation and dissolution affects the assemblage to a minor extent. Consequently, our data set can be used with confidence regarding the influence of fragmentation.

As already mentioned, planktonic foraminifera responds to other environmental variables and in upwelling regions the biological primary productivity could produce a bias in the temperature estimates, as suggested by previous studies (e.g., Ravelo et al., 1990;

Andreasen and Ravelo, 1997; Watkins and Mix, 1998). Modern oceanic summer and winter primary productivity for each sample is based on satellite data of Antoine et al., (1996). Comparison of the temperature residuals to modern biological productivity (Fig. 11) reveals no correlation for the winter season for both techniques, but a slight significant correlation appears for the summer season with r^2=0.18, r^2=0.27, and r^2=0.37 for the IK, SIMMAX dw, SIMMAX ndw SST, respectively. Therefore, this variable does not bias the transfer function estimates of winter SST, but could influence the summer SST estimates, the season when upwelling occurs. The range of residuals, however, is higher in regions where productivity is low and where upwelling occurs only occasionally or not at all. This observation suggests that a bias in our calibration can not be excluded, but only outside of the seasonal upwelling influence.

Nevertheless, given the very high correlations between winter and summer SST in the calibration data sets it remains nearly impossible to provide any statistically sound evidence that the two variables can be reconstructed independently.

2.4.3. Paleo SST reconstructions

To test the validity of the regional calibrations and to examine the impact of each technique on paleo-SST reconstructions for the Late Holocene, IK, SIMMAX dw and ndw options were applied to two box-cores located at the Portuguese margin under (SO83-9GK) and outside (M39022-1) the direct upwelling influence (Fig. 2, Appendix 1). The box cores SO83-9GK and M39022-1 cover the last 1680 and 4290 years, respectively (Salgueiro et al., in preparation). In each core, the SST estimates were compared to planktonic isotope data from the same level. The $\delta^{18}O$ of *Globigerina bulloides*, the most abundant species during the summer upwelling, was compared with the summer SST, while the $\delta^{18}O$ values of *Globigerinoides ruber* (white) and *Globorotalia inflata*, species characteristic of winter hydrographic conditions, were compared with the winter SST (Fig. 12a and 13a). For a simple comparison between temperature changes indicated by the shell $\delta^{18}O$ values and the transfer function derived SST values, we apply the Shackleton (1974) equation (Δ1‰ = Δ4.3°C) and neglect any potential salinity changes in the $\delta^{18}O$ signal.

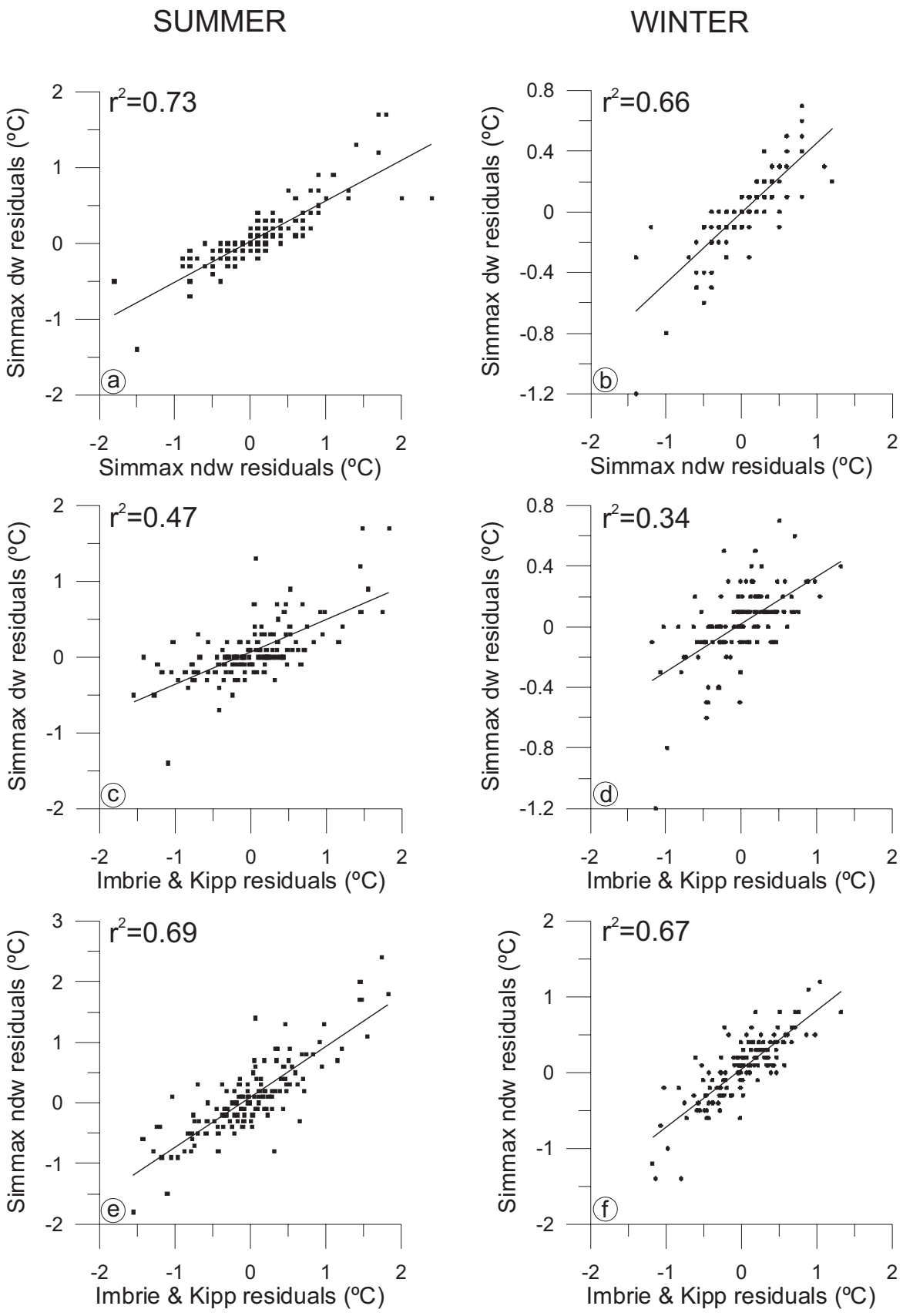

Fig. 10 Assessment of the degree of independence in sea surface temperature estimates produced by Imbrie & Kipp and SIMMAX (dw and ndw) techniques.

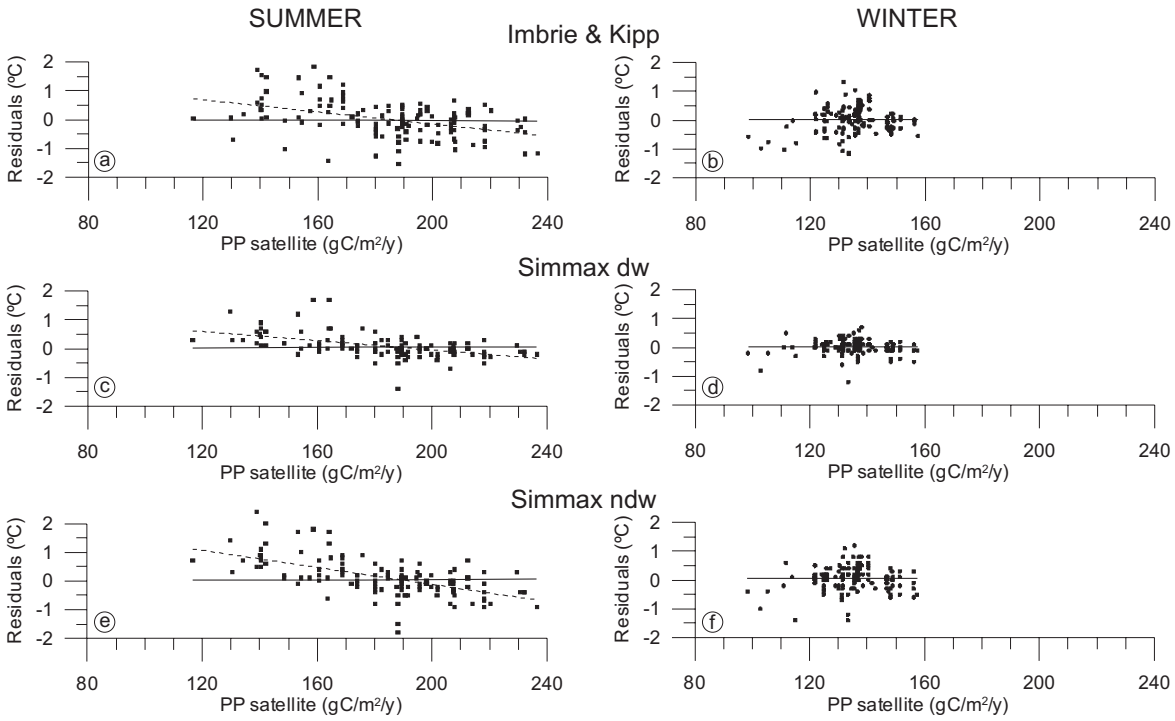

Fig. 11 Scatter plots of the SST residuals versus satellite-derived primary productivity for the summer and winter seasons for the Imbrie & Kipp (a, b), SIMMAX distance weighting (dw; c, d) and without distance weighting (ndw; e, f) techniques, respectively.

SO83-9GK core

The mean satellite-derived SST at this site is 19.7ºC in summer and 15.6ºC in winter.

Downcore SST estimated for summer to winter seasons by the IK, SIMMAX dw and ndw options, vary from 19.3 to 20.5ºC and 15 to 16ºC, and have mean values of ~19.8ºC and ~15.5ºC, respectively (Fig.12b). All three methods appear to have succeeded in reconstructing the absolute SST value observed in the satellite-derived SST. The estimated SST amplitudes of 1-1.2ºC are lower than the $\delta^{18}O$ derived temperature amplitudes (0.4‰ VPBD = 1.72ºC) (Fig.12a). However, downcore estimated SSTs and $\delta^{18}O$ derived temperature show similar amplitudes for both seasons, but the pattern is not always coincident. $\delta^{18}O$ derived temperature does not show the major warm event at 32.5 cm in summer and winter season. SIMMAX dw and ndw options show a similar trend, but SIMMAX dw shows the lowest SST variability for both seasons.

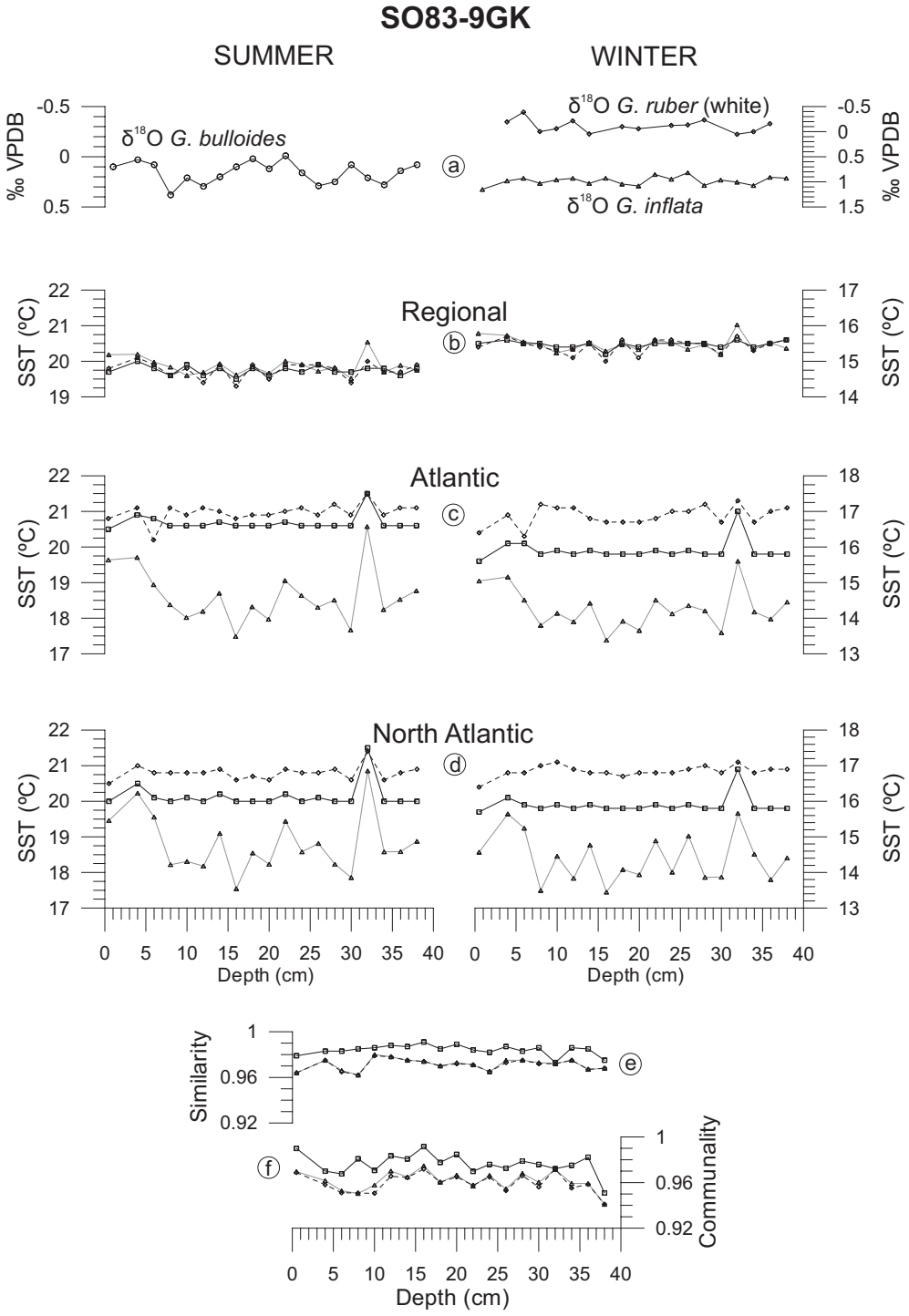

Fig. 12 Paleo-SST reconstructions in core SO83-9GK. Planktonic foraminifera isotope values are shown in (a). Paleo-SST were calculated with the regional data set (b), the Atlantic data set of Pflaumann et al., (1996) (c), and the North Atlantic data set (d; Kucera et al., 2005). Similarity and communality from each data set resulting from the Imbrie & Kipp and the two SIMMAX techniques are shown in (e) and (f), respectively. For figures (b) to (d), Imbrie & Kipp related results are shown in grey, SIMMAX distance weighting results in black and SIMMAX non-distance weighting results as dashed, black line. For figures (e) and (f), regional data set related results are shown in black, Atlantic data set results in grey and North Atlantic results as dashed, black line.

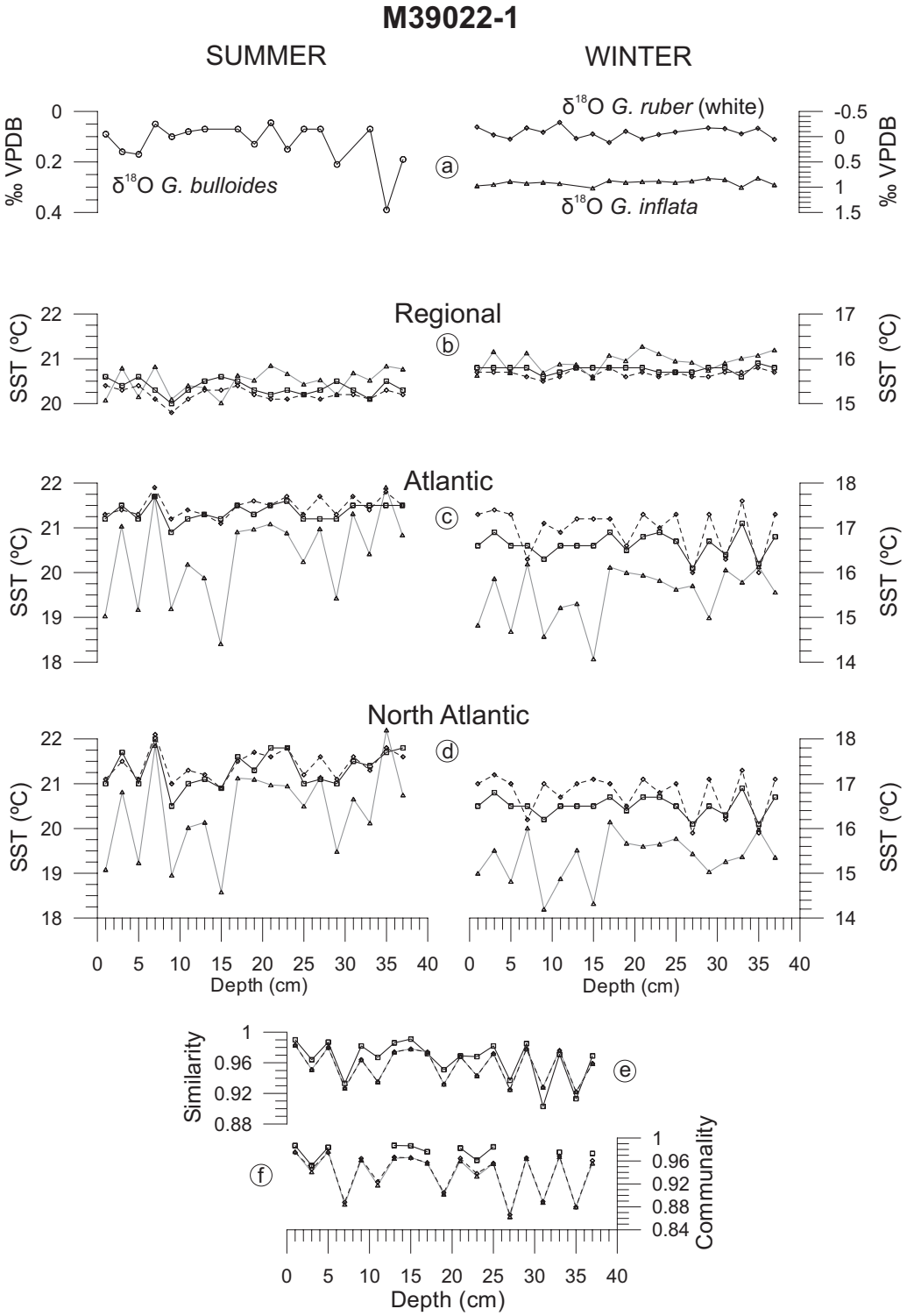

Fig. 13 Paleo-SST reconstructions in core M39022-1. isotope values are shown in (a). Paleo-SST were calculated with the regional data set (b), the Atlantic data set of Pflaumann et al., (1996) (c), and the North Atlantic data set (d; Kucera et al., 2005). Similarity and communality from each data set resulting from the Imbrie & Kipp and the two SIMMAX techniques are shown in (e) and (f), respectively. For figures (b) to (d), Imbrie & Kipp related results are shown in grey, SIMMAX distance weighting results in black and SIMMAX non-distance weighting results as dashed, black line. For figures (e) and (f), regional data set related results are shown in black, Atlantic data set results in grey and North Atlantic results as dashed, black line.

If we use the calibration data set from the Atlantic (Pflaumann et al., 2003) or the North Atlantic (Kucera et al., 2005) instead of our regional data set, the range and the pattern of the estimated SST by all techniques differs (Fig. 12c, d). For both calibration data sets, the IK SST estimates show higher amplitudes (~3.1 and 2.2ºC for summer and winter, respectively) than indicated by the $\delta^{18}O$ derived temperature (<1.72ºC), are on average 1ºC cooler during both seasons than the IK SST estimated with our regional calibration data set. The SIMMAX dw and ndw SSTs show amplitudes for both seasons, which are comparable to the planktonic foraminiferal $\delta^{18}O$ values. Comparison of the downcore SIMMAX SSTs from our regional calibration to summer SSTs estimated with the other two data bases always show less variation, especially for the Atlantic calibration data set. With the Atlantic data set (Fig. 12c), SSTs have a mean value of 20.7 - 21ºC in summer and of 15.9 - 16.9ºC in winter with the dw and ndw options, respectively. For the North Atlantic data set (Fig. 12d), values are 20.1ºC and 20.8ºC in summer and 15.9ºC and 16.9ºC, in winter for dw and ndw options, respectively. In summary, for the Atlantic and North Atlantic calibration data sets the IK based SSTs are 1ºC lower in both seasons than the SIMMAX derived SSTs. Also, the dw SIMMAX SST are nearly always colder than the ndw ones and are more similar to the regional calibration values.

The communality and similarity values are lower for the Atlantic and North Atlantic calibration data sets than for our regional calibration data set (Fig. 12e, f).

M39022-1 core

The mean satellite-derived SST at this site is 21ºC for summer and 16.3ºC for winter.

Downcore SST results, for all three methods calculated with our regional calibration data set, are similar with ranges of 20 – 20.9ºC and 15.5 – 16.3ºC and means of ~20.4ºC and ~15.8ºC, and summer and winter, respectively (Fig. 13b). However, downcore IK SST data shows higher amplitude and sometimes even an opposite trend to the SIMMAX derived SST records.

The maximum amplitude in the summer SSTs estimated by all options ranges from 0.6 to 0.9ºC, which agrees with the $\delta^{18}O$ *G. bulloides* data (0.15‰ VPBD = 0.7ºC, except for 35 cm depth), while the winter SST varies between 0.3 and 0.7ºC, which is slightly lower than the isotopic values of *G. ruber* (white) (0.4‰ VPBD = 1.72ºC) and *G. inflata* (0.2‰ VPBD = 0.8ºC) (Fig. 13a). However, the downcore, especially in the older part of

the core, $\delta^{18}O$ derived temperature variation does not follow the estimated SST by all methods and both seasons, coinciding with an interval lacking communality and with low similarity (Fig. 13e, f).

If we estimate the paleo - SST of this core using the calibration data set from the Atlantic Ocean (Pflaumann et al., 2003) and the North Atlantic (Kucera et al., 2005), the problems of a reduced number of analogs, which is most probably causing the low communality and similarity values in the Gulf of Cadiz in the regional data base, are eliminated (Fig. 13f). For the two former data sets, the downcore IK SST estimates show again consistently higher amplitudes (3.5ºC for summer; 2ºC for winter) than implied by the $\delta^{18}O$ derived temperature variations. In addition, they are on average ~0.5ºC lower for the summer season than the IK SST estimated with the regional calibration data set.

The two SIMMAX options (Fig. 13c, d), show similar amplitudes of ~1ºC - 1.5ºC for both seasons and both Atlantic data sets and a mean SST of ~21.5ºC and ~17ºC for summer and winter, respectively. However, while the SST trends are similar for both calibration data sets, the North Atlantic based SST shows a higher variability. In addition, differences between dw and ndw SSTs, especially in the summer records, are much smaller than in the upwelling influenced site SO83-9GK.

From the comparison of techniques and data sets, Atlantic and North Atlantic calibration data, it is evident that the IK SSTs are colder than the SIMMAX ones, sometimes by more than 1ºC, and more similar to SST range of the regional calibration data set.

2.5. Discussion

2.5.1. Biological and hydrographic implications of the planktonic foraminiferal factors

The principal component analysis showed that the planktonic foraminifera distribution off Iberian margin can be explained by three factors. Their biological and hydrographic implications are discussed bellow.

Factor 1: Upwelling factor

Factor 1 (Fig. 3f, Table 2) is nearly exclusively defined by *G. bulloides*. This species thrives in areas of nutrient-rich mixing zones and episodic phytoplankton blooms (e.g., Schiebel et al., 1997; Thiede et al., 1997; Schiebel et al., 2004) and has often been encountered in other upwelling areas (e.g. Thunell et al., 1983; Curry et al., 1992; Ortiz and Mix, 1992; Thunell and Sautter, 1992; Giraudeau, 1993).

G. bulloides is the most abundant and widespread species along the Iberian margin. Its distribution pattern (Fig. 3b) matches the satellite-derived SST data (Fig. 1a), high chlorophyll pigment concentrations (Fig. 1b), as well as the diatom abundance distribution patterns on both surface sediments and the water column during a typical upwelling period (Abrantes and Moita, 1999). This indicates a close relationship between the abundance of this species and the spatial location of coastal upwelling on the western Iberian margin. Moreover, the highest percentages of *G. bulloides* are located off the most important Portuguese rivers (Douro and Tagus) apparently also reflecting the river nutrient input and related winter/spring season productivity.

Upwelling determines the production patterns observed off Iberia (Prego and Bao, 1997; Abrantes and Moita, 1999). The geographic distribution of the high factor loadings (Fig. 3f) also seems to reflect the upwelling associated with cold and productive waters close to the coast, with the highest values off Capes Roca, Espichel and S. Vicente, where upwelling generated plumes first appear under favorable wind conditions. Off the Guadiana River (8.6ºW), the high loading values may be related to the plume that occurs in the region during favorable westerly wind events (Fiúza, 1983; 1984).

Nowadays an important upwelling filament, with cold waters and high primary production, is located off Cape Finisterra (Haynes et al., 1993; Álvarez-Salgado et al., 2001). This filament is not evidenced by this factor, possibly because our database does not have enough samples in this region.

Low factor loadings are observed along the northwestern coast off Galicia, where seasonal upwelling also occurs during the summer (Fraga, 1981; Tenore et al., 1995). This could be related to: (1) a change in the upwelling source water (ENACWsp instead of ENACWst) and an associated higher abundance of cold water species like *N. pachyderma* (dextral) rather than *G. bulloides*; (2) the narrowness of the upwelling band on the Galician coast which practically reaches the coastline and penetrates into the Rias Baixas (Prego and Bao, 1997); (3) the planktonic foraminifera assemblages in samples located off the

Rias Baixas constitute a parautochtonous fauna, due to the frequent shelf-ocean exchange processes in this particular area (Álvarez-Salgado et al., 2003; Nogueira et al., 2003).

Factor 2: Portugal Current factor

Factor 2 (Fig. 3g, Table 2) is dominated by *N. pachyderma* (dextral) and *G. inflata*. *N. pachyderma* (dextral) is considered a subpolar species by Bé and Tolderlund (1971) and Bé (1977) and occurs in waters relatively colder than preferred by *G. bulloides*. In general, it also occupies a deeper habitat in more stable waters than *G. bulloides* (thermally stratified upper water column) just below the thermocline (Fairbanks et al., 1982; Marchant et al., 1998). This species has also been associated with upwelling areas (e.g. Sautter and Thunell, 1991; Thunell and Sautter, 1992; Giraudeau, 1993; Ufkes and Zachariasse, 1993) occurring in maximum concentrations during periods of high fertility (diatoms blooms). Isotopic records from sediment traps in the San Pedro Basin (Thunell and Sautter, 1992) suggest that during upwelling it migrates to shallower depths in order to maintain a preferred temperature. At the Portuguese margin, *N. pachyderma* (dextral) is the second most important species (Fig. 3c), dominating along the coast north of 39ºN. The water temperature is colder (1.5ºC) in the north than in the south all year round (Fig. 1), not only due to winter circulation, but also due to the source of the upwelled waters (ENACWsp) during the upwelling season. *N. pachyderma* (dextral) appears to reflect this north/south temperature division, but probably also the increased fertilisation generated by the higher river runoff and nutrient input in the north, which also contribute to a higher productivity all year round, a pattern similar to the one of the small forms of the diatom genus *Thalassiosira* (Abrantes and Moita, 1999). In particular, the high percentage of this species off the Rias Baixas could be related to the high productivity and well stratified waters in this region associated with the transition period between upwelling and downwelling seasons. Downwelling occurs during winter, when the Portuguese Coastal Countercurrent (PCCC) (poor in nutrients) confines the Rias Baixas waters (with high primary productivity) to the continental shelf; waters whose outwelling is typical and very intense during the upwelling season (Teixeira et al., 2003).

G. inflata is the other major contributor to the factor 2 assemblage (Fig. 3d). This species is considered to be a typical indicator of transitional waters (Bé and Tolderlund, 1971; Fairbanks et al., 1980; Deuser et al., 1981; Ravelo et al., 1990; Giraudeau, 1993). On

the Portuguese margin, higher relative abundances of *G. inflata* (>15%) (Fig. 4c) occur at the west boundary of the upwelling front and coincide with oligotrophic waters in agreement with the transitional assemblage of Bé (1977) and its distribution in the Atlantic database of Pflaumann et al., (2003).

In the eastern North Atlantic, Ottens (1991) found *N. pachyderma* (dextral) and *G. inflata* associated with North Atlantic Drift waters. This supports our interpretation that factor 2 represents the Portugal Current, the descending branch of the North Atlanic Drift. Due to the upwelling in summer and the coastal poleward flow in winter, the influence of the Portugal Current is more strongly felt west of 10°W and in the northwest (Perez et al., 2001), conform the spatial distribution of high loadings for factor 2 (Fig. 3g).

Factor 3: Azores Current Eastern branch factor

Factor 3 (Fig. 3h, Table 2) is defined by high abundances of the tropical to subtropical species *G. ruber* (white) and *G. trilobus trilobus*, and also *G. inflata*.

The geographic distribution of the high abundance of tropical to subtropical species (Fig. 3e) and the highest factor loadings (Fig. 3h) show their dominance on the southern margin, where upwelling only occurs occasionally (Fiúza, 1983) and offshore of the south western coast, outside of the direct influence of coastal upwelling (well stratified surface waters). These are the regions most strongly influenced by Azores Current waters, either in form of the wintertime PCCC (Peliz et al., 2005) or the ENACWst. The ecology of *G. inflata*, a non-upwelling, transitional, and oligotrophic species, also points to an offshore source.

2.5.2. Modern SST calibrations

Both IK, SIMMAX dw and ndw techniques detected the lowest communality and similarity coefficients of the best analog samples outside the direct influence of upwelling. These techniques recognized the same samples in the calibration data set as no- or less-analogs by the low communality and the similarity index. However, there is no correlation between temperature residuals (summer, winter) versus communality or similarity, exhibiting that most species abundance combinations and SST patterns are well

represented in the calibration data set and there is no large error produced by more "exotic" assemblages.

The lowest root-mean square error of prediction (RMSEP) was produced for the SIMMAX dw option (summer: 0.4ºC; winter: 0.25ºC), as was also shown in previous works (Malmgren et al., 2001; Kucera et al., 2005). IK and SIMMAX ndw, on the other hand, produced RMSEP about 0.2ºC larger than SIMMAX dw for both seasons. For the North Atlantic data set (Kucera et al., 2005), SIMMAX dw produced a RMSEP (summer: 0.9ºC; winter: 1.4ºC) 0.5ºC lower than SIMMAX ndw for both seasons. The lower RMSEP obtained for SIMMAX dw are not decisive to select this technique to be used primarily on the western Iberian margin, given that Telford et al., (2004) reported that SIMMAX dw always underestimates RMSEP because it uses geographic information that reduces the independence of the samples during cross validation. Therefore all methods will be discussed.

SIMMAX dw SST resulted in higher linear correlation coefficients for the estimated versus measured satellite-derived SST from 13º to 23ºC, and displayed a more homogeneous scatter with a lower significant deviation and with more samples inside the RMSEP limits for summer or winter seasons than SIMMAX ndw option and IK technique (Fig. 6b).

The relationship between temperature residuals and observed satellite temperature of the single sample sites for both techniques in summer and winter (Fig. 7), also shows that the techniques did not produce any significant SST related bias (distribution of the residual values around zero). But there is a general trend for overestimating the higher SST and for underestimating the lower SST. The SIMMAX dw option, however, shows the lowest deviation. This observation is also supported by the temperature residuals versus latitudinal distribution. The largest positive deviation for all options was found above 20.6ºC (summer) and below 16.2ºC (winter) coinciding with samples located at latitudes 36º-37ºN with low communalities and similarities. The largest negative deviation for both options was found below 18.8ºC (summer) and below 14ºC (winter) coincident with samples located north of 41ºN, especially north of 43ºN, and coincident with low communality and similarity values. The cause for both deviations might the lack of sufficient modern analogs with similar assemblages or the respective temperature range in applied database. In general, the largest residuals produced by the different techniques correspond to the same sample of the calibration data set (Fig. 8).

Both techniques appear to underestimate SST at the southern Portuguese margin, an area mainly occupied by warm waters where upwelling occurs only occasionally, and overestimate SST on the northern part of the Portuguese coast, where cold waters are mostly present year round. Furthermore, both methods were more successful in predicting temperatures for the winter season, most probably due to the high hydrographic variability caused by the waxing and waning of upwelling features. From all the methods, SIMMAX dw seems to perform slightly better with a lower amplitude of residuals, suggesting that it may have been more successful in dealing with the poor sample coverage in the south (warm analogs) and the north (cold analogs) of the western Iberian margin.

Lower deviations between measured and estimated SST for the SIMMAX dw technique than for the IK technique are in good agreement with the findings of Pflaumann et al., (1996), who compared these two techniques for surface sediments from the North and the South Atlantic between 87ºN and 40ºS, 35ºE and 60ºW.

When the similarity of both techniques was studied (Fig. 9), SIMMAX dw and IK showed the lowest correlation, providing an adequate degree of independence among SST estimates derived from both techniques. Seasonality, however, shows a similar range of values for both techniques, evidencing well the presence of cold waters from the upwelling (low values) and warm waters without influence of the upwelling (high values), however only SIMMAX dw mirrors the upwelled waters off Capes Roca and Espichel.

In this study, SIMMAX dw provides better fits to the modern satellite-derived SST pattern. For paleo-SST reconstructions, however, it might not necessarily be more useful than the SIMMAX ndw option and the IK technique, as hydrographic changes unrelated to upwelling could produce artificially cold or warm SST.

To evaluate, if our regional transfer function is biased for paleo-SST reconstruction, we tested the different techniques in two Holocene records from the western Iberian margin.

2.5.3. Paleo SST reconstructions

The summer and winter paleo-SST of core SO83-9GK (Fig. 12), under the influence of seasonal upwelling, and core M39022-1 (Fig. 13), outside of the direct influence of

seasonal upwelling, were estimated with the IK and SIMMAX dw and ndw regional calibration to evaluate the performance of each one.

For both cores and seasons, all methods yield SST of a similar range and a similar average, the later of which is equal to the modern SST at site SO83-9GK, but underestimates the modern values by 1ºC for core M39022-1. The SST amplitudes are always within the range, mostly even a bit lower than the $\delta^{18}O$ derived temperature amplitudes, which could point to underestimation of the actual SST variability. Along core SO83-9GK, the SST estimated by all techniques and the corresponding $\delta^{18}O$ derived temperature variations does not show the same pattern downcore. At 32.5 cm both seasons show an increase in SST that it was not marked by $\delta^{18}O$ records, these SST increase may is due the more influence of warm winter-time Azores Current given that in the foraminiferal assemblage is visible an increase of the sub-tropical species and an decrease of *N. pachyderma* (dextral), and similar relative abundance of *G. bulloides*. However the SST estimated and $\delta^{18}O$ derived temperature show more fluctuations during the summer than during the winter, thereby reflecting the changes in upwelling intensification through time. At site M39022-1, outside the modern upwelling, $\delta^{18}O$ derived temperature correspond a little bit worse to the SST estimated by all techniques. As mentioned before, this is most probably caused by an inefficient number of modern analogs in the calibration database, as the warm-water sphere of the Azores current is currently poorly represented.

In general, SST estimates by the two SIMMAX versions are more closely related, while the IK results deviate more, especially in core M39022-1. The high correlation between IK and SIMMAX ndw methods (Fig. 10f) is not evident in the fossil samples of either core. Using the Atlantic (Pflaumann et al., 2003) and North Atlantic (Kucera et al., 2005) data sets instead of our regional database calculations result in different SST ranges and patterns (Fig. 12, 13). In each core, the IK based SST estimates show consistently higher amplitudes than derived from the planktonic $\delta^{18}O$ values and are on average 1ºC lower than the two SIMMAX variants. The SIMMAX based SST amplitudes, on the other hand, are inside the $\delta^{18}O$ range of temperature change.

At site SO83-9GK, the SST estimated with Atlantic and North Atlantic databases indicate fairly stable temperature conditions and imply no or only minor intensification of the upwelling through time, in contrast to the higher variability evident in the summer SST record from the regional calibration data set (Fig. 12).

When the SST of core M39022-1 were estimated with the Atlantic or North Atlantic databases, the no analog problem, that affects our regional data set, is resolved and the SST show higher variability in both seasons than estimated from the regional data set (Fig. 13). The paleo-reconstruction confirms what was already indicated by the high residual deviations for samples in the eastern Gulf of Cadiz. A comparison between the results shows that with our regional database SST are underestimated for about 1ºC colder than the modern SST and the SIMMAX dw and ndw results from Atlantic and North Atlantic calibrations data set, respectively. So one aim for the future is to increase the regional database by adding more warm water analogs from the inner and outer Gulf of Cadiz to our data set.

The better accuracy of SIMMAX dw and ndw over the IK technique is well evidenced by the reconstructed paleo-SST in both cores. SIMMAX dw, in spite of being applied to an upwelling area, does not seem to produce biased SST estimates. The dw results are more consistent along the cores than the SIMMAX ndw ones.

Summer productivity does not seem to influence the SST estimated by all methods in the regional calibration, as the variation of upwelling intensity is well marked in core SO83-9GK.

2.5.4. Caveats

The biggest weakness of our regional approach is the lack of analogs for the colder subpolar and polar temperature range, where *N. pachyderma* (sinistral) is more abundant. This species is known to reach high percentages on the western Iberian margin during cold events like the Heinrich events (Cayre et al., 1999; de Abreu et al., 2003). Consequently, our regional transfer function can only be used to reconstruct SST during interglacial periods.

One way to solve this problem well as the lack of warm analogs would be to include our data set into the North Atlantic reference data set of Kucera et al., (2005).

Another possible approach to solve this calibration problem is to follow the Mix et al., (1999) strategy, and look into past variability along the Portuguese margin samples to

define faunal assemblages that covary through time rather than modern samples to define assemblages that covary geographically with the actual hydrographic conditions.

2.6. Conclusions

Along the western Iberian margin, *G. bulloides* is the most abundant and widespread species and its distribution pattern shows a close relationship to the present-day spatial occurrence of coastal upwelling. Its importance in the planktonic foraminifera fauna is further highlighted by the fact that the prominent factor 1, upwelling factor, of the Q-mode factor analysis is defined mainly by this species. The other two factors are interpreted as representing two other important hydrographic features on the Iberian margin: the Portugal Current (factor 2; characterized by *N. pachyderma* (dextral) and *G. inflata*) and the warm Eastern branch of the Azores Current (factor 3; defined by *G. ruber* (white), *G. trilobus trilobus*, and *G. inflata*). The geographical relevance of the upwelling factor permits to conclude that the foraminiferal distribution pattern on the Iberian margin is linked to actual hydrographic conditions, especially to the various upwelling features.

In an attempt to better reconstruct the seasonally highly variable hydrographic conditions along the western Iberian margin, in particular the summer upwelling features, we use the foraminiferal assemblages in 134 core top samples and satellite-derived summer and winter SST to develop a regional transfer function with the Imbrie & Kipp (IK) and SIMMAX (dw - with distance weighting, ndw - without distance weighting) techniques.

The regional transfer function calibrations show that the SIMMAX dw results have the lowest RMSEP, the highest correlation coefficients and the lowest deviation in residuals for both seasons. Both techniques appear to underestimate SST at the southern Portuguese margin, an area mainly occupied by warm waters where upwelling occurs only occasionally, and to overestimate SST at the northwestern Iberian margin, where cold waters are mostly present year round. Furthermore, low communality and similarity are identified by both methods for the same samples.

The regional transfer function calibrations produced by both methods, where applied to cores SO83-9GK, under influence of seasonal upwelling, and M39022-1 in the Gulf of Cadiz. Estimated summer and winter SST for the Late Holocene are within a similar range and show an average SST that coincides with the actual SST at site SO83-9GK, but

underestimate SST at site M39022-1 by 1ºC. The SIMMAX dw values are more consistent downcore than the ones from the other methods.

The SST estimated with the regional calibration data set downcore in SO83-9GK exhibit higher SST variations during the summer than the results from any of the other databases, highlighting how important is a sufficient regional coverage of modern analogs for the reconstruction of upwelling intensity variations. Currently, our regional data set is underestimating SSTs in the warmer parts of the Gulf of Cadiz. The lack of a sufficient number of modern analogs is clearly shown by the differences in the SST variations calculated for core M39022-1 where the Atlantic and North Atlantic calibration data sets yield a higher variability than suggested by the regional transfer function.

Therefore, to solve this lack of analogs for the Azores current/ subtropical warm water sphere and the lack of analogs for (sub) polar conditions on the western Iberian margin (*N. pachyderma* left coiling caveat) the best approach would currently be to include our regional data set into the MARGO reference data set of the North Atlantic (Kucera et al., 2005) or by using past variability of species to define modern faunal assemblages (Mix et al., 1999).

As our regional transfer function is doing so well in reconstructing the upwelling related SST patterns along the Iberia margin, a future study intends to extend the regional coverage to the upwelling area off NW Africa, which belongs to the same upwelling system. Like our regional study has shown, it is important to increase the number of analogs for upwelling features in a regionally restricted or the North Atlantic database in order to obtain more reliable paleo-SST estimates for the upwelling regions in the eastern North Atlantic.

Acknowledgements

We are particularly grateful to the Department of Geologia Marinha of INETI, (former IGM), for providing the sediment samples, and to Ana Margarida Silva and Celia Trindade for technical assistance. We thank Isabelle Gil, Susana Lebreiro and Lúcia de Abreu, for collecting surface samples during various cruises. Lúcia de Abreu, Cristina Lopes and Michal Kucera gave constructive comments to an earlier version of this manuscript. This study was funded by “Fundação para a Ciência e a Tecnologia (FCT)” and “Fundo Social Europeu (FSE) no âmbito do III Quadro Comunitáro de Apoio”

fellowship SFRH/BD/11743/2003, and project INGMAR PLE/4/98. The EU PALEOSTUDIES project supported the *Globogerinoides ruber* (white) and *Globorotalia inflata* isotope measurements from the SO83-9GK and M39022-1 cores. We are also grateful to the Deutsche Forschungsgemeinschaft as part of the DFG-Research Center Ocean Margins (RCOM) of the University of Bremen for technical support.

Appendix 1 Detailed information on the 134 surface sediment samples and the 2 box-cores (SO83-9GK, M39022-1) used in this study including geographical position, water depth, cruise and sampling device. Satellite-derived SST as 18 year average for winter and summer (NOAA-1985-2003) and seasonality are also given.

Sample	Longitude (W)	Latitude (N)	Water Depth (m)	Cruise Name	Device	Author	SSTwinter (ºC)	SSTsummer (ºC)	Seasonality (ºC)
VB033	-9.1500	41.3733	140	VIABOA	shipeck grab	E. S.	14.1	18.0	3.9
VB057	-9.2233	41.0867	160	VIABOA	shipeck grab	E. S	14.3	18.2	3.9
VB060	-8.9050	41.0867	65	VIABOA	shipeck grab	E. S	13.8	18.1	4.3
VB073	-9.2033	40.8083	140	VIABOA	shipeck grab	E. S	14.3	18.5	4.1
VB075	-9.0817	40.8100	95	VIABOA	shipeck grab	E. S	14.3	18.4	4.1
VB094	-9.4917	40.4067	155	VIABOA	shipeck grab	E. S	14.5	18.9	4.4
VB095	-9.4333	40.4200	145	VIABOA	shipeck grab	E. S	14.5	18.9	4.4
VB098	-9.1917	40.4300	100	VIABOA	shipeck grab	E. S	14.4	18.8	4.4
VB106	-9.5150	39.9750	145	VIABOA	shipeck grab	E. S	14.7	19.3	4.6
VB108	-9.3150	39.9633	120	VIABOA	shipeck grab	E. S	14.5	19.0	4.5
VB133	-9.4667	39.7150	140	VIABOA	shipeck grab	E. S	14.7	19.2	4.5
VB135	-9.5367	39.7167	155	VIABOA	shipeck grab	E. S	14.8	19.3	4.5
VB136	-9.8500	39.3000	205	VIABOA	shipeck grab	E. S	14.9	19.3	4.4
VB138	-9.7833	39.3000	155	VIABOA	shipeck grab	E. S	14.9	19.1	4.3
VB156	-9.6650	39.0833	94	VIABOA	shipeck grab	E. S	14.8	19.0	4.2
VB161	-9.7983	39.0833	130	VIABOA	shipeck grab	E. S	14.8	19.1	4.3
VB164	-9.9417	39.0850	154	VIABOA	shipeck grab	E. S	15.0	19.4	4.5
VB165	-10.0833	38.8767	415	VIABOA	shipeck grab	E. S	15.1	19.6	4.5
VB172	-9.7833	38.8667	105	VIABOA	shipeck grab	E. S	15.0	19.2	4.2
VB176	-9.6300	38.8667	110	VIABOA	shipeck grab	E. S	14.9	18.9	4.0
LV010	-7.5000	36.9100	405	LIVRA	Van Veen grab	E. S	16.3	21.7	5.5
LV044	-8.1667	36.8667	84	LIVRA	Van Veen grab	E. S	15.9	20.9	5.0
LV051	-8.8667	36.9417	100	LIVRA	Van Veen grab	E. S	15.7	20.4	4.7
LV053	-8.8667	36.9067	110	LIVRA	Van Veen grab	E. S	15.8	20.3	4.5
LV059	-8.4317	36.9000	107	LIVRA	Van Veen grab	E. S	15.9	20.6	4.7
LV072	-8.6667	36.9833	74	LIVRA	Van Veen grab	E. S	15.7	20.5	4.8
LV073	-8.6667	36.9683	80	LIVRA	Van Veen grab	E. S	15.8	20.5	4.8
LV075	-8.6667	36.9333	98	LIVRA	Van Veen grab	E. S	15.9	20.5	4.6
LV078	-8.6667	36.8833	105	LIVRA	Van Veen grab	E. S	16.0	20.4	4.4
LV079	-8.6667	36.8750	110	LIVRA	Van Veen grab	E. S	16.0	20.4	4.4
LV085	-8.9750	37.2500	96	LIVRA	Van Veen grab	E. S	15.0	19.8	4.8
LV087	-9.0417	37.2500	122	LIVRA	Van Veen grab	E. S	15.5	19.9	4.5
LV099	-9.0633	36.8833	157	LIVRA	Van Veen grab	E. S	15.8	20.1	4.3
LV102	-9.0267	37.4150	180	LIVRA	Van Veen grab	E. S	15.5	19.7	4.2
LV119	-8.9500	37.5833	145	LIVRA	Van Veen grab	E. S	15.4	19.6	4.2
LV122	-9.0000	37.5833	172	LIVRA	Van Veen grab	E. S	15.5	19.6	4.1
LV124	-9.0350	37.5883	212	LIVRA	Van Veen grab	E. S	15.5	19.6	4.1
LV125	-9.0533	37.5833	245	LIVRA	Van Veen grab	E. S	15.6	19.6	4.0
LV126	-9.1000	37.5817	305	LIVRA	Van Veen grab	E. S	15.6	19.6	4.0
LV127	-9.1317	37.7417	385	LIVRA	Van Veen grab	E. S	15.5	19.5	3.9
LV131	-8.9900	37.7467	152	LIVRA	Van Veen grab	E. S	15.4	19.5	4.1
LV134	-8.9333	37.7433	130	LIVRA	Van Veen grab	E. S	15.0	19.8	4.8
LV144	-8.9917	37.9142	138	LIVRA	Van Veen grab	E. S	15.4	19.4	4.0
LV148	-9.1533	38.0867	335	LIVRA	Van Veen grab	E. S	15.5	19.4	3.9
LV171	-9.0000	38.2133	143	LIVRA	Van Veen grab	E. S	15.3	19.4	4.1
LV173	-8.9333	38.2250	128	LIVRA	Van Veen grab	E. S	15.1	19.8	4.8
SO75 09KG	-9.8467	37.8433	2331	SONNE75	box corer	E. S	15.7	20.4	4.7
SO75 13KG	-9.2733	37.5550	636	SONNE75	box corer	N. L..	15.7	19.7	4.0
SO75 15KG	-9.4150	37.5750	986	SONNE75	box corer	N. L..	15.7	19.9	4.2
SO75 25KG	-9.5450	37.8550	1300	SONNE75	box corer	N. L..	15.6	20.0	4.4
SO75 30KG	-9.5983	37.4633	1699	SONNE75	box corer	N. L..	15.9	20.4	4.5
SO75 33KG	-9.6417	37.3967	1871	SONNE75	box corer	N. L..	15.9	20.4	4.5
SO83 07GK	-9.7117	37.8400	2010	SONNE83	box corer	E. S.	15.7	20.2	4.5
SO83 10GK	-9.2533	37.8150	498	SONNE83	box corer	N. L..	15.5	19.6	4.1
SO83 11GK	-9.0767	37.8150	267	SONNE83	box corer	N. L..	15.5	19.5	4.0
PO01(2)	-9.1117	37.3267	246	POSEIDON 200-10	box corer	N. L..	15.6	19.8	4.2
PO03(1)	-9.3100	37.3250	822	POSEIDON 200-10	box corer	N. L..	15.8	19.9	4.1
PO05(1)	-9.2650	37.8983	550	POSEIDON 200-10	box corer	J. M.	15.5	19.6	4.1
PO06(1)	-9.5033	37.8217	1085	POSEIDON 200-10	box corer	J. M.	15.6	19.9	4.3
M39002-3	-7.7750	36.0272	1205	METEOR 39/1	multi corer	N. L..	16.7	22.5	5.8

Appendix 1 Continued

Sample	Longitude (W)	Latitude (N)	Water Depth (m)	Cruise Name	Device	Author	SSTwinter (ºC)	SSTsummer (ºC)	Seasonality (ºC)
M39003-2	-7.2227	36.1108	800	METEOR 39/1	multi corer	N. L..	16.5	22.5	6.0
M39004-2	-7.7289	36.2367	967	METEOR 39/1	multi corer	N. L..	16.5	22.4	5.9
M39016-2	-7.7056	36.7783	580	METEOR 39/1	multi corer	N. L..	16.3	21.7	5.4
M39017-4	-7.4101	36.6500	532	METEOR 39/1	multi corer	N. L..	16.3	22.2	5.9
M39021-5	-8.2547	36.6050	900	METEOR 39/1	box corer	N. L..	16.4	21.3	4.9
M39022-3	-8.2599	36.7117	668	METEOR 39/1	multi corer	N. L..	16.3	21.0	4.7
M39023-3	-8.2621	36.7350	728	METEOR 39/1	box corer	N. L..	16.3	21.0	4.7
M39029-6	-8.2333	36.0497	1918	METEOR 39/1	multi corer	N. L..	16.7	22.3	5.6
M39035-3	-9.5010	37.8217	1082	METEOR 39/1	multi corer	N. L..	15.6	19.9	4.3
M39058-1	-10.6795	39.0393	1977	METEOR 39/1	box corer	N. L..	15.2	20.5	5.3
M39059-2	-10.5352	39.0665	1605	METEOR 39/1	box corer	N. L..	15.2	20.3	5.1
M39070-1	-9.3917	43.6183	1220	METEOR 39/1	box corer	N. L..	13.2	18.2	5.0
M39072-1	-9.4350	43.7867	2170	METEOR 39/1	box corer	N. L..	13.1	18.4	5.3
PE151-01A	-9.8668	38.7667	133	IBERIA 2000	box corer	E. S.	15.1	19.2	4.2
PE151-03B	-8.8203	36.8522	312	IBERIA 2000	box corer	E. S.	16.0	20.2	4.3
PE151-04A	-7.2792	37.0157	61	IBERIA 2000	box corer	E. S.	15.8	22.1	6.3
PO287-3-1B	-10.4993	39.0738	1505	PALEO I	box corer	E. S.	15.2	20.3	5.1
PO287-5-1B	-8.9985	41.3740	87	PALEO I	box corer	E. S.	14.0	17.9	3.9
PO287-8-1B	-9.0128	41.2910	88	PALEO I	box corer	E. S.	14.0	18.0	4.0
PO287-13-1B	-9.0125	41.1562	81	PALEO I	box corer	E. S.	14.0	18.0	4.0
PO287-15-1B	-9.2537	39.7362	111	PALEO I	box corer	E. S.	14.5	19.0	4.5
PO287-19-1B	-9.2332	39.8480	101	PALEO I	box corer	E. S.	14.5	19.0	4.5
PO287-21-1B	-9.3753	39.9670	128	PALEO I	box corer	E. S.	14.6	19.1	4.5
PO287-26-1B	-9.3640	38.5582	96	PALEO I	box corer	H. B.-J.	15.0	19.0	4.0
PO287-27-1B	-9.4542	38.6340	85	PALEO I	box corer	H. B.-J.	14.9	18.9	4.0
PO287-28-1B	-9.5145	38.6243	105	PALEO I	box corer	H. B.-J.	14.9	18.9	4.0
PO287-33-1B	-8.9092	37.6780	119	PALEO I	box corer	E. S.	15.1	19.9	4.8
PO287-34-1B	-8.8610	37.6758	90	PALEO I	box corer	E. S.	15.1	19.9	4.8
PO287-40-1B	-9.2242	37.6892	493	PALEO I	box corer	E. S.	15.6	19.6	4.0
PO287-41-1B	-9.1432	37.6905	380	PALEO I	box corer	E. S.	15.6	19.6	4.0
PO287-44-1B	-10.6607	39.0425	1866	PALEO I	box corer	E. S.	15.2	20.5	5.3
PO287-45-1B	-10.3742	39.0833	1216	PALEO I	box corer	E. S.	15.1	20.1	5.0
PO201/10-702	-8.6900	43.8433	402	POSEIDON 201-10	box corer	A. V.	13.3	18.6	5.2
PO201/10-703	-8.7367	43.9667	583	POSEIDON 201-11	box corer	A. V.	13.2	18.6	5.4
ATL-FP1-04B	-9.8750	42.9194	2130	Atalante	multi corer	A. V.	13.5	18.1	4.6
ATL-FP1-05B	-10.1892	42.8361	2953	Atalante	multi corer	A. V.	13.5	18.5	5.1
ATL-FP1-08A	-9.3439	38.0306	987	Foram Prox	multi corer	A. V.	15.5	19.6	4.1
ATL-FP1-09A	-9.7644	37.5283	3124	Foram Prox	multi corer	A. V.	15.9	20.5	4.6
ATL-FP1-10B	-9.6383	37.1933	1863	Foram Prox	multi corer	A. V.	16.0	20.5	4.5
64PE218-16	-8.9333	38.2667	430	Canyons 2003	multi corer	A. V.	15.3	19.5	4.3
64PE218-21	-9.2672	38.4998	498	Canyons 2003	multi corer	A. V.	15.0	19.0	4.0
64PE218-22	-9.3296	38.4130	1463	Canyons 2003	multi corer	A. V.	15.2	19.1	4.0
64PE218-36-1	-9.1584	38.2707	1409	Canyons 2003	box corer	A. V.	15.3	19.3	4.0
64PE225-1-21	-9.5808	38.0833	1742	Canyons 2004	multi corer	E. S.	15.5	19.9	4.4
64PE225-1-26	-9.4001	39.5990	1118	Canyons 2004	multi corer	E. S.	14.7	19.3	4.6
64PE225-2-02	-9.3843	38.4330	301	Canyons 2004	multi corer	E. S.	15.2	19.1	4.0
64PE225-3-03	-9.3266	38.3330	1856	Canyons 2004	multi corer	E. S.	15.3	19.2	3.9
64PE225-06	-9.9753	38.0080	2945	Canyons 2004	multi corer	E. S.	15.7	20.4	4.7
64PE225-07	-10.0043	38.1060	4451	Canyons 2004	multi corer	A. V.	15.6	20.4	4.8
64PE225-25	-10.9999	39.7740	4804	Canyons 2004	multi corer	A. V.	14.8	20.4	5.6
64PE225-22	-11.1565	39.8980	4975	Canyons 2004	multi corer	A. V.	14.7	20.3	5.6
64PE225-27	-9.6831	39.5660	1009	Canyons 2004	multi corer	E. S.	14.8	19.5	4.7
MD04-2811	-10.1647	37.8040	3162	Privilege	kasten corer	E. S.	15.8	20.6	4.8
MD04-2814	-9.8577	40.5945	2449	Alienor	kasten corer	E. S.	14.5	19.5	5.0
MD04-2817	-9.7993	42.1618	2365	Alienor	kasten corer	A. V.	13.9	18.6	4.7
M2004-13	-7.3000	36.1940	742	MOUNDFORCE	box corer	A. V.	16.5	22.5	6.1
M2004-28	-7.4010	36.0930	815	MOUNDFORCE	box corer	A. V.	16.6	22.5	5.9
SWIM04-42 SW	-7.5278	35.8855	1172	SWIM 2004	sw corer	A. V.	16.6	22.6	6.0
GeoB9014-1	-7.7800	36.5970	716	GAP	multi corer	A. V.	16.4	21.9	5.5
ZS-5	-9.0496	42.0606	125	Investigador	shipeck grab	R. G.-Á.	13.7	17.9	4.1
ZS-9	-9.1953	41.9887	139	Investigador	shipeck grab	R. G.-Á.	13.8	17.9	4.1
ZS-13	-9.3408	41.9170	192	Investigador	shipeck grab	R. G.-Á.	14.0	18.0	4.0
ZS-17	-9.0322	42.1477	122	Investigador	shipeck grab	R. G.-Á.	13.7	17.8	4.1

Appendix 1 Continued

Sample	Longitude (W)	Latitude (N)	Water Depth (m)	Cruise Name	Device	Author	SSTwinter (ºC)	SSTsummer (ºC)	Seasonality (ºC)
ZS-21	-9.1747	42.0751	145	Investigador	shipeck grab	R. G.-Á.	13.8	17.8	4.0
ZS-26	-9.3526	41.9835	244	Investigador	shipeck grab	R. G.-Á.	14.0	18.0	4.0
ZS-30	-9.2323	42.1355	171	Investigador	shipeck grab	R. G.-Á.	13.9	17.9	4.0
ZS-36	-9.0188	42.2358	120	Investigador	shipeck grab	R. G.-Á.	13.6	17.7	4.1
ZS-42	-9.0119	42.3045	104	Investigador	shipeck grab	R. G.-Á.	13.5	17.7	4.2
ZS-51	-9.2715	42.2822	203	Investigador	shipeck grab	R. G.-Á.	13.9	17.8	3.9
ZS-55	-9.1267	42.3481	135	Investigador	shipeck grab	R. G.-Á.	13.6	17.7	4.1
ZS-57	-9.0520	42.3813	105	Investigador	shipeck grab	R. G.-Á.	13.5	17.6	4.1
ZS-63	-9.1153	42.4410	113	Investigador	shipeck grab	R. G.-Á.	13.6	17.6	4.0
ZS-68	-9.2983	42.4268	205	Investigador	shipeck grab	R. G.-Á.	13.8	17.7	3.9
ZS-71	-9.1938	42.4784	123	Investigador	shipeck grab	R. G.-Á.	13.5	17.6	4.1
* SO83-9GK	-9.3733	37.8083	900	SONNE83	Box-corer	N. L ./ E. S.	15.6	19.7	4.1
* M39022-1	-8.2599	36.7117	667	METEOR 39/1	Box-corer	E. S..	16.3	21	4.7

Appendix 2 Estimated temperature (est.) and seasonality with their respective residuals (resid.) obtained for each sample by the three transfer function techniques used in this study.

	Imbrie & Kipp						**SIMMAX dw**						**SIMMAX ndw**					
	Winter		Summer		Seasonality		Winter		Summer		Seasonality		Winter		Summer		Seasonality	
Station	SST		SST		SST		SST		SST		SST		SST		SST		SST	
	est.	resid.	est.	resid.	est.	resid.	est.	resid.	est.	resid.	est.	resid.	est.	resid.	est.	resid.	est.	resid.
VB033	13.9	0.2	18.4	-0.4	4.5	-0.6	14.1	0.0	18.4	-0.4	4.3	-0.4	14.0	0.1	18.5	-0.5	4.5	-0.6
VB057	14.2	0.1	18.8	-0.6	4.6	-0.7	14.2	0.1	18.5	-0.3	4.3	-0.4	14.1	0.2	18.7	-0.5	4.5	-0.6
VB060	14.9	-1.1	19.2	-1.1	4.3	0.0	15.0	-1.2	19.5	-1.4	4.4	-0.1	15.2	-1.4	19.6	-1.5	4.5	-0.2
VB073	13.9	0.4	18.0	0.5	4.2	-0.1	14.2	0.1	18.4	0.1	4.2	-0.1	13.9	0.4	18.2	0.3	4.3	-0.2
VB075	14.4	-0.1	18.5	-0.1	4.2	-0.1	14.2	0.1	18.5	-0.1	4.2	-0.1	14.1	0.2	18.3	0.1	4.2	-0.1
VB094	14.3	0.2	18.6	0.3	4.3	0.1	14.5	0.0	18.8	0.1	4.3	0.1	14.4	0.1	18.8	0.1	4.4	0.0
VB095	14.7	-0.2	19.5	-0.6	4.8	-0.4	14.7	-0.2	19.1	-0.2	4.4	0.0	14.7	-0.2	19.2	-0.3	4.5	-0.1
VB098	14.5	-0.1	18.7	0.1	4.2	0.2	14.3	0.1	18.5	0.3	4.2	0.2	14.2	0.2	18.4	0.4	4.2	0.2
VB106	14.8	-0.1	19.2	0.1	4.4	0.2	14.9	-0.2	19.3	0.0	4.5	0.1	15.0	-0.3	19.4	-0.1	4.4	0.2
VB108	15.0	-0.5	19.2	-0.2	4.3	0.2	15.0	-0.5	19.3	-0.3	4.3	0.2	15.1	-0.6	19.5	-0.5	4.4	0.1
VB133	14.7	0.0	19.0	0.2	4.3	0.2	14.8	-0.1	19.2	0.0	4.5	0.0	14.8	-0.1	19.1	0.1	4.3	0.2
VB135	15.3	-0.5	19.6	-0.3	4.4	0.1	14.9	-0.1	19.3	0.0	4.5	0.0	15.1	-0.3	19.5	-0.2	4.4	0.1
VB136	14.7	0.2	19.2	0.1	4.5	-0.1	14.9	0.0	19.2	0.1	4.4	0.0	14.6	0.3	19.0	0.2	4.5	-0.1
VB138	15.2	-0.3	19.9	-0.8	4.7	-0.4	14.9	0.0	19.3	-0.2	4.4	-0.1	14.9	0.0	19.3	-0.2	4.4	-0.1
VB156	15.1	-0.3	19.4	-0.4	4.3	-0.1	15.2	-0.4	19.7	-0.7	4.5	-0.3	15.3	-0.5	19.8	-0.8	4.5	-0.3
VB161	14.8	0.0	19.1	0.0	4.3	0.0	14.8	0.0	19.2	-0.1	4.4	-0.1	14.7	0.1	19.1	0.0	4.4	-0.1
VB164	14.9	0.1	19.5	-0.1	4.7	-0.2	14.8	0.2	19.2	0.2	4.4	0.1	14.7	0.3	19.1	0.3	4.4	0.1
VB165	15.4	-0.3	19.9	-0.3	4.5	0.0	15.2	-0.1	19.6	0.0	4.5	0.0	15.3	-0.2	19.7	-0.1	4.5	0.0
VB172	15.3	-0.3	19.7	-0.5	4.4	-0.2	15.1	-0.1	19.4	-0.2	4.4	-0.2	15.2	-0.2	19.5	-0.3	4.4	-0.2
VB176	14.8	0.1	19.1	-0.2	4.2	-0.2	15.0	-0.1	19.2	-0.3	4.3	-0.3	14.9	0.0	19.1	-0.2	4.3	-0.3
LV010	15.8	0.5	20.2	1.5	4.4	1.1	15.6	0.7	20.0	1.7	4.5	1.0	15.5	0.8	20.0	1.7	4.5	1.0
LV044	15.3	0.6	19.7	1.2	4.4	0.6	15.9	0.0	20.5	0.4	4.6	0.4	15.4	0.5	20.0	0.9	4.5	0.5
LV051	15.3	0.4	19.7	0.7	4.4	0.3	15.8	-0.1	20.3	0.1	4.6	0.1	15.6	0.1	20.0	0.4	4.5	0.2
LV053	15.3	0.5	19.8	0.5	4.5	0.0	15.7	0.1	20.4	-0.1	4.7	-0.2	15.6	0.2	20.1	0.2	4.5	0.0
LV059	15.2	0.7	19.7	0.9	4.4	0.3	15.7	0.2	20.3	0.3	4.6	0.1	15.5	0.4	20.0	0.6	4.5	0.2
LV072	15.3	0.4	19.7	0.8	4.4	0.4	15.8	-0.1	20.3	0.2	4.6	0.2	15.2	0.5	19.7	0.8	4.5	0.3
LV073	15.4	0.4	19.9	0.6	4.4	0.4	15.8	0.0	20.4	0.1	4.6	0.2	15.6	0.2	20.2	0.3	4.6	0.2
LV075	15.3	0.6	19.8	0.7	4.5	0.1	15.8	0.1	20.4	0.1	4.7	-0.1	15.5	0.4	20.3	0.2	4.8	-0.2
LV078	15.5	0.5	20.0	0.4	4.5	-0.1	15.7	0.3	20.4	0.0	4.7	-0.3	15.4	0.6	20.0	0.4	4.6	-0.2
LV079	16.0	0.0	20.5	-0.1	4.5	-0.1	15.7	0.3	20.2	0.2	4.6	-0.2	15.6	0.4	20.0	0.4	4.5	-0.1
LV085	15.5	-0.5	19.9	-0.1	4.4	0.4	15.6	-0.6	20.1	-0.3	4.5	0.3	15.5	-0.5	20.0	-0.2	4.5	0.3
LV087	15.5	0.0	19.9	0.0	4.4	0.1	15.5	0.0	19.8	0.1	4.3	0.2	15.4	0.1	19.9	0.0	4.4	0.1
LV099	15.8	0.0	20.3	-0.2	4.5	-0.2	15.6	0.2	20.1	0.0	4.5	-0.2	15.6	0.2	20.1	0.0	4.6	-0.3
LV102	15.4	0.1	19.8	-0.1	4.4	-0.2	15.4	0.1	19.8	-0.1	4.4	-0.2	15.4	0.1	19.8	-0.1	4.4	-0.2
LV119	15.4	0.0	19.9	-0.3	4.4	-0.2	15.3	0.1	19.8	-0.2	4.6	-0.4	15.4	0.0	19.9	-0.3	4.5	-0.3
LV122	15.3	0.2	19.6	0.0	4.3	-0.2	15.3	0.2	19.7	-0.1	4.4	-0.3	15.2	0.3	19.5	0.1	4.3	-0.2
LV124	15.5	0.0	19.8	-0.2	4.4	-0.3	15.5	0.0	19.6	0.0	4.1	0.0	15.3	0.2	19.6	0.0	4.3	-0.2
LV125	14.9	0.7	19.2	0.4	4.3	-0.3	15.5	0.1	19.6	0.0	4.1	-0.1	15.0	0.6	19.4	0.2	4.4	-0.4

Appendix 2 Continued

	Imbrie & Kipp						SIMMAX dw						SIMMAX ndw					
	Winter		Summer		Seasonality		Winter		Summer		Seasonality		Winter		Summer		Seasonality	
Station	SST		SST		SST		SST		SST		SST		SST		SST		SST	
	est.	resid.	est.	resid.	est.	resid.	est.	resid.	est.	resid.	est.	resid.	est.	resid.	est.	resid.	est.	resid.
LV126	15.1	0.5	19.5	0.1	4.3	-0.3	15.5	0.1	19.6	0.0	4.1	-0.1	15.3	0.3	19.5	0.1	4.2	-0.2
LV127	15.0	0.5	19.6	-0.1	4.6	-0.7	15.4	0.1	19.6	-0.1	4.2	-0.3	15.1	0.4	19.6	-0.1	4.5	-0.6
LV131	15.1	0.3	19.3	0.2	4.3	-0.2	15.3	0.1	19.7	-0.2	4.3	-0.2	15.1	0.2	19.4	0.1	4.2	-0.2
LV134	15.4	-0.4	19.8	0.0	4.4	0.4	15.5	-0.5	19.7	0.1	4.2	0.6	15.4	-0.4	19.8	0.0	4.3	0.5
LV144	15.4	0.0	19.8	-0.4	4.4	-0.4	15.3	0.1	19.7	-0.3	4.5	-0.5	15.2	0.2	19.6	-0.2	4.4	-0.4
LV148	14.6	0.9	19.2	0.2	4.6	-0.7	15.2	0.3	19.5	-0.1	4.3	-0.4	15.0	0.5	19.5	-0.1	4.5	-0.6
LV171	15.4	-0.1	19.7	-0.3	4.4	-0.3	15.3	0.0	19.6	-0.2	4.3	-0.2	15.2	0.1	19.5	-0.1	4.3	-0.2
LV173	15.0	0.1	19.3	0.5	4.3	0.5	15.2	-0.1	19.5	0.3	4.2	0.6	15.1	0.0	19.5	0.3	4.4	0.4
SO75 09KG	16.0	-0.3	20.7	-0.3	4.8	-0.1	15.5	0.2	20.2	0.2	4.6	0.1	15.5	0.2	20.2	0.2	4.7	0.0
SO75 13KG	15.4	0.3	19.8	-0.1	4.5	-0.5	15.5	0.2	19.7	0.0	4.2	-0.2	15.4	0.3	19.9	-0.1	4.4	-0.4
SO75 15KG	15.1	0.6	19.4	0.5	4.3	-0.1	15.4	0.3	19.6	0.3	4.2	0.0	15.2	0.5	19.5	0.4	4.3	-0.1
SO75 25KG	15.6	0.0	20.2	-0.2	4.5	-0.1	15.5	0.1	20.1	-0.1	4.6	-0.2	15.6	0.0	20.3	-0.3	4.7	-0.3
SO75 30KG	15.6	0.3	20.1	0.3	4.5	0.0	15.5	0.4	20.1	0.3	4.6	-0.1	15.6	0.3	20.3	0.1	4.7	-0.2
SO75 33KG	15.9	0.0	20.4	0.0	4.5	0.0	15.7	0.2	20.2	0.2	4.4	0.1	15.7	0.2	20.2	0.2	4.5	0.0
SO83 07GK	16.2	-0.5	20.8	-0.6	4.6	-0.1	15.6	0.1	20.0	0.2	4.5	0.0	15.6	0.1	20.2	0.0	4.6	-0.1
SO83 10GK	14.7	0.8	19.0	0.6	4.3	-0.2	15.4	0.1	19.5	0.1	4.1	0.0	14.7	0.8	19.0	0.6	4.2	-0.1
SO83 11GK	14.8	0.7	19.2	0.3	4.3	-0.3	15.4	0.1	19.5	0.0	4.2	-0.2	14.9	0.6	19.3	0.2	4.4	-0.4
PO01(2)	15.3	0.3	19.6	0.2	4.3	-0.1	15.5	0.1	19.7	0.1	4.2	0.0	15.5	0.1	19.6	0.2	4.2	0.0
PO03(1)	15.7	0.1	20.1	-0.2	4.5	-0.4	15.5	0.3	19.9	0.0	4.3	-0.2	15.4	0.4	19.7	0.2	4.3	-0.2
PO05(1)	15.1	0.4	19.4	0.2	4.3	-0.2	15.4	0.1	19.6	0.0	4.2	-0.1	15.1	0.4	19.4	0.2	4.2	-0.1
PO06(1)	16.1	-0.5	21.2	-1.3	5.1	-0.8	15.7	-0.1	20.4	-0.5	4.8	-0.5	15.7	-0.1	20.7	-0.8	5.0	-0.7
M39002-3	16.5	0.2	22.3	0.2	5.8	0.0	16.5	0.2	22.2	0.3	5.7	0.1	16.3	0.4	21.8	0.7	5.5	0.3
M39003-2	16.1	0.4	21.9	0.6	5.8	0.3	16.5	0.0	22.3	0.2	5.8	0.2	16.4	0.1	22.0	0.5	5.6	0.4
M39004-2	16.4	0.1	21.4	1.0	5.0	0.9	16.4	0.1	21.8	0.6	5.4	0.5	16.1	0.4	21.1	1.3	5.0	0.9
M39016-2	16.5	-0.2	21.2	0.5	4.8	0.6	16.0	0.3	21.0	0.7	5.0	0.4	15.8	0.5	20.4	1.3	4.6	0.8
M39017-4	16.0	0.3	20.7	1.5	4.7	1.2	16.1	0.2	21.0	1.2	4.9	1.0	15.8	0.5	20.5	1.7	4.7	1.2
M39021-5	15.8	0.6	21.4	-0.1	5.6	-0.7	16.2	0.2	21.3	0.0	5.1	-0.2	16.0	0.4	21.1	0.1	5.2	-0.3
M39022-3	15.6	0.7	20.1	0.9	4.5	0.2	15.7	0.6	20.4	0.6	4.7	0.0	15.5	0.8	20.0	1.0	4.5	0.2
M39023-3	16.2	0.1	20.9	0.1	4.8	-0.1	15.9	0.4	20.9	0.1	5.0	-0.3	15.7	0.6	20.4	0.6	4.8	-0.1
M39029-6	16.6	0.1	21.9	0.4	5.3	0.3	16.4	0.3	21.8	0.5	5.4	0.2	16.2	0.5	21.4	0.9	5.2	0.4
M39035-3	15.9	-0.3	20.4	-0.5	4.5	-0.2	15.6	0.0	19.9	0.0	4.3	0.0	15.6	0.0	20.0	-0.1	4.4	-0.1
M39058-1	15.6	-0.4	20.0	0.5	4.4	0.9	15.2	0.0	19.6	0.9	4.4	0.9	15.3	-0.1	19.6	0.9	4.4	0.9
M39059-2	15.0	0.2	20.3	0.0	5.3	-0.2	15.0	0.2	19.6	0.7	4.7	0.4	15.0	0.2	19.8	0.5	4.8	0.3
M39070-1	14.0	-0.8	17.9	0.3	3.9	1.1	13.5	-0.3	18.5	-0.3	5.0	0.0	14.6	-1.4	19.0	-0.8	4.5	0.5
M39072-1	14.1	-1.0	18.4	0.0	4.3	1.0	13.9	-0.8	18.0	0.4	4.1	1.2	14.1	-1.0	18.3	0.1	4.1	1.2
PE151-01A	14.9	0.2	19.1	0.1	4.2	0.0	14.9	0.2	19.0	0.2	4.1	0.1	14.7	0.4	18.8	0.4	4.2	0.0
PE151-03B	14.7	1.3	19.0	1.2	4.4	-0.1	15.6	0.4	20.0	0.2	4.5	-0.2	15.2	0.8	19.5	0.7	4.3	0.0
PE151-04A	15.8	0.0	20.3	1.8	4.5	1.8	15.7	0.1	20.4	1.7	4.7	1.6	15.7	0.1	20.3	1.8	4.6	1.7
PO287-3-1B	15.2	0.0	19.6	0.7	4.4	0.7	15.1	0.1	19.9	0.4	4.8	0.3	15.1	0.1	19.5	0.8	4.3	0.8
PO287-5-1B	14.4	-0.4	18.6	-0.7	4.2	-0.3	14.0	0.0	18.1	-0.2	4.1	-0.2	14.2	-0.2	18.4	-0.5	4.2	-0.3
PO287-8-1B	14.6	-0.6	18.8	-0.8	4.2	-0.2	14.1	-0.1	18.1	-0.1	4.0	0.0	14.5	-0.5	18.8	-0.8	4.3	-0.3
PO287-13-1B	15.2	-1.2	19.6	-1.6	4.4	-0.4	14.1	-0.1	18.5	-0.5	4.4	-0.4	15.2	-1.2	19.8	-1.8	4.6	-0.6
PO287-15-1B	14.6	-0.1	18.8	0.2	4.2	0.3	14.6	-0.1	19.0	0.0	4.4	0.1	14.8	-0.3	18.9	0.1	4.2	0.3
PO287-19-1B	14.5	0.0	18.6	0.4	4.2	0.3	14.4	0.1	18.8	0.2	4.3	0.2	14.2	0.3	18.3	0.7	4.2	0.3
PO287-21-1B	15.0	-0.4	19.3	-0.2	4.3	0.2	15.0	-0.4	19.2	-0.1	4.3	0.2	15.2	-0.6	19.3	-0.2	4.1	0.4
PO287-26-1B	15.2	-0.2	19.8	-0.8	4.6	-0.6	15.1	-0.1	19.1	-0.1	4.0	0.0	15.3	-0.3	19.5	-0.5	4.2	-0.2
PO287-27-1B	15.5	-0.6	20.1	-1.2	4.6	-0.6	15.0	-0.1	19.1	-0.2	4.1	-0.1	15.4	-0.5	19.8	-0.9	4.5	-0.5
PO287-28-1B	15.4	-0.5	19.9	-1.0	4.6	-0.6	15.0	-0.1	19.1	-0.2	4.1	-0.1	15.4	-0.5	19.8	-0.9	4.4	-0.4
PO287-33-1B	15.1	0.0	19.4	0.5	4.3	0.5	15.4	-0.3	19.5	0.4	4.1	0.7	15.0	0.1	19.2	0.7	4.2	0.6
PO287-34-1B	15.4	-0.3	19.9	0.0	4.5	0.3	15.5	-0.4	20.1	-0.2	4.6	0.2	15.5	-0.4	20.1	-0.2	4.7	0.2
PO287-40-1B	15.3	0.3	19.6	0.0	4.4	-0.4	15.5	0.1	19.6	0.0	4.1	-0.1	15.3	0.3	19.5	0.1	4.2	-0.2
PO287-41-1B	15.3	0.3	19.7	-0.1	4.4	-0.4	15.5	0.1	19.6	0.0	4.1	-0.1	15.3	0.3	19.5	0.1	4.2	-0.2
PO287-44-1B	15.6	-0.4	20.2	0.3	4.5	0.8	15.2	0.0	20.4	0.1	5.2	0.1	15.2	0.0	19.8	0.7	4.7	0.6
PO287-45-1B	14.1	1.0	18.5	1.6	4.4	0.6	14.8	0.3	19.2	0.9	4.4	0.6	14.6	0.5	19.0	1.1	4.4	0.6
PO201/10-702	14.0	-0.7	18.6	0.0	4.6	0.6	13.5	-0.2	18.5	0.1	5.0	0.2	13.9	-0.6	18.3	0.3	4.4	0.8
PO201/10-703	14.3	-1.1	19.0	-0.4	4.7	0.7	13.5	-0.3	18.5	0.1	4.9	0.5	13.9	-0.7	18.3	0.3	4.4	1.0
ATL-FP1-04B	14.3	-0.8	18.9	-0.8	4.7	-0.1	13.7	-0.2	18.5	-0.4	4.9	-0.3	13.9	-0.4	18.6	-0.5	4.7	-0.1
ATL-FP1-05B	14.1	-0.6	18.7	-0.2	4.6	0.5	13.7	-0.2	18.3	0.2	4.5	0.6	13.9	-0.4	18.4	0.1	4.5	0.6
ATL-FP1-08A	15.7	-0.2	20.3	-0.7	4.6	-0.5	15.6	-0.1	19.9	-0.3	4.4	-0.3	15.5	0.0	19.9	-0.3	4.4	-0.3
ATL-FP1-09A	16.7	-0.8	21.9	-1.4	5.2	-0.6	15.9	0.0	20.5	0.0	4.7	-0.1	16.1	-0.2	21.1	-0.6	5.0	-0.4

Appendix 2 Continued

	Imbrie & Kipp						**SIMMAX dw**						**SIMMAX ndw**					
	Winter		Summer		Seasonality		Winter		Summer		Seasonality		Winter		Summer		Seasonality	
Station	SST		SST		SST		SST		SST		SST		SST		SST		SST	
	est.	resid.	est.	resid.	est.	resid.	est.	resid.	est.	resid.	est.	resid.	est.	resid.	est.	resid.	est.	resid.
ATL-FP1-10B	16.6	-0.6	21.5	-1.0	4.9	-0.4	15.8	0.2	20.3	0.2	4.5	0.0	15.8	0.2	20.4	0.1	4.6	-0.1
64PE218-16	15.3	0.0	19.8	-0.3	4.5	-0.2	15.3	0.0	19.6	-0.1	4.2	0.1	15.2	0.1	19.6	-0.1	4.4	-0.1
64PE218-21	15.4	-0.4	19.9	-0.9	4.5	-0.5	15.1	-0.1	19.2	-0.2	4.1	-0.1	15.4	-0.4	19.8	-0.8	4.4	-0.4
64PE218-22	15.5	-0.3	20.1	-1.0	4.6	-0.6	15.2	0.0	19.4	-0.3	4.2	-0.2	15.5	-0.3	20.0	-0.9	4.5	-0.5
64PE218-36-1	15.2	0.1	19.5	-0.2	4.4	-0.4	15.2	0.1	19.8	-0.5	4.6	-0.6	15.2	0.1	19.7	-0.4	4.6	-0.6
64PE225-1-21	15.3	0.2	20.2	-0.3	5.0	-0.6	15.6	-0.1	19.9	0.0	4.3	0.1	15.6	-0.1	20.1	-0.2	4.5	-0.1
64PE225-1-26	14.7	0.0	19.1	0.2	4.4	0.2	15.2	-0.5	19.3	0.0	4.1	0.5	15.3	-0.6	19.5	-0.2	4.2	0.4
64PE225-2-02	15.4	-0.2	19.9	-0.8	4.4	-0.4	15.3	-0.1	19.4	-0.3	4.1	-0.1	15.3	-0.1	19.7	-0.6	4.4	-0.4
64PE225-3-03	15.5	-0.2	19.9	-0.7	4.4	-0.5	15.3	0.0	19.4	-0.2	4.2	-0.3	15.4	-0.1	19.9	-0.7	4.5	-0.6
64PE225-06	15.5	0.2	20.0	0.4	4.4	0.3	15.4	0.3	19.8	0.6	4.4	0.3	15.3	0.4	19.8	0.6	4.5	0.2
64PE225-07	16.1	-0.5	21.6	-1.2	5.6	-0.8	15.7	-0.1	20.5	-0.1	4.7	0.1	15.9	-0.3	20.8	-0.4	4.9	-0.1
64PE225-25	15.8	-1.0	21.1	-0.7	5.3	0.3	14.8	0.0	20.1	0.3	5.3	0.3	15.0	-0.2	20.1	0.3	5.1	0.5
64PE225-22	14.9	-0.2	20.2	0.1	5.3	0.3	14.2	0.5	19.0	1.3	4.8	0.8	14.1	0.6	18.9	1.4	4.8	0.8
64PE225-27	14.8	0.0	19.2	0.3	4.4	0.3	14.8	0.0	19.2	0.3	4.4	0.3	14.9	-0.1	19.3	0.2	4.4	0.3
MD04-2811	15.6	0.2	20.3	0.3	4.7	0.1	15.3	0.5	19.9	0.7	4.7	0.1	15.0	0.8	19.7	0.9	4.7	0.1
MD04-2814	14.2	0.3	18.8	0.7	4.6	0.4	14.4	0.1	18.8	0.7	4.4	0.6	14.1	0.4	18.7	0.8	4.6	0.4
MD04-2817	13.9	0.0	18.5	0.1	4.5	0.2	13.9	0.0	18.2	0.4	4.3	0.4	13.8	0.1	18.3	0.3	4.5	0.2
M2004-13	15.5	1.0	20.8	1.7	5.3	0.8	16.3	0.2	21.9	0.6	5.6	0.5	15.2	1.2	20.1	2.4	4.9	1.2
M2004-28	15.7	0.9	21.0	1.5	5.3	0.6	16.3	0.3	21.9	0.6	5.7	0.2	15.5	1.1	20.5	2.0	5.0	0.9
SWIM04-42 SW	16.4	0.2	22.5	0.1	6.1	-0.1	16.5	0.1	22.3	0.3	5.8	0.2	16.4	0.2	21.9	0.7	5.5	0.5
GeoB9014-1	16.3	0.1	21.8	0.1	5.5	0.0	16.5	-0.1	22.1	-0.2	5.7	-0.2	16.4	0.0	22.0	-0.1	5.6	-0.1
ZS-5	13.7	0.0	17.8	0.1	4.1	0.0	13.6	0.1	17.8	0.1	4.1	0.0	13.7	0.0	17.9	0.0	4.2	-0.1
ZS-9	13.3	0.5	17.5	0.4	4.1	0.0	13.9	-0.1	17.9	0.0	4.0	0.1	13.8	0.0	18.0	-0.1	4.2	-0.1
ZS-13	13.7	0.3	18.2	-0.2	4.5	-0.5	13.9	0.1	18.0	0.0	4.1	-0.1	13.8	0.2	18.0	0.0	4.2	-0.2
ZS-17	14.3	-0.6	18.5	-0.7	4.1	0.0	13.7	0.0	17.8	0.0	4.1	0.0	14.0	-0.3	18.1	-0.3	4.1	0.0
ZS-21	13.4	0.4	17.1	0.7	3.7	0.3	13.9	-0.1	17.9	-0.1	4.1	-0.1	13.8	0.0	18.1	-0.3	4.3	-0.3
ZS-26	13.4	0.6	17.7	0.3	4.3	-0.3	13.9	0.1	18.0	0.0	4.1	-0.1	13.9	0.1	18.1	-0.1	4.2	-0.2
ZS-30	13.5	0.4	17.7	0.2	4.2	-0.2	13.8	0.1	17.9	0.0	4.0	0.0	13.8	0.1	18.0	-0.1	4.2	-0.2
ZS-36	14.0	-0.4	18.1	-0.4	4.1	0.0	13.6	0.0	17.8	-0.1	4.1	0.0	14.0	-0.4	18.1	-0.4	4.1	0.0
ZS-42	13.8	-0.3	17.8	-0.1	4.0	0.2	13.6	-0.1	17.7	0.0	4.1	0.1	14.0	-0.5	18.1	-0.4	4.1	0.1
ZS-51	13.7	0.2	17.8	0.0	4.1	-0.2	13.8	0.1	17.9	-0.1	4.1	-0.2	13.7	0.2	18.1	-0.3	4.3	-0.4
ZS-55	13.6	0.0	17.8	-0.1	4.2	-0.1	13.9	-0.3	17.9	-0.2	4.0	0.1	13.9	-0.2	18.0	-0.3	4.2	-0.1
ZS-57	13.8	-0.3	17.8	-0.2	4.1	0.0	13.6	-0.1	17.7	-0.1	4.1	0.0	13.8	-0.3	18.0	-0.4	4.2	-0.2
ZS-63	13.9	-0.3	18.0	-0.4	4.1	-0.1	13.6	0.0	17.7	-0.1	4.1	-0.1	13.9	-0.2	18.0	-0.4	4.1	-0.1
ZS-68	14.1	-0.3	18.9	-1.2	4.8	-0.9	13.8	0.0	17.9	-0.2	4.1	-0.2	13.8	0.0	18.1	-0.4	4.3	-0.4
ZS-71	13.5	0.0	17.6	0.0	4.1	0.0	13.6	-0.1	17.7	-0.1	4.1	0.0	13.8	-0.3	18.0	-0.4	4.2	-0.1

References

Abrantes, F., Sancetta, C., 1985. Diatom assemblages in surface sediments reflect coastal upwelling off Southern Portugal. Oceanologica Acta, 8: 7-12.

Abrantes, F., 1988. Diatom Assemblages as Upwelling Indicators in Surface Sediments Off Portugal. Marine Geology, 85: 15-39.

Abrantes, F., Moita, M.T., 1999. Water column and recent sediment data on diatoms and coccolithophorids, off Portugal, confirm sediment record of upwelling events. Oceanologica Acta, 22: 319-336.

Álvarez-Salgado, X.A., Doval, M.D., Borges, A.V., Joint, I., Frankignoulle, M., Woodward, E.M.S., Figueiras, F.G., 2001. Off-shelf fluxes of labile materials by an upwelling filament in the NW Iberian Upwelling System. Progress in Oceanography, 51(2-4): 321-337.

Álvarez-Salgado, X.A., Figueiras, F.G., Perez, F.F., Groom, S., Nogueira, E., Borges, A., Chou, L., Castro, C.G., Moncoiffe, G., Rios, A.F., Miller, A.E.J., Frankignoulle, M., Savidge, G., Wollast, R., 2003. The Portugal coastal counter current off NW Spain: new insights on its biogeochemical variability. Progress in Oceanography, 56(2): 281-321.

Andreasen, D.J., Ravelo, A.C., 1997. Tropical Pacific Ocean thermocline depth reconstructions for the last glacial maximum. Paleoceanography, 12(3): 395-413.

Antoine, D., Andre, J.M., Morel, A., 1996. Oceanic primary production .2. Estimation at global scale from satellite (coastal zone color scanner) chlorophyll. Global Biogeochemical Cycles, 10(1): 57-69.

Bé, A.W.H., Hamlin, W.H., 1967. Ecology of recent planktonic foraminifera. Part3: Distribution in the North Atlantic during the summer of 1962. Micropaleontology, 13: 87-106.

Bé, A.W.H., Tolderlund, D.S., 1971. Distribution and ecology of living planktonic foraminifera in surface waters of the Atlantic and Indian Oceans. In: Funnel, B.M., Riedel, W. R. (eds.) (Eds.), The Micropaleontology of Oceans. Cambridge University Press,New York, pp. 105–149.

Bé, A.W.H., 1977. An ecological, zoogeographic and taxonomic review of Recent planktonic foraminifera. In: Ramsay, A.T.S. (Eds.), Oceanic Micropaleontology. Academic,San Diego, California, pp. 1-100.

Birks, H.J.B., 1995. Quantitative palaeoenvironmental reconstructions. In: Maddy, D., Brew, J.S. (Eds.), Statistical Modelling of Quaternary Science Data. Technical Guide 5. Quaternary Research Association,Cambridge, pp. 161-254.

Cayre, O., Lancelot, Y., Vincent, E., 1999. Paleoceanographic reconstructions from planktonic foraminifera off the Iberian Margin: Temperature, salinity, and Heinrich events. Paleoceanography, 14(3): 384-396.

Chen, M.T., Huang, C.C., Pflaumann, U., Waelbroeck, C., Kucera, M., 2005. Estimating glacial western Pacific sea-surface temperature: methodological overview and data compilation of surface sediment planktic foraminifer faunas. Quaternary Science Reviews, 24(7-9): 1049-1062.

Curry, W.B., Ostermann, D.R., Guptha, M.V.S., Ittekkot, V., 1992. Foraminiferal production and monsoonal upwelling in the Arabian Sea: evidence from sediment traps. In: Summerhayes, C.P., Prell, W.L., Emeis, K.C. (Eds.), Upwelling Systems: Evolution Since the Early Miocene. Geological Society Special Publication, 64, pp. 93-106.

Darling, K.F., Wade, C.M., Stewart, I.A., Kroon, D., Dingle, R., Brown, A.J.L., 2000. Molecular evidence for genetic mixing of Arctic and Antarctic subpolar populations of planktonic foraminifers. Nature, 405(6782): 43-47.

Darling, K.F., Kucera, M., Wade, C.M., von Langen, P., Pak, D., 2003. Seasonal distribution of genetic types of planktonic foraminifer morphospecies in the Santa Barbara Channel and its paleoceanographic implications. Paleoceanography, 18(2): doi:10.1029/2001PA000723.

de Abreu, L., Shackleton, N.J., Schonfeld, J., Hall, M., Chapman, M., 2003. Millennial-scale oceanic climate variability off the Western Iberian margin during the last two glacial periods. Marine Geology, 196(1-2): 1-20.

de Vargas, C., Renaud, S., Hilbrecht, H., Pawlovski, J., 2001. Pleistocene adaptive radiation in Globorotalia truncatulinoides: genetic, morphologic, and environmental evidence. Paleobiology, 27: 104-25.

Deuser, W.G., Ross, E.H., Hemleben, C., Spindler, M., 1981. Seasonal changes in species composition, numbers, mass, size, and isotopic composition of planktonic foraminifera settling into the deep sargasso sea. Palaeogeography, Palaeoclimatology, Palaeoecology, 33(1-3): 103-127.

Fairbanks, R.G., Wiebe, P.H., Bé, A.W.H., 1980. Vertical Distribution and Isotopic Composition of Living Planktonic Foraminifera in the Western North Atlantic. Science, pp. 61-63.

Fairbanks, R.G., Sverdlove, M., Free, R., Wiebe, P.H., Be, A.W.H., 1982. Vertical distribution and isotopic fractionation of living planktonic foraminifera from the Panama Basin. Nature, 298(5877): 841-844.

Fiúza, A.F.G., 1983. Upwelling Patterns off Portugal. In: Suess, E., Thiede, J. (Eds.), Coastal Upwelling its sediment record. Plenum Press,New York, pp. 85-98.

Fiúza, A.F.G., 1984. Hidrologia e Dinamica das Aguas Costeiras de Portugal, Faculdade de Ciências da Universidade de Lisboa, Lisbon, 294 pp.

Fiúza, A.F.G., Hamann, M., Ambar, I., Diaz del Rio, G., Gonzalez, N., Cabanas, J.M., 1998. Water masses and their circulation off western Iberia during May 1993. Deep Sea Research Part I: Oceanographic Research Papers, 45(7): 1127-1160.

Fraga, F., 1981. Upwelling off the Galician Coast, Northwest Spain. In: Richards, F.A. (Eds.), Coastal Upwelling. American Geophysical Union,Washington, pp. 176-182.

Giraudeau, J., 1993. Planktonic Foraminiferal Assemblages in Surface Sediments from the Southwest African Continental-Margin. Marine Geology, 110: 47-62.

Haynes, R., Barton, E., Pilling, I., 1993. Development, persistence, and variability of upwelling filaments off the Atlantic coast of the Iberian Peninsula. Journal of Geophysical Research, 98(C12): 22681-22692.

Hemleben, C., Spindler, M., Anderson, O.R., 1989. Modern Planktonic Foraminifera. Springer-Verlang, Berlin, 363 pp.

Huber, B.T., Bijma, J., Darling, K., 1997. Cryptic speciation in the living planktonic foraminifer Globigerinella siphonifera (d'Orbigny). Paleobiology, 23(1): 33-62.

Hutson, W.H., 1977. Transfer-Functions under No-Analog Conditions - Experiments with Indian-Ocean Planktonic Foraminifera. Quaternary Research, 8(3): 355-367.

Hutson, W.H., 1980. The Agulhas Current During the Late Pleistocene - Analysis of Modern Faunal Analogs. Science, 207(4426): 64-66.

Imbrie, J., Kipp, N.G., 1971. A new micropaleontological method for quantitative paleoclimatology: Application to a late Pleistocene Caribbean core. In: Turekian, K.K., ed. (Eds.), The late Cenozoic glacial ages. Yale University Press, New Haven, Conneticut, pp. 71–181.

Imbrie, J., van Donk, J., Kipp, N.G., 1973. Paleoclimatic investigation of a late Pleistocene Caribbean deep-sea core: comparision of isotopic and faunal methods. Quaternary Research, 3: 10-38.

Kearns, E.J., Hanafin, J.A., Evans, R.H., Minnett, P.J., Brown, O.B., 2000. An Independent Assessment of Pathfinder AVHRR Sea Surface Temperature Accuracy Using the Marine Atmosphere Emitted Radiance Interferometer (MAERI). Bulletin of the American Meteorological Society, 81(7): 1525-1536.

Kennett, J., 1982. Marine Geology, Marine Geology. Prentice-Hall Inc., Englewood Cliffs, pp. 538-559.

Kennett, J.P., Srinivasan, M.S., 1983. Neogene planktonic Foraminifera. A phylogenetic atlas. Hutchinson Ross Pulbishing Company, Stroudsburg, 263 pp.

Kucera, M., Weinelt, M., Kiefer, T., Pflaumann, U., Hayes, A., Weinelt, M., Chen, M.-T., Mix, A., Barrows, T., Cortijo, E., Duprat, J., Juggins, S., Waelbroeck, C., 2005. Reconstruction of sea-surface temperatures from assemblages of planktonic foraminifera: multi-technique approach based on geographically constrained calibration data sets and its application to glacial Atlantic and Pacific Oceans. Quaternary Science Reviews, 24: 951-998.

Le, J., 1992. Paleotemperature estimation methods: Sensitivity test on two western Equatorial Pacific cores. Quaternary Science Reviews, 11: 801-820.

Le, J., Shackleton, N.J., 1994. Reconstructing paleoenvironment by transfer function: Model evaluation with simulated data. Marine Micropaleontology, 24(2): 187-199.

Levy, A., Mathieu, R., Poignant, A., Rosset-Moulinier, M., Ubaldo, M.L., Lebreiro, S., 1995. Foraminiferes actuels de la Marge Continental Portuguese - Inventaire et Distribuition, 32. Memórias do Instituto Geológico e Mineiro, Lisboa, 116 pp.

Malmgren, B.A., Nordlund, U., 1997. Application of artificial neural networks to paleoceanographic data. Palaeogeography Palaeoclimatology Palaeoecology, 136: 359-373.

Malmgren, B.A., Kucera, M., Nyberg, J., Waelbroeck, C., 2001. Comparison of statistical and artificial neural network techniques for estimating past sea surface temperatures from planktonic foraminifer census data. Paleoceanography, 16(5): 520-530.

Marchant, M., Hebbeln, D., Wefer, G., 1998. Seasonal flux patterns of planktic foraminifera in the Peru-Chile Current. Deep-Sea Research Part I-Oceanographic Research Papers, 45(7): 1161-1185.

Mix, A.C., Morey, A.E., Pisias, N.G., Hostetler, S.W., 1999. Foraminiferal faunal estimates of paleotemperature: Circumventing the no-analog problem yields cool ice age tropics. Paleoceanography, 14(3): 350-359.

Monteiro, J.H., Dias, J.A., Gaspar, L.C., Possolo, A.M., 1980. Recent marine sediments of the Portuguese continental shelf. Actual problems of oceanography in Portugal. JNICT and Nato Marine Science Panel, Lisbon.

Monteiro, J.H., Abrantes, F., Alveirinho-Dias, J.M., Gaspar, L., 1983. Upwelling records in recent sediments from southern Portugal: a reconnaissance survey. In: Suess, E., Thiede, J. (Eds.), Coastal Upwelling: Its Sediment Record. Part B; Sedimentary Record of Ancient Coastal Upwelling. NATO Conference Series, Plenum,New York, pp. 145-162.

Nogueira, E., González-Nuevo, G., Morán, X.A.G., Varela, M., Bode, A., 2003. Hydrological structures along the N and NW Iberian Shelf during the winter-spring transition, 4rd Symposium on the Iberian Atlantic Continental Margin, Vigo, Spain, pp. 65-66.

Ortiz, J.D., Mix, A.C., 1992. The spatial distribution and seasonal succession of planktonic foraminifera in the California Current off Oregon, September 1987 - September 1988. In: Summerhayes, C.P., Prell, W.L., Emeis, K.C. (Eds.), Upwelling Systems: Evolution Since the Early Miocene. Geological Society Special Publication, 64, London, pp. 197-213.

Ortiz, J.D., Mix, A.C., 1997. Comparison of Imbrie-Kipp transfer function and modern analog temperature estimates using sediment trap and core top foraminiferal faunas. Paleoceanography, 12(2): 175-190.

Ottens, J.J., 1991. Planktic Foraminifera as North-Atlantic Water Mass Indicators. Oceanologica Acta, 14(2): 123-140.

Peliz, A., Dubert, J., Santos, A.M.P., Oliveira, P.B., Le Cann, B., 2005. Winter upper ocean circulation in the Western Iberian Basin - Fronts, Eddies and Poleward Flows: an overview. Deep-Sea Research Part I-Oceanographic Research Papers, 52(4): 621-646.

Perez, F.F., Castro, C.G., Alvarez-Salgado, X.A., Rios, A.F., 2001. Coupling between the Iberian basin - scale circulation and the Portugal boundary current system: a chemical study. Deep-Sea Research Part I-Oceanographic Research Papers, 48(6): 1519-1533.

Pflaumann, U., Duprat, J., Pujol, C., Labeyrie, L.D., 1996. SIMMAX: A modern analog technique to deduce Atlantic sea surface temperatures from planktonic foraminifera in deep-sea sediments. Paleoceanography, 11(1): 15-35.

Pflaumann, U., Jian, Z., 1999. Modern distribution patterns of planktonic foraminifera in the South China Sea and western Pacific: a new transfer technique to estimate regional sea-surface temperatures. Marine Geology, 156: 41-83.

Pflaumann, U., Sarnthein, M., Chapman, M., d'Abreu, L., Funnell, B., Huels, M., Kiefer, T., Maslin, M., Schulz, H., Swallow, J., van Kreveld, S., Vautravers, M., Vogelsang, E., Weinelt, M., 2003. Glacial North Atlantic: Sea-surface conditions reconstructed by GLAMAP 2000. Paleoceanography, 18(3): 1065, doi: 10.1029/2002PA000774.

Prego, R., Bao, R., 1997. Upwelling influence on the Galician coast: Silicate in shelf water and underlying surface sediments. Continental Shelf Research, 17(3): 307-318.

Prell, W.L., 1985. The stability of low-latitude sea-surface temperatures: An evaluation of the CLIMAP reconstruction with emphasis on the positive SST anomalies. U.S. Dep. Energy. Spec. Publ. TRO 25,Washington, DC, pp. 60.

Ravelo, A.C., Fairbanks, R.G., Philander, S.G.H., 1990. Reconstructing tropical Atlantic hydrography using planktontic foraminifera and an ocean model. Paleoceanography, 5(3): 409-431.

Relvas, P., Barton, E.D., 2002. Mesoscale patterns in the Cape São Vicente (Iberian Peninsula) upwelling region. Journal Geophysical Research, 107(C10): 28-1-28-23.

Ríos, A.F., Pérez, F.F., Fraga, F., 1992. Water masses in the upper and middle North-Atlantic Ocean east of the Azores. Deep-Sea Research Part A-Oceanographic Research Papers, 39(3-4): 645-658.

Salgueiro, E., Voelker, A., Abrantes, F., Meggers, H., Loncaric, N., Moreno, J., in preparation. Productivity and hydrographic changes off SW and S Portugal: Foraminiferal evidence for the Late Holocene.

Sautter, L.R., Thunell, R.C., 1991. Planktonic Foraminiferal Response to Upwelling and Seasonal Hydrographic Conditions - Sediment Trap Results from San-Pedro-Basin, Southern California Bight. Journal of Foraminiferal Research, 21(4): 347-363.

Schiebel, R., Bijma, J., Hemleben, C., 1997. Population dynamics of the planktic foraminifer Globigerina bulloides from the eastern North Atlantic. Deep-Sea Research Part I-Oceanographic Research Papers, 44(9-10): 1701-1713.

Schiebel, R., Zeltner, A., Treppke, U.F., Waniek, J.J., Bollmann, J., Rixen, T., Hemleben, C., 2004. Distribution of diatoms, coccolithophores and planktic foraminifers along atrophic gradient during SW monsoon in the Arabian Sea. Marine Micropaleontology, 51(3-4): 345-371.

Schlitzer, R., 2000. Ocean Data View, http://www.awi-bremerhaven.de/GEO/ODV.

Shackleton, N.J., 1974. Attainment of isotopic equilibrium between ocean water and the benthonic foraminifera genus Uvigerina: Isotopic changes in the ocean during the last glacial. In: C.N.R.S., C.I.d. (Editor), Les méthodes quantitatives d´étude des variations du climat au cours du Pléistocène, pp. 203-209.

Sieger, R., Gersonde, R., Zielinski, U., 1999. A new extended software package for quantitative paleoenvironmental reconstructions. EOS (Trans. Am. Geophys. Union), Electronic Suppl.

Sousa, F.M., Bricaud, A., 1992. Satellite-Derived phytoplankton pigment structures in the Portuguese Upwelling Area. Journal of Geophysical Research, 97(C7): 11,343-11,356.

Teixeira, I., F.G., F., Castro, C.G., 2003. Hydrography, microplankton composition and primary production associated with the transition priod between upwelling and downwelling seasons in Galicia waters (NW Spain). 4rd Symposium on the Iberian Atlantic Continental Margin, Vigo, Spain, pp. 201.

Telford, R.J., Andersson, C., Birks, H.J.B., Juggins, S., 2004. Biases in the estimation of transfer function prediction errors. Paleoceanography, 19(4): PA4014, doi:1029/2004PA001072.

Tenore, K.R., Alonso-Noval, M., Alvarez-Ossorio, M., Atkinson, L.P., Cabanas, J.M., Cal, R.M., Campos, H.J., Castillejo, F., Chesney, E.J., Gonzalez, N., Hanson, R.B., McClain, C.R., Miranda, A., Roman, M.R., Sánchez, J., Santiago, G., Valdés, L., Varela, M., Yoder, J., 1995. Fisheries and oceanography off Galicia, NW Spain: Mesoscale spatial and temporal changes in physical processes and resultan patterns of biological productivity. J. geophys. Res., 100(C6): 10943-10966.

Thiede, J., Nees, S., Schulz, H., DeDeckker, P., 1997. Oceanic surface conditions recorded on the sea floor of the Southwest Pacific Ocean through the distribution of foraminifers and biogenic silica. Palaeogeography Palaeoclimatology Palaeoecology, 131(3-4): 207-239.

Thunell, R., Sautter, L.R., 1992. Planktonic foraminiferal faunal and stable isotopic indices of upwelling: a sediment trap study in the San Pedro Basin, Southern California Bight. In: Summerhayes, C.P., Prell, W.L., Emeis, K.C. (Eds.), Upwelling Systems: Evolution Since the Early Miocene. Geological Society Special Publication, 64, pp. 77-91.

Thunell, R.C., Curry, W.B., Honjo, S., 1983. Seasonal variation in the flux of planktonic foraminifera: time series sediment trap results from the Panama basin. Earth and Planetary Science Letters, 69: 44-55.

Ufkes, E., Zachariasse, W.-J., 1993. Origin of coiling differences in living neogloboquadrinids in the Walvis Bay region, off Namibia, southwest Africa. Micropaleontology, 39: 283-287.

Waelbroeck, C., Labeyrie, L., Duplessy, J.C., Guiot, J., Labracherie, M., Leclaire, H., Duprat, J., 1998. Improving past sea surface temperature estimates based on planktonic fossil faunas. Paleoceanography, 13(3): 272-283.

Watkins, J.M., Mix, A.C., 1998. Testing the effects of tropical temperature, productivity, and mixed-layer-depth on foraminiferal transfer functions. Paleoceanography, 13(1): 96-105.

Wooster, W., Bakun, A., McLain, D., 1976. The seasonal upwelling cycle along the eastern boundary of the North Atlantic. Journal of Marine Research, 34(2): 131-141.

CHAPTER 3

Productivity and hydrographic changes off Southwest and South Portugal: Foraminiferal evidence for the Late Holocene

Emília Salgueiro[a,b], Antje Voelker[a], Fátima Abrantes[a], Neven Lončarić[c,d], Helge Meggers[b], João Moreno[d], Gerold Wefer[b]

[a] Departamento de Geologia Marinha, Instituto Nacional de Engenharia, Tecnologia e Inovação I.P., (INETI-DGM), Estrada da Portela – Zambujal, Apartado 7586, 2721-866 Alfragide, Portugal
[b] Fachbereich Geowissenschaften Universität Bremen, Postfach 33 04 40, D-28359 Bremen, Germany
[c] Nederlands Instituut voor Onderzoek der Zee (NIOZ), Postbus 59, 1790 AB, Den Burg, Texel, The Nederlands
[d] INETI-DGM former collaborator, Estrada da Portela – Zambujal, Apartado 7586, 2721-866 Alfragide, Portugal

To be submitted to Quaternary Research

Abstract

The sedimentary record off the Portuguese margin is mainly influenced by seasonal coastal upwelling between May and September, generating high productivity along this margin, and by the Mediterranean Outflow Water (MOW), centered in two main cores between 500 and 1200 m water depth along the southwestern and southern margin. This work discusses the productivity and surface and deep-water hydrographic conditions for the last 2500 yr along the southwestern and southern Portuguese margin, and how they might be linked to the varying atmosphere/ocean forcing mechanisms. Multi-proxy data including planktonic and benthic foraminifera abundances, planktonic foraminifera assemblages, stable isotope data and organic carbon abundances will be used in six box/multi-cores, four recovered along an E-W transect off Sines between 900-2331 m water depth, and two along a N-S transect off Albufeira between 667-1978 m water depth. The productivity conditions off Sines were more stable during the major warm European North Atlantic periods, Roman Warm Period (RWP) and Medieval Warm Period (MWP), than during the cold ones, Dark Ages (DA) and Little Ice Age (LIA) of the latest Holocene. While the opposite was observed off Albufeira. Alternate intensification of northerly (upwelling at southwest margin) and westerly winds (upwelling at south margin) during the summer of warm and cold climatic periods during the last 2500 yr, could explain such results. No major changes between the different climatic periods were observed in both transects in terms of water masses signal. The intermediate and deep bottom currents (MOW and NACW) were fairly consistent and at same position than today throughout the studied intervals.

Keywords: Portuguese margin; Holocene; Paleoproductivity; Paleoceanography; upwelling; foraminifera.

3.1. Introduction

The Holocene, the current climate period, was for long considered to be a period of persistent stable climate, but Denton & Karlén's (1973) study showed that this period had a more dynamic climate than previously thought, with significant variability on millennial/centennial time scales. Since then other studies have contributed to a better understanding of the Holocene and its short-term climate variability (e.g., Bond et al., 1997; Bianchi, 1999; deMenocal et al., 2000; Bond et al., 2001).

The major European and partly North Atlantic-wide climate events of the last 2000 yr, i.e. the Roman Warm Period (RWP), the Dark Ages (DA), the Medieval Warm Period (MWP), and the Little Ice Age (LIA), are clearly recorded in high-resolution marine sediment cores from the Iberian margin (Diz et al., 2002; Abrantes et al., 2005; Bartels-Jonsdóttir et al., 2006; Gil et al., 2006; Lebreiro et al., in press). The global significance of these climate intervals (mainly an alternating sequence of the warm and cold periods) with worldwide expression (Broecker, 2001; Jones et al., 2001), and the boundaries between them are still under debate. At the Tagus Prodelta site, which is located in the vicinity of our study area, biogeochemical changes allow to define the RWP lasted from ~1950-1600 cal. yr BP, the DA between ~1550 and 1250 cal. yr BP, the MWP from ~1150 to 750 cal. yr BP, and the youngest period, the LIA, between ~650 – 200 cal. yr BP (Lebreiro et al., in press). However pollen data from northwest Iberia suggest that RWP started early around 2200 yr (Desprat et al., 2003), in agreement with other studies in Northern Europe (e.g., Hass, 1996).

In the Tagus Prodelta record, ocean circulation (productivity and coastal upwelling) dominates the warm period of the MWP whereas precipitation (river flux and continental inputs into the shelf) takes over during the cold period of the LIA, and inclusively the cold period of the DA could have been as warm as the MWP (Abrantes et al., 2005; Lebreiro et al., in press), and associated an increased of upwelling (Gil et al., 2006).

Besides the changes in solar irradiance (Stuiver et al., 1997; Crowley, 2000), atmospheric/oceanic forcing such as the North Atlantic Oscilation (NAO), seems to be the dominant factor behind these climate oscillations (Hurrell, 1995; Broecker et al., 1999; Hurrell et al., 2001; Visbeck, 2002).

The NAO is an index calculated as the difference in atmospheric pressure at sea level between the Stykkidhólmur (Icelandic Low) and the Lisbon (Azores High) (Hurrell et al.,

2001). A positive NAO phase, i.e. a large meridional pressure gradient due to the enhancement of both the Icelandic and the Azores pressure centers, leads relatively strong and frequent winter storms cross the North Atlantic, and winters become warmer and wetter at high latitudes in Europe. The opposite situation, when both centers are weakened, the negative NAO phase, leads to colder winters in the northern latitudes and increased precipitation at the southern latitudes of Europe. Consequently, increased precipitation and river discharge in Portugal during cold and winter periods is associated with a negative NAO index (Abrantes et al., 2005), while a positive NAO induces strong northerly and westerly winds during warmer periods and thereby intense upwelling along the southwest Portuguese margin. Upwelling off Portugal is associated to the southward flowing cool Portugal Current, which intensifies close to the coast under the influence of northerly winds in summer (Fiúza, 1983; 1984). In winter, a warm poleward current, which may also be forced by southerly winds, occurs off Portugal. Along the southwestern and southern Portuguese margin, it is this coastal upwelling that generates enhanced productivity, that is, the atmospheric/oceanic forcing determines not only the hydrography but also the productivity levels in this region.

The present work aims to reconstruct the oceanographic conditions along the Portuguese margin during the latest Holocene (2500 yr to Present) and investigate their links to the varying atmosphere/ocean forcing mechanisms. Previous works on the Portuguese Margin for that period are based on shallow sedimentary sequences influenced by terrestrial input. Here, a multi-proxy study was preformed on two transects: an E-W transect (southwest Portugal off Sines; Fig. 1), a region that is under persistent influence of upwelling induced by northerly winds, and a N-S transect (on the southern/Algarve coast off Albufeira), where upwelling influence is sporadic and induced by westerly winds. As both study regions are under the influence of the Mediterranean Outflow Water (MOW), which flows mainly at 600 and 1200 m, it is believed this water mass has been fairly constant in position and intensity throughout the Holocene. Nevertheless it is necessary to distinguish the effects of this warmer, salty, and high velocity bottom current influence on the sediment productivity signal.

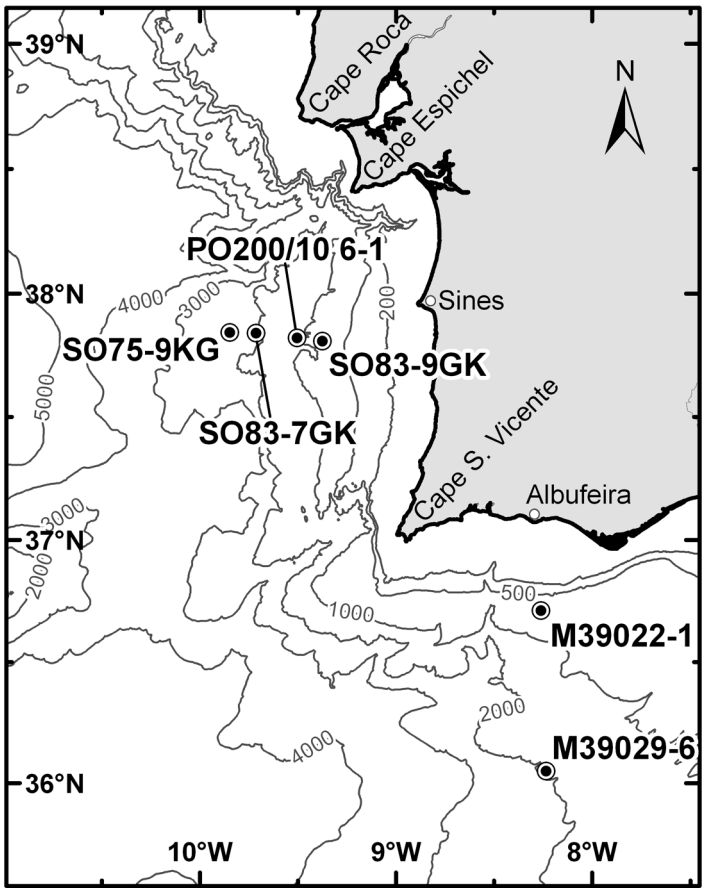

Fig. 1 Geographical distribution of the 6 box-multi-cores used in this study and listed in Table 1. Depth contours drawn are 200 and 500 m and then every 1000 m between 1000 and 5000 m. Capes mentioned in the text are also indicated.

Table 1 Detailed information on the 6 box-multi-cores used in this study including geographical position, water depth, core length, cruise and sampling device.

Sample ID	Longitude (ºW)	Latitude (ºN)	Water Depth (m)	Core length (cm)	Cruise Name	Cruise Year	Device
SO75-09KG	-9.8467	37.8433	2331	24	SONNE75	1991	box-corer
SO83-07GK	-9.7117	37.8400	2010	39	SONNE83	1992	box-corer
PO200/10 6-1	-9.5033	37.8217	1085	51	POSEIDON 200-10	1993	box-corer
SO83-9GK	-9.3733	37.8083	900	39	SONNE83	1992	box-corer
M39022-1	-8.2599	36.7117	667	38	METEOR 39/1	1997	box-corer
M39029-6	-8.2333	36.0497	1918	33	METEOR 39/1	1997	multi-corer

3.2. Oceanographic Setting

The surface circulation off the SW Portuguese margin is related to strong seasonality in the wind system, which show reversing patterns between summer and winter mainly due the annual cycle of the atmospheric systems (e.g. Fiúza, 1984). From May to September,

coastal upwelling occurs at the west coast due to the strong northerly winds (Portuguese Trade winds) blowing nearly parallel to the coast and associated with the northward displacement of the Azores High and the weakening of the Iceland Low-pressure cell (Wooster et al., 1976; Fiúza et al., 1982; Fiúza, 1984). Cold nutrient–rich upwelled water is transported southwards by the Portugal Coastal Current (PCC), a fast flowing branch of the southward Portugal Current (PC), that flows close to the west coast (Fiúza, 1984). However, along the south coast, the summer wind pattern is affected by the establishment of a low pressure center of thermal origin over the Iberian Peninsula, which causes westerly wind off southern Portugal and induces local upwelling (Fiúza et al., 1998; Relvas and Barton, 2002). Modulated by topographic features like submarine ridges and coastal morphologic capes, filaments or plumes of cold water and high pigment concentrations (e.g., Fiúza, 1984; Sousa and Bricaud, 1992; Haynes et al., 1993) are observed in our study area off Cape Roca to Espichel, Cape Sines and Cape São Vicente (Fig. 1). Waters upwelled off Cape São Vicente can flow around the cape and then continue further to the east over the shelf on the southern coast (e.g., Fiúza et al., 1982). This eastward intrusion of cold water, either deived from the west coast upwelling or from locally induced upwelling, forces the warm surface water body formed on the shallow continental shelf between Faro and Cadiz further to the east and to intrude into the strait of Gibraltar (Sousa and Bricaud, 1992; Folkard et al., 1997).

Especially during winter, coastal convergence conditions prevail under southerly winds that result from the intensification of the Iceland Low associated with a large southward displacement of the Azores High-pressure cell, and the most relevant transport mechanism during this period is the poleward Portugal Coastal Countercurrent (PCCC) (Fiúza, 1984; Fiúza et al., 1998). Its subtropical waters originate from the Azores front between 35-36°N, which extends towards the southern Portuguese margin deflecting northward in vicinity of the coast (Peliz et al., 2005). This poleward flow has also been associated with the interaction of the meridional density gradient with the continental slope and shelf (Huthnance, 1984; Peliz et al., 2003).

Below the ocean surface layer (approximately 100 m), along the Portuguese margin flows the Eastern North Atlantic Central Water (ENACW), the source of the upwelled water, with subtropical (ENACWst) or a subpolar origin (ENACWsp), and depending on the wind strength either type can be upwelled. North of Lisbon, however, the importance of the subtropical branch decreases. Thus in our study region the waters are typically of

subtropical origin. The poleward flowing ENACWst, the subsurface component of the PCC, is formed along the Azores front during winter and is lighter, warmer and saltier than the southward flowing ENACWsp branch and contains less nutrients (Fiúza, 1984; Rios et al., 1992; Fiúza et al., 1998).

Deeper in the water column the dominant water masses are the Mediterranean Outflow Water (MOW) and the North Atlantic Deep Water (NADW). The MOW, characterized by high temperatures and salinities (Ambar and Howe, 1979a; Ambar and Fiúza, 1994), flows along the Portuguese margin.Here, the MOW appears divided into two main cores: an upper core centered between 500-800 m and a more saline and denser lower core around 1200 m (Ambar and Howe, 1979a,b; Ambar et al., 2002). The upper core shows a stronger tendency to follow the slope contours along the Portuguese continental margin, while the lower core spreads more northwesterly after passing between Cape São Vicente and the Goringe Bank (Ambar, 1983; Zenk and Armi, 1990). Below the MOW, around 2000 m, the prevailing deep-water masses are controlled by the thermohaline equilibrium between the North Atlantic Deep Water (NADW), with poor stratification and a high oxygen content, and the carbonate corrosive Antarctic Bottom Water (AABW) (e.g., Fiúza, 1984).

3.3. Material and methods

The material used in this study was obtained from six box- or multi-cores recovered from two transects: along 37˚ 50´N, off Sines and spanning water depths from 900 to 2331 m (SO83-9GK, PO200/10 6-1, SO83-7GK, SO75-09GK); and along 8˚ 15´W off Albufeira on the Algarve coast at 667 and 1978 m water depth (M39022-1, M39029-6). The cores were recovered during the POSEIDON 200/10, SONNE 75, SONNE 83, and METEOR 39 cruises (Fig. 1, Table 1).

The box-cores were sampled continuously in 2 cm thick intervals and the multi-core from station M39029-6 was sampled in 2 cm of interval resolution in 1 cm thick. Each sediment sample was divided into two sub-sample sets for the different analyses: (1) 2 cc were dried at 40ºC and crushed for the carbonate and carbon content analyses; (2) 8-23 cc were weighted, dried at 40ºC and weighted again to allow dry bulk density calculations. The dried sediment was then dispersed with a 0.005 mol sodium hexametaphosphate

solution and washed with distilled water through a sieve stack of 2 mm, 150 μm, and 63 μm mesh-size for foraminifera assemblage, stable isotope and grain size >63 μm analyses.

Total carbon content was determined with a CHNS-932 LECO Elemental Analyzer at the Marine Geology Laboratory of INETI. Two replicates of dried and homogenized sediment (2 mg) were analyzed per level. The same set of samples was later subjected to combustion for 8 hours through a predefined stepwise increase in temperature up to 400ºC, to remove organic carbon and re-analyzed for inorganic carbon. The organic carbon content (C_{org}) was calculated as the difference between total carbon and inorganic carbon concentration. The relative precision of repeated measurements of both samples and standards was 0.03 wt%. The results are presented as Accumulation Rate (AR) calculated for each component as the product of this fraction/weight and the bulk mass accumulation rate (derived from the dry bulk densities and sedimentation rates).

For planktonic and benthic foraminifera quantification and planktonic foraminifera assemblage identification, the fraction 150 μm – 2 mm was split to obtain 300-600 specimens and planktonic foraminifera identified following the taxonomic criteria of Bé and Hamlin (1967), Bé (1977), Kennett and Srinivasan (1983), and Hemleben et al., (1989). After the counting, the relative abundance of each planktonic foraminifera species was calculated. Quantitative abundances of planktonic and benthic foraminifera were transformed into AR by the multiplying the bulk mass accumulation rate by the number of foraminifera per gram of dry sediment, taking into account the weight of the total sample and the number of times that the >150 μm fraction was split prior to the counting procedure.

Stable isotope measurements were performed on planktonic (*Globigerina bulloides*, *Globorotalia inflata*, *Globigerinoides ruber* (white)) and benthic (*Cibicidoides* sp., *Uvigerina* sp.) foraminifera species. Samples contained on average 25 planktonic and 6 benthic specimens picked from the fraction >250 μm (mainly between 250 and 350 μm). All samples, except from core PO200/10 6-1, were measured in the Finnigan MAT 252 mass spectrometer of the RCOM of the Bremen University. The $^{18}O/^{16}O$ ratio is reported in δ permil (‰) notation relative to the Vienna Peedee Belemnite (VPDB) standard. Analytical standard deviation is ±0.07 and ±0.05‰ for $\delta^{18}O$ and $\delta^{13}C$, respectively. For core PO200/10 6-1 isotope measurements were performed of the Leibniz laboratory at Kiel University. Duplicate sample analyses give maximal standard deviation of ±0.05‰ for $\delta^{18}O$ and ±0.04‰ for $\delta^{13}C$. In all *Cibicidoides* sp. $\delta^{18}O$ values were corrected by +0.64‰

to be equivalent to the *Uvigerina* sp. data (Shackleton, 1974) and the combination of both species is referred to as benthic $\delta^{18}O$.

The % sand is calculated from the weight of the sand fraction (63 μm to 2 mm) and the dry weight of the respective sample.

Sea surface temperature (SST) reconstruction was derived from 22 taxonomic categories of planktonic foraminifera with the modern analog technique SIMMAX 28 (distance weighted) (Pflaumann et al., 1996; 2003) applied to regional conditions (restrict Iberian margin data base and satellite derived SST) (Salgueiro et al., submitted).

All data presented in this paper will be stored at the World Data Centre MARE (http:/www.wdc-mare.org).

3.4. Chronology

The chronology of each studied core is based on AMS 14C ages that were measured on mono-specific (*Globigerina bulloides*) planktonic foraminifera samples picked from the fraction 250 μm – 2 mm (mainly between 250 and 350 μm). The ages were measured in three different laboratories: the National Ocean Sciences AMS Facility (NOSAMS), Woods Hole Oceanographic Institution, USA (OS code); the AMS 14C Dating Laboratory at University of Aarhus, Denmark (AAR code); and the Leibniz Labor für Altersbestimmung und Isotopenforschung, Christian Albrechts Universität Kiel, Germany (KIA code) (Table 2).

Ages were corrected for a marine reservoir-effect of 400 years according to modern values determined in the area (Bard, 1988; Abrantes et al., 2005) and converted to calendar ages with the INTCAL04 data (Reimer et al., 2004). Calendar ages were calculated considering 1 σ and 2 σ errors (Table 3), for the establishment of the final age model (Fig. 2) for which mostly the interval with the highest probability within the 2 σ range was used. Two of the ages, SO83-7GK (2 cm) and PO200/10 6-1 (2 cm), were not considered because they appear to be too young and too old respectively, relative to the ages for others levels used the construction of the age model. Given the recovery of the water/sediment interface in all cores, the age at the surface (= 0 cm) of each core was set to be equal to the year of core retrieval (Table 1) converted into years BP (Before Present = 1950 AD). All ages mentioned in this text will be calibrated years (yr) BP.

Sedimentation rates (SR) were determined by linear interpolation between all accepted control points and the surface age (Fig. 2). Except for box-core SO83-9GK it was possible to establish lines that fit all accepted control points. For core SO83-9GK we assume the sediment surface to be intact and gave it a higher weight to the surface age as control point. The age offset at 8 cm depth between the current age model and the youngest 2 σ calibration range is 7 years and therefore nearly negligible. In the cores of the Sines profile SR varies between 17.8 and 21.6 cm/ky, except for box-core PO200/10 6-1 where SR increases to 51.6 cm/ky between 1027 - 1260 yr, and decreases to 13.1 cm/ky in the part of the core older than 1260 yr. In the profile off Albufeira the SR is 9.2 cm/ky in core M39029-6 and varies from 7.4 cm/ky to 10.7 cm/ky at 1359 yr in box-core M39022-1. The SR changes in cores, PO200/10 6-1 and M39022-1, located at depths influenced by Mediterranean Outflow Water, might be due to contourite deposits, which will be discussed later in the text.

Table 2 Radiocarbon ages for the box-multi-cores used in this study.

Sample ID (cm)	Lab. code	Planktnic foraminifera species	Reservoir corrected [(a)] ^{14}C age ± 1σ error (yr BP)
SO75-09KG (23 cm)	OS 29454	*G. bulloides*	1200 ± 55
SO83-07GK (2 cm)	OS 30364	*G. bulloides*	-365 ± 60
SO83-07GK (38 cm)	OS 37761	*G. bulloides*	2120 ± 160
PO200/10 6-1 (2 cm)	AAR 2033	*G. bulloides*	855 ± 65
PO200/10 6-1 (19 cm)	AAR 5281	*G. bulloides*	1060 ± 45
PO200/10 6-1 (33 cm)	AAR 5282	*G. bulloides*	1345 ± 50
PO200/10 6-1 (51 cm)	AAR 6801	*G. bulloides*	2569 ± 52
SO83-9GK (8 cm)	OS 29452	*G. bulloides*	465 ± 40
SO83-9GK (20 cm)	OS 30360	*G. bulloides*	910 ± 95
SO83-9GK (30 cm)	OS 29453	*G. bulloides*	1420 ± 45
M39022-1 (15 cm)	KIA 23351	*G. bulloides*	1480 ± 30
M39022-1 (35 cm)	OS 30363	*G. bulloides*	3710 ± 95
M39029-6 (30.5 cm)	OS 30359	*G. bulloides*	3070 ± 85

[(a)] 400 year reservoir correction has been applied.

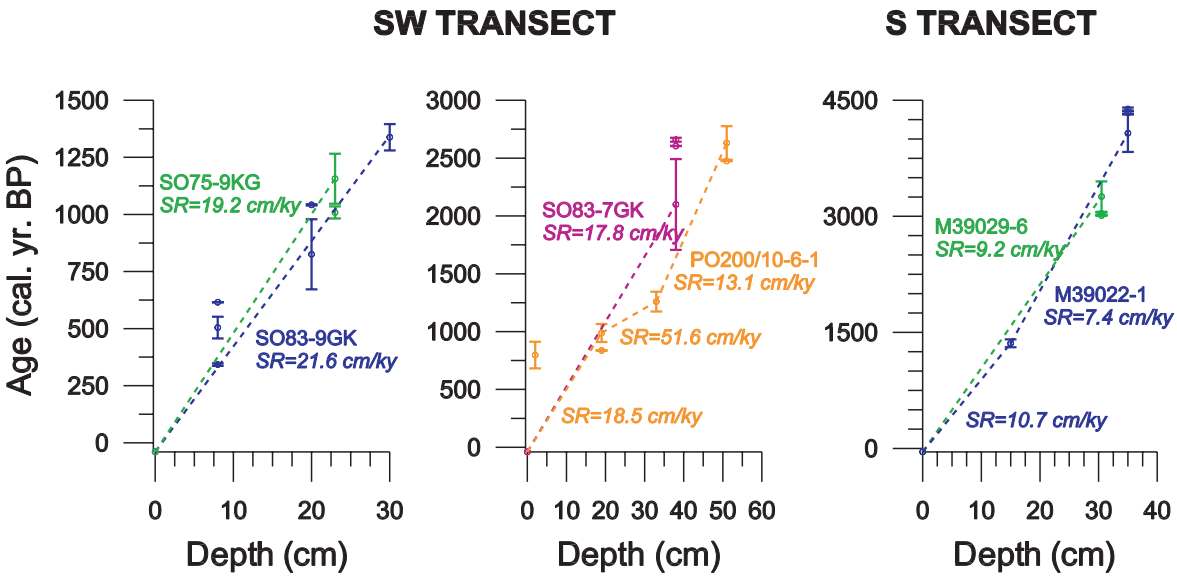

Fig. 2 Age models and sedimentation rates (SR) for 6 box-multi-cores used in this study.

Table 3 Calendar ages with 1 σ and 2 σ errors for the box-multi-cores used in this study.

Sample ID (cm)	1σ Calendar age (yr BP)	1σ Calendar age (yr AD/BC)	2σ Calendar age (yr BP)	2σ Calendar age (yr AD/BC)
SO75-09KG (23 cm)	**1119 ± 61**	**831 ± 61**	**1157 ± 110**	**794 ± 110**
"	1219 ± 10	731 ± 10	1009 ± 27	942 ± 27
SO83-07GK (2 cm)[a]	0	------	0	------
SO83-07GK (38 cm)	**2130 ± 185**	**-180 ± 185**	**2099 ± 392**	**-149 ± 392**
"	1936 ± 2	15 ± 2	2605 ± 2	-655 ± 2
"	------	------	2659 ± 17	-709 ± 17
PO200/10 6-1 (2 cm)[a]	**745 ± 53**	**1206 ± 53**	**797 ± 115**	**1153 ± 115**
"	884 ± 14	1066 ± 14	------	------
"	820 ± 2	1131 ± 2	------	------
PO200/10 6-1 (19 cm)	**959 ± 30**	**992 ± 30**	**988 ± 78**	**962 ± 78**
"	1042 ± 10	909 ± 10	837 ± 2	1113 ± 2
PO200/10 6-1 (33 cm)	**1275 ± 33**	**676 ± 33**	**1260 ± 86**	**691 ± 86**
"	1194 ± 9	756 ± 9	------	------
PO200/10 6-1 (51 cm)	**2727 ± 29**	**-777 ± 29**	**2631 ± 145**	**-681 ± 145**
"	2566 ± 25	-616 ± 25	2475 ± 2	-525 ± 2
"	2626 ± 11	-676 ± 11	------	------
"	2522 ± 4	-572 ± 4	------	------
SO83-9GK (8 cm)	**516 ± 17**	**1435 ± 17**	**505 ± 48**	**1446 ± 48**
"	------	------	343 ± 6	1608 ± 6
"	------	------	616 ± 1	1335 ± 1
SO83-9GK (20 cm)	**838 ± 80**	**1113 ± 80**	**826 ± 154**	**1125 ± 154**
"	749 ± 6	1202 ± 6	1042 ± 3	908 ± 3
SO83-9GK (30 cm)	**1322 ± 28**	**629 ± 28**	**1338 ± 58**	**612 ± 58**
M39022-1 (15 cm)	**1365 ± 28**	**585 ± 28**	**1359 ± 51**	**591 ± 51**
M39022-1 (35 cm)	**4033 ± 125**	**-2083 ± 125**	**4075 ± 243**	**-2125 ± 243**
"	4175 ± 2	-2225 ± 2	4340 ± 17	-2390 ± 17
"	4214 ± 11	-2264 ± 11	4387 ± 20	-2437 ± 20
M39029-6 (30.5 cm)	**3292 ± 91**	**-1342 ± 91**	**3255 ± 196**	**-1305 ± 196**
"	------	------	3010 ± 5	-1060 ± 5
"	------	------	3037 ± 16	-1087 ± 16

Values **in bold** correspond to ages mean of high probability
[a] Ages not considered for the age model

3.5. Results

3.5.1. Southwest transect off Sines (37° 50´N, 900-2331 m water depth)

3.5.1.1. Productivity

Planktonic foraminifera and organic carbon evidence

Along the southwestern Portuguese margin profile *G. bulloides* is the most abundant planktonic foraminifera species in the three shallower cores (SO83-9KG: 900 m depth, PO200/10-6-1: 1085 m depth, SO83-7GK: 2010 m depth), while *G. inflata* is the most abundant species in the deepest, furthest offshore core (SO75-9KG: 2331 m depth). On average, during the last 2000 yr *G. bulloides* abundance decreases seawards from 45% to 23% (Fig. 3a). The nearshore site (SO83-9GK) exhibits higher percentages of *G. bulloides* with values from 34 to 54%, while the percentages at the other 3 sites vary from 10 to 32%. Site PO200/10-6-1 relatively to these 3 sites has a slightly higher (27%) mean value and a more stable record, even though all cores show low variation over time between 2650 and 750 yr. In the two shallowest cores, % *G. bulloides* increases slightly (5-10%) from 750 to 500 yr decreasing to the older values at 300 yr. In the two deepest cores, *G. bulloides* decreases slightly (8%) until 500 yr and rise back up to the older values also at 300 yr. Between 300 yr and the Present the three shallowest cores show an increase of 5-15% until 200 yr while the deepest site (SO75- 9KG) shows a decrease of 17% until 200 yr. All cores display values within a close range at 300 yr and at Present.

C_{org} accumulation rate (AR) (Fig. 3b) along the four sites oscillates between 0.02 to 0.26 g/cm^{2}ky, with mean values close to 0.08 g/cm^{2}ky between 1550-1250 yr and 650-200 yr, and 0.12 g/cm^{2}ky in the remaining time period. The only exception is site PO200/10-6-1 that shows the highest values at the base of the core. High C_{org} AR were kept until 1000 yr decreasing then drastically from 0.26 to 0.09 g/cm^{2}ky and then staying more or less constant until the present. The other cores reveal high variability between 650-200 yr, whereby core SO83-7KG shows always the lowest C_{org} AR.

All records show mean C/N values of 3 between 1250-1550 yr and 650-200 yr, and of 4 during the remaining period (Fig. 3c).

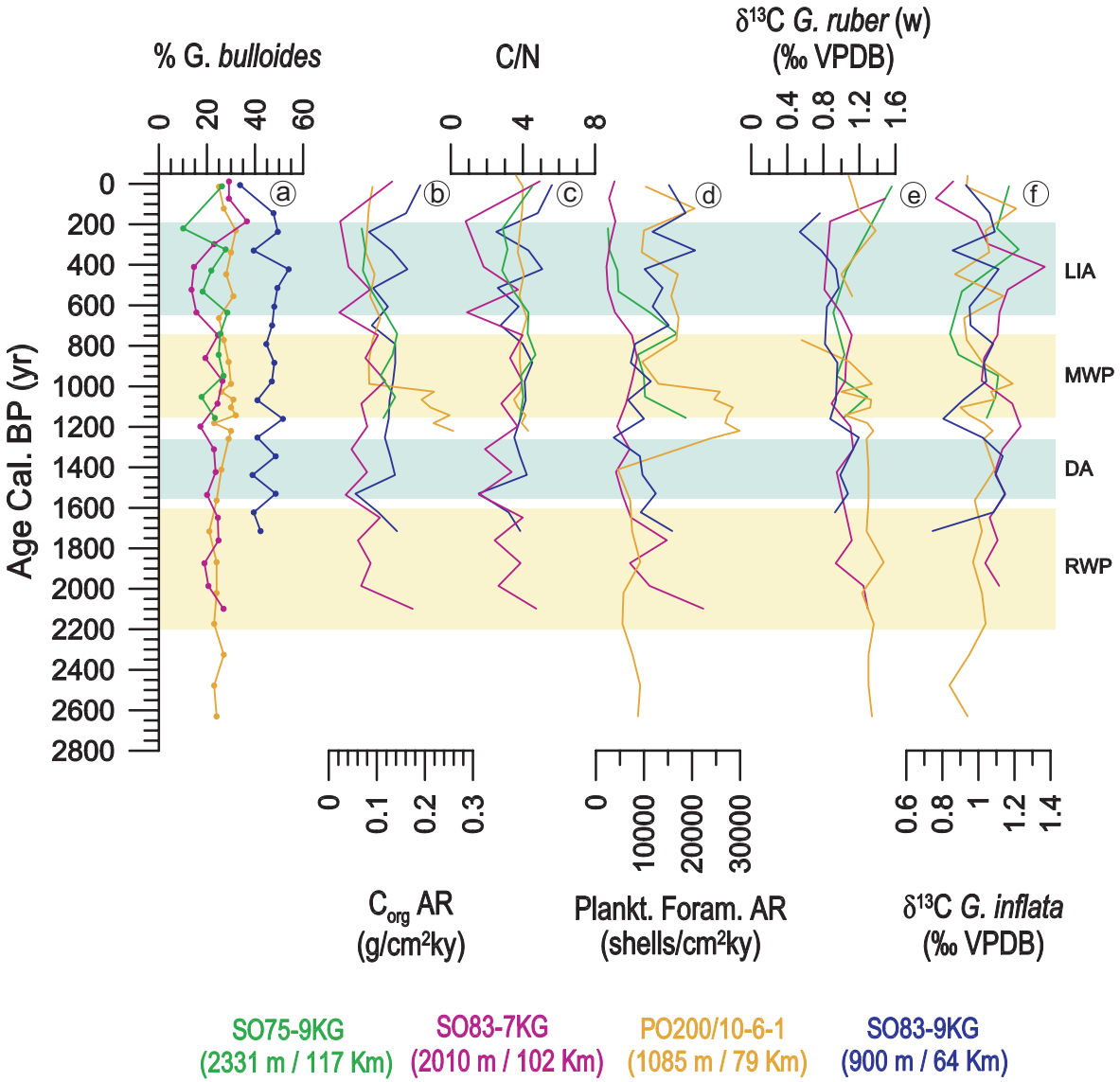

Fig. 3 Comparison of planktonic foraminifera and organic productivity indicators from southwest transect off Sines: a) % *G. bulloides*; b) C_{org} accumulation rate (AR); c) C/N; d) planktonic foraminifera AR; e) $\delta^{13}C$ *G. ruber* (white); f) $\delta^{13}C$ *G. inflata*. The major warm European North Atlantic periods (yellow bands), Roman Warm Period (RWP) and Medieval Warm Period (MWP), and the cold periods (light green bands), Dark Ages (DA) and Litle Ice Age (LIA) of the latest Holocene were based in recent works in the region (Lebreiro et al., in press and Desprat et al., 2003).

In general, the four sites display a low variation with similar values of planktonic foraminifera AR around 9000 shells/cm^{2}ky until 750 yr (Fig. 3d). Core PO200/10-6-1, however, has an abrupt increase in planktonic foraminifera to 30000 shells/cm^{2}ky between 1400-1000 yr. At site SO83-7KG planktonic foraminifera AR decreases between 2100 and 1900 yr and at site SO75-9GK between 1150-1075 yr to the average values of 22000 and 19000 shells/cm^{2}ky, respectively. From 750 to 150 yr planktonic foraminifera AR at sites

SO83-9GK and PO200/10-6-1 varied between 6700 and 14000 shells/cm^{2}ky, and 9600 and 14000 shells/cm^{2}ky, respectively. While at sites SO83-7KG and SO75-9GK planktonic foraminifera AR fall to mean values of 4000 shells/cm^{2}ky.

Carbon isotope values for *G. ruber* (white) fluctuate between 0.5 and 1.6‰ throughout time along the transect (Fig. 3e). Similar values among the sites are observed until 600 yr, with mean values of 1.2‰ until 1250 yr and 1‰ between 1250 and 600 yr. Between 600 and 200yr, higher amplitude variations in *G. ruber* (white) $\delta^{13}C$ are seen in all cores, and with the exception of PO200/10-6-1, which shows values similar to SO75-9KG, the values increase from the shallowest to the deepest site.

Carbon isotope values of *G.inflata*, show similar values for all sites with a mean value of 1.0‰ (Fig. 3f).

Benthic foraminifera evidence

The benthic foraminifera accumulation rate decreases from the site closest to the coast to the open ocean (Fig. 4a); with exception for the interval between 1400-1000 yr when PO200/10-6-1 exhibits higher values than SO83-9KG. While the AR varies through time in cores SO83-9KG and PO200/10-6-1, the SO83-7KG and SO75-9GK records show similar and nearly constant values. From 2650 to 850 yr benthic foraminifera AR oscillates between 800 (SO83-9KG) and 250 shells/cm^{2}ky (SO75-9GK), with the exception of core PO200/10-6-1 where it reaches 2000 shells/cm^{2}ky between 1400 and 1000 yr. From 850 yr until the present the deepest sites, SO83-7KG and SO75-9GK, have constant values of 250 and 350 shells/cm^{2}ky. The PO200/10-6-1 record has a mean of 900 shells/cm^{2}ky, with a slight increase to 1200 shells/cm^{2}ky at 750 and 150 yr. Core SO83-9GK's data gradually increases from 3500 to 16000 shells/cm^{2}ky.

Cibicidoides sp. and *Uvigerina* sp. $\delta^{13}C$ display average values of 1.1‰ and 0.3‰, respectively, at the two shallower sites and 0.7‰ and –0.2‰, respectively, at the deeper sites (Fig. 4b,c). $\Delta\ \delta^{13}C$ *Cibicidoides* sp. - *Uvigerina* sp. oscillates between 0.5 and 1.3‰, with 0.7‰ as an average in the shallower cores, in particular SO83-9KG, and with 1.0‰ in the deeper cores, especially SO83-7KG (Fig. 4d).

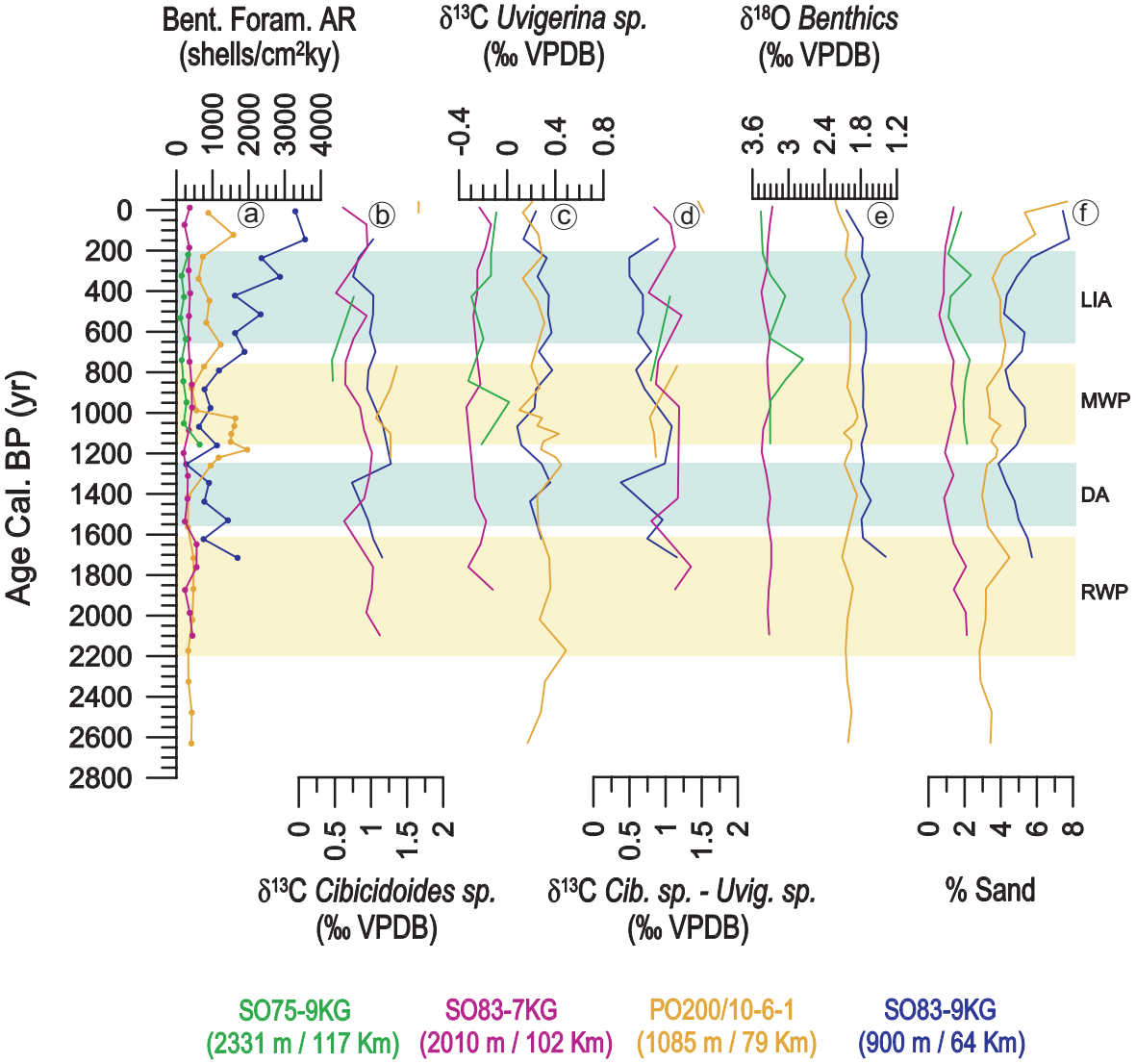

Fig. 4 Comparison of benthic foraminifera and textural indicators from southwest transect off Sines: a) benthic foraminifera AR; b) $\delta^{13}C$ *Cibicidoides* sp.; c) $\delta^{13}C$ *Uvigerina* sp.; d) $\Delta\ \delta^{13}C$ benthics; e) $\delta^{18}O$ benthics; f) % sand. The major warm European North Atlantic periods (yellow bands), Roman Warm Period (RWP) and Medieval Warm Period (MWP), and the cold periods (light green bands), Dark Ages (DA) and Litle Ice Age (LIA) of the latest Holocene were based in recent works in the region (Lebreiro et al., in press and Desprat et al., 2003).

3.5.1.2. Hydrography

Planktonic foraminifera evidence

The relative abundance of *G. inflata*, the most abundant species over time at the deepest core site, varies within the four studied cores between 7 – 33% (Fig. 5a). The two shallower cores, SO83-9KG and PO200/10-6-1, exhibit low downcore variability with mean values of 10-20%, respectively. Site SO83-7KG and SO75-9GK, on the other hand,

experience small changes only until 750 yr and then show an increase up to 33% at 400 yr and 200 yr, respectively.

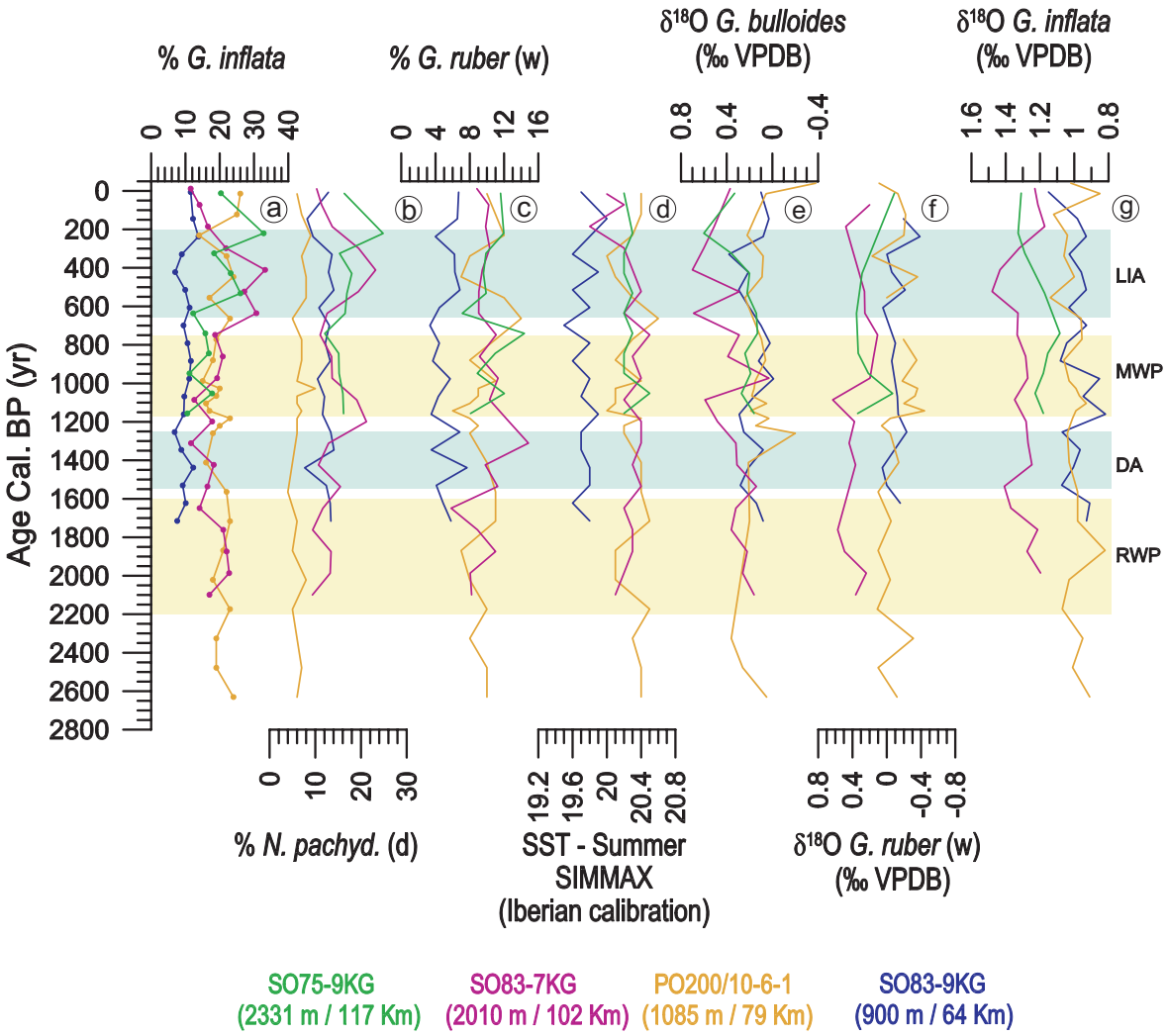

Fig. 5 Comparison of planktonic foraminifera hydrographic indicators from southwest transect off Sines: a) % *G. inflata*; b) % *N. pachyderma* (dextral); c) % *G. ruber* (white); d) transfer function derived sea surface temperature (SST); e) $\delta^{18}O$ *G. bulloides*; f) $\delta^{18}O$ *G. ruber* (white); g) $\delta^{18}O$ *G. inflata*. The major warm European North Atlantic periods (yellow bands), Roman Warm Period (RWP) and Medieval Warm Period (MWP), and the cold periods (light green bands), Dark Ages (DA) and Litle Ice Age (LIA) of the latest Holocene were based in recent works in the region (Lebreiro et al., in press and Desprat et al., 2003).

The percentage of *N. pachyderma* (dextral) along this transect fluctuates between 4 and 24%. Site PO200/10-6-1 has the lowest percentage (mean of 7%) during the studied interval (Fig. 5b). In general, the remaining cores show similar trends with an increase (on average 12 – 16%) of this species from the shallowest to the deepest site. These three records reveal high values (20 – 25%) around 1200 and between 650-200 yr.

The other important species at the southwestern Portuguese margin is *G. ruber* (white). This species displays a clear difference of downcore relative abundance between site SO83-9KG (values around 5%), closest to the coast, and the other sites (values around 10%) (Fig. 5c). In addition, the three deeper sites show a slight increase between 1600 and 750 yr.

Satellite-derived SST integrated over an 18 year period for summer show gradual increase from the coast to offshore of 19.7, 19.9, 20.2, 20.4ºC, to four sites. Summer sea surface temperature (SST) estimated with SIMMAX from the planktonic foraminifera assemblage shows similar range of values from 19.5 to 20.5ºC (Fig. 5d). The core closest to the coast always exhibits colder temperatures around 19.7ºC, like at Present-day, while the remaining cores have average temperatures around 20.3ºC, and no thermal gradient between them is observed.

Planktonic foraminifera oxygen isotope values exhibit lighter values for SO83-9KG and PO200/10-6-1 than for SO83-7KG and SO75-9GK (Fig. 5e, f and g). $\delta^{18}O$ *G. bulloides* values oscillate between –0.4 and 0.4‰ nearshore with mean values close to 0.2‰ between 1250-1550 yr and between 650-200 yr, and 0.1‰ in the remaining time period, while in the two deeper cores $\delta^{18}O$ *G. bulloides* values become heavier, on average close to 0.3‰, but varying between 0.1 and 0.7‰ (Fig. 5e). $\delta^{18}O$ *G. ruber* (white) and $\delta^{18}O$ *G. inflata* show similar trends with values around -0.15 and 1‰, respectively in the shallower cores (SO83-9KG, PO200/10-6-1) and 0.3 and 1.3‰ for the deeper cores (SO83-7KG, SO75-9GK) (Fig. 5f and g).

Benthic foraminifera and grain size evidence

The benthic foraminifera $\delta^{18}O$ records of the four sites from the southwestern profile show constant and similar values in the two shallower cores as well as in the two deeper ones (Fig.4e). The shallower sites have lighter values of about 1.9‰ than the deeper sites with values around 3.3‰. While the values are fairly constant through time at site SO83-7KG, the deepest site (SO75-9KG) experienced some oscillation between 950-200 yr with somewhat lighter values, 2.8‰ to 3.1‰ at 750 yr and 400 yr, respectively.

All cores display a low percentage (1-8%) of sand, which consists purely of foraminifera (Fig.4f). The shallower cores SO83-9KG and PO200/10-6-1 display a similar trend until 500 yr (5%) and 200 yr (4%), respectively, and an increase to values close to

8% afterwards. The deepest cores record lower percentages of sand with values of about 2% downcore.

3.5.2. South transect off Albufeira (8° 15´W, 667-1978 m water depth)

3.5.2.1. Productivity

Planktonic foraminifera and organic carbon evidence

Along the southern Portuguese margin profile *G. bulloides* is also the most abundant planktonic foraminifera species within the core closer to the coast (M39022-1; 667 m depth), while *G. ruber* (white) is the most abundant species in the open ocean core (M39029-6; 1978 m depth). At core M39022-1 *G. bulloides* percentages are on average 36%, while in core M39029-6 has on average a relative abundance of 13% (Fig. 6a). The later, offshore core also shows lower variability throughout. The nearshore core, on the other hand, reveals an abundance increase (reaching 46-50%) between 1600-1250 yr and between 650 yr and the Present.

The C_{org} AR (Fig. 6b) fluctuates between 0.03 and 0.09 g/cm^{2}ky in both cores with values around 0.05 g/cm^{2}ky until 1600 yr and 0.06 g/cm^{2}ky between 1600 yr and the Present, but M39022-1 has two maxima between 1400-1150 yr and 650-400 yr. For both sites C/N varies from 3 to 10, but shows mean values of 5 and 6 in the periods prior and after 1600 yr, respectively (Fig. 6c).

For M39022-1, the planktonic foraminifera AR exhibits large variation between 3500 and 650 yr ranging from 13000 to 67000 shells/cm^{2}ky, while the remaining time show values close to 13000 shells/cm^{2}ky. The highest peaks with 67000 shells/cm^{2}ky occur around 2700 yr and between 1600 and 1350 yr, while two smaller maxima (33000 and 39000 shells/cm^{2}ky) are observed at 3260 and 1000 yr, respectively. In contrast, the planktonic foraminifera AR in core M39029-6 has downcore values of around 12500 shells/cm^{2}ky downcore (Fig. 6d).

The δ^{13}C of *G. ruber* (white) shows similar values for both sites (close to 1.2‰) with a small deviation of plus 0.5‰ at site M39029-6 between 3500 and 2700 yr and 750 to Present (Fig. 6e). Contrarily the δ^{13}C of *G. inflata* exhibits large variations between 0.8 and 1.2‰ during the studied intervals in both cores (Fig. 6f).

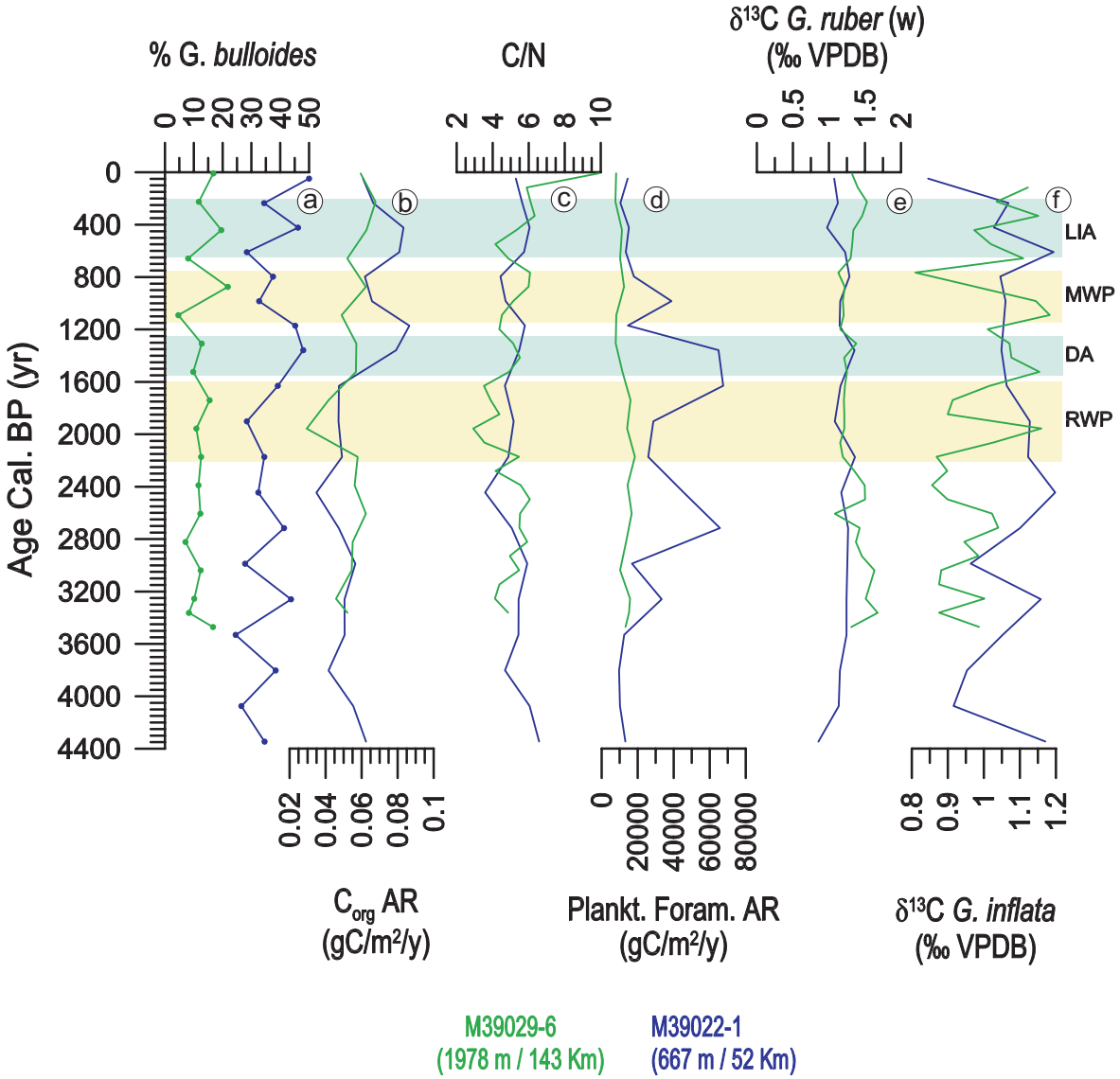

Fig. 6 Comparison of planktonic foraminifera and organic productivity indicators from south transect off Albufeira: a) % *G. bulloides*; b) C_{org} accumulation rate (AR); c) C/N; d) planktonic foraminifera AR; e) $\delta^{13}C$ *G. ruber* (white); f) $\delta^{13}C$ *G. inflata*. The major warm European North Atlantic periods (yellow bands), Roman Warm Period (RWP) and Medieval Warm Period (MWP), and the cold periods (light green bands), Dark Ages (DA) and Litle Ice Age (LIA) of the latest Holocene were based in recent works in the region (Lebreiro et al., in press and Desprat et al., 2003).

Benthic foraminifera evidence

Benthic foraminifera AR (Fig. 7a) display a similar trend to the planktonic foraminifera AR for both cores, but differ in absolute values. For M39022-1, benthic foraminifera AR varies between 3500 and 750 yr, from 1900 to 9500 shells/cm^{2}ky, with four relevant peaks: around 3260 yr (5000 shells/cm^{2}ky), 2700 yr (7600 shells/cm^{2}ky), 1350 yr (9500 shells/cm^{2}ky), and 1000 yr (7800 shells/cm^{2}ky). The remaining time

intervals have low variability around 1900 shells/cm^{2}ky. M39029-6 has low values of 200 shells/cm^{2}ky throughout the whole sequence (Fig. 7a).

δ^{13}C of *Cibicidoides* sp. and of *Uvigerina* sp. are generally higher at the shallower site (Fig.7b, c). The mean values of δ^{13}C *Cibicidoides* sp. are 1.26 and 0.84‰ for cores M39022-1 and M39029-6, respectively, while the mean values of δ^{13}C *Uvigerina* sp. are 0.46 and 0.2‰, respectively. Δ δ^{13}C *Cibicidoides* sp. - *Uvigerina* sp. fluctuates between 0.0 and 1.3‰ for core M39022-1, and between 0.4 and 0.9‰ in core M39029-6. Between 1200 and 400 yr, both sites show similar values.

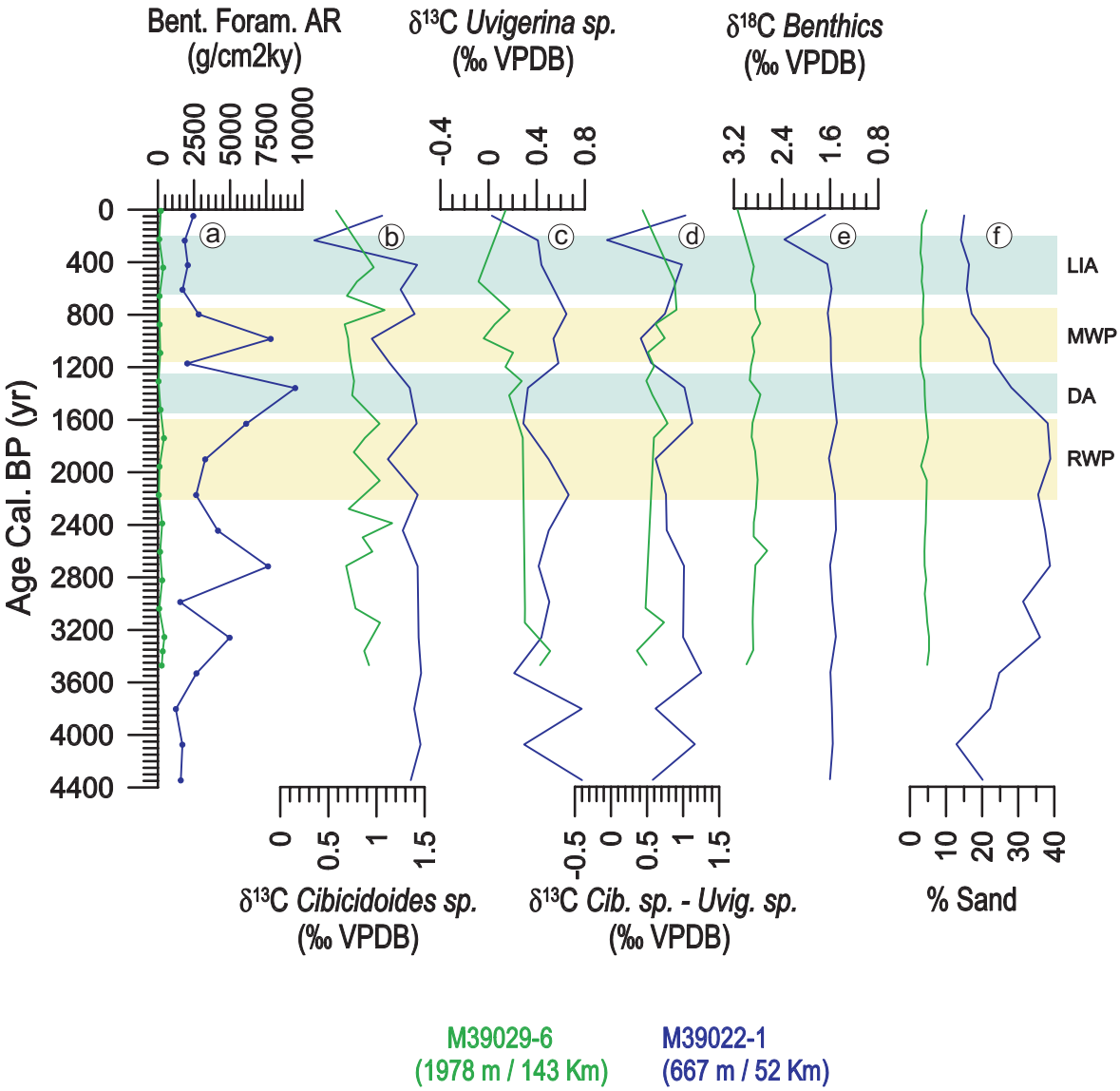

Fig. 7 Comparison of benthic foraminifera and textural indicators from south transect off Albufeira: a) benthic foraminifera AR; b) δ^{13}C *Cibicidoides* sp.; c) δ^{13}C *Uvigerina* sp.; d) Δ δ^{13}C benthics; e) δ^{18}O benthics; f) % sand. The major warm European North Atlantic periods (yellow bands), Roman Warm Period (RWP) and Medieval Warm Period (MWP), and the cold periods (light green bands), Dark Ages (DA) and Litle Ice Age (LIA) of the latest Holocene were based in recent works in the region (Lebreiro et al., in press and Desprat et al., 2003).

3.5.2.2. Hydrography

Planktonic foraminifera evidence

The relative abundance of *G. inflata* displays similar trends and values over time in the two studied cores with percentages ranging between 6 and 14%. Both cores show lower values during 3800-3000 yr and 1550-1250 yr intervals (Fig. 8a).

The shallow core, M39022-1 has higher percentages of *N. pachyderma* (dextral), with a mean value of 8% while at the deeper core, M39029-6, the mean value is 4%. At site M39022-1, % *N. pachyderma* (dextral) shows values lower than the mean between 4400 and 3800 yr and during the last 650 yr (Fig. 8b).

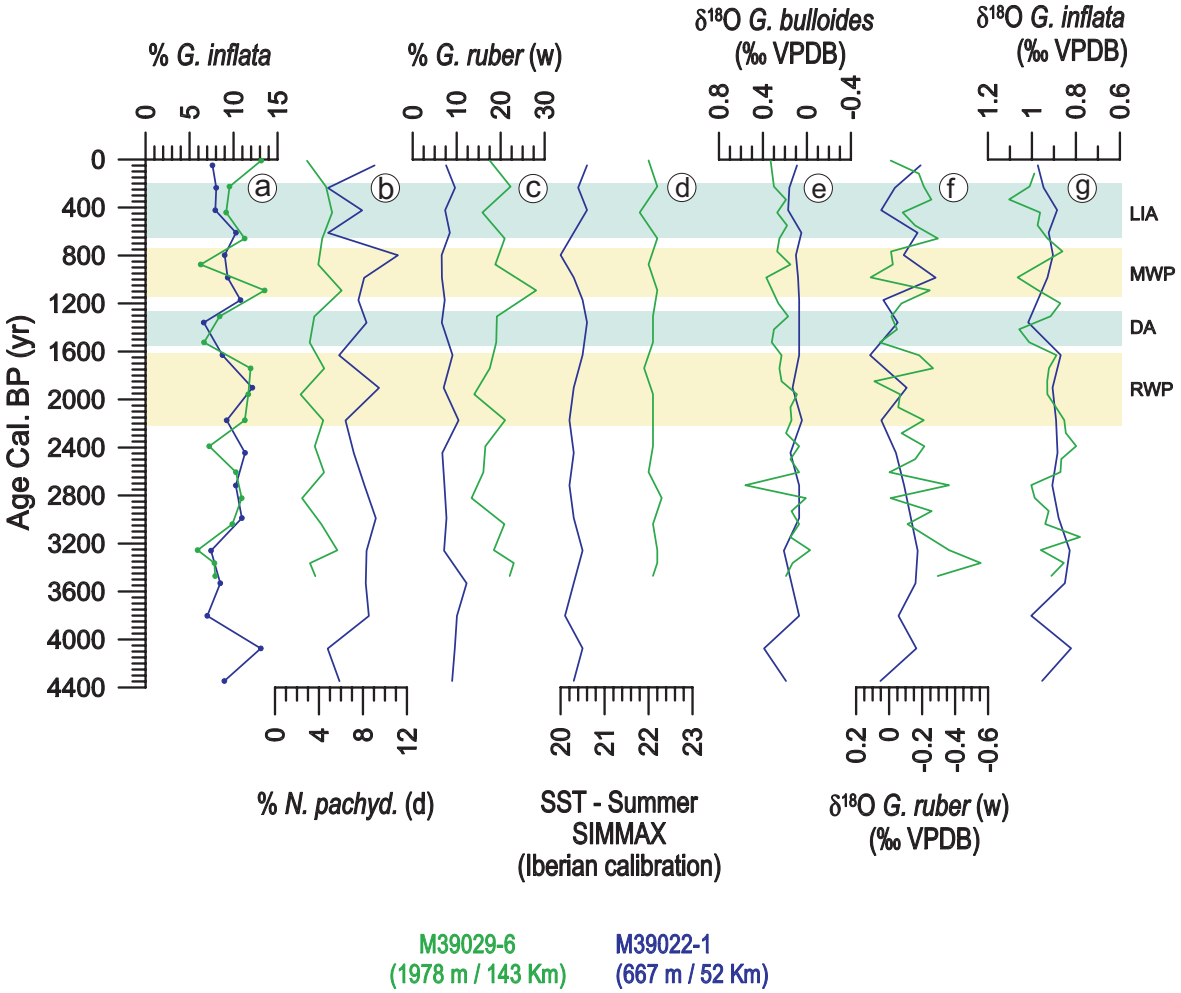

Fig. 8 Comparison of planktonic foraminifera hydrographic indicators from south transect off Albufeira: a) % *G. inflata*; b) % *N. pachyderma* (dextral); c) % *G. ruber* (white); d) transfer function derived sea surface temperature (SST); e) $\delta^{18}O$ *G. bulloides*; f) $\delta^{18}O$ *G. ruber* (white); g) $\delta^{18}O$ *G. inflata*. The major warm European North Atlantic periods (yellow bands), Roman Warm Period (RWP) and Medieval Warm Period (MWP), and the cold periods (light green bands), Dark Ages (DA) and Litle Ice Age (LIA) of the latest Holocene were based in recent works in the region (Lebreiro et al., in press and Desprat et al., 2003).

G. ruber (white), the most abundant species throughout time in the deep core, varies between 7 and 12 % in core M39022-1, and between 13 and 28% in core M39029-6 (Fig. 8c).

Satellite-derived summer sea surface temperature (SST) integrated over an 18 year period for summer show corresponding SSTs of 21ºC and 22.3ºC to M39022-1 and M39029-6, respectively. Simmax estimated SST exhibit values close to modern ones with low variability around 20.4ºC at the near coast site and increase to 22.1 °C offshore (Fig. 8d).

Planktonic foraminifera oxygen isotope data display similar values for both sites (Fig. 8e, f. g). However, $\delta^{18}O$ *G. bulloides* is heavier by 0.1‰ at site M39029-6 relatively to M39022-1 for the last 1600 yr core (Fig. 8e). After 1600 yr, $\delta^{18}O$ *G. ruber* (white) increase from values of –0.2 and –0.5‰ to values of 0.0‰ (Fig. 8f). $\delta^{18}O$ *G. inflata* ranges between 0.8 and 1.0‰ in the shallow core, and between 0.8 and 1.1‰ in the deep site (Fig. 8g).

Benthic foraminifera and Grain size evidence

The benthic foraminifera $\delta^{18}O$ records of the two cores of the southern profile show comparable values, but with lighter values (around 1.6‰) at the shallower site than at the deeper site (around 2.9‰) (Fig.7e).

The site closer to the coast exhibits higher percentages of sand content (purely foraminifera; 13-39%) than the open ocean core (3-5%) (Fig.7f). Sand content increases within core M39022-1 from 17% to 39% between 3500 and 750 yr.

3.6. Discussion

The sediment cores along the southwestern profile off Sines (37˚ 50´N, 900-2331 m water depth) are presently under the influence of the prominent and recurrent southern coastal upwelling band and the Cape Roca and Espichel upwelling filaments that develop along the Portuguese margin during summer, as evidenced by satellite sea surface temperature and chlorophyll pigment pictures (e.g., Fiúza, 1983; Sousa and Bricaud, 1992). During the winter season all southwestern sites are influenced by the warmer, nutrient poor Portugal Coastal Countercurrent (PCCC) (Salgueiro et al., submitted). Sites

SO83-9KG and PO200/10-6-1 have water depths within the MOW influence (Ambar and Howe, 1979a, b; Ambar et al., 2002), while site SO83-7KG and SO75-9KG are bathed by the NADW (Fiúza, 1984).

The hydrography at the south coast profile off Albufeira (8° 15´W, 667-1978 m water depth) is characterized by the presence of a warm coastal countercurrent over the continental shelf. This is interrupted during the summer by local upwelling episodes, which can be strong at times (Relvas and Barton, 2002), and also by the Cape São Vicente filament and upwelling waters displaced from the west coast. During winter months the surface waters at the southern coast derive from the PCCC (Fiúza, 1984; Peliz et al., 2005). Presently, the site closest to the coast (M39022-1) is under the influence of upwelled waters and inside the upper MOW core.

The productivity changes in both transects mainly reflect summer conditions.

3.6.1. Paleoproductivity conditions

On the Portuguese margin particle size and composition of surface sediments are sensitive to the MOW current (Schönfeld, 1997; Abrantes et al., 2001). So to reconstruct the surface paleoproductivity conditions at the southwestern and southern Portuguese margins some of the traditional productivity proxies like organic carbon, planktonic and benthic foraminifera accumulation rates (AR) need to be used with caution, because they can be partially affected by changes in the sediment's grain size caused by the MOW actions on bottom sediments. Therefore they cannot be considered as a simple index of paleoproductivity (Abrantes et al., 2001). Benthic $\delta^{13}C$ can also be partly determined by the MOW characteristics, reason why they it should be interpreted more in terms of ventilation changes than as nutrient indicator (Zahn and Sarnthein, 1987; Sierro et al., 1999; Abrantes et al., 2001).

The composition of the planktonic foraminifera assemblage and $\delta^{13}C$ of *G. ruber* (white), however, can be used with confidence because they are independent of the MOW action (Abrantes et al., 2001). An increase in the relative abundance of *G. bulloides* is an indicator of productivity related to coastal upwelling (e.g., Thunell and Sautter, 1992; Ufkes and Zachariasse, 1993; Salgueiro et al., submitted). $\delta^{13}C$ of *G. ruber* (white), becomes more negative during increased upwelling of subsurface waters enriched in ^{12}C

and can therefore be used as a nutrient availability proxy (Ganssen and Sarnthein, 1983; Sarnthein and Winn, 1990; Mortlock et al., 1991). However, previous studies have shown that the interpretation of the stable composition of foraminiferal shells in upwelling areas can be difficult, and often hampered by the dynamic character of such settings (Kroon and Ganssen, 1989; Curry et al., 1992; Thunell and Sautter, 1992).

Bias associated with the Mediterranean Outflow Water

Fictitious increases of productivity due to MOW influence (e.g., contourite layers) are well detected at sites SO83-9GK and PO200/10-6-1 in the southwest transect, and at site M39022-1 in the south by sandy foraminifera-rich layers, a notable excess of the C_{org} AR and a drastic change in the sedimentation rate. Cores SO83-9GK and PO200/10-6-1 show high planktonic and benthic foraminifera AR between ~750 yr and 150 yr coincident with a slight increase in sand percentage (3-4%) during the last 500 yr at the shallowest site and during the last 200 yr at both sites (Fig. 4). PO200/10-6-1 also exhibits high values of C_{org}, planktonic and benthic foraminifera AR during 1400-1000 yr. Planktonic and benthic AR, and sand content also display high values between 3500-750 yr at M39022-1. Three periods reflect high energy bottom current influence and are in the range of the youngest contouritic deposit in the Gulf of Cadiz as reported by several authors (e.g., 0-3000 yr: Faugeres et al., 1994; 2100-4400 yr: Voelker et al., 2006). The higher sand content of the core located off Albufeira may be explained by the fact it experiences a MOW with higher velocities (Schönfeld, 2002), which result in a more efficient winnowing of the finer fraction and in the accumulation of the coarser sediments, i.e. the foraminifera shells, than observed in the cores located off Sines (Schönfeld, 1997; Abrantes et al., 2001). The lower sedimentation rate on the southwest margin also allows for a longer residence time within the upper mixed layer of the near surface sediment and therefore the energy of currents would act longer, producing also a more efficient winnowing of sediment. At the same time more generations of benthic organisms would rework the mixed layer, favouring the winnowing in this margin (Sierro et al., 1999).

Productivity signals during the latest Holocene

Upwelling determines the production patterns along the Portuguese margin (Abrantes and Sancetta, 1985; Abrantes, 1988; Abrantes and Moita, 1999), and the related planktonic foraminifera, *G. bulloides* exhibits a decrease in productivity (~20%) from East to West

along the southwestern transect and North to South along the southern transect (Fig. 3a, 6a), in accordance with the present-day productivity gradient induced by upwelling (e.g., Fiúza, 1983; Fiúza, 1984). In the surface sediments along the margin *G. bulloides* distribution closely matches the upwelling features shown in satellite-derived sea surface temperature and chlorophyll pigment concentration images as well as in the high diatom abundance found both in the surface sediments as in the water column during a typical upwelling period (Sousa and Bricaud, 1992; Abrantes and Moita, 1999; Salgueiro et al., submitted). As such, *G. bulloides* percentage appears as a very reliable upwelling indicator for this region.

Along the southwest transect the higher percentages (45%) of *G. bulloides* throughout core SO83-9GK reflect the upwelled nutrient-rich waters close to the coast, induced by summer upwelling that occurs on the western margin under northerly winds. The two westernmost core locations (SO83-7GK and SO75-9KG), on the other hand, reveal lower percentages on average and a higher temporal variability, a pattern-likely related to the fact that at present above these sites productivity only increases during strong upwelling events and filaments development off the Cape Roca and Espichel. Core PO200/10-6-1's position seems to be at present located at the boundary between the coastal upwelling band and the filaments position, which is likely to have been maintained at all times because it reveals a lower productivity (less percentage) than the nearshore site but higher productivity than the westernmost sites (Fig. 3a). The relative abundance of *G. bulloides* along the southern transect is also higher (nearby 36%) within the nearshore core M39022-1, which seems to indicate a strong influence of the Cape São Vicente filament in conjunction with the southern coastal upwelling (Fiúza, 1983; Relvas and Barton, 2002) (Fig. 6a). The filament is a prominent and frequent feature from late spring until early autumn induced by northerly winds, while coastal upwelling is linked to westerly winds and occurs as short-term episodes in particular in summer.

According to *G. bulloides* evidence C_{org} AR and $\delta^{13}C$ *G. ruber* (white) lower values, which indicate abundant nutrients in the surface water, productivity was higher along the southwestern transect than at the southern transect indicating a continuous stronger upwelling influence on the western margin (Fig. 3, 6). The C_{org} AR, however, is only reliable in those cores outside of the MOW influence, i.e. the deeper sites. C_{org} can be of either marine or continental origin and usually the C/N ratio is the first approach used to distinguish between marine (4-10) and continental (>20) sources of sedimentary organic

matter (Meyers, 1994; 1997). The study's records show mean C/N values of 4 in the southwest transect and of 5 in the southern transect (Fig. 3c, 6c), indicating a marine origin at all sites. However, in sediments that contain low values of total organic carbon, as it is the case in our cores, a progressive masking of the original C/N ratio occurs (Wagner and Dupont, 1999) and hence the results may not be directly interpreted. Thus, caution is also required in the interpretation of the C_{org} AR in the deeper cores, even though they mirror the % *G. bulloides* productivity trends.

Recent studies using satellite imagery show that the frequency of occurrence of upwelling in the south coast is about 50% of the west coast upwelling occurrences (Relvas and Barton, 2002). According to the same authors west coast upwelling is mainly concentrated in the summer months, while in the south coast, upwelling events are more distributed through the year, but most intense and mainly limited to the area immediately to the east of Cape São Vicente. If one looks at the planktonic foraminifera AR (Fig. 3d, 6d) in the deeper sites, however, they exhibit lower values for the transect off Sines than for the one off Albufeira – so contrary to what the upwelling intensity would suggest. An explanation for this could be dilution by fine terrigenous material as indicated by the low sand contents of only 1-2% (Fig. 4f) and the relative high sedimentation rates (Fig. 2).

In general, all used proxies at all cores, excluding those influenced by the MOW, show that considerable temporal productivity changes occurred both off Sines and Albufeira at times contemporary with the widely recognized European climate periods of the Roman Warm Period (RWP), the Dark Ages (DA), the Medieval Warm Period (MWP), and the Little Ice Age (LIA).

Along the southwestern profile, stable upwelling conditions and an increase of productivity during the RWP and MWP, mainly during the last, are indicated by the high percentage of upwelling related planktonic foraminifera species, the C_{org} content and the *G. ruber* (white) carbon isotope values. During the cold periods, the DA and the LIA, the upwelling related proxies show a higher variability with an, on average, decreasing productivity (Fig. 3), and most probably caused by the spatial and/or intensity variations of the Cape Roca and Espichel filaments through time. Recent studies using various productivity proxies (e.g., foraminiferal assemblage, diatoms assemblage, alkenones) in sediment records from the Tagus Prodelta, also under the influence of the Cape Roca and Espichel filaments during the summer, enhanced productivity and warmer surface waters are also indicated for the MWP, while cold and low productivity conditions are indicated

the LIA (Abrantes et al., 2005; Bartels-Jonsdóttir et al., 2006; Gil et al., 2006; Lebreiro et al., in press).

Off the south Portuguese margin, in spite of the lower sedimentation rate relatively to the southwest transect, an opposite trend is observed: the productivity indicators (% *G. bulloides* and C_{org} AR) decreased during the warm periods (RWP and MWP) and increased during the cold periods (DA and LIA) in the upwelling influenced site M39022-1 (Fig. 6). In addition, both southern cores display a change towards higher values of % *G. bulloides*, % *N. pachyderma* (dextral) and C_{org} AR during the last 1600 yr, especially in the nearshore core. These changes could be related to an intensification either of the Cape São Vicente filament or/and of the southern coastal upwelling during the last 1600 yr. A possible explanation for the opposite productivity trends observed in the two transects during the last 2500 yr climatic periods of could be a shift in the intensification and wind direction from northerly winds warm periods to westerly winds during cold periods observed during the different North Atlantic Oscillations (NAO) phases. Warm periods are characterized by a prevalent positive NAO phase, induced strong northerly winds and an increase of upwelling at the southwestern margin, is likely to occur. Concurrently, a dominate negative NAO phase during the cold periods would lead to strong westerly winds and the occurrence of upwelling on the southern Iberian margin.

3.6.2. Paleohydrographic conditions

Surface water conditions

Planktonic foraminifera upwelling related species *G. bulloides* was discussed in detail in the paleoproductivity section (3.6.1) however, this species is also indicative of the relative temperature of the upwelled water. In the sites closer to the coast of both records, SO83-9GK off Sines and M39022-1 off Albufeira, was observed the highest percentage of *G. bulloides*, the coldest SST and the lowest percentage the subtropical species, *G. ruber* (white) (Fig. 3a, 5c and d, 6a, 8c and d). Also colder transfer function derived summer SST´s reflect surface waters nearshore, although 1ºC warmer in the south, that we attribute to the previously described less persistent upwelling along the southern coast.

Another indicator of SST is the $\delta^{18}O$ of planktonic foraminifera. Along the southwest transect the two shallower sites (SO83-9GK, PO200/10-6-1) reveal lighter $\delta^{18}O$ *G.*

bulloides values than the deeper sites (SO83-7GK and SO75-9KG), that is warmer or less saline waters, contrarily to the expected (Fig. 5e). Two possible explanations can be advanced, the first hypothesis is based in the pronounced migration of *G. bulloides* from below the thermocline prior to upwelling to the surface during the upwelling (Thunell and Sautter, 1992). The reconstruction of calcification temperatures in the NW Arabian Sea (SW monsoon upwelling area) suggest that most of the calcite is precipitated at a depth level just below the deep chlorophyll maximum, but above the main thermocline. Consequently, the average calcification temperature of *G. bulloides* is lower than the SST (Peeters et al., 2002), which in our area could be the case in the two nearshore cores. The second hypothesis is based on the persistent presence of a warm water intrusion observed in summer satellite images off Sines. Such intrusion interspersed between the cool coastal and offshore waters may influence sites SO83-9GK, PO200/10-6-1, while sites SO83-7GK and SO75-9KG are still influenced by the offshore cold waters. This intrusion may either correspond to an anticyclonic eddy or, more probably, a result of the offshore southward advection of waters upwelled further north (Fiúza, 1983; P. Oliveira, personal communication 2003). As the shallow site in the southern transect also exhibits lighter $\delta^{18}O$ values for *G. bulloides* after the productivity increase around 1600 yr than recorded at the offshore site (Fig. 8e), the first hypothesis is considered the most probable.

The % *N. pachyderma* (dextral) is slightly increased in the two deeper cores of the southwest coast (Fig. 5b), which based on the surface distribution of this species (Salgueiro et al., submitted) seems to be indicative of a more offshore flowing eastern branch of the Portugal current (PC), a descending branch of the North Atlantic Drift. However, the *N. pachyderma* (dextral) has also been associated with upwelling areas (e.g., Thunell and Sautter, 1992; Ufkes and Zachariasse, 1993).

The nearshore core also shows high values of this species, but here the increase seems to result from the temperature of the upwelled water.

The other important superficial current along the study area is the wintertime warm Portugal Coastal Countercurrent (PCCC) that flows eastward along the south coast and northward along the southwest coast (Peliz et al., 2005). In our data this current is mainly characterized by the presence of the surface dwelling subtropical species *G. ruber* (white). High percentages of *G. ruber* (white) and warmer SST, indicate that this current affected the three deeper sites off Sines, with some spatial variations through time (Fig. 5c,d). Off Albufeira higher percentages of this species at the deeper site reflect the PCCC' more

offshore position. A stronger influence of this current during the last ~2000 yr is recorded by an increase in % *G. ruber* (white) at the deeper site and lighter $\delta^{18}O$ *G. ruber* (white) values at both sites (Fig. 8c,f). Thus, beside the probable increase of upwelling during the summer, also an increase in PCCC intensity, during the winter, is observed along the south coast between 2000 and 1600 yr.

G. inflata, a deep dwelling, non-upwelling, transitional and oligotrophic species, is also related to the PC and PCCC (Salgueiro et al., submitted) and is associated with the winter mixed layer. So both *G. ruber* (white) and *G. inflata* are related to the PCCC and reflect the winter hydrographic conditions. The $\delta^{18}O$ values of both species, but especially of *G. inflata*, are lighter in the two shallower than in the deeper cores of the southwestern transect (Fig. 5f,g) in accordance with the modern wintertime circulation pattern. Peliz et al., (2005) mapped a recurrent warm signature in SST satellite images that is likely a nearshore northward recirculation of the PCCC around Cape Sines. This recirculation influences the two cores closer to the coast as evidenced by an increase in the sediment´s coccolithophores abundance at the same position (Abrantes and Moita, 1999). The similar $\delta^{18}O$ differences between *G. ruber* (white) and *G. inflata* along the whole transect can probably be attributed to stable temperature conditions in the waters derived from the Azores front, i.e. the PCCC and the ENACWst upwelling source water, throughout the studied period. In terms of nutrient content the $\delta^{13}C$ values of *G. inflata* exhibit almost constant values downcore, indicating low nutrient variability in the winter mixed layer (ENACWst) (Fig. 3f).

Along the southern transect, $\delta^{18}O$ of *G. inflata* reveals slightly heavier values for both cores during the last ~1600 yr (Fig. 8g), but overall, the data agrees with the observations relative to the winter conditions along the southwest transect. $\delta^{13}C$ of *G. inflata,* however, indicate much more nutrient variations in the Gulf of Cadiz, especially during the last 1600 yr and at the offshore site (Fig. 6f). This seems that Azores front produced water with same SST conditions through time but variable preformed nutrients, variable productivity at the Azores front latitude.

Intermediate and Deep water conditions

The benthic $\delta^{18}O$ values reveal stable conditions in the NADW and MOW throughout the last 2500 yr. The stability, furthermore, indicates that both MOW and NADW must have flowed at the same water depths as today. Also in terms of ventilation

both the deep water and the MOW were fairly consistent through time, whereby the MOW is slightly better ventilated than the NADW in the studied transects. Higher $\Delta\ \delta^{13}C$ are observed within the MOW depth level, reflecting the influence of the higher $\delta^{13}C$ MOW relatively to the NADW (Abrantes et al., 2001). In the southwestern profile, however, this is less obvious due to the continuing entrainment of ENACWst into the MOW and thus the modification of its properties along its way northwards.

3.7. Conclusions

The productivity indicators, % *G. bulloides*, C_{org} AR and $\delta^{13}C$ *G. ruber* (white) values, but the C_{org} AR only reliable in cores outside of the Mediterranean Outflow Water (MOW) influence, show spatial higher productivity along the southwestern transect relatively to the southern transect, what is attributed to the stronger and more persistent upwelling influence on the western Portuguese margin such as at present-day conditions. Considerable temporal productivity changes at both the Sines and Albufeira transects, reflect the widely recognized European climate periods: Roman Warm Period (RWP); Dark Ages (DA); Medieval Warm Period (MWP); Little Ice Age (LIA).

Off Sines during warm periods, in particular the MWP, stable upwelling conditions and increased productivity dominate, while during cold periods, DA and LIA, higher upwelling variability with an average decrease in productivity most probably caused by spatial and temporal variations in the Cape Roca and Espichel filaments intensity. Off Albufeira, opposite trend is observed, with productivity indicators (% *G. bulloides* and C_{org} AR) decreasing during the warm periods (RWP and MWP) and increasing during the cold periods (DA and LIA).

The shift in direction and intensification of the winds observed on the Portuguese margin during the different North Atlantic (NAO) phases could explain our results. During warm periods a prevalent positive NAO phase induced strong northerly winds and an increase of upwelling at the southwestern margin, is likely to occur. While during the cold periods a dominant negative NAO phase would lead to strong westerly winds and the occurrence of upwelling on the southern Iberian margin. However, the southwestern transect shows higher productivity than the southern transect through time, which is attributed to a stronger and more persistent upwelling influence on the western Portuguese

margin such as today. In both transects no other major changes occurred in the hydrographic conditions between warm and cold climatic periods.

Summer cold coastal upwelling waters and wintertime warm waters flowed by the northward Portugal Coastal Countercurrent are at Present the two major currents, and can also be identified from the planktonic foraminifera assemblages and transfer function derived summer temperatures along both transects with similar patterns thought time.

North Atlantic Deep Water and MOW are considered to have flowed during the all time internal considered, at the same water depths as today. The sites influenced by MOW record the youngest reported contourite deposit from Gulf of Cadiz along both transects.

Acknowledgements

We thank Célia Trindade, David Jerónimo, Cremilde Monteiro, Ana Margarida Silva of the Department of Geologia Marinha of INETI for analytical assistance. Susana Lebreiro for helpful data discussions on the early stage of this manuscript. The EU PALEOSTUDIES project supported some foraminifera stable isotopes measurements. Monika Segl is acknowledged for her help with the isotope measurements. This study was funded by "Fundação para a Ciência e a Tecnologia (FCT)" and "Fundo Social Europeu (FSE) no âmbito do III Quadro Comunitário de Apoio" fellowship SFRH/BD/11743/2003, and project INGMAR PLE/4/98. We are also grateful to the Deutsche Forschungsgemeinschaft as part of the DFG-Research Center Ocean Margins (RCOM) at the University of Bremen for technical support.

References

Abrantes, F., and Sancetta, C. (1985). Diatom assemblages in surface sediments reflect coastal upwelling off Southern Portugal. Oceanologica Acta 8, 7-12.

Abrantes, F. (1988). Diatom Assemblages as Upwelling Indicators in Surface Sediments Off Portugal. Marine Geology 85, 15-39.

Abrantes, F., and Moita, M. T. (1999). Water column and recent sediment data on diatoms and coccolithophorids, off Portugal, confirm sediment record of upwelling events. Oceanologica Acta 22, 319-336.

Abrantes, F., Loncaric, N., Moreno, J., Mil-Homens, M., and Pflaumann, U. (2001). Paleoceanographic Conditions along the Portuguese Margin during the Last 30 ka: A Multiple Proxy Study. Comunicações do Instituto Geológico e Mineiro 88, 161-184.

Abrantes, F., Lebreiro, S., Rodrigues, T., Gil, I., Bartels-Jonsdottir, H., Oliveira, P., Kissel, C., and Grimalt, J. O. (2005). Shallow-marine sediment cores record climate variability and earthquake activity off Lisbon (Portugal) for the last 2000 years. Quaternary Science Reviews 24, 2477-2494.

Ambar, I., and Howe, M. R. (1979a). Observations of the Mediterranean Outflow .1. Mixing in the Mediterranean Outflow. Deep-Sea Research Part a-Oceanographic Research Papers 26, 535-554.

Ambar, I., and Howe, M. R. (1979b). Observations of the Mediterranean Outflow .2. Deep Circulation in the Vicinity of the Gulf of Cadiz. Deep-Sea Research Part a-Oceanographic Research Papers 26 A, 555-568.

Ambar, I. (1983). A Shallow Core of Mediterranean Water Off Western Portugal. Deep-Sea Research Part a-Oceanographic Research Papers 30, 677-680.

Ambar, I., and Fiúza, A. F. G. (1994). Some Features of the Portugal Current System: a Poleward Slope Undercurrent, an Upwelling-Related Summer Southward Flow and an Autumn-Winter Poleward Coastal Surface Current. In "Second International Conference on Air-Sea interaction and on Meteorology and Oceanography of the Coastal Zone." (I. Ambar, Ed.), pp. 286-287. American Meteorological Society.

Ambar, I., Serra, N., Brogueira, M. J., Cabecadas, G., Abrantes, F., Freitas, P., Goncalves, C., and Gonzalez, N. (2002). Physical, chemical and sedimentological aspects of the Mediterranean outflow off Iberia. Deep-Sea Research Part Ii-Topical Studies in Oceanography 49, 4163-4177.

Bard, E. (1988). Correction of accelerator mass spectometry 14C ages measured in planktonic foraminifera: Paleoceanographic implications. Paleoceanography 3, 635-645.

Bartels-Jonsdóttir, H. B., Knudsen, K. L., Abrantes, F., Lebreiro, S., and Eiriksson, J. (2006). Climate variability during the last 2000 years in the Tagus Prodelta, western Iberian Margin: Benthic foraminifera and stable isotopes. Marine Micropaleontology 59, 83-103.

Bé, A. W. H., and Hamlin, W. H. (1967). Ecology of recent planktonic foraminifera. Part3: Distribution in the North Atlantic during the summer of 1962. Micropaleontology 13, 87-106.

Bé, A. W. H. (1977). An ecological, zoogeographic and taxonomic review of Recent planktonic foraminifera. In "Oceanic Micropaleontology." (A. T. S. Ramsay, Ed.), pp. 1-100. Academic, San Diego, California.

Bianchi, G. G., McCave, N. (1999). Holocene periodicity in North Atlantic climate and deep-ocean flow south of Iceland. Nature 397, 515-517.

Bond, G., Showers, W., Cheseby, M., Lotti, R., Almasi, P., deMenocal, P., Priore, P., Cullen, H., Hajdas, I., and Bonani, G. (1997). A pervasive millennial-scale cycle in North Atlantic Holocene and glacial climates. Science 278, 1257-1266.

Bond, G., Kromer, B., Beer, J., Muscheler, R., Evans, M. N., Showers, W., Hoffmann, S., Lotti-Bond, R., Hajdas, I., and Bonani, G. (2001). Persistent solar influence on north Atlantic climate during the Holocene. Science 294, 2130-2136.

Broecker, W. S., Sutherland, S., and Peng, T.-H. (1999). A Possible 20th-Century Slowdown of Southern Ocean Deep Water Formation. Nature 286, 1132-1135.

Broecker, W. S. (2001). Paleoclimate - Was the medieval warm period global? Science 291, 1497-1499.

Crowley, T. (2000). Causes of climate change over the past 1000 years. Science 289, 270-277.

Curry, W. B., Ostermann, D. R., Guptha, M. V. S., and Ittekkot, V. (1992). Foraminiferal production and monsoonal upwelling in the Arabian Sea: evidence from sediment traps. In "Upwelling Systems: Evolution Since the Early Miocene." (C. P. Summerhayes, W. L. Prell, and K. C. Emeis, Eds.), pp. 93-106. Geological Society Special Publication.

deMenocal, P., Ortiz, J., Guilderson, T., and Sarnthein, M. (2000). Coherent High- and Low-latitude climate variability during the holocene warm period. Science 288, 2198-2202.

Denton, G. H., and Karlen, W. (1973). Holocene Climatic Variations-Their Pattern and Possible Cause. Quaternary Research 3, 155-205.

Desprat, S., Goni, M. F. S., and Loutre, M. F. (2003). Revealing climatic variability of the last three millennia in northwestern Iberia using pollen influx data. Earth and Planetary Science Letters 213, 63-78.

Diz, P., Frances, G., Pelejero, C., Grimalt, J. O., and Vilas, F. (2002). The last 3000 years in the Ria de Vigo (NW Iberian Margin): climatic and hydrographic signals. Holocene 12, 459-468.

Faugeres, J.-C., Gonthier, E., Monteiro, H., and Vergnaud-Grazzini, C. (1994). Sedimentary records of deep contour currents: an example, the Mediterranean Outflow in the late Quaternary. Comunicações do Instituto Geológico e Mineiro 80, 71-88.

Fiúza, A. F. D., Demacedo, M. E., and Guerreiro, M. R. (1982). Climatological Space and Time Variation of the Portuguese Coastal Upwelling. Oceanologica Acta 5, 31-40.

Fiúza, A. F. G. (1983). Upwelling Patterns off Portugal. In "Coastal Upwelling its sediment record." (E. Suess, and J. Thiede, Eds.), pp. 85-98. Plenum Press, New York.

Fiúza, A. F. G. (1984). "Hidrologia e Dinamica das Aguas Costeiras de Portugal." Faculdade de Ciências da Universidade de Lisboa.

Fiúza, A. F. G., Hamann, M., Ambar, I., Diaz del Rio, G., Gonzalez, N., and Cabanas, J. M. (1998). Water masses and their circulation off western Iberia during May 1993. Deep Sea Research Part I: Oceanographic Research Papers 45, 1127-1160.

Folkard, A. M., Davies, P. A., Fiuza, A. F. G., and Ambar, I. (1997). Remotely sensed sea surface thermal patterns in the Gulf of Cadiz and the Strait of Gibraltar: Variability, correlations, and relationships with the surface wind field. Journal of Geophysical Research-Oceans 102, 5669-5683.

Ganssen, G., and Sarnthein, M. (1983). Stable-isotope composition of foraminifers: the surface and bottom water record of coastal upwelling. In "Coastal upwelling: Its sediment record. PartA: Responses of the sedimentary regime to present coastal upwelling." (E. Suess, and J. Thiede, Eds.), pp. 99-121. Plenum, New York and London.

Gil, I. M., Abrantes, F., and Hebbeln, D. (2006). The North Atlantic Oscillation forcing through the last 2000 years: Spatial variability as revealed by high-resolution marine diatom records from N and SW Europe. Marine Micropaleontology 60, 113-129.

Hass, H. C. (1996). Northern Europe climate variations during the late Holocene: evidence from marine Skagerrak. Palaeogeography, Palaeoclimatology, Palaeoecology 123, 121-145.

Haynes, R., Barton, E., and Pilling, I. (1993). Development, persistence, and variability of upwelling filaments off the Atlantic coast of the Iberian Peninsula. Journal of Geophysical Research 98, 22681-22692.

Hemleben, C., Spindler, M., and Anderson, O. R. (1989). "Modern Planktonic Foraminifera." Springer-Verlang, Berlin.

Hurrell, J. (1995). Deacadal trends in the North Atlantic Oscillation: regional temperatures and precipitation. Science 269, 676-679.

Hurrell, J. W., Kushnir, Y., and Visbeck, M. (2001). The North Atlantic Oscillation. Science 291, 603-605.

Huthnance, J. M. (1984). Slope currents and "JEBAR". Journal Phys. Oceanogr. 14, 795-810.

Jones, P. D., Osborn, T. J., and Briffa, K. R. (2001). The Evolution of Climate Over the Last Millennium. Science 292, 662-667.

Kennett, J. P., and Srinivasan, M. S. (1983). "Neogene planktonic Foraminifera. A phylogenetic atlas." Hutchinson Ross Pulbishing Company, Stroudsburg.

Kroon, D., and Ganssen, G. (1989). Northern Indian Ocean upwelling cells and the stable isotope composition of living planktonic foraminifers. Deep Sea Research 36, 1219-1236.

Lebreiro, S. M., Francés, G., Abrantes, F. F. G., Diz, P., Bartels-Jonsdottir, H., Stroynowski, Z., Gil, I. M., Pena, L., Rodrigues, T., Jones, P., Nombela, M. A., Alejo, I., Briffa, K., Harris, I., and Grimalt, J. O. (in press). Climate change and coastal hydrographic response along the Atlantic Iberian margin (Tagus Prodelta and Muros Ría) during the last two millenia. Holocene.

Meyers, P. (1994). Preservation of elemental and isotopic source identification od sedimentary organic matter. Chemical Geology 114, 289-302.

Meyers, P. (1997). Organic geochemical proxies of paleoceanographic, paleolimnologic, and paleoclimatic processes. Organic Geochemistry 27, 213-250.

Mortlock, R. A., Charles, C. D., Froelich, P. N., Zibello, M. A., Saltzman, J., Hays, J. D., and Burckle, L. H. (1991). Evidence for lower productivity in the Antarctic Ocean during the last glaciation. Science 351, 220-223.

Peeters, F. J. C., Brummer, G.-J. A., and Ganssen, G. (2002). The effect of upwelling on the distribution and stable isotope composition of Globigerina bulloides and Globigerinoides ruber (planktic foraminifera) in modern surface waters of the NW Arabian Sea. Global and Planetary Change 34, 269-291.

Peliz, A., Dubert, J., Haidvogel, D. B., and Le Cann, B. (2003). Generation and unstable evolution of a density-driven Eastern Poleward Current: The Iberian Poleward Current. Journal of Geophysical Research-Oceans 108, 3268, doi: 10.1029/20002JC001443.

Peliz, A., Dubert, J., Santos, A. M. P., Oliveira, P. B., and Le Cann, B. (2005). Winter upper ocean circulation in the Western Iberian Basin - Fronts, Eddies and Poleward Flows: an overview. Deep-Sea Research Part I-Oceanographic Research Papers 52, 621-646.

Pflaumann, U., Duprat, J., Pujol, C., and Labeyrie, L. D. (1996). SIMMAX: A modern analog technique to deduce Atlantic sea surface temperatures from planktonic foraminifera in deep-sea sediments. Paleoceanography 11, 15-35.

Pflaumann, U., Sarnthein, M., Chapman, M., d'Abreu, L., Funnell, B., Huels, M., Kiefer, T., Maslin, M., Schulz, H., Swallow, J., van Kreveld, S., Vautravers, M., Vogelsang, E., and Weinelt, M. (2003). Glacial North Atlantic: Sea-surface conditions reconstructed by GLAMAP 2000. Paleoceanography 18, 1065, doi: 10.1029/2002PA000774.

Reimer, P. J., Baillie, M. G. L., Bard, E., Bayliss, A., Beck, J. W., Bertrand, C. J. H., Blackwell, P. G., Buck, C. E., Burr, G. S., Cutler, K. B., Damon, P. E., Edwards, R. L., Fairbanks, R. G., Friedrich, M., Guilderson, T. P., Hogg, A. G., Hughen, K. A., Kromer, B., McCormac, G., Manning, S., Ramsey, C. B., Reimer, R. W., Remmele, S., Southon, J. R., Stuiver, M., Talamo, S., Taylor, F. W., Plicht, J. v. d., and Weyhenmeyer, C. E. (2004). INTCAL04 Terrestrial Radiocarbon Age calibration, 0–26 cal kyr BP. Radiocarbon 46, 1029 -1058.

Relvas, P., and Barton, E. D. (2002). Mesoscale patterns in the Cape São Vicente (Iberian Peninsula) upwelling region. Journal Geophysical Research 107, 28-1-28-23.

Rios, A. F., Perez, F. F., and Fraga, F. (1992). Water Masses in the Upper and Middle North-Atlantic Ocean East of the Azores. Deep-Sea Research Part a-Oceanographic Research Papers 39, 645-658.

Salgueiro, E., Voelker, A., Abrantes, F., Meggers, H., Pflaumann, U., Loncaric, N., González-Álvarez, R., Oliveira, P., Bartels-Jonsdottir, H., Moreno, J., and Wefer, G. (submitted). Planktonic Foraminifera from Modern Sediments Reflect Upwelling Patterns off Iberia: Insights from a Regional Transfer Function. Marine Micropaleontology.

Sarnthein, M., and Winn, K. (1990). Reconstruction of Low and Middle latitude export productivity, 30,000 years BP to Present: Implications for Global Carbon Reservoirs. In "Proc. of NATO ARCO "Climate-Ocean Interation"." pp. 319-342. Kluwer Academic Publishers.

Schönfeld, J. (1997). The impact of the Mediterranean Outflow Water (MOW) on benthic foraminiferal assemblages and surface sediments at the southern Portuguese continental margin. Marine Micropaleontology 29, 211-236.

Schönfeld, J. (2002). A new benthic foraminiferal proxy for near-bottom current velocities in the Gulf of Cadiz, northeastern Atlantic Ocean. Deep-Sea Research Part I-Oceanographic Research Papers 49, 1853-1875.

Shackleton, N. J. (1974). Attainment of isotopic equilibrium between ocean water and the benthonic foraminifera genus Uvigerina: Isotopic changes in the ocean during the last glacial. In "Les méthodes quantitatives d´étude des variations du climat au cours du Pléistocène." (C. I. d. C.N.R.S., Ed.), pp. 203-209.

Sierro, F. J., Flores, J. A., and Baraza, J. (1999). Late glacial to recent paleoenvironmental changes in the Gulf of Cadiz and formation of sandy contourite layers. Marine Geology 155, 157-172.

Sousa, F. M., and Bricaud, A. (1992). Satellite-Derived phytoplankton pigment structures in the Portuguese Upwelling Area. Journal of Geophysical Research 97, 11,343-11,356.

Stuiver, M., Braziunas, T. F., Grootes, P. M., and Zielinski, G. A. (1997). Is there evidence for solar forcing of climate in the GISP2 oxygen isotope record? Quaternary Research 48, 259-266.

Thunell, R., and Sautter, L. R. (1992). Planktonic foraminiferal faunal and stable isotopic indices of upwelling: a sediment trap study in the San Pedro Basin, Southern California Bight. In "Upwelling Systems: Evolution Since the Early Miocene." (C. P. Summerhayes, W. L. Prell, and K. C. Emeis, Eds.), pp. 77-91. Geological Society Special Publication.

Ufkes, E., and Zachariasse, W.-J. (1993). Origin of coiling differences in living neogloboquadrinids in the Walvis Bay region, off Namibia, southwest Africa. Micropaleontology 39, 283-287.

Visbeck, M. (2002). The ocean's role in Atlantic climate variability. Science 297, 2223-2224.

Voelker, A. H. L., Lebreiro, S. M., Schonfeld, J., Cacho, I., Erlenkeuser, H., and Abrantes, F. (2006). Mediterranean outflow strengthening during northern hemisphere coolings: A salt source for the glacial Atlantic? Earth and Planetary Science Letters 245, 39-55.

Wagner, T., and Dupont, L. M. (1999). Terrestrial Organic Matter in Marine Sediments: Analytical Approaches and Eolian-Marine Records in the Central Equatorial Atlantic. In "Use of Proxies in Paleoceanography: Examples from the South Atlantic." (G. Fischer, and G. Wefer, Eds.), pp. 547-574. Springer-Verlag.

Wooster, W., Bakun, A., and McLain, D. (1976). The seasonal upwelling cycle along the eastern boundary of the North Atlantic. Journal of Marine Research 34, 131-141.

Zahn, R., and Sarnthein, M. (1987). Benthic isotope evidence for changes of the Mediterranean Outflow during the late Quaternary. Paleoceanography 2, 543-559.

Zenk, W., and Armi, L. (1990). The complex spreading pattern of Mediterranean Water off the Portuguese continental slope. Deep-Sea Research 37, 1805-1823.

CHAPTER 4

Temperature and Productivity Changes off the Western Iberian Margin during the last 150 ky

E. Salgueiro [a,c], A. Voelker [a], L. de Abreu [a,b], F. Abrantes [a], H. Meggers [c], G. Wefer [c]

[a] Dept. Geologia Marinha, Instituto Nacional de Engenharia, Tecnologia e Inovação I.P., Alfragide, Portugal;
[b] School of Earth & Ocean Science, National Oceanography Centre, Southampton, UK.
[c] FB Geowissenschaften, Universität Bremen, Bremen, Germany.

Submitted to Quaternary Science Reviews (16 August 2006)

Abstract

Present day hydrographic conditions along the western Iberian margin are characterized by seasonal upwelling with filaments that can penetrate more than 200 km into the open ocean and constitute areas of high productivity. In order to investigate spatial and temporal gradients in temperature and productivity conditions during the last 150 ky, high-resolution proxy records for 3 cores (SU92-03, MD95-2040, MD95-2042), which form a N-S profile along the margin, were generated. In all cores, planktonic foraminifera census counts are used to reconstruct summer sea surface temperature (SST_{su}) and export productivity ($Pexp_{su}$) using the modern analog technique SIMMAX 28. Values similar to the modern SST_{su} and $Pexp_{su}$ are observed throughout the Holocene and Eemian periods for each one of the three sites, indicating fairly stable conditions equivalent to the modern ones. The North - South transect reveals a SST increase of 2-3ºC and a Pexp decrease of 30-40 $gC/m^2/yr$. Glacial periods are characterized by a SST_{su} increase of 3-4ºC from north to south, but no change in $Pexp_{su}$. The northernmost core SU92-03 reveals the coldest conditions with records closer to MD95-2040 than to MD95-2042, the later of which is, as at present, more affected by subtropical waters. Core SU92-03 shows higher interglacial productivity similar to open ocean mid- to high latitude sites, while the other two cores monitor higher glacial productivity conform with other sites from more southern mid-latitude upwelling areas. A boundary between differences in glacial/ interglacial productivity appears to be present in our study between 43º12´N and 40º35´N. Coldest SSTsu and lowest Pexpsu are found during Heinrich events (H)1 – H8 and H10 - H11 at all sites. Only at the southernmost site MD95-2042, less influenced by H, does the lowest $Pexp_{su}$ not coincide with all of these events.

Keywords: Paleotemperatur, Paleoproductivity, Iberian margin, Heinrich events, Foraminifera, Transfer function.

4.1. Introduction

Abrupt and large amplitude climatic changes during the last glacial - interglacial cycle detected in high-resolution paleoclimatic records from Greenland ice cores (e.g., Dansgaard et al., 1993; Grootes et al., 1993) were also found in North Atlantic deep-sea cores including the Iberian margin (Shackleton et al., 2000; de Abreu et al., 2003; Voelker et al., 2006). These millennial-scale abrupt climate oscillations with periodicity of ~ 1500 years (Grootes and Stuiver, 1997) are characterized by Dansgaard-Oeschger (D-O) cycles of interstadial (warm) and stadial (cold) phases. Some stadial phases with intervals 5-10 ky coincide with episodes of extreme iceberg discharges into the North Atlantic, so called the Heinrich events (H) (Heinrich, 1988; Bond et al., 1992; Elliot et al., 1998).

The drastic reduction in both sea surface temperature (SST) and salinity (SSS) during those massive iceberg discharges (Labeyrie et al., 1995; Maslin et al., 1995) led to the reduction or shutdown of North Atlantic Deep Water (NADW) formation (Sarnthein et al., 1994; Oppo and Lehman, 1995; Vidal et al., 1997; Sarnthein et al., 2001; Elliot et al., 2002), and thereby affected the Atlantic's thermohaline circulation. Changes in the thermohaline circulation seem to be directly linked to the D-O cycles and are even thought to be one possible cause for their oscillatory behavior (Boyle, 2000; van Kreveld et al., 2000; Ganopolski and Rahmstorf, 2002; Wunsch, 2003; Kaspi et al., 2004). The recent review by Hemming (2004) of the various mechanisms that have been proposed for the origin of H, however, resulted in the recommendation of additional studies to better understand these episodes.

Even though, the abrupt climatic changes are largely correlated with variations in SST and SSS data, their impacts on ocean productivity (primary and export) are still poorly understood and under discussion. Some studies in North Atlantic within and northward of Ice Rafted Debris (IRD) belt (Ruddiman, 1977) point to an increase in primary productivity associated with lateral shifts of the polar front (Weinelt et al., 2003) and with iceberg discharges (H), possibly associated with sea ice. These are thought to sustain high production due to turbulent mixing, enhanced density stratification, and nutrient input (Sancetta, 1992). However, low productivity was also reported in North Atlantic sediments based on the reduction of foraminifera production during the H, which was linked to the extreme cooling of surface waters or the impediment of light penetration due to icebergs

and sea ice cover (Heinrich, 1988; Bond et al., 1992; Broecker et al., 1992). Recent high-resolution mapping of diatom abundances within the H4 and H1 intervals in the open North Atlantic (Nave, 2005) also reveals a severe decrease of these primary producers, which is especially evident in the western North Atlantic basin where the IRD flux was higher. For the eastern boundary upwelling systems – areas of significant biological productivity – increased productivity contemporary with H was reported based on planktonic foraminifera data from the Iberian margin (Lebreiro et al., 1997; Abrantes et al., 1998) as well as from the edge of the upwelling cells off Northwest Africa (Kiefer, 1998). Low total alkenone concentrations in the upwelling cell off Cape Yubi (NW-Africa), however, indicate decreased coccolithophores production during the stadials of the last 50 ky (Meggers et al., personal communication, 2006). Based on these results, productivity changes associated with different Heinrich events may have been variable depending on the latitudinal position of the polar front and the degree of disturbance of the meridional overturning cell in the North Atlantic.

Upwelling regions constitute one important process of carbon export from the euphotic zone into deep ocean sediments, i.e. the export productivity (Pexp) or "biological pump" (Eppley and Peterson, 1979; Berger and Keir, 1984; Berger et al., 1989). According to (Lampitt et al., 1995), these areas may contribute about 40% to the total marine organic carbon accumulation in sediments. JGOFS (Joint Global Ocean Flux Study) data from the time-series programs near Bermuda and Hawaii and process studies, however, provided evidence that the efficiency of the biological pump is not easily parameterized and differs considerably between sites and within seasons at any given site (Ducklow et al., 2001). The ratio of export to total production varies between 10% and 50%, with highest export efficiency in cold, productive regions and high diatom abundance coinciding with upwelling areas of mid latitudes (Laws et al., 2000; Doney et al., 2001; Moore et al., 2002). Thus, productivity variations in upwelling regions play an important role in global carbon cycling and provide a feedback mechanism to climate change (Broecker, 1982; Sarnthein and Winn, 1988; Berger et al., 1989).

In order to better understand the influence of abrupt climate change, in particular of Heinrich events, on the North Atlantic's eastern boundary upwelling systems, we have investigated hydrography and productivity variations during the last 150 ky BP (kilo year before present) along a N-S transect through the western Iberian upwelling system. At present, the western Iberian coastal upwelling cells mark the northern boundary of the

North Atlantic's upwelling system, but during H the presence of IRD on this margin confirm that floating icebergs and sea ice reached these latitudes and must have affected the upwelling systems off Portugal (Lebreiro et al., 1996; Zahn et al., 1997; Cayre et al., 1999; de Abreu et al., 2003).

While basing our conclusions on results from the N-S core transect, special attention is given to the northernmost core, more likely to be influenced by polar front movements. SST and Pexp reconstructions are derived from planktonic foraminifera census counts and the modern analog technique SIMMAX 28 (Pflaumann et al., 1996; 2003). For the transfer functions the modern analog database for the North Atlantic (Kucera et al., 2005) was increased by 134 surface samples from the Iberian margin allowing a much more accurate reconstruction of the SST (Salgueiro et al., submitted) and productivity variations off western Iberia.

4.2. Oceanographic Settings

The western Iberian margin is located on the eastern edge of the subtropical gyre and modern surface water characteristics are influenced by the southward branch of the North Atlantic Drift (Portugal Current), by the Portugal Coastal Countercurrent (PCC) and by a seasonal (May to September) coastal upwelling regime (Fiúza, 1984). The poleward flowing PCC is the prominent oceanographic feature in winter and has a surface and a subsurface component. Its subtropical waters originate from the Azores front between 35-36°N and can penetrate along the coast all the way up to the Galician margin (e.g., Peliz et al., 2005). Eastern North Atlantic Central Water (ENACW) upwells under the influence of the northerly Portuguese Trade Winds and forms a cold and nutrient-rich water band along the western coast (Fig. 1a, c) (Fiúza, 1984; Fiúza et al., 1998). These bands are generally around 50 km wide (Fiúza, 1983) with offshore extensions, filaments and plumes, mainly in the vicinity of the capes. These filaments and plumes may reach distances of more than 200 km from the coast (Sousa and Bricaud, 1992).

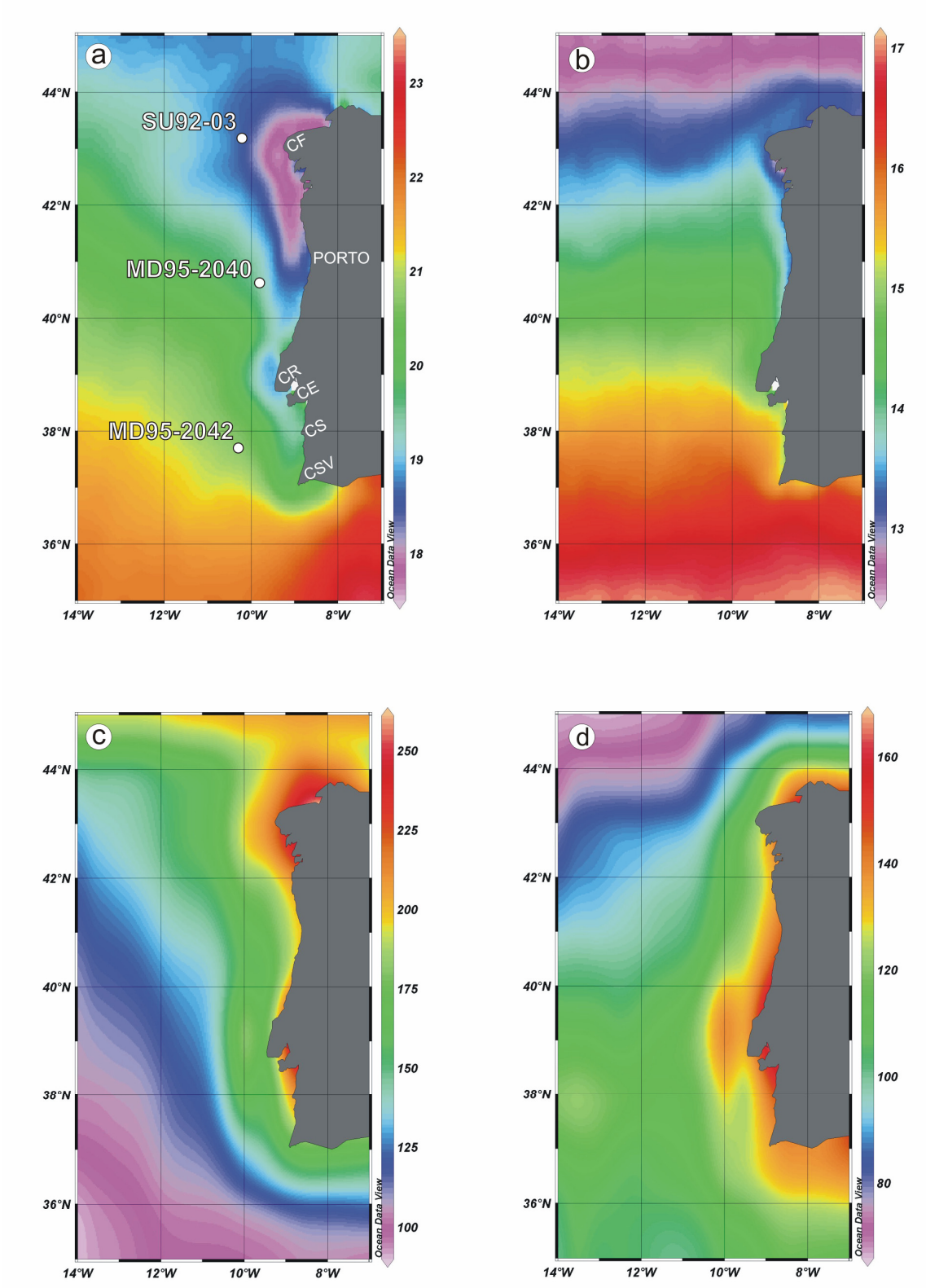

Fig. 1 Sea surface temperature and chlorophyll concentration along the Iberian margin. Mean satellite-derived SST (NOAA: 1985-2003) for summer (a) and for winter (b). Mean satellite primary productivity (PP; 8 years average, (Antoine et al., 1996) for summer (c) and for winter (d). In a) is including the location of the sediment cores used in this study and listed in Table 1. CF: Cape Finisterra; CR: Cape Roca; CE: Cape Espichel; CS: Cape Sines ; CSV: Cape São Vicente. The data was mapped with the Ocean Data View program of (Schlitzer, 2000). Note different scale in all maps.

Table 1 Detail information on the 3 studied cores: SU92-03, MD95-2040, and MD95-2042.

Core	Latitude (N)	Longitude (W)	Water depth (m)	Plank. Foram. $\delta^{18}O$	Bent. Foram. $\delta^{18}O$	Plank. Foram. counts	Detrital Grain counts	Carbonate content	AMS ^{14}C Ages
SU92-03	43º11.75'	10º6.78'	3005	this study	this study	this study	this study	this study	this study
MD95-2040	40º34.91'	9º51.67'	2465	(a)	------	(a)	------	------	(a)
MD95-2042	37º47.99'	10º9.99'	3146	(b)	------	(c)	------	------	(b)

(a) de Abreu et al., (2003); (b) Shackleton and Hall (2000); (c) Cayre et al., (1999)

ENACW, which occupies the depths of the permanent thermocline, has either a subtropical (ENACWst) or a subpolar origin (ENACWsp) and depending on the wind strength either type can be upwelled. The poleward flowing ENACWst, the subsurface component of the PCC, is lighter, relatively warmer and saltier than the southward flowing ENACWsp branch and contains less nutrients. The denser ENACWsp, which flows below the subtropical ENACWst, is formed in the eastern North Atlantic at 46ºN (Fiúza, 1984; Rios et al., 1992; Fiúza et al., 1998) and can penetrate as far south as 30-35°N.

Intermediate depth circulation is dominated by the Mediterranean Outflow Water (MOW), which is characterized by high temperature and salinity (Ambar and Howe, 1979). Below the MOW, around 2000 m, the prevailing deep-water masses are controlled by the thermohaline equilibrium between the North Atlantic Deep Water (NADW), with low stratification and a high oxygen content, and the carbonate corrosive Antarctic Bottom Water (AABW) (Fiúza, 1984). Mainly in the northwest of the Iberian margin, where the MOW's influence is less pronounced, fresh and colder Labrador Sea Water (LSW) can intrude between the MOW and NADW (Saunders, 1986). At the present day, all studied sites are under the influence of NADW.

4.3. Material and Methods

Piston core SU92-03 off Cape Finisterra, was recovered in 1992 during the PALEOCINAT II cruise of the integrated EPOCH program with the Research Vessel (RV*) Le Suroît* (Labeyrie and Party, 1990). Core MD95-2040 from the southeastern flank of the Oporto Seamount and core MD95-2042 off Cape Sines were collected during the first International Marine Global Change Study (IMAGES) cruise in 1995 using the CALYPSO

giant piston corer on board of RV *Marion Dufresne* (Bassinot and Labeyrie, 1996) (Fig. 1, Table 1).

Core SU92-03 specific proxy data

Core SU92-03 was sampled at a 5 cm resolution with 1 cm thick slices, except for the intervals of H1 and H4 that were sampled continuously in 1.5 cm thick intervals. Sediment samples were divided into two sample sets for the different analyses: (1) 2cc were dried at 40ºC and crushed for the carbonate and carbon content analyses; (2) 20-25cc were weighted wet, dried at 40ºC and weighted again to allow dry bulk density calculations. The dried sediment was dispersed with a 0.005 mol sodium hexametaphosphate solution and washed with distilled water through a sieve stack of 2 mm, 150 μm, and 63 μm mesh-size.

Total carbon content was determined in the CHNS-932 LECO Elementar Analyzer of the Marine Geology Laboratory at INETI. Two replicates of dried and homogenized sediment (2 mg) were analyzed per level. The same set of samples was later subjected to combustion for 8 hours through a predefined stepwise increase in temperature up to 400ºC to remove organic carbon and re-analyzed for inorganic carbon. The organic carbon content (C_{org}) was calculated as the difference between total carbon and inorganic carbon concentration. The relative precision of repeated measurements of both samples and standards was 0.03wt%. C_{org} accumulates in the fine fraction and its values can be reduced every time that coarse grains (heavier) are present in the sediment like during the H. So to compensate for the grain size and density effect C_{org} was first calculated considering the total sediment sample and then recalculated assuming that the sediment sample was composed of the fraction <63 μm only. The two records reveal similar tendencies, but with high values for the second calculation, so that we assume that grain size and density affect the C_{org} AR along the studied core. Consequently, only the C_{org} calculated for the sediment sample fraction <63 μm is show in this study. The results are presented as Accumulation Rate (AR). The component specific AR was calculated as the product of the fraction of each component and the bulk mass accumulation rate (derived from the dry bulk densities and sedimentation rates).

For quantitative planktonic foraminiferal identification, the fraction 150 μm – 2 mm was split to obtain 300-600 planktonic foraminifera specimens that were identified

following the taxonomic criteria of Hemleben et al., (1989). In the same split, the number of detrital grains was determined. After the counting, the relative abundance of each planktonic foraminifera species were calculated. Quantitative abundances of planktonic foraminifera and lithic grains were calculated as numbers per gram of dry sediment taking into account the weight of the total sample and the number of times that the >150 μm fraction was split prior to the counting procedure, and as AR. The relative abundance of the polar species *Neogloboquadrina pachyderma* (sinistral) was used to monitor southward penetrations of the (sub)polar waters (e.g., Bond et al., 1992; de Abreu et al., 2003) and the relative abundance of *Globigerina bulloides* and *Neogloboquadrina pachyderma* (dextral) to indicate productivity related to coastal upwelling (e.g. Thunell and Sautter, 1992; Salgueiro et al., submitted).

Stable isotopes measurements were performed on planktonic (*Globigerina bulloides*, *Globorotalia inflata*, *Globigerinoides ruber* (white)) and benthic (*Cibicidoides* spp., *Uvigerina* spp.) foraminifera species. Samples contained on average 25 planktonic or 6 benthic foraminiferal specimens picked from the fraction >250 μm (mainly between 250 and 330 μm) and were measured in the Finnigan MAT 252 mass spectrometer of the RCOM at Bremen University. The $^{18}O/^{16}O$ ratio is reported in permil (‰) relative to the Vienna Peedee Belemnite (VPDB) standard. Analytical standard deviation is ±0.07‰ for $\delta^{18}O$. The *Cibicidoides* spp. $\delta^{18}O$ values were corrected by +0.64‰ to be equivalent to the *Uvigerina* spp. data (Shackleton, 1974) and the combination of both species is referred to as benthic $\delta^{18}O$.

For AMS ^{14}C dating on average 1100 specimens of the planktonic foraminifera *G. bulloides* species were picked from the fraction >250 μm (mainly between 250 and 330 μm) from 4 selected levels. All ages were measured in the Leibniz laboratory for Radiocarbon Dating of the Kiel University, Germany (Table 2). Ages were corrected for a marine reservoir-effect of 400 years according to modern values determined in the area (Bard, 1988; Abrantes et al., 2005). The reservoir age was assumed to be constant through time, as no data exists for the region that could reveal paleo-reservoir age increases due to the southward advance of polar surface waters or the upwelling of aged ENACW. The ^{14}C ages younger than 20 ky were calibrated to calendar years with INTCAL04 (Reimer et al., 2004); for the older ^{14}C age the data of Hughen et al., (2004) was used.

Table 2 Radiocarbon ages, species used, calendar ages for core SU92-03.

Event	Depth (cm)	Species	Age (cal. Y)	
Holocene	7.5	*G. bulloides*	2830 (± 40)	♦
Holocene	47.5	*G. bulloides*	13860 (± 80)	♦
Holocene	112.5	*G. bulloides*	19930 (± 120)	♦
H2	147.5		24080	*
-	167.5		25780	*
-	197.5	*G. bulloides*	28700	Δ
Base H3	217.5		30220	*
Top H4	271.8		38360	*
Base H4	287.5		40160	*
D-O 12	332.5		45380	*
D-O 17	402.5		58300	*
D-O 18	452.5		62050	*
top D-O 19	487.5		67250	*
D-O 20	504.5		73000	¥
Top 5b	537.5		84000	¥
5b	552.5		92000	+
5c	600.5		109000	¥
peak 5e	635.5		126000	¥
6	652.5		134000	¥
-	687.5		140000	¥

♦ ^{14}C calibrated INTCAL04 (Reimer et al., 2004)
Δ ^{14}C corrected with Cariaco (Hughen et al., 2004)
* Stuiver and Grootes (2000)
¥ Lisiecki and Raymo (2005)
+ Martinson et al., (1987)

Temperature and productivity data

To reconstruct sea surface temperature (SST) and Export Productivity (Pexp), 27 taxonomic categories of planktonic foraminifera census counts were used with the modern analog technique SIMMAX 28 (Pflaumann et al., 1996; 2003) To the 26 taxonomic groups widely used and listed in (Kucera et al., 2005), *Turborotalita humilis* was added in our calibration as it is associated with the PCC source region (Meggers et al., 2002). The modern analog file is based on the Iberian margin database (Salgueiro et al., submitted) combined with the North Atlantic surface samples used by the MARGO project (Kucera et al., 2005). This results in a total of 1020 analogs for SST and 999 for Pexp. Modern SSTs

for 10 m water depth were taken from the World Ocean Atlas 1998 using the webpage of the MARGO project (http://www.palmod.uni-bremen.de/~csn/woasample.html). Modern oceanic primary productivity (PP) is obtained for each site by averaging 12 monthly primary productivity values for a 8 year period (1978-1986) that were estimated from satellite color data (CZCS) and gridded at 0.5º latitude - longitude fields (Antoine et al., 1996). Export Productivity (Pexp) was calculated from the PP values following the empirical relationship *(1)*

(1) $$Pexp=PP^2/400$$

for primary production below 200 $gC/m^2/yr$, and the empiric relationship *(2)*

(2) $$Pexp=PP/2$$

for primary production above 200 $gC/m^2/yr$ (Eppley and Peterson, 1979; Sarnthein and Winn, 1988). Paleo-SST and paleo-Pexp were calculated using the same procedures as in Pflaumann et al., (1996; 2003), including the consistent use of 10 best analogs, the scalar-product similarity index with no threshold, and the geographical distance-weighting.

The relationship between modern SST and Pexp for 999 samples are not correlated to annual (r=0.1) and not significantly correlated to spring (r=0.32) and summer (r=0.30) seasons. Iberian margin samples to summer season are located in graphic area where there are not correlation (Fig. 2). Consequently the same data set can be used to reconstruct these two variables independently.

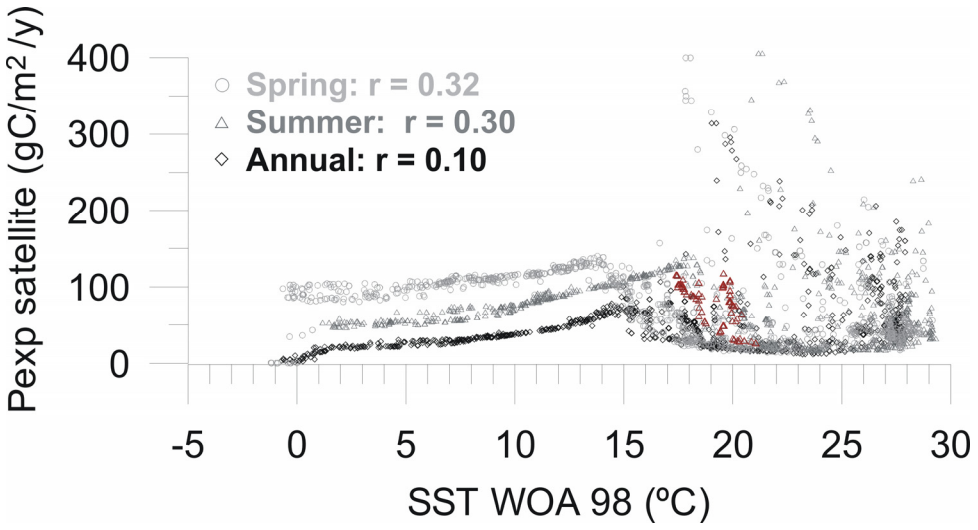

Fig. 2 Scatter plots export productivity (Pexp) of satellite versus sea surface temperature (WOA 98, at 10 m depth) to annual (black), spring (light grey), and summer (red to Iberian samples and dark grey to remaining samples). "r" is the correlation coefficient.

The validity of our reference database for paleo-SST and paleo-Pexp reconstructions was assessed by "leave-one-out" cross-validation of the modern data set. In this approach, the predicted values are generated consecutively *n* times (1020 for SST; 999 for Pexp) using a training set of the size (*n*-1). In each of the *n* predictions, one sample is left out in turn and the transfer function based on the (*n*-1) sites in the data set is applied to the one sample in the test set and omitted from the data set, giving a predicted value for that sample (Birks, 1995).

The SST and Pexp prediction error, the root-mean-square error prediction (RMSEP), was calculated as the square root of the mean of the squared differences between the observed and predicted values for all samples from the test set. For SST estimation the RMSEP is 0.72ºC for annual, 0.73ºC for spring and 0.84ºC for summer, and for Pexp the RMSEP is 15 $gC/m^2/yr$ for annual, 19 $gC/m^2/yr$ for spring, and 20 $gC/m^2/yr$ for summer. For the North Atlantic data set by itself and using the same transfer function technique, Kucera et al., (2005) got a slightly higher prediction error for annual (0.8ºC) and summer (0.9ºC) SST.

Estimated versus measured SST for summer or winter seasons are significantly correlated ($p<0.001$) with correlation coefficients of 0.995 for annual, spring and summer, and display a homogeneous scatter with no significant deviation (Fig. 3a). Estimated versus measured Pexp is also significantly correlated ($p<0.001$) with high correlation coefficients for annual and spring (0.92), and summer (0.90) seasons (Fig. 3b).

The distribution of SST and Pexp residuals (observed minus predicted values) versus the latitude of the individual sample site for annual, spring and summer show that the residuals are generally well distributed around the zero (Fig. 3c, d). Positive residuals indicate that SST and Pexp are underestimated by the regression function, while negative residuals indicate an overestimation (Niebler and Gersonde, 1998). For SST, both positive and negative residuals have similar amplitudes throughout the North Atlantic without a preferential area for under- or overestimation. A different scenario is seen in the amplitude of positive and negative Pexp residuals. Pexp residual values on the western Iberian margin (36 - 44ºN) reveal that quasi all, positive or negative, fall inside the confidence intervals of the RMSEP. This consistency corroborates the use of 10 modern analogs for the Pexp reconstruction in the studied cores. Highly underestimated Pexp values correspond to the high-productivity areas of NW-Africa, because the database currently lacks enough modern analogs with Pexp values >200 $gC/m^2/yr$. Underestimated samples between 40 and

50°N are from the Labrador Sea or are influenced by the Labrador Current and could therefore be affected by a seasonal ice cover. On the other hand, overestimation at low latitudes is observed in samples from the open ocean where productivity is low. The transfer function approach is valid for our study area, but it is clearly necessary to increase the number of analogs for the eastern boundary high productivity zones before the transfer function can be successfully applied to those more productive regions.

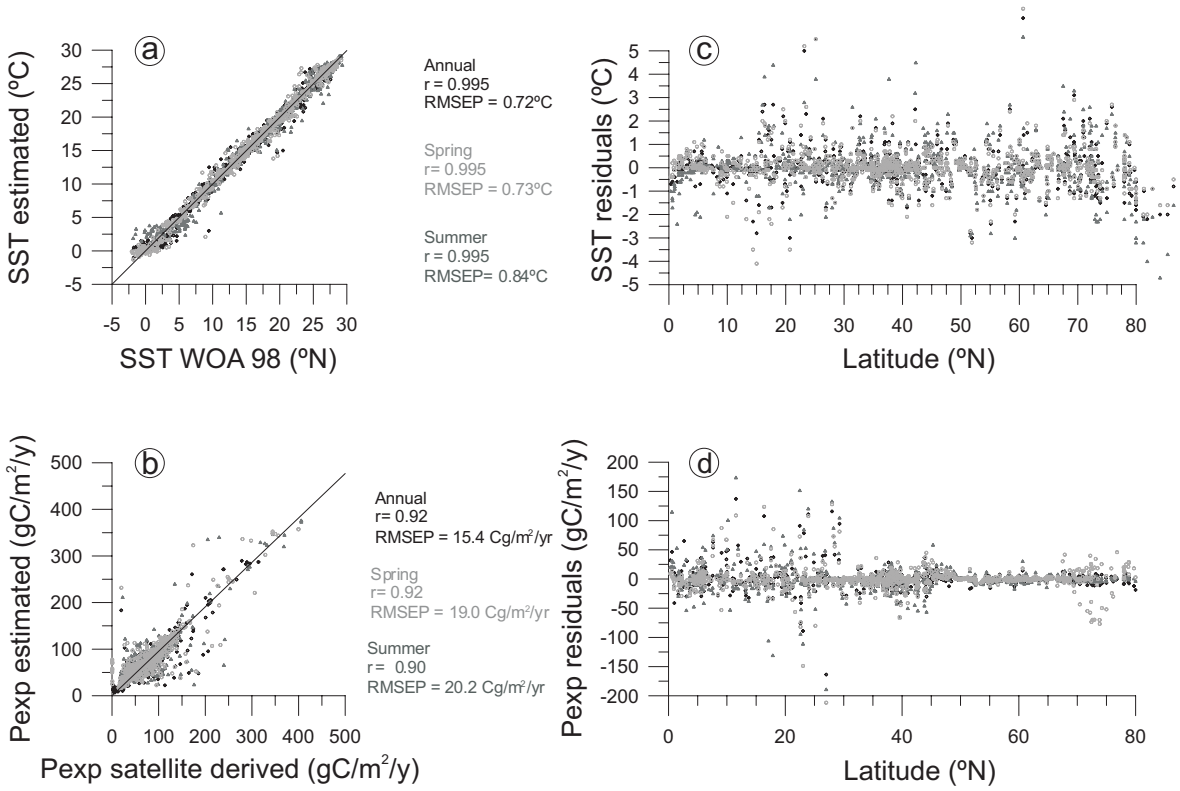

Fig. 3 Annual (black), spring (light grey), and summer (dark grey) comparison between the sea surface temperature (SST; WOA 98, 10 m depth) data and the SST estimated with SIMMAX (a), and export productivity (Pexp; 8 years average) data and Pexp estimated with SIMMAX (b). "r" is the correlation coefficient. RMSEP is the predicted error. Solid line represents linear regression line. Latitudinal distribution of annual (black), spring (light grey), and summer (dark grey) SST residuals from SIMMAX technique (c), and Pexp residuals from SIMMAX technique (d).

For core MD95-2040, the planktonic foraminifera census counts used in this study are from *de* Abreu et al., (2003) and for core MD95-2042 they are those of Cayre et al., (1999). In order to estimate the error in SST and Pexp due to counts by different observers 5 samples from warm and cold periods of core MD95-2040 were counted by L. de Abreu and E. Salgueiro, respectively. Differences in the counts resulted in a maximum offset of

0.6ºC for summer SST and 5 gC/m^2/yr for summer Pexp in warm periods. Both values are inside the prediction error, indicating that observer-specific bias is negligible.

For the comparison of the three cores summer season values for temperature and productivity are used, because they are directly linked to the upwelling of cool and nutrient-rich deep waters, which is at maximum intensity in August, i.e. one month after the northerly wind maxima (Coste et al., 1986).

In this study, the mean values shown for each period and for each indicator were calculated without taking into consideration abrupt changes, such as observed during Heinrich events.

4.4. Chronostratigraphy

The age model of core SU92-03 is primarily based on the planktonic and benthic oxygen isotope data and radiocarbon dates for the upper part. In the vicinity of the Heinrich events, the age model was refined using the abundance of detrital grains and the relative abundance of *N. pachyderma* (sinistral) (Fig. 4).

Both the benthic and *G. bulloides* $\delta^{18}O$ records clearly mirror the global isotopic stacks (SPECMAP: Martinson et al., (1987); LR04: Lisiecki and Raymo (2005)) and allow the identification of Marine Isotope Stages (MIS) 1 to 6. Tuning to these two stacks provided age control for part of MIS 5 and MIS 6, while the Holocene to Last Glacial Maximum (LGM) chronology is purely based on the calibrated ^{14}C ages (Table 2). From H2 to Dansgaard-Oeschger (DO) interstadial 19 the $\delta^{18}O$ record of *G. bulloides* was correlated with the pattern of millennial-scale oscillations of the GISP2 $\delta^{18}O$ record (Stuiver and Grootes, 2000) (Table 2). H are clearly marked by > 80% *N. pachyderma* (sinistral) and the presence of ice rafted debris, with the exception of H8 and probably H7 (Fig. 4). As % *N. pachyderma* (sinistral) drops rapidly below 15% at most H / interstadial transitions, these transitions were preferentially used as correlation points (Fig. 4). Sedimentation rates were calculated by linear interpolation between all accepted control points (Table 2).

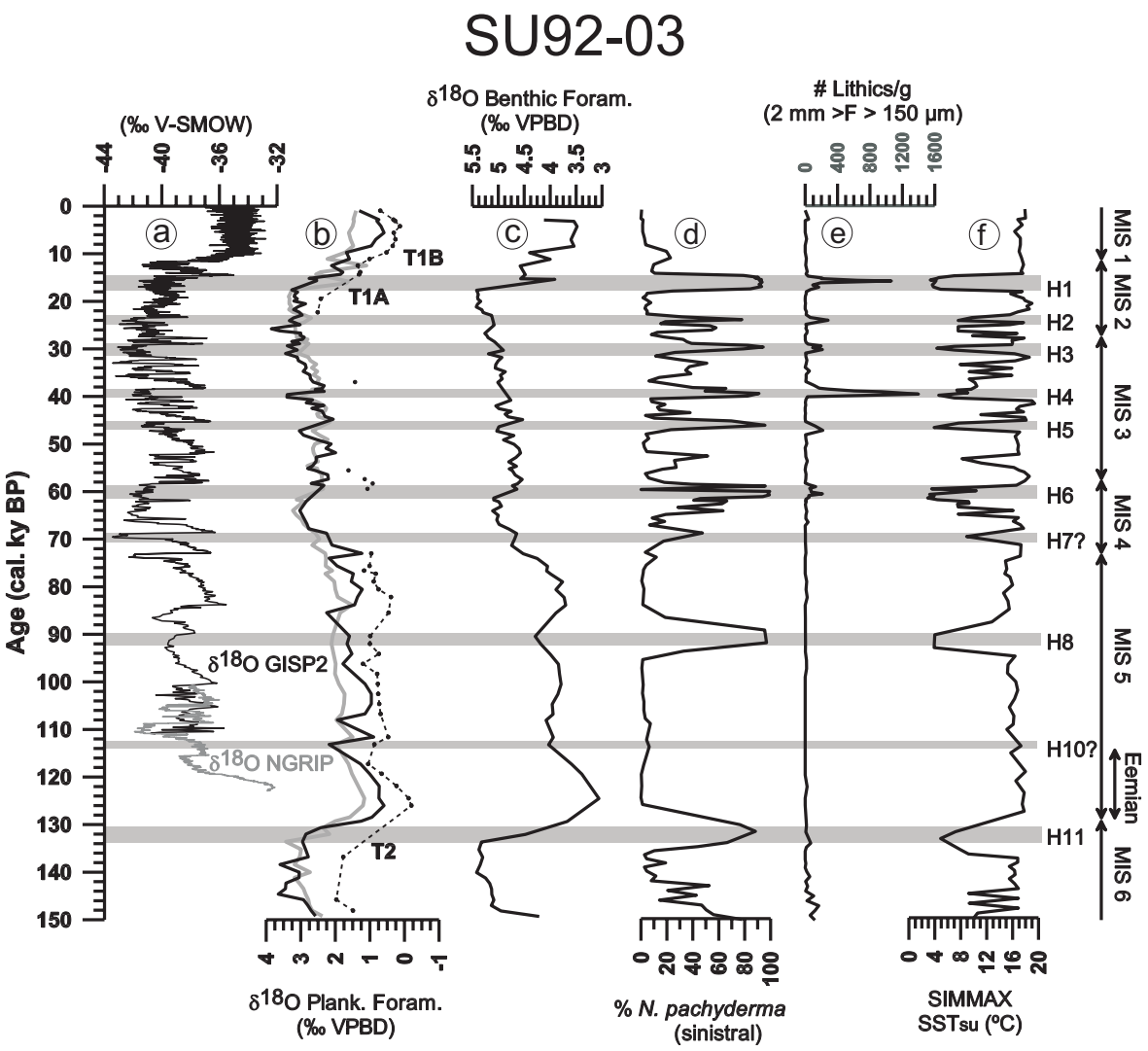

Fig. 4 Core SU92-03: correlation of ice cores $\delta^{18}O$ GISP (black: Stuiver and Grootes, 2000) and $\delta^{18}O$ NGRIP (grey: NGRIP-members, 2004) (a), with planktonic foraminifera isotope data, $\delta^{18}O$ *G. bulloides* (black), $\delta^{18}O$ *G. inflata* (light grey), and $\delta^{18}O$ *G. ruber* (white) (dashed, black line) (b); (c) benthic foraminifera isotope data, $\delta^{18}O$ values were adjusted by +0.64‰ (Shackleton et al., 1974); (d) relative abundance of *N. pachyderma* (sinistral); (e) absolute abundance of lithics; (f) summer sea surface temperature estimated with SIMMAX technique.

The study of rapid climatic variability needs a common chronostratigraphy between all the studied cores. So to synchronize the three cores in regard of timing, graphic correlation was done between SU92-03 and the other 2 cores by comparing the $\delta^{18}O$ *G. bulloides* and the relative abundance of *N. pachyderma* (sinistral) records (Fig. 5, 6).

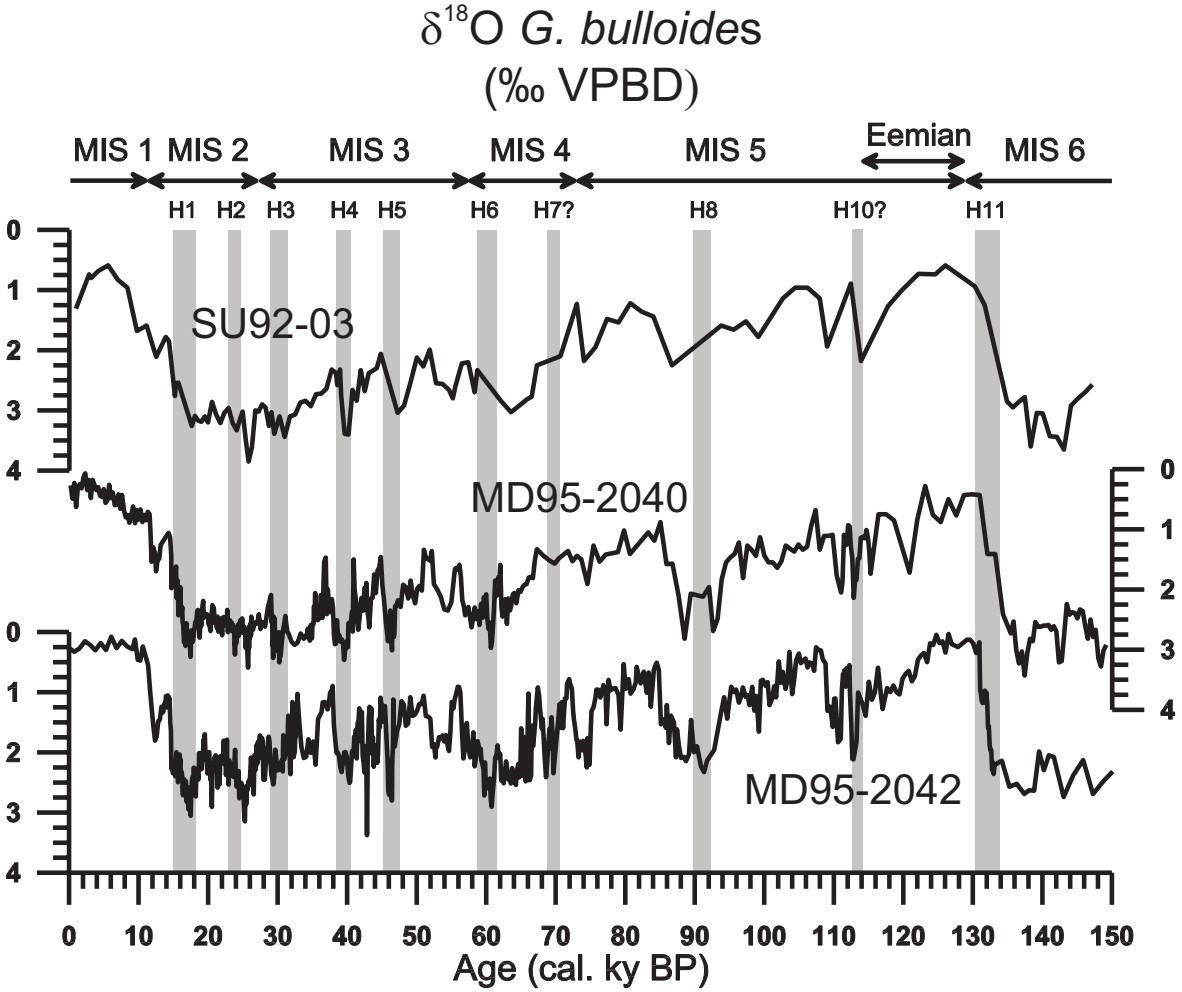

Fig. 5 Comparison of $\delta^{18}O$ *G. bulloides* of the cores, SU92-03, MD95-2040, and MD95-2042.

Planktonic isotope (*G. bulloides*) data for core MD95-2040 was taken from de Abreu et al., (2003), and for core MD95-2042 from Cayre et al., (1999) and Shackleton et al., (2000). Samples of both cores were measured at the Godwin Laboratory, Cambridge University.

The chronology of core MD95-2040 is derived from de Abreu et al., (2003) with small adjustments around H2, at the base of D-O interstadial 11, and in the MIS 6 interval. The age model of core MD95-2042 is based on the correlation of its *G. bulloides* $\delta^{18}O$ record with the GISP2 ice core chronology (Shackleton et al., 2000), with small adjustments in relation to MD95-2040 between D-O 6 and H4 and below 80 ky. The resulting age - depth relationship for each core is shown in the Fig. 7.

The revised age models and all other data presented in this paper will be stored at the World Data Centre MARE (http://www.wdc-mare.org).

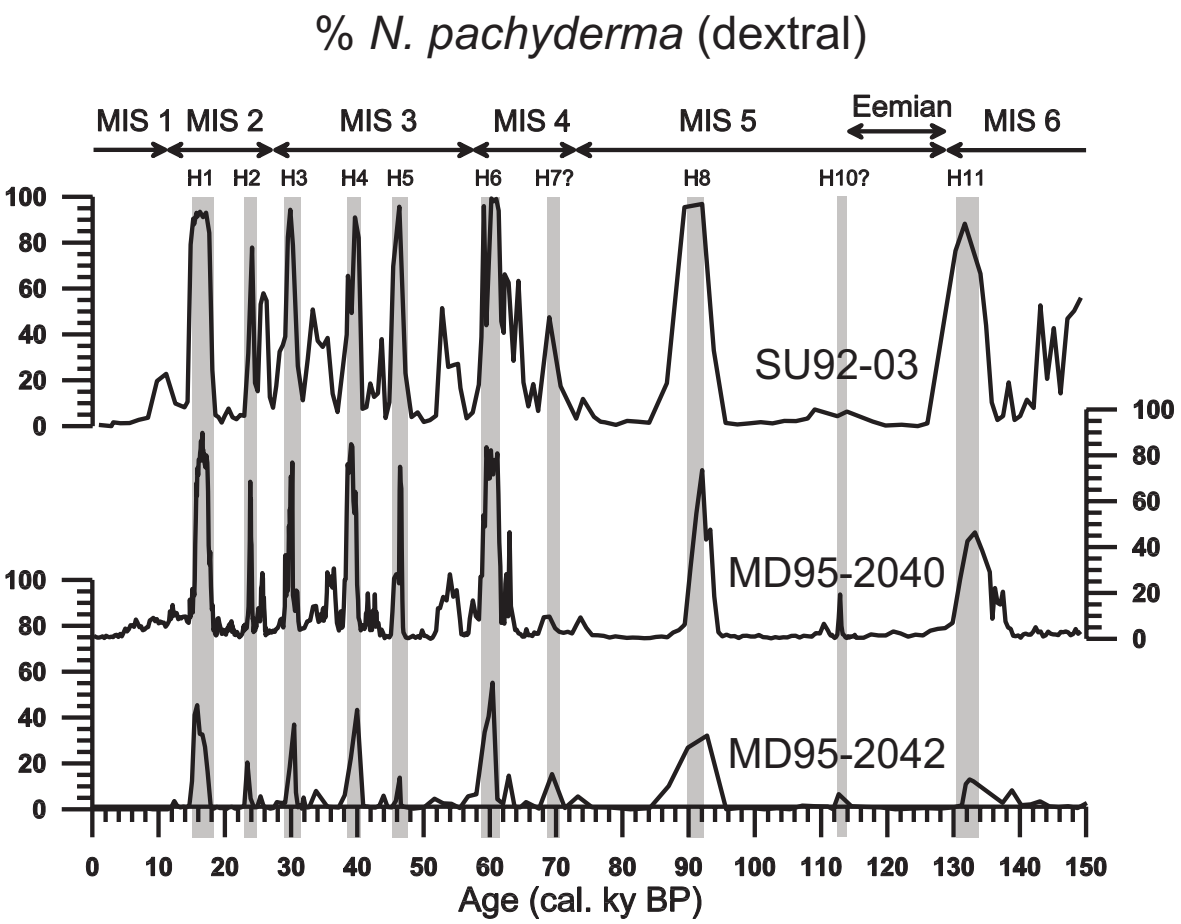

Fig. 6 Comparison of *N. pachyderma* (sinistral) from cores SU92-03, MD95-2040, and MD95-2042.

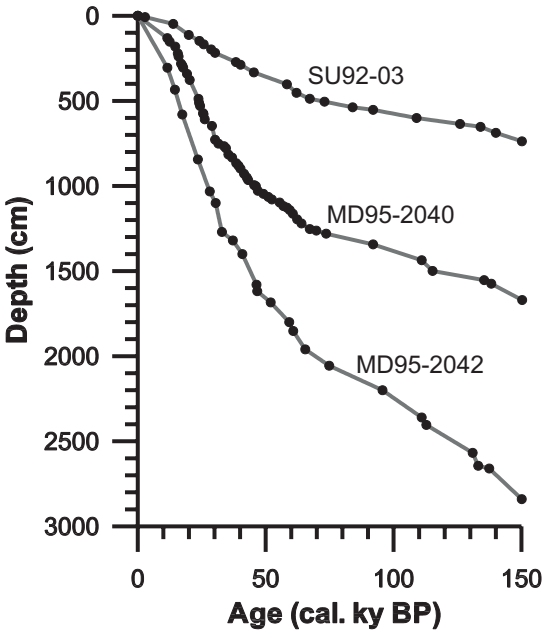

Fig. 7 Age versus depth plots for cores SU92-03, MD95-2040, and MD95-2042.

4.5. Results

4.5.1. Paleotemperature

The $\delta^{18}O$ records of the different planktonic foraminifera species from core SU92-03 generally show the same trend downcore for the last two glacial – interglacial cycles (Fig. 4b). *G. bulloides* $\delta^{18}O$ values vary between 0.6 and 3.9‰. The lightest average values occur during the interglacial intervals, the Eemian (~ 1.1‰) and the Holocene (~ 1‰). Heavy values correspond to the glacial periods, mainly MIS 6 (~ 3.1‰) and 2 (~ 3‰), and some Heinrich events (H) (3.2 – 3.5‰). The heaviest value (3.8‰) was found around 25.8 ky BP. The $\delta^{18}O$ curves of *G. bulloides* and *G. inflata* show similar values during the glacial periods (mainly during the MIS 3), but during the interglacial periods, MIS 5.3 and 5.1 *G. inflata* $\delta^{18}O$ is heavier by 0.4 – 0.8‰. In contrast, during periods correlated with abrupt climate change like H11, H3 – H1, and the Younger Dryas *G. inflata* is lighter by 0.5 – 0.9‰. The surface dwelling (upper 50 m) species G. *ruber* (white), when present, always exhibits lighter values (0.4 – 1.2‰) than the upper water column (up to 100 m) species *G. bulloides*, and the deep dwelling (100-300 m) species *G. inflata*. G. *ruber* (white) is considered to reflect conditions in the warm waters of the wintertime Portugal Coastal Countercurrent, *G. inflata* those in the winter mixed layer, and *G. bulloides* the summer upwelling (Salgueiro et al., submitted). Sudden decreases of $\delta^{18}O$ in the three planktonic foraminifera species coincide with the last two deglaciations (Terminations; T), T2 and T1, whereby for T1 events A and B (Duplessy et al., 1981) can be detected. *G. bulloides* $\delta^{18}O$ reaches values of 2.2 and 2.0‰ during T2 and T1, respectively.

Comparing the *G. bulloides* $\delta^{18}O$ records of the three cores (SU92-03, MD95-2040, MD95-2042) reveals that the northernmost core SU92-03 always shows heavier values than the other cores, but with varying amplitude over time (Fig. 5). During the Eemian and the Holocene, the difference between SU92-03 and the southernmost core MD95-2042 is 0.5 and 0.7‰, respectively, during MIS 6 and 2 1‰, during MIS 4 0.7‰, and during MIS 3 0.9‰.

The benthic foraminifera $\delta^{18}O$ record from SU92-03 (Fig. 4c) reflects to a large extent the global ice volume signal (Shackleton and Opdyke, 1973), and its lightest values

correspond to the Eemian (3.1‰) and the Holocene (3.5‰), while the heaviest values (5.4‰) clearly belong to the glacial maximum of MIS 6 and the LGM (equivalent to MIS 2.2, Martinson et al., (1987)). At this site the LGM is dated to 21.5-18 ky, in accordance with the "Last Isotope Maximum" or LGM definition of GLAMAP 2000 (Sarnthein et al., 2003). During MIS 5, the colder substages MIS 5.2 and 5.4 and the warmer substages MIS 5.1, and 5.3 (Martinson et al., 1987) were also recognized in the benthic $\delta^{18}O$ data.

Along core SU92-03 the relative abundance of the polar species *N. pachyderma* (sinistral) varied between 0 and 95% with peak abundances during MIS 4 to 2 and 6, and with persistent low abundances (0 – 0.5 %) during the Eemian, MIS 5.3, 5.1, and the Holocene. Eight clearly defined periods with values exceeding 80% of the polar species (Fig. 4d) coincide with H11, H8, H1 - H6 and another less defined period with 40% may represent H7. Except for H8, the probable H7, and H10, those time periods are also associated with increased amounts of lithic grains (>200 lithics/g), which are interpreted as Ice Rafted Debris (IRD) and mark the presence of icebergs on the northwestern Iberian margin (Fig. 4e). The highest amount of IRD with 1400 and 1100 lithics/g was deposited during H4 and H1, respectively.

In core MD95-2040, the percentage of *N. pachyderma* (sinistral) varies between 0 and 90 % and in MD95-2042 between 0 and 55 % (Fig. 6). Like SU92-03 both cores show the minimal percentages during Eemian, MIS 5.3, 5.1, and the Holocene, and the highest peaks coinciding with the H as defined by de Abreu et al., (2003)(MD95-2040) and Cayre et al., (1999) (MD95-2042).

Summer sea surface temperatures (SST_{su}), estimated from the planktonic foraminifera assemblage, range from 2.9 to 19.4ºC at site SU92-03, 4.7 to 19.9ºC at MD95-2040, and 7.8 to 21.4ºC at MD95-2042 (Fig. 4f, 8). During MIS 1 and 5 SST_{su} are fairly stable in all three records, while the glacial SST_{su} records show more variability with short-termed relative stable periods and abrupt SST_{su} drops, especially during the H. However, the short term, but low amplitude variability (~2ºC) seems to be still present at least during the Holocene in our higher-resolution record (MD95-2040). These results suggest that the mechanism(s) behind this high-frequency variability are a common feature during interglacials and their effects can still be detected in the sea-surface environment.

In core SU92-03, the interglacial periods have a mean SST_{su} of 17.3ºC. If the H are excluded, mean SST_{su} during glacial MIS 6 is 13ºC, and during MIS 4, 3 and 2, 13.6ºC, 15.3ºC and 15.6ºC, respectively (Table 3). The LGM has 17.4ºC as average, with a

maximum value of 19ºC around 20 ky coinciding with the presence of *G. ruber* (white) (~ 1.5%) in the planktonic foraminifera assemblage. SST_{su} drops rapidly at the onsets of H by as much as 14.7ºC of SST_{su} difference for H4 and as little as 5.1ºC for H6. H8, H6-H3, and H1 are associated with values between 3.9 and 4.5ºC, the minimum temperatures of the whole record (Fig. 4f and Fig. 8).

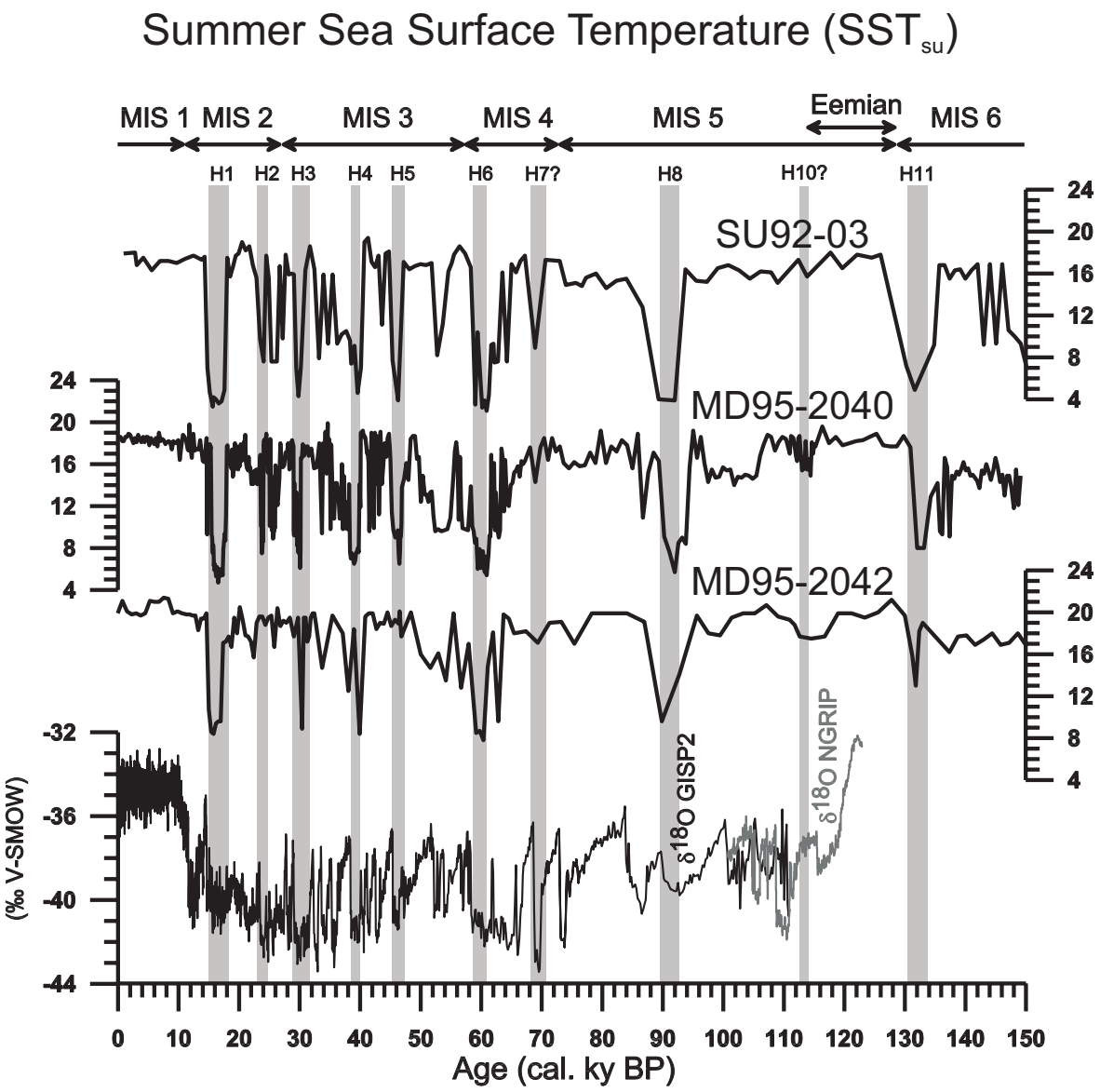

Fig. 8 Summer sea surface temperature estimated with SIMMAX technique of the 3 studied cores, SU92-03, MD95-2040, and MD95-2042, and their correlation with ice cores: $\delta^{18}O$ GISP (black: Stuiver and Grootes, 2000) and $\delta^{18}O$ NGRIP (grey: NGRIP-members, 2004).

Table 3 Average estimated summer sea surface temperature and estimated export productivity with SIMMAX technique of cores SU92-03, MD95-2040, and MD95-2042.

*SST_{su} (ºC)	Holocene	Eemian	MIS 2	MIS 3	MIS 4	MIS 6	LGM
SU92-03	17.3	17.2	15.6	15.3	13.6	13.0	17.4
MD95-2040	18.3	17.6	15.7	15.4	14.8	14.7	16.5
MD95-2042	20.4	19.0	18.7	18.2	17.4	16.8	18.4
*$Pexp_{su}$ ($gC/m^2/yr$)	Holocene	Eemian	MIS 2	MIS 3	MIS 4	MIS 6	LGM
SU92-03	108	108	96	96	89	89	100
MD95-2040	79	89	95	86	94	99	108
MD95-2042	65	79	91	87	83	99	85

*average without consider the Heinrich events

In core MD95-2040, Eemian SST_{su} have a mean value of 17.6ºC and the Holocene ones of 18.3ºC, while the glacial (without H) SST_{su} show a mean around 14.8ºC during MIS 6 and 4, and in the range of 15.5 to 15.7ºC during MIS 3 - 2 (Table 3). During the LGM SST_{su} is on average at 16.5ºC, but reveals also a maximum of 18.3ºC around 20 ky. During the H SST_{su} drops abruptly to minimum temperatures of 4.7 and 5ºC during H8, H6, H3, and H1 (Fig. 8). The SST_{su} estimated here are slightly colder than those by de Abreu et al., (2003) who used the modern analog database of Pflaumann et al., (2003) with 947 analogs from the whole Atlantic and modern SSTs from the World Ocean Atlas 1994.

In the southernmost core MD95-2042, the Eemian has a mean SST_{su} of 19ºC and the Holocene of 20.4ºC, while the glacial periods MIS 6, 4, 3, and 2 range between 16.8ºC, 17.4ºC, 18.2ºC, and 18.7ºC, respectively (Table 3). During the LGM mean SST_{su} is 18.4ºC, with a maximum value of 20.4ºC around 20 ky. The coldest SST_{su} of 7.8 to 8.2ºC correspond to H6, H4, and H1 (Fig. 8).

4.5.2. Paleoproductivity

G. bulloides and *N. pachyderma* (dextral) constitute 0 to 70% of the total planktonic foraminifera assemblage throughout core SU92-03 (Fig. 9a). Lowest relative abundances of these species are associated with H, even dropping to 0% during H8, H6, and H1. High *G. bulloides* average abundances are observed during glacials. High *N. pachyderma* (dextral) average abundances coincide with the end of MIS 6, MIS 5, and the Holocene.

The planktonic foraminifera accumulation rate (AR) (Fig. 9b) along core SU92-03 has minimum values during the H11, H8, H6, and H5 (330-1000 shells/cm^{2}ky) and maximum values (>25000 shells/cm^{2}ky) during the late MIS 5.1, the Holocene and in the D-O interstadials following H5, H4 and H1. The fragmentation index is on average 6.4% suggesting that mechanical fragmentation and dissolution affected the assemblage only to a minor extend (Fig. 9c). Fragmentation is higher during H, especially during H6, and is probably related to dissolution caused by the shoaling of the AABW/ NADW interface (Shackleton et al., 2000; Skinner and Shackleton, 2004) and thus the presence of poorly ventilated and carbonate corrosive AABW at the site (confirmed by the benthic δ^{13}C data; not shown).

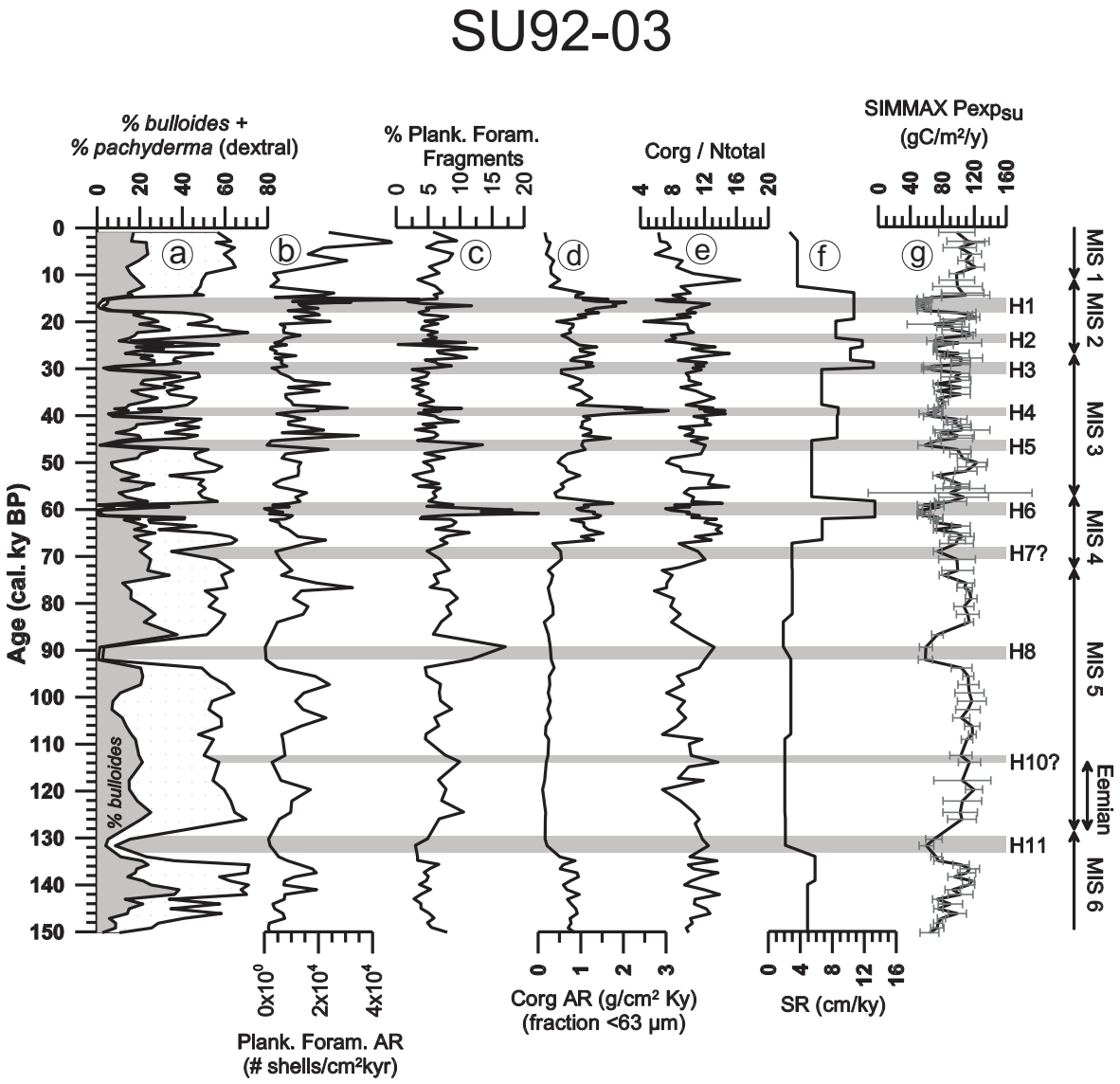

Fig. 9 Core SU92-03: (a) relative abundance of upwelling species of Iberian margin (*G. bulloides* and *N. pachyderma* (dextral)); (b) accumulation rate of planktonic foraminifera; (c) relative abundance of fragments of planktonic foraminifera (d) accumulation rate of C_{org} within fraction < 63µm; (e) C/N ratio; (f) sedimentation rate; (g) summer export productivity estimated with SIMMAX technique.

The C_{org} AR oscillates between 10 and 305 g/cm^{2}ky, with values close to zero during the Eemian and the Holocene and high values during the MIS 4 – MIS 2 (Fig. 9e). Typical C/N values of marine sources are normally between 7 and 9, and those >15 are of terrestrial origin (Wefer et al., 1999). Thus during the Younger Dryas, the C/N values >15 indicate an input of C_{org} of terrestrial origin (Fig. 9f).

The sedimentation rate is low during MIS 5 and the Holocene and highest during H and both Terminations (Fig. 9g).

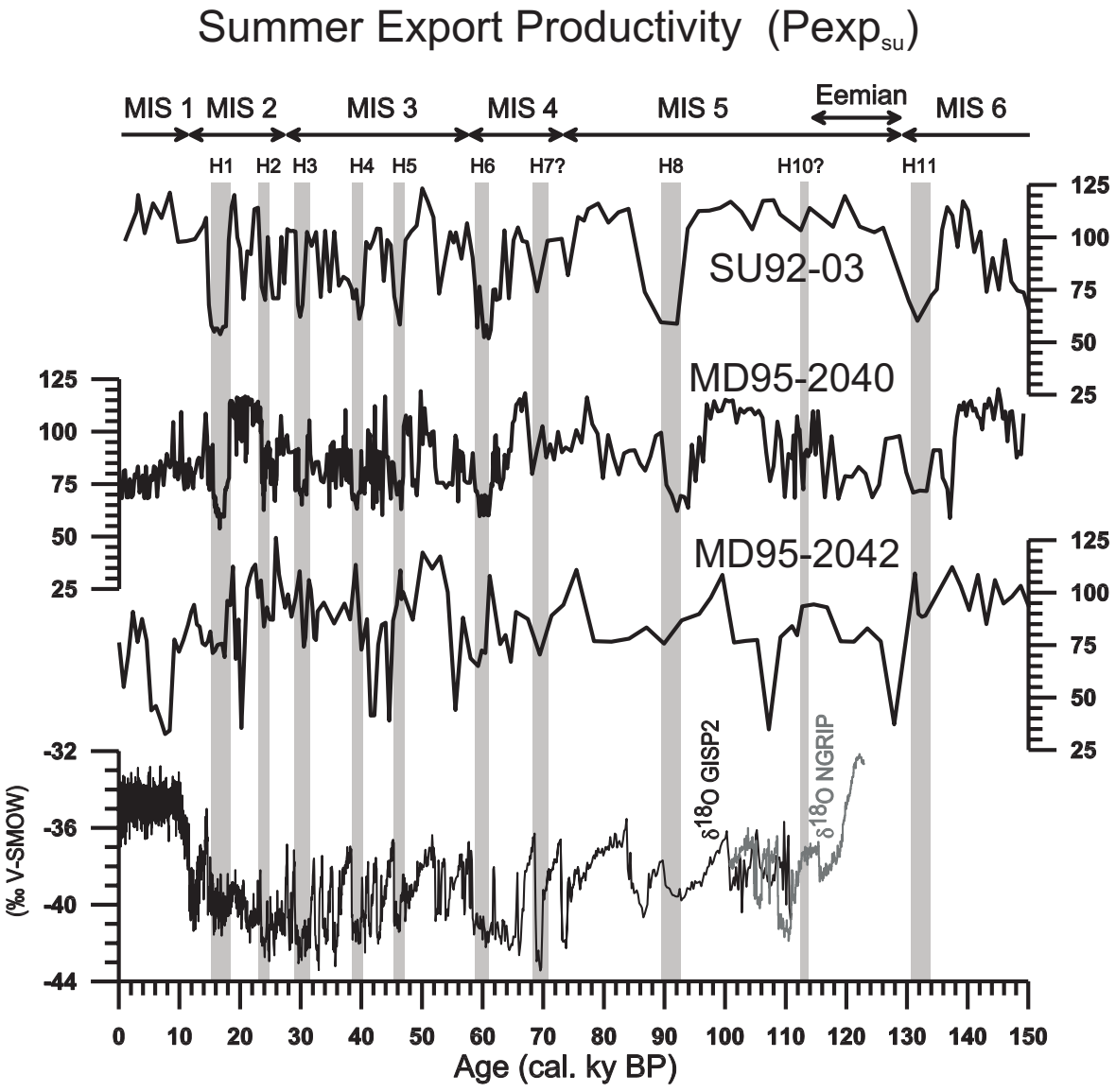

Fig. 10 Summer export productivity estimated with SIMMAX technique of the 3 studied cores, SU92-03, MD95-2040, and MD95-2042, and their correlation with ice cores: δ^{18}O GISP (black: Stuiver and Grootes, 2000) and δ^{18}O NGRIP (grey: NGRIP-members, 2004).

Summer export productivity ($Pexp_{su}$) values range from 52 to 123 $gC/m^2/yr$ in core SU92-03, from 54 to 120 $gC/m^2/yr$ in core MD95-2040, and from 33 to 126 $gC/m^2/yr$ in core MD95-2042 (Fig. 9h, 10). At site SU92-03 the Eemian and the Holocene $Pexp_{su}$ is on average 108 $gC/m^2/yr$, while glacials (without H) MIS 6 and 4 have an average of 89 $gC/m^2/yr$ and MIS 3 and 2 of 96 $gC/m^2/yr$ (Table 3). During the LGM mean $Pexp_{su}$ is 100 $gC/m^2/yr$, with a minimum value of 70 $gC/m^2/yr$ along with the SST maximum around 20 ky. $Pexp_{su}$ drops during the H to values of 23 $gC/m^2/yr$ during H6 and 73 $gC/m^2/yr$ during H1 (Fig. 9h, 10).

In core MD95-2040 the Eemian has a mean $Pexp_{su}$ of 89 $gC/m^2/yr$, the Holocene of 79 $gC/m^2/yr$, the glacial periods MIS 6, 4, 2 of 95 - 99 $gC/m^2/yr$, and MIS 3 of 86 $gC/m^2/yr$ (Table 3). The LGM $Pexp_{su}$ is on average 108 $gC/m^2/yr$, with a short-termed minimum of 81 $gC/m^2/yr$ around 20 ky. During the H $Pexp_{su}$ sinks as low as 15 $gC/m^2/yr$ during H6 and 65 $gC/m^2/yr$ during H1 (Fig. 10).

At site MD95-2042 mean $Pexp_{su}$ is 79 $gC/m^2/yr$ during the Eemian, 65 $gC/m^2/yr$ during the Holocene, between 83 - 99 $gC/m^2/yr$ during MIS 6, 4, 3 and 2 (Table 3). The LGM has a mean $Pexp_{su}$ of 85 $gC/m^2/yr$, with a minimum value of 31 $gC/m^2/yr$ around 20 ky. Different from the other two cores, $Pexp_{su}$ drops to minimum values during warm periods like in the beginning of the Eemian and MIS 5.3, MIS 3 and the Holocene (Fig. 10).

4.6. Discussion

4.6.1. Hydrographic changes

Along the north - souths transect, the studied sites record similar $\delta^{18}O$ *G. bulloides* patterns during the last 150 ky with millennial-scale variability, related to Heinrich events and Dansgaard-Oeschger cycles (Fig. 6). Gradients in the absolute values reflect the different hydrographic conditions. The higher % *N. pachyderma* (sinistral) and heavier planktonic $\delta^{18}O$ and lower SST_{su} values (Fig. 5, 6 and 8) clearly show that core SU92-03 (43º12´N) was more influenced by polar water masses than the other two cores, not only in the surface waters but similar to the modern conditions most probably also through the

ENACW. While SU92-03 reveals the coldest conditions, its records are more similar to MD95-2040 (40º35´N) than to MD95-2042 (37º48´N), in accordance with a actual stronger subtropical influence on the southern margin. Differences between the sites and time periods will be discussed in detail below.

Interglacial (MIS 1 and MIS 5) variability

At present the mean of SST_{su} at SU92-03 site, under influence of the cold ENACWsp and the persistent Cape Finisterra filament, is of 17.8ºC. While SST_{su} at MD95-2040 site, influenced by the cold band of seasonal upwelled waters, is 18.6ºC, and at the southernmost site MD95-2042, the most affected by the warm ENACWst, is 20.0ºC. These data show an actual north-south SST_{su} increase of 2ºC.

During the last 150 ky the interglacial periods, Eemian (MIS 5.5) and Holocene (MIS 1), are the most stable and warmest periods at the 3 sites. The SST_{su} and planktonic foraminifera $\delta^{18}O$ data also reveal that temperature increased 2º and 3ºC from 43º12´N to 37º48´N during the Eemian and Holocene, respectively. The Holocene SST_{su} gradient between the 3 latitudes fully reflects the modern conditions, with colder temperatures off Cape Finisterra and warmer (subtropical) temperatures off southwest Iberia, and demonstrates the efficiency of our transfer function.

During the Eemian, usually understood as an interval with climate as warm or warmer than today (e.g., Kukla et al., 2002), alkenone based SST values for cores MD95-2040 and –2042 show temperatures that are 1.5 - 2ºC warmer than during the Holocene (Pailler and Bard, 2002). This contrasts our foraminiferal based data with slightly heavier and colder values during the Eemian than the Holocene. However, our data reflects mainly summer conditions while alkenones on the Iberian margin more likely correspond to winter/spring temperatures (Abrantes and Moita, 1999; Abrantes et al., 2005). The warmer Eemian wintertime SSTs seem to be linked to a stronger influence of the PCC, which is associated with *G. ruber* (white) on the western Iberian margin (Salgueiro et al., submitted). So in core SU92-03, the wintertime poleward flow of subtropical waters is reflected by the $\delta^{18}O$ values of *G. ruber* (white), which are lighter (warmer SST) during the Eemian than the Holocene. Alkenone-derived SST at site MD95-2037 (Calvo et al., 2001) near the Azores (37º05´N, 32º02´W) and therefore the source region for PCC waters were slightly warmer during the Eemian than the Holocene, so that the warmer SST off western

Iberia seem to originate from the Azores current. The larger difference between summer and winter SSTs also indicates a stronger seasonality during the Eemian and the Holocene.

Climatic conditions during the Eemian and the Holocene appear to be similar to today, with upwelling being the main hydrographic feature during the summer season. As such, the colder SST_{su} observed during the Eemian relatively to the Holocene for cores MD95-2040 and MD95–2042 point to more intense or persistent upwelling. There is also a slightly higher $Pexp_{su}$ during the Eemian than in the Holocene, but the difference is within the $Pexp_{su}$ calibration error (Fig. 10, Table 3). An alternative hypothesis is that stronger winds like during some periods at present time (Fiúza, 1983; Fiúza, 1984; Relvas and Barton, 2002) cause the colder and deeper ENACWsp to be preferentially upwelled in the Eemian.

The SST_{su} record, with the current temporal resolution, appears fairly stable during the two interglacials at all 3 sites, although the MD95-2042 record shows a bit more variability with a gradual cooling between 128 ky and 123 ky that lasts until the end of the Eemian and a cold spell starting at the beginning of the Holocene and ending between 3 – 2 ky (Fig. 8). These rapid climatic changes are further supported by pollen and dinocyst data from the same core and its twin core SU81-18, where the cooling is marked by a distinct change to a less Mediterranean and more oceanic vegetation (Sánchez-Goñi et al., 2000b).

For the complete MIS 5 (129 - 74 ky) the story looks different. While site SU92-03 reveals a gradual cooling of about 2°C during MIS 5, except for H8 when SST_{su} dropped by 12ºC, the other two sites experienced more variable conditions with some short-term cold periods, but in general SST_{su} as warm in MIS 5.3 and 5.1 as in the Eemian. This contrast between the sites might again be related to the stronger influence of the ENACWsp at site SU92-03. Colder but relative homogenous conditions in the deep winter mixed layer during most of MIS 5 are indicated by the heavier $\delta^{18}O$ *G. inflata* values and a relative constant offset between *G. inflata* and *G. bulloides* $\delta^{18}O$ (Fig. 4b). The $\delta^{18}O$ difference between these two species reflects the seasonal temperature gradient in the upper water column, which was about 2 – 3ºC during the warm intervals of MIS 5, yet smaller than during most of the Holocene (~3.4ºC). The gradual cooling during MIS 5 observed at SU92-03 is also evident in North Atlantic sites from the northern subtropical gyre. At site SU90-03 (40ºN, 32ºW) foraminifera based SST cooled in the order of 5ºC (Chapman and Shackleton, 1998) and at sites SU90-08 (43º30´N, 30º24´W) and MD95-

2037 alkenone derived SST (winter SST) reveal a cooling of 4ºC (Calvo et al., 2001). All of them, however, show a higher short-term variability than SU92-03.

The short-term cold periods during the MIS 5 that are detected at the two MD sites off western Iberia seem to be connected to a series of cooling episodes associated with the repeated southward expansion of polar water masses and IRD deposition in the North Atlantic region (e.g., McManus et al., 1994; Fronval and Jansen, 1997; Chapman and Shackleton, 1998; Martrat et al., 2004). The Portugal current, the descending branch of the North Atlantic Drift, transported this signal down to the Portuguese margin, where SST_{su} cooled 4°C (reaching 14ºC) between 116-114 ky at site MD95-2040 and 3°C (reaching 17ºC) between 118-112 ky at site MD95-2042. These SST_{su} drops coincide with D-O stadial 26 in the NGRIP $\delta^{18}O$ record (NGRIP-members, 2004) and with the Shackleton et al., (2002) cool event C24 in both cores, and probably also cool event C25 in core MD95-2042. Both cold events appear to be contemporary with the Early Weichselian Mélisey I stadial, which is characterized by cold and dry conditions as indicated by the shift from arboreal to steppic pollen (Sánchez-Goñi et al., 1999; Sánchez-Goñi et al., 2000b; Shackleton et al., 2002). In core MD95-2040, event C24, which coincides with the MIS 5.4 $\delta^{18}O$ maximum, was detected by a peak (19%) of the polar species *N. pachyderma* sinistral and is referred to as a probable H10 in de Abreu et al., (2003). Given that this event is not well noted at the northernmost site SU92-03 like the other H are, it might be that the PC had a different route during this period, possibly closer to the coast than today. In the Alboran Sea H10 is also well marked at ODP site 977A (36º2´N, 1º57´W) with a sudden alkenone SST decrease by 6.0º. This cold event seems to be recorded in the SU90-08 and MD95-2037 alkenone SST records with a cooling in the order of 4-5ºC down to 16.5 – 17ºC (Calvo et al., 2001) and a SST drop of 6ºC down to 15ºC at site SU90-03 (Chapman and Shackleton, 1998). Cold events C23 and C22 (Chapman and Shackleton, 1999), equivalent to D-O stadials 24 and 23 in the Greenland $\delta^{18}O$ records (Stuiver and Grootes, 2000; members, 2004; NGRIP-members, 2004), are also marked in core MD95-2040 between 106 and 96 ky, when SST_{su} decreased 4ºC, and less clearly in MD95-2042 (SST_{su} drop of 2ºC). H8 (~ C21) (Chapman and Shackleton, 1999), is recorded in all cores by a SST_{su} decline from north to south of 12, 14, and 10ºC (down to 4, 5, and 9ºC) and by an increased abundance of polar species (95, 70, and 30%) at 43º12´N, 40º35´N, and 37º48´N, respectively. This is the most pronounced cold excursion within MIS 5 along the western Iberian margin and coincides with the coldest part of MIS 5.2 as indicated by the *G.*

bulloides $\delta^{18}O$ records (Fig. 6), as well as in Alboran Sea (ODP-977A (Martrat et al., 2004)). However, for this event the studied cores recorded lower SST_{su} and higher percentages of polar species than sites in the open North Atlantic, where SST dropped from north to south only by 1, 4 and 2.5ºC at sites SU90-08, SU90-03, and MD95-2037, respectively, reaching SST around 15-16ºC (Chapman and Shackleton, 1998; Calvo et al., 2001). The minor decrease evidenced at SU90-08 and MD95-2037 are also seen in their alkenone SST records. Even sites in the eastern North Atlantic (V29-191: 54º16´N, 16º47´W; DSDP 609: 49º53´N, 24º14`N) only cooled in the order of 4ºC (McManus et al., 2002) during H8, despite relative high abundances of polar species (V29-191: 62%; DSDP 609: 44%; (McManus et al., 1994)). So it seems that the cold waters recorded off western Iberia do not originate from the North Atlantic drift/ Portugal current system, but might have a more local source region like the British and Amorican margins. Strong surface water cooling off the Celtic/Amorican margin is evidenced at site MD03-2692 (46º50´N, 9º31´W), where the % *N. pachyderma* (sinistral) exceeded 50% during H8 and reached about 50% during H10 (Mojtahid et al., 2005).

The youngest cooling event in MIS 5, refered to as D-O stadial 21 by Shackleton (2001) and the NGRIP-members (2004) and possibly corresponding to cold event C20 of Chapman and Shackleton (1999), is observed in both MD cores around 75 ky, with a SST_{su} lowering of the same amplitude as for cold events C23 and C22 for each core. This cold event is also well represented in the above mentioned North Atlantic sites, where SST dropped by 3ºC on average (Chapman and Shackleton, 1998; Calvo et al., 2001), similar to the value we found off the Iberian margin.

Glacial (MIS 2-4 and MIS 6) variability

In particular, the two northernmost cores display millennial-scale variability as recorded in the Greenland ice cores (e.g., Stuiver and Grootes, 2000; NGRIP-members, 2004) (Fig. 7). Without taking the H into consideration, SST_{su} at 43º12´N are on average 0-2ºC colder than at 40º35´N, and 3-4ºC colder than at 37º48´N (Fig. 8, Table 3). Cores SU92-03 and MD95-2040 display colder conditions and higher variability than the MD95-2042 record, which again seems to reflect the stronger subtropical influence in the south, but could partly also be related to the latter's lower temporal resolution. Like for the interglacial periods, SU92-03 shows the coldest SST_{su} and highest SST amplitude over

time, in agreement with the strongest influence of glacial polar front movements and the southward penetration of subpolar to polar water masses, not only in the surface water but in accordance with modern conditions most probably also in the ENACWsp. This is supported by the heavier $\delta^{18}O$ *G. bulloides* values and the higher abundance of *N. pachyderma* (sinistral) recorded at sites SU92-03 and MD95-2040 (Fig. 5, 6). Based on a four core SST transect (BOFS 5K; DSDP 609; SU90-03; ODP 658C) from the subpolar to subtropical North Atlantic, Chapman et al., (2000) could show that the glacial temperature gradient sometimes increased to 10ºC between 50ºN to 40ºN and to half as much or less between 40ºN and 20ºN.

During glacial periods *G. bulloides* and *G. inflata* $\delta^{18}O$ values are very similar at site SU92-03 (Fig. 4b), indicating that both species are either influenced by the same water mass (ENACWsp) or that the seasonal temperature gradient in the water column was greatly reduced. The picture changes for H1 and the Younger Dryas, when $\delta^{18}O$ *G. inflata* becomes lighter than $\delta^{18}O$ *G. bulloides*. A possible explanation for this could be a fresher winter mixed layer due to meltwater influx, supported by the increased abundance of *N. pachyderma* (sinistral) in both periods and an IRD increase during H; meltwater, which might orginate from the proximate NW European ice-sheets (Peck et al., 2006).

Glacial SST_{su} averages, with the H not considered, differ minimaly in the three cores; in agreement with previous foraminifera based SST calculations for cores MD95-2040 (de Abreu et al., 2003) and MD95-2042 (Cayre et al., 1999) or with the alkenone SST for the same cores (Pailler and Bard, 2002). Cayre et al., (1999) related these small changes in the glacial environment off the Iberian margin to the dominance of the polar front migrations, and the occurrence of abrupt iceberg discharge events and their effects on the evolution of Iberian continental climate.

At all 3 sites the late glacial MIS 6 is marked by the lowest SST_{su} (12.7-16.8ºC) and the heaviest *G. bulloides* $\delta^{18}O$ mean values (2-3‰) within the last 150 ky, excluding the melting events. Specifically between 142-135 ky, the penultimate glacial maximum (coincident with the heaviest benthic $\delta^{18}O$ values), SST_{su} were lower than during the LGM confirming that MIS 6 had climatically a stronger impact than MIS 4-2 at this latitude, in agreement with the global sea level record and the well-developed continental ice sheets (Shackleton and Opdyke, 1973), which had a larger extension in the Northern Hemisphere during MIS 6 than during the last glacial (e.g., Crowley, 1994; VanAndel and Tzedakis, 1996). However, SST_{su} for the late MIS 6 were never below 9ºC along the north-south

transect, while during the H SST_{su} would drop as low as 2ºC. For the entire MIS 6 in core MD95-2040, de Abreu et al., (2003) reported 8ºC as the lowest SST_{su} value with polar species contributing less to the total assemblage than during MIS 4-2. These authors confirm that the polar front did not reach as far south as during the last glacial (as before referred by Lebreiro et al., 1996; Lebreiro et al., 1997; Cayre et al., 1999; Calvo et al., 2001). Thus making the penultimate glacial, in general, a warmer period in this region. The warmer ocean waters may have led to rapid melting and resulted in comparatively fewer icebergs reaching this site. Our data partially supports this hypothesis. Between 150 and 142 ky, SST_{su} decreased by 10ºC at site SU92-03, accompanied by an increase to 58% of the polar species and a slight increase in IRD (Fig. 4, 6), none of which are observed at the more southern MD sites. Furthermore, two warming SST peaks of 7ºC amplitude are observed at 146 ky and 143 ky in the SU92-03 record, which are equivalent to the SST oscillations of D-O interstadials 4 and 3 in MIS 3 and less prominent in the MD cores.

During the MIS 4-2 interval mean $\delta^{18}O$ *G. bulloides*, not considering the H for average, are within the same range of those from core MD95-2042, but are slightly lighter (0.2 - 0.5‰) during MIS 4 and 3 than MIS 2 in the two northern cores. This could indicate that temperature and salinity conditions in the glacial ENACWst were more stable than in the ENACWsp, which was formed closer the NW European ice sheet margins. In general, MIS 4 SST_{su} were 1-2ºC colder (~13.6-17.4ºC) than their MIS 3 and 2 counterparts, which are of similar degree (~15.5-18.5ºC).

As part of MIS 2 (Fig. 8), LGM (21.5-18 ky) SST_{su} were relatively warm (16.5-18.4ºC) off Iberia, in agreement with previous reconstructions based on foraminiferal (Abrantes et al., 1998; de Abreu et al., 2003), alkenone (Pailler and Bard, 2002) and pollen data (Roucoux et al., 2005). A SST_{su} increase around 20 ky to 18.3-20.4ºC, in the range of modern SST, and the presence (2%) of the subtropical species *G. ruber* (white) imply the northward advance of warm waters all the way up to site SU92-03. This warm poleward flow, however, was restricted to a nearshore position. Like CLIMAP, the GLAMAP and EPILOG reconstructions show the glacial North Atlantic drift flowing east along the arctic front between 40 and 42ºN and turning south as the cold Portugal and Canary Current along the eastern margin of the subtropical gyre (Pflaumann et al., 2003). Off the western Iberian margin, the arctic water masses are only recorded at the Tore Seamount (39.05ºN, 12.58ºW), i.e. further offshore (Lebreiro et al., 1997) as suggested by Abrantes et al., (1998). So for the LGM summer, the circulation scheme off the western Iberian margin

looked very much like the modern winter circulation (Peliz et al., 2005) with a warm poleward flow – the PCC – along the coast and the influence of the colder Portugal Current restricted to the west of the Iberian winter front, i.e. today to about 10°W north of 40°N and 11°W south of this latitude. As the modern day Iberian winter front is meandering more strongly north of 40°, the LGM SST_{su} at MD95-2040, which are on average colder than at the other two sites, might partly be caused by incursions of subpolar waters.

As previously mentioned, during the glacial periods all cores show a high SST_{su} variability with short-term cold periods coeval with ten H (H11-H10 and H8-H1) and D-O stadials. During the H and D-O stadials, the weakened thermohaline circulation caused a southward shift of the polar front, which in turn allowed the arrival of polar water and icebergs to the latitude of southern Iberia (Lebreiro et al., 1997; Cayre et al., 1999; Thomson et al., 1999; de Abreu et al., 2003; Martrat et al., 2004; Voelker et al., 2006), and caused the coldest and certainly driest periods on the Iberian peninsula (Roucoux et al., 2001; Sánchez-Goñi et al., 2002; Roucoux et al., 2005). The wind-regime became dominantly westerly on the Iberian Coast (Wyputta and Grieger, 1999) and thus probably less favorable for coastal upwelling. In our sediment cores, these periods are well marked by increased percentages of *N. pachyderma* (sinistral), consequently colder SST, heavier planktonic foraminifera $\delta^{18}O$ values and for most H also the presence of small amounts of IRD (Fig. 4) (Cayre et al., 1997; de Abreu et al., 2003). In the northernmost core, SU92-03, % *N. pachyderma* (sinistral) reaches the same range (>90%) during the H as in cores from the subpolar North Atlantic and closer to the major northern hemisphere ice sheets; cores like SU90-24 (62º40´N, 37º22´W, (Elliot et al., 1998)) and SO82-5 (59°N, 31°W; (van Kreveld et al., 2000)). On the other hand, core SU90-03 (Chapman et al., 2000), at a similar latitude as MD95-2040, but in the open subtropical North Atlantic, recorded 6-8ºC warmer SST during H6, H5, H3 and H2 highlighting how strongly MD95-2040 and the western Iberian margin were influenced by the arctic waters transported with the paleo-Portugal Current. The Iberian margin itself experienced strong temperature gradients during the H, which ranged from 0.5 to 2ºC between 43º12´N and 40º12´N, and 4 to 14ºC between 43º12´N and 37º48´N, confirming that the increasing SST caused icebergs to melt rapidly on their way south as proposed by Lebreiro et al., (1997). Baas et al., (1997) also related the intensified melting of icebergs south of 39.6ºN to warmer SST and at least for H10, H7, H5, and H2, this is corroborated by the data from core MD95-2042 (Fig. 8).

The H5a event, first identified in cores from the Labrador Sea and the northwest Atlantic Ocean (Stoner et al., 1996; Sarnthein et al., 2001; Rashid et al., 2003), correlates with stadial 15 in the GISP2 $\delta^{18}O$ record (Stuiver and Grootes, 2000) and is marked in particular in the two northernmost sites by an increase in % *N. pachyderma* (sinistral) to 50% and 26% in cores SU92-03 and MD95-2040, respectively, (Fig. 6), and by $\delta^{18}O$ values of *G. bulloides* of 2.4 to 2.1‰ (Fig. 5). Furthermore, SST decreased northward from 14°C at site MD95-2042 to 8ºC at site SU92-03 (Fig. 8). The H5a values are equivalent to those obtained for H7 in terms of SST_{su} and % polar species, and seem to record a short cold event less proximal to the ice margins.

H7 is equivalent with D-O stadials 20 and cold event C19 of McManus et al., (1994). It is one of the rapid change events punctuating the MIS 4 record, which for the marine record were first defined in DSDP site 609 (McManus et al., 1994). The other cold events are C18/ D-O stadial 19 and C17/ D-O stadial 18 (H6) and all 3 coolings are well defined in our 3 records (Fig. 8). Furthermore, they are recorded in the SST records of subtropical gyre core SU90-03 (Chapman et al., 2000) and Alboran sea core ODP977A (Matrat et al., 2004). Off western Iberia margin, the minimum temperatures reached during the cold events are within the range of those at DSDP 609, which reflects conditions in the North Atlantic drift, but colder than at site SU90-03. The amplitude of SST_{su} change at the onset of cold events C19 and C18, however, is larger off Iberia than at DSDP site 609.

Warm SST_{su} during MIS 4-2 are related to the D-O interstadials (Fig. 8). Some MIS 3 D-O interstadials exhibit SST_{su} that were as warm or even 1ºC warmer than the observed interglacial SST_{su}. In the two northernmost cores, the interval encompassing D-O interstadials 16-9 particularly recorded warmer SST_{su}. Since essentially warmer conditions during early MIS 3 are less evident in the pollen data (Sánchez-Goñi et al., 2000a), they might mainly be restricted to the ocean. On the other hand, most other North Atlantic records from the subpolar and subtropical gyre, show SST values that are lower during the D-O interstadials than during the last two interglacial periods (e.g., CH69-K09 - 41º45´N, 47º21´W (Labeyrie et al., 1999); SU90-08; MD95-2037 (Calvo et al., 2001); SU90-03 (Chapman et al., 2000); ODP977A (Matrat et al., 2004). Most of these records also show a declining trend in the maximum interstadial SST from the early MIS 3 to MIS 2, maybe related to the warm Azores current, however, this is not observed in our SST or the alkenone SST records at MD cores (Pailler and Bard, 2002).

As already mentioned by other authors (e.g., van Kreveld et al., 2000) SST_{su} rose rapidly at the onset of each D-O interstadial in MIS 3-2, but D-O interstadial 8 along the western Iberian margin is one exception to this rule, with SST_{su} as cold as at the beginning of some D-O stadials.

4.6.2. Paleoproductivity conditions

At present, productivity along the Iberian margin is induced (1) by the seasonal (May to September) upwelling of cold and nutrient-rich ENACW; (2).by river input of nutrients, mainly in winter and early spring and mostly in the northern area. The sediments productivity record is however not depend only on the surface productivity but also on the export efficiency and preservation at the bottom (Dittert et al., 1999).

Interglacial (MIS 1 and MIS 5) variability

At present the mean summer export productivity ($Pexp_{su}$) at SU92-03, MD95-2040, and MD95-2042 sites is 96, 68, and 77 $gC/m^2/yr$, respectively. Evidencing the highest productivity at 43º12´N.

The northernmost site SU92-03 also records higher $Pexp_{su}$ during the Eemian and the Holocene (108 $gC/m^2/yr$) than the other two cores (Fig. 10, Table 3). From 43º12´N to 37º48´N $Pexp_{su}$ decreased by 30 and 40 $gC/m^2/yr$ during the Eemian and Holocene, respectively. Eemian and Holocene differences in $Pexp_{su}$ are twice as high (20 to 30 $gC/m^2/yr$) between cores MD95-2040 and SU92-03 as between cores MD95-2040 and MD95-2042. Within the three cores the difference between the Eemian and the Holocene is small and within the $Pexp_{su}$ prediction error.

The Holocene latitudinal $Pexp_{su}$ gradient agrees well with the phytoplankton productivity indicated by the satellite-based pigment distribution data at the 3 core sites (Antoine et al., 1996). This is also a demonstration of the accuracy of our transfer function calibration. At present, the high $Pexp_{su}$ values off Cape Finisterra are related to the quasi-permanent or persistent occurrence of one of the most important upwelling filaments off the Iberian margin (Haynes et al., 1993; Álvarez-Salgado et al., 2001). Besides, the

ENACW upwelled in this area generally shows characteristics of the subpolar branch, which is colder and richer in nutrients (Fiúza, 1984; Rios et al., 1992; Fiúza et al., 1998).

During both interglacials, SU92-03 shows a higher $Pexp_{su}$, but lower % *G. bulloides* and a lower C_{org} accumulation rate (AR) than during the glacial periods. The planktonic foraminifera AR also exhibits higher values in the Holocene than during the glacials, but a similar range between the Eemian and the glacial periods (Fig. 9). The lower interglacial C_{org} AR as well as the lower Eemian planktonic foraminifera AR could be related to dissolution/preservation. For the planktonic foraminifera this is corroborated by the fragmentation index (Fig. 9), which during the Eemian is higher than during MIS 6 and in the range of the other glacials. Even though the planktonic foraminifera assemblage represents a composite mixture of different seasons over several years, it is still possible to link it to general primary production patterns in the surface ocean. The relative abundance of *G. bulloides* is lower in core SU92-03 than in the other two cores and replaced in the fauna by *N. pachyderma* (dextral) (Fig. 9); conform with the modern surface sediment record (Salgueiro et al., submitted). This change could be related to temperature changes in the prevailing water mass and/or to a change in the primary producer fauna and thereby food availability, as *G. bulloides* apparently prefers less spinose diatoms and possibly coccolithophores (Abrantes et al., 2002).

The $Pexp_{su}$ record of SU92-03 is fairly stable during the full MIS 5 and Holocene with an average 108 $gC/m^2/yr$, SST_{su} was fairly stable during the Eemian and Holocene with 17.3ºC on average and with 15.5ºC during the remaining MIS 5 (excluding H). $Pexp_{su}$ maxima within MIS 5 (120 $gC/m^2/yr$) occurred around 119.5 ky during the Eemian, and at 8 and 3 ky during the Holocene. The 114 ky, 6 and 3 ky peaks of high $Pexp_{su}$ coincide with an increase of % *G. bulloides* and SST_{su} decrease, clearly denoting times of intense upwelling during the interglacials. The $Pexp_{su}$ minimum of 60 $gC/m^2/yr$ within MIS 5 is related to H8.

For the full MIS 5 and the Holocene both MD sites show a higher variability, with the MD95-2042 data revealing a larger amplitude and lower $Pexp_{su}$ (Fig. 10). The interglacial periods have lower $Pexp_{su}$ and warmer SST_{su} (~80-90 $gC/m^2/yr$ and 18ºC) than MIS 5.3 and MIS 5.1 (96 $gC/m^2/yr$ and 16ºC). Like in the SU92-03 core both show low $Pexp_{su}$ during H8 with 60 and 75 $gC/m^2/yr$ at site MD95-2040 and MD95–2042, respectively. Furthermore, H10 is recorded by a minimum of 65 $gC/m^2/yr$ in core MD95-2040. In contrast to the H, short-term cooling periods, i.e. the SST minima of D-O stadial

26, 24-23, and 21, are associated with increased Pexp in the MD cores (Fig. 10), possibly related to a higher nutrient content in the subpolar waters. At site MD95-2042 $Pexp_{su}$ minima (< 50 $gC/m^2/yr$) are also observed at the MIS 6/Eemian transition, during D-O stadial 25, and at 7-8 ky and 0.5 ky, all of which coincide with slightly warmer SST_{su} in this core.

Pailler and Bard (2002), using the two southern cores, MD95-2040 and MD95–2042 alkenone and carbonate data, observed also an anticorrelation between productivity proxies, total C37 alkenones AR and C_{org} AR, and the SST alkenone records for the full MIS 5 and MIS 1. The authors suggest a connection between the strength of the upwelling and the biological productivity off Portugal with weaker coastal upwelling being caused by a weakening or a shift in the atmospheric circulation over the North Atlantic during MIS 5 and the Holocene. This regime fits well with our interglacial data for the same cores, but does not agree with site SU92-03's data, as this site at 43º12´N records colder SST_{su} and higher Pexp than the two MD sites at 40º35´N and 37º48´N. Our data suggests another cause, the type of ENACW being upwelled. In Fig. 11 the $Pexp_{su}$ values for each core are plotted versus their respective SST_{su} and clear trends are visible. $Pexp_{su}$ seems to increase with SST_{su} until 16ºC and then to decrease along with rising SST. This temperature threshold agrees with the modern temperature range of the $ENACW_{sp,}$, which is preferentially upwelled at site SU92-03. So the difference in productivity is more likely related to the upwelled water mass and its nutrient content.

Higher interglacial than glacial primary productivity as shown by our SU92-03 record was also observed in the mid- to high latitude band between 48º and 58ºN by benthic foraminifera (Thomas et al., 1995) or planktonic foraminifera AR and carbonate mass AR in core T88-9P (48º23´N, 25º06´W (van Kreveld et al., 1996)) or the organic carbon content in sediments from the Feni Drift (54º-56ºN (Stein and Stax, 1991; Van Weering and Rijk, 1991)); so regions close to where $ENACW_{sp}$ is formed. At high latitudes of the Southern Ocean productivity was also higher during interglacials (e.g., Berger and Wefer, 1991; Shemesh et al., 1993). In contrast, primary productivity was higher during glacial than interglacial periods - like in our MD sites - in regions and upwelling areas of the low latitude North Atlantic (Muller et al., 1983; Pokras, 1987; Sarnthein et al., 1992) and at lower mid-latitude sites in the eastern boundary upwelling system (Sarnthein and Winn, 1988; Lebreiro et al., 1997; Abrantes, 2000; Freudenthal et al., 2002). The geographic boundary between these different glacial/interglacial

productivity regimes seems to be located in our study transect between SU92-03 and MD95-2040 cores and thus between 43º12´N and 40º35´N.

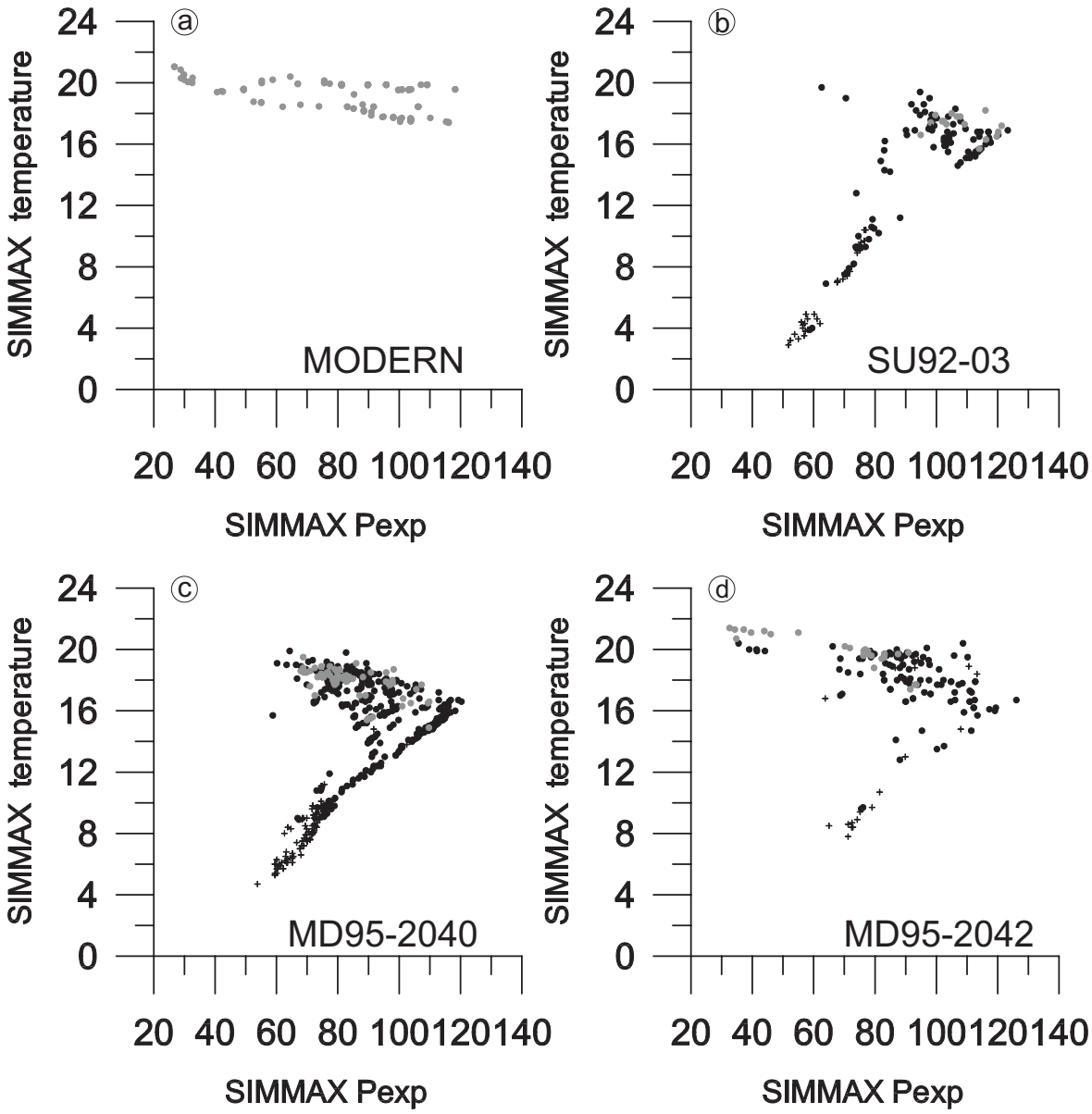

Fig. 11 (a) Satellite derived summer export productivity versus summer sea surface temperature (WOA 98, at 10 m depth) from samples of database located off Iberian margin. Estimated summer export productivity versus estimated summer sea surface temperature with SIMMAX technique of the 3 studied cores: SU92-03 (b), MD95-2040 (c), and MD95-2042 (d).Grey circles represent the interglacial samples; black circles represent the glacial samples; black crosses represent the Heinrich events samples.

Glacial (MIS 2-4 and MIS 6) variability

During glacial periods of the last 150 ky mean $Pexp_{su}$, excluding the H, varies along the latitudinal transect between 83 and 99 $gC/m^2/yr$ within the $Pexp_{su}$ calibration error (Fig. 10, Table 3). Like the SST_{su} records, glacial $Pexp_{su}$ shows higher-frequency oscillations than recorded during the interglacial periods, in particular at the two northernmost cores.

Similar to the interglacial periods, MD95-2042 shows the lowest $Pexp_{su}$ values and highest $Pexp_{su}$ amplitude variability over time, which should reflect the variability of the upwelling filament off Cape Sines and also Cape Roca and Espichel in regard to intensity, persistence, spatial extension, and nutrient availability or a combination of some of these factors over the last 150 ky. In contrast, site MD95-2040, located closer to the coast, recorded a more constant coastal upwelling and thus a narrower $Pexp_{su}$ amplitude.

In core SU92-03, higher sedimentation rates and C_{org} AR are related to the glacials (Fig. 9). The relative abundance of *G. bulloides* follows the same trend as the C_{org} AR, so that both seem to indicate increased productivity off Cape Finisterra and thereby periods of upwelling intensification. However, both MIS 6 and MIS 4 C/N ratios are higher than 10 and lower than 15, suggesting an increase of terrestrial C_{org} input, but it is during the Younger Dryas that values of C/N higher than 15 clearly indicate a substantial input of terrestrial C_{org} (Fig. 9e).

In the two MD cores, Pailler and Bard (2002) have also correlated the high C_{org} AR, $CaCO_3$ AR, total C37 alkenone AR, and the SST alkenone record for the last 140 ky, which reveals about 4ºC colder SST than in the Holocene, with more intense upwelling.

Favorable upwelling conditions under glacial conditions result from the southward migration of the polar front, which seems to generate an intensification of the Azores anticyclonic cell and consequently also a probable increase in wind circulation with stronger northerlies off Iberia, and turned upwelling into the major promoter of productivity (Pailler and Bard, 2002 and references within).

For all cores, relatively warm SST_{su} and high $Pexp_{su}$ values (85 - 108 $gC/m^2/yr$) comparatively with actual SST_{su} and $Pexp_{su}$ are observed during the LGM, in accordance with a polar front position more at 40-42ºN (Pflaumann et al., 2003). A $Pexp_{su}$ short drop around 20 ky supports a northward advance of warm ENACWst like during the modern winter circulation (Fig. 10). As already mentioned above, site MD95-2040 does not record

this warm incursion as strongly as the other cores and shows high productivity close to the coast what could be related to the incursion of nutrient-rich subpolar waters.

For cores SU92-03 and MD95-2040, the lowest $Pexp_{su}$ values coincide with the H (including H5a) and D-O stadials – with similar values at both sites –, while in the southern core MD95-2042 $Pexp_{su}$ was reduced during H1 to H3, H6 and H7 and to a lesser extend during H6, H8 and H10, but spiked during H4 and H5 (Fig. 10). Glacial $Pexp_{su}$ minima in this core, on the other hand, coincide with interstadials and the warm water incursion at 20 ky and their values are the lowest recorded in all three records. So, the productivity history was much more complex in the south and probably related to the varying interplay between southward advances of the polar front and northward advances of subtropical waters, over which we have also. To consider the variability in intensity, and/or persistence and direction of the upwelling filament which affected this site nearly throughout the whole last 150 ky (Fig. 11). Besides H4 and H5 the reduced H $Pexp_{su}$ values at site MD95-2042 are in the range of those found in two northern sites, so that the incursions of subpolar freshwater probably had a similar effect at all sites, i.e. causing an increased water column stratification and suppressing wind induced upwelling. As subpolar surface waters advanced into the Gulf of Cadiz (Voelker et al., 2006) and the Mediterranean Sea (Cacho et al., 1999; Martrat et al., 2004) during H4 and H5, the productivity peaks at site MD95-2042 might be linked to upwelling at the polar front. The lowest productivity during H can also result from the quasi monospecific (high relative abundances of *Nq. pachyderma* (sinistral)) assemblages found at those levels. However, recent model (Schmittner, 2005) shows evidence, as our results, for the disruption of Atlantic meridional overturning circulation to result into a stronger decline in biomass, less than half, particularly in the North Atlantic plankton stocks, due to the rapid shoaling of winter mixed layers and their associated separation from the deep ocean nutrient reservoir. These analysis of the simulation also indicates an increase of nutrients and stronger upwelling that fertilize the ocean along the Iberian margin (40ºN, 20ºW) during the D-O stadials, but with exception three stadials at 37º48´N (MD95-2042) site, our data indicate that D-O interstadials are associated with high $Pexp_{su}$ values. At site SU92-03 furthermore indicated by increased C_{org} AR after H6, H5, H4, H3 and planktonic foraminifera AR, which generally follow the C_{org} record. In some cases such as at the end of H1 (Nave et al., 2005) at the southern limit of the Ruddiman-belt, as the upwelling cell off Cape Yubi (NW-Africa) (Meggers et al., personal communication , 2006).

4.7. Conclusions

Millennial-scale variability, related to Heinrich events and Dansgaard-Oeschger cycles is evidenced along a north - south transect off the Western Iberian margin (SU92-03, MD95-2040, MD95-2042) by $\delta^{18}O$ *G. bulloides* record similar patterns for the last 150 ky.

At all sites, planktonic foraminifera census counts were used to reconstruct summer sea surface temperature and summer export productivity during the last 150 ky with the modern analog technique SIMMAX 28. For this purpose the North Atlantic modern analog database from planktonic foraminifera counts was expanded by Iberian margin surface samples leading to a total of 1020 analogs for SST and 999 for Pexp.

The higher relative abundances of *N. pachyderma* (sinistral), heavier planktonic $\delta^{18}O$ and lower SST_{su} values clearly show that the northernmost core SU92-03 was more influenced by polar water masses than the other two cores. While SU92-03 reveals the coldest conditions over time, its records are more similar to MD95-2040 than to MD95-2042, in accordance with a stronger subtropical influence on the southern margin. The highest relative abundances of *N. pachyderma* (sinistral) (>80%), the presence of Ice Rafted Debris, low mean SST_{su} (< 7ºC), and low mean $Pexp_{su}$ (< 70 $gC/m^2/yr$) at site SU92-03 are associated with Heinrich events (H)1 - H6, H8, H11, and probably H7 and H10. These events are also marked by heavy planktonic and benthic $\delta^{18}O$ values. A similar pattern was also found on the other two cores. However, the core MD95-2042 lowest $Pexp_{su}$ estimates seem to coincide with different factors as probably determined by the varying interplay between southward advances of the polar front and northward advances of subtropical waters. Associated may also be the variability in intensity and/or persistence of the upwelling filament which affected this site nearly throughout the whole last 150 ky.

The interglacial periods, Eemian and Holocene are the most stable and warmest periods at the 3 sites during the last 150 ky with a clear north-south increase in SST_{su} (2-3ºC) and a decrease in $Pexp_{su}$ (30-40 $gC/m^2/yr$). This north-south variation between the 3 latitudes fully reflects the modern conditions, with colder temperatures off Cape Finisterra and warmer (subtropical) temperatures off southwest Iberia, and demonstrates the efficiency of our transfer function.

During the glacial periods all cores show high SST_{su} and $Pexp_{su}$ variability with the H well marked by short cold periods. The mean SST_{su} without considering the H, also record a north-south temperature increase (3-4ºC), but no variation is seen in the mean $Pexp_{su}$ (without H).

SU92-03 shows higher interglacial than glacial $Pexp_{su}$ like other North Atlantic sites at mid to high latitudes. Contrarily the other two cores show higher glacial than interglacial $Pexp_{su}$ as also recorded in low latitude regions and upwelling areas of the North Atlantic. The geographic boundary between these differences in glacial/ interglacial productivity estimates seems to be between 43º12´N and 40º35´N.

For all cores relatively warm SST_{su} (16.5-18.4ºC) and high $Pexp_{su}$ (85 - 108 $gC/m^2/yr$) were observed during the Last Glacial Maximum (21.5-18 ky), in agreement with the reconstructions of the GLAMAP group (Sarnthein et al., 2003). A short increase in SST_{su}, and a drop in $Pexp_{su}$ around 20 ky, and the presence of the subtropical species *G. ruber* (white) imply the northward advance of warm waters all the way up to site SU92-03 and a circulation like during the modern winter.

The northernmost core SU92-03 shows the coldest SST_{su} and highest SST_{su} amplitude over time, in agreement with the strongest influence of the glacial polar front movements and the southward penetration of subpolar to polar water masses, not only in the surface waters but in accordance with modern conditions most probably also in ENACW. In contrast, the southernmost core MD95-2042 shows the highest $Pexp_{su}$ amplitude indicating that while the upwelling filament of Sines was likely present during most of the studied interval, it underwent major changes in its direction, intensity and/or nutrient availability. Core MD95-2040, located closer to the coast, where the upwelling is more constant, suffers less variations in Pexp.

Acknowledgements

We thank Célia Trindade, Cremilde Monteiro, Ana Margarida Silva, and Maria José Custódio of the Department of Geologia Marinha of INETI (former IGM) for analytical assistance. The EU PALEOSTUDIES project supported the planktonic and benthic foraminifera stable isotopes measurements from the SU92-03 core. Cristina Lopes is acknowledged for extracting the modern analog primary productivity data from the

Antoine´s data base and Monika Segl for her help with the isotope measurements. This study was funded by "Fundação para a Ciência e a Tecnologia (FCT)" and "Fundo Social Europeu (FSE) no âmbito do III Quadro Comunitáro de Apoio" fellowship SFRH/BD/11743/2003, and project INGMAR PLE/4/98. "Fundação Calouste Gulbenkian" is acknowledge for travel support to E. Salgueiro. We are also grateful to the Deutsche Forschungsgemeinschaft as part of the DFG-Research Center Ocean Margins (RCOM) of the University of Bremen for technical support.

References

Abrantes, F., 2000. 200 000 yr diatom records from Atlantic upwelling sites reveal maximum productivity during LGM and a shift in phytoplankton community structure at 185 000 yr. Earth and Planetary Science Letters, 176 (1), 7-16.

Abrantes, F. et al., 1998. Sediment fluxes along the northeastern European Margin: inferring hydrological changes between 20 and 8 kyr. Marine Geology, 152 (1-3), 7-23.

Abrantes, F. et al., 2005. Shallow-marine sediment cores record climate variability and earthquake activity off Lisbon (Portugal) for the last 2000 years. Quaternary Science Reviews, In Press, Corrected Proof.

Abrantes, F. et al., 2002. Fluxes of micro-organisms along a productivity gradient in the Canary Islands region (29°N): implications for paleoreconstructions. Deep Sea Research Part II: Topical Studies in Oceanography, 49 (17), 3599-3629.

Abrantes, F. and Moita, M.T., 1999. Water column and recent sediment data on diatoms and coccolithophorids, off Portugal, confirm sediment record of upwelling events. Oceanologica Acta, 22, 319-336.

Álvarez-Salgado, X.A., Gago, J., Miguez, B.M. and Perez, F.F., 2001. Net ecosystem production of dissolved organic carbon in a coastal upwelling system: the Ria de Vigo, Iberian margin of the North Atlantic. Limnology and Oceanography, 46 (1), 135-147.

Ambar, I. and Howe, M.R., 1979. Observations of the Mediterranean Outflow .1. Mixing in the Mediterranean Outflow. Deep-Sea Research Part a-Oceanographic Research Papers, 26 (5), 535-554.

Antoine, D., Andre, J.M. and Morel, A., 1996. Oceanic primary production .2. Estimation at global scale from satellite (coastal zone color scanner) chlorophyll. Global Biogeochemical Cycles, 10 (1), 57-69.

Baas, J.H., Mienert, J., Abrantes, F. and Prins, M.A., 1997. Late Quaternary sedimentation on the Portuguese continental margin: Climate-related processes and products. Palaeogeography Palaeoclimatology Palaeoecology, 130 (1-4), 1-23.

Bard, E., 1988. Correction of accelerator mass spectometry ^{14}C ages measured in planktonic foraminifera: Paleoceanographic implications. Paleoceanography, 3, 635-645.

Bassinot, F. and Labeyrie, L., 1996. IMAGES 101 Report, Institut Français pour la Recherche et la Technologie Polaires, Plouzané.

Berger, W.H. and Keir, R.S., 1984. Glacial-Holocene Changes in Atmospheric CO2 and the Deep-Sea Record. In: M. Ewing (Editor), Climate Processes and Climate Sensitivity. Am. Geophysical Union, pp. 337-351.

Berger, W.H., Smetacek, V.S. and Wefer, G., 1989. Productivity of the Ocean : Present and Past, Report of the Dahlem Workshop on Berlin, 1988, April 24-29, Productivity of the Ocean : Present and Past. Life Sciences Research Reports - Nº 44. John Wiley & Sons, Chichester, pp. 471.

Berger, W.H. and Wefer, G., 1991. Productivity of the oceans: Discussion of the iron hypothesis. Paleoceanography, 36, 1899-1918.

Birks, H.J.B., 1995. Quantitative palaeoenvironmental reconstructions. In: D. Maddy and J.S. Brew (Editors), Statistical Modelling of Quaternary Science Data. Technical Guide 5. Quaternary Research Association, Cambridge, pp. 161-254.

Bond, G. et al., 1992. Evidence for Massive Discharges of Icebergs into the North-Atlantic Ocean During the Last Glacial Period. Nature, 360 (6401), 245-249.

Boyle, E.A., 2000. Is ocean thermohaline circulation linked to abrupt stadial/interstadial transitions? Quaternary Science Reviews, 19 (1-5), 255-272.

Broecker, W., Bond, G., Miecyslawa, K., Clark, E. and McManus, J., 1992. Origin of the northern Atlantic's Heinrich events. Climate Dynamics, 6, 265–273.

Broecker, W.S., 1982. Ocean Chemistry During Glacial Time. Geochimica Et Cosmochimica Acta, 46 (10), 1689-1705.

Cacho, I. et al., 1999. Dansgaard-Oeschger and heinrich event imprints in Alboran Sea paleotemperatures. Paleoceanography, 14 (6), 698-705.

Calvo, E., Villanueva, J., Grimalt, J.O., Boelaert, A. and Labeyrie, L., 2001. New insights into the glacial latitudinal temperature gradients in the North Atlantic. Results from U-37(K ') sea surface temperatures and terrigenous inputs. Earth and Planetary Science Letters, 188 (3-4), 509-519.

Cayre, O., Lancelot, Y. and Vincent, E., 1999. Paleoceanographic reconstructions from planktonic foraminifera off the Iberian Margin: Temperature, salinity, and Heinrich events. Paleoceanography, 14 (3), 384-396.

Chapman, M.R. and Shackleton, N.J., 1998. Millennial-scale fluctuations in North Atlantic heat flux during the last 150,000 years. Earth and Planetary Science Letters, 159, 57-70.

Chapman, M.R. and Shackleton, N.J., 1999. Global ice-volume fluctuations, North Atlantic ice-rafting events, and deep-ocean circulation changes between 130 and 70 ka. Geology, 27 (9), 795-798.

Chapman, M.R., Shackleton, N.J. and Duplessy, J.C., 2000. Sea surface temperature variability during the last glacial-interglacial cycle: assessing the magnitude and pattern of climate change in the North Atlantic. Palaeogeography Palaeoclimatology Palaeoecology, 157 (1-2), 1-25.

Coste, B., Fiuza, A.F.G. and Minas, H.J., 1986. Hydrological and Chemical Conditions Associated with the Portuguese Coastal Upwelling During Late Summer. Oceanologica Acta, 9 (2), 149-158.

Crowley, T.J., 1994. Pleistocene Temperature-Changes. Nature, 371 (6499), 664-664.

Dansgaard, W. et al., 1993. Evidence for General Instability of Past Climate from a 250-Kyr Ice-Core Record. Nature, 364 (6434), 218-220.

de Abreu, L., Shackleton, N.J., Schonfeld, J., Hall, M. and Chapman, M., 2003. Millennial-scale oceanic climate variability off the Western Iberian margin during the last two glacial periods. Marine Geology, 196 (1-2), 1-20.

Dittert, N. et al., 1999. Carbonate Dissolution in the Deep-Sea: Methods, Quantification and Paleoceanographic Application. In: G. Fischer and G. Wefer (Editors), Use of Proxies in Paleoceanography: Examples from the South Atlantic. Springer-Verlag, pp. 255-284.

Doney, S.C. et al., 2001. Marine Biogeochemical Modeling: Recent Advances and Future Challenges. Oceanography, 14 (4), 93-107.

Ducklow, H.W., Steinberg, D.K. and Buesseler, K.O., 2001. Upper Ocean carbon export and the biological pump. Oceanography, 14 (4), 50-58.

Duplessy, J.C., Delibrias, G., Turon, J.L., Pujol, C. and Duprat, J., 1981. Deglacial Warming of the Northeastern Atlantic Ocean : Correlation with the Paleoclimatic Evolution of the European Continent. Elsevier Scientific Publishing Company, Amsterdam, pp. 121-144.

Elliot, M. et al., 1998. Millennial-scale iceberg discharges in the Irminger Basin during the last glacial period: Relationship with the Heinrich events and environmental settings. Paleoceanography, 13 (5), 433-446.

Elliot, M., Labeyrie, L. and Duplessy, J.-C., 2002. Changes in North Atlantic deep-water formation associated with the Dansgaard-Oeschger temperature oscillations (60-10ka). Quaternary Science Reviews, 21 (10), 1153-1165.

Eppley, R.W. and Peterson, B.J., 1979. Particulate Organic-Matter Flux and Planktonic New Production in the Deep Ocean. Nature, 282 (5740), 677-680.

Fiúza, A.F.G., 1983. Upwelling Patterns off Portugal. In: E. Suess and J. Thiede (Editors), Coastal Upwelling its sediment record. Plenum Press, New York, pp. 85-98.

Fiúza, A.F.G., 1984. Hidrologia e Dinamica das Aguas Costeiras de Portugal, Faculdade de Ciências da Universidade de Lisboa, Lisbon, 294 pp.

Fiúza, A.F.G. et al., 1998. Water masses and their circulation off western Iberia during May 1993. Deep Sea Research Part I: Oceanographic Research Papers, 45 (7), 1127-1160.

Freudenthal, T. et al., 2002. Upwelling intensity and filament activity off Morocco during the last 250,000 years. Deep Sea Research Part II: Topical Studies in Oceanography, 49 (17), 3655-3674.

Fronval, T. and Jansen, E., 1997. Eemian and early Weichselian (140-60 ka) paleoceanography and paleoclimate in the Nordic seas with comparisons to Holocene conditions. Paleoceanography, 12 (3), 443-462.

Ganopolski, A. and Rahmstorf, S., 2002. Abrupt Glacial Climate Change due to Stochastic Resonance. Physical Review Letters, 88 (3), DOI: 10.1103/PhysRevLett.88.038501.

Grootes, P.M. and Stuiver, M., 1997. $^{18}O/^{16}O$ variability in Greenland snow and ice with 10^{-3} to 10^{5} year time resolution. Journal Geophysical Research, 102, 26455-26470.

Grootes, P.M., Stuiver, M., White, J.W.C., Johnsen, S. and Jouzel, J., 1993. Comparison of oxygen isotope records from the GISP2 and GRIP Greenland ice cores. Nature, 366, 552–554.

Haynes, R., Barton, E. and Pilling, I., 1993. Development, persistence, and variability of upwelling filaments off the Atlantic coast of the Iberian Peninsula. Journal of Geophysical Research, 98 (C12), 22681-22692.

Heinrich, H., 1988. Origin and Consequences of Cyclic Ice Rafting in the Northeast Atlantic-Ocean During the Past 130,000 Years. Quaternary Research, 29 (2), 142-152.

Hemleben, C., Spindler, M. and Anderson, O.R., 1989. Modern Planktonic Foraminifera. Springer-Verlang, Berlin, 363 pp.

Hemming, S.R., 2004. Heinrich events: Massive late Pleistocene detritus layers of the North Atlantic and their global climate imprint. Rev. Geophys., 42 (1), 1-43.

Hughen, K. et al., 2004. C-14 activity and global carbon cycle changes over the past 50,000 years. Science, 303 (5655), 202-207.

Kaspi, Y., Sayag, R. and Tziperman, E., 2004. A "triple sea-ice state" mechanism for the abrupt warming and synchronous ice sheet collapses during Heinrich events. Paleoceanography, 19 (3), -.

Kiefer, T., 1998. Productivity and temperatures in the sutropical North Atlantic: Cyclic and abrupt changes during the Late Quaternary, University Kiel, Kiel, 127 pp.

Kucera, M. et al., 2005. Reconstruction of sea-surface temperatures from assemblages of planktonic foraminifera: multi-technique approach based on geographically constrained calibration data sets and its application to glacial Atlantic and Pacific Oceans. Quaternary Science Reviews, 24, 951-998.

Kukla, G.J. et al., 2002. Last interglacial climates. Quaternary Research, 58 (1), 2-13.

Labeyrie, L. et al., 1999. Temporal variability of the surface and deep waters of the North West Atlantic Ocean at orbital and millennial scales. In: P.U. Clark, R.S. Webb and L.D. Keigwin (Editors), Mechanisms of Global Climate Change at Millennial Time Scales. AGU, Washington, D.C., pp. 77–98.

Labeyrie, L. and Party, S.S., 1990. Rapport Preliminaire de PALEOCINAT I (Paleocirculation de l´Atlantique nord), IFREMER, INSU.

Labeyrie, L. et al., 1995. Surface and deep hydrology of the Northern Atlantic Ocean during the past 150 000 years. Phil. Trans. R. Soc. Lond., 348, 255-264.

Lampitt, R.S., Raine, R.C.T., Billett, D.S.M. and Rice, A.L., 1995. Material supply to the European continental slope: A budget based on benthic oxygen demand and organic supply. Deep-Sea Research Part I-Oceanographic Research Papers, 42 (11-12), 1865-&.

Laws, E.A., Falkowski, P.G., Smith, W.O., Ducklow, H.W. and McCarthy, J.J., 2000. Temperature effects on export production in the opean ocean. Global Biogeochemical Cycles, 14, 1231-1246.

Lebreiro, S.M., Moreno, J.C., Abrantes, F.F. and Pflaumann, U., 1997. Productivity and paleoceanographic implications on the Tore Seamount (Iberian Margin) during the last 225 kyr: Foraminiferal evidence. Paleoceanography, 12 (5), 718-727.

Lebreiro, S.M., Moreno, J.C., McCave, I.N. and Weaver, P.P.E., 1996. Evidence for Heinrich layers off Portugal (Tore Seamount: 39 degrees N, 12 degrees W). Marine Geology, 131 (1-2), 47-56.

Lisiecki, L.E. and Raymo, M.E., 2005. A Pliocene-Pleistocene stack of 57 globally distributed benthic delta O-18 records. Paleoceanography, 20 (1), -.

Martinson, D.G. et al., 1987. Age Dating and Orbital Theory of the Ice Ages: Development of a High-Resolution 0 to 300,00-Year Chronostratigraphy. Quaternary Research, 27, 1-29.

Martrat, B. et al., 2004. Abrupt temperature changes in the western Mediterranean over the past 250,000 years. Science, 306, 1762-1765.

Maslin, M.A., Shackleton, N.J. and Pflaumann, U., 1995. Surface-Water Temperature, Salinity, and Density Changes in the Northeast Atlantic During the Last 45,000 Years - Heinrich Events, Deep-Water Formation, and Climatic Rebounds. Paleoceanography, 10 (3), 527-544.

McManus, J.F. et al., 1994. High-Resolution Climate Records from the North-Atlantic During the Last Interglacial. Nature, 371 (6495), 326-329.

McManus, J.F., Oppo, D.W., Keigwin, L.D., Cullen, J.L. and Bond, G.C., 2002. Thermohaline circulation and prolonged interglacial warmth in the North Atlantic. Quaternary Research, 58 (1), 17-21.

Meggers, H. et al., 2002. Assessment of geochemical and micropaleontological sedimentary parameters as proxies of surface water properties in the Canary Islands region. Deep Sea Research Part II: Topical Studies in Oceanography, 49 (17), 3631-3654.

members, N., 2004. High-resolution record of Northern Hemisphere climate extending into the last interglacial period. Nature, 431 (7005), 147-151.

Mojtahid, M. et al., 2005. Palaeoclimatology and palaeohydrography of the glacial stages on Celtic and Armorican margins over the last 360 000 yrs. Marine Geology, 224 (1-4), 57-82.

Moore, J.K., Doney, S.C., Glover, D.M. and Fung, I.Y., 2002. Iron cycling and nutrient-limitation patterns in surface waters of the World Ocean. Deep-Sea Research Part Ii-Topical Studies in Oceanography, 49 (1-3), 463-507.

Muller, A., Erlenkeuser, H. and von Grafenstein, R., 1983. Glacial-interglacial cycles on oceanic productivity inferred from organic carbon contens in eastern North Atlantic cores. In: E. Suess and J. Thiede (Editors), Coastal Upwelling. Plenum Press, New York, pp. 365-398.

Nave, S., 2005. Changements de la productivité océanique lors des variations rapides du climat (Événements de Heinrich). PhD. Thesis, Université Paris XI, Orsay.

NGRIP-members, 2004. High-resolution record of Northern Hemisphere climate extending into the last interglacial period. Nature, 431 (7005), 147-151.

Niebler, H.-S. and Gersonde, R., 1998. A planktic foraminiferal transfer function for the southern South Atlantic Ocean. Marine Micropaleontology, 34 (3-4), 213-234.

Oppo, D.W. and Lehman, S.J., 1995. Suborbital Timescale Variability of North-Atlantic Deep-Water During the Past 200,000 Years. Paleoceanography, 10 (5), 901-910.

Pailler, D. and Bard, E., 2002. High frequency palaeoceanographic changes during the past 140 000 yr recorded by the organic matter in sediments of the Iberian Margin. Palaeogeography, Palaeoclimatology, Palaeoecology, 2799, 1-22.

Peck, V.L. et al., 2006. High resolution evidence for linkages between NW European ice sheet instability and Atlantic Meridional Overturning Circulation. Earth and Planetary Science Letters, 243 (3-4), 476-488.

Peliz, A., Dubert, J., Santos, A.M.P., Oliveira, P.B. and Le Cann, B., 2005. Winter upper ocean circulation in the Western Iberian Basin - Fronts, Eddies and Poleward Flows: an overview. Deep-Sea Research Part I-Oceanographic Research Papers, 52 (4), 621-646.

Pflaumann, U., Duprat, J., Pujol, C. and Labeyrie, L.D., 1996. SIMMAX: A modern analog technique to deduce Atlantic sea surface temperatures from planktonic foraminifera in deep-sea sediments. Paleoceanography, 11 (1), 15-35.

Pflaumann, U. et al., 2003. Glacial North Atlantic: Sea-surface conditions reconstructed by GLAMAP 2000. Paleoceanography, 18 (3), 1065, doi: 10.1029/2002PA000774.

Pokras, E.M., 1987. Diatom record of the late Quaternary climatic change in the eastern equatorial Atlantic and tropical Africa. Paleoceanography, 2, 273-286.

Rashid, H., Hesse, R. and Piper, D.J.W., 2003. Evidence for an additional Heinrich event between H5 and H6 in the Labrador Sea. Paleoceanography, 18 (4), -.

Reimer, P.J. et al., 2004. INTCAL04 Terrestrial Radiocarbon Age calibration, 0–26 cal kyr BP. Radiocarbon, 46, 1029 -1058.

Relvas, P. and Barton, E.D., 2002. Mesoscale patterns in the Cape São Vicente (Iberian Peninsula) upwelling region. Journal Geophysical Research, 107 (C10), 28-1-28-23.

Rios, A.F., Perez, F.F. and Fraga, F., 1992. Water Masses in the Upper and Middle North-Atlantic Ocean East of the Azores. Deep-Sea Research Part a-Oceanographic Research Papers, 39 (3-4A), 645-658.

Roucoux, K.H., De Abreu, L., Shackleton, N.J. and Tzedakis, P.C., 2005. The response of NW Iberian vegetation to North Atlantic climate oscillations during the last 65 kyr. Quaternary Science Reviews, 24 (14-15), 1637-1653.

Roucoux, K.H., Shackleton, N.J., de Abreu, L., Schonfeld, J. and Tzedakis, P.C., 2001. Combined marine proxy and pollen analyses reveal rapid Iberian vegetation response to North Atlantic. Quaternary Research, 56 (1), 128-132.

Ruddiman, W.F., 1977. Late Quaternary deposition of ice-rafted sand in the subpolar North Atlantic (lat 40º to 65ºN). Geological Society of America Bulletin, 88, 1813-1827.

Salgueiro, E. et al., submitted. Planktonic Foraminifera from Modern Sediments Reflect Upwelling Patterns off Iberia: Insights from a Regional Transfer Function. Marine Micropaleontology.

Sancetta, C., 1992. Primary production in the glacial North Atlantic and North Pacific oceans. Nature, 360, 249-251.

Sánchez-Goñi, M.F. et al., 2002. Synchroneity between marine and terrestrial responses to millennial scale climatic variability during the last glacial period in the Mediterranean region. Climate Dynamics, 19, 95-105.

Sánchez-Goñi, M.F., Eynaud, F., Turon, J.L. and Shackleton, N.J., 1999. High resolution palynological record off the Iberian margin: direct land-sea correlation for the Last Interglacial complex. Earth and Planetary Science Letters, 171 (1), 123-137.

Sánchez-Goñi, M.F., Turon, J.L., Eynaud, F. and Glendreau, S., 2000a. European climatic response to millennial-scale changes in the atmosphere-ocean system during the last glacial period. Quaternary Research, 54, 394–403.

Sánchez-Goñi, M.F., Turon, J.-L., Eynaud, F., Schackleton, N.J. and Cayre, O., 2000b. Direct land/sea correlation of the Eemian, and its comparison with the Holocene: a high-resolution palynological record off the Iberian margin. Geologie en Mijnbouw / Netherlands Journal of Geosciences, 79 (2/3), 345-354.

Sarnthein, M., Pflaumann, U., Ross, R., Tiedemann, R. and Winn, K., 1992. Transfer Functions to reconstruct ocean paleoproductivity: a comparison. In: C.P. Summerhayes, W.L. Prell and K.C. Emeis (Editors), Upwelling Systems: Evolution Since the Early Miocene. Geological Society Special Publication, pp. 411-427.

Sarnthein, M., Pflaumann, U. and Weinelt, M., 2003. Past extent of sea ice in the northern North Atlantic inferred from foraminiferal paleotemperature estimates. Paleoceanography, 18 (2), -.

Sarnthein, M. et al., 2001. Fundamental modes and abrupt changes in North Atlantic circulation and climate over the last 60 ky – Numerical modelling and reconstruction. In: P. Schäfer, W. Ritzrau, M. Schlüter and J. Thiede (Editors), The Northern North Atlantic: A changing environment. Springer Verlag, Heidelberg, pp. 365–410.

Sarnthein, M. and Winn, K., 1988. Global variations of surface ocean productivity in Low and Mid latitudes: Influence on CO2 reservoirs of the deep ocean and atmosphere during the last 21,000 years. Paleoceanography, 3 (3), 361-399.

Sarnthein, M. et al., 1994. Changes in East Atlantic Deep-Water Circulation over the Last 30,000 Years - 8 Time Slice Reconstructions. Paleoceanography, 9 (2), 209-267.

Saunders, P.M., 1986. The accuracy of measurement of salinity, oxygen and temperature in the deep ocean. Journal of Physical Oceanography, 16 (1), 1274-1285.

Schmittner, A., 2005. Decline of the marine ecosystem caused by a reduction in the Atlantic overturning circulation. Nature, 434 (7033), 628-633.

Shackleton, N., 2001. Paleoclimate - Climate change across the hemispheres. Science, 291 (5501), 58-59.

Shackleton, N., Hall, M.A. and Vicent, E., 2000. Phase relationships between millennial-scale events 64,000-24,000 years ago. Paleoceanography, 15 (6), 565-569.

Shackleton, N.J., 1974. Attainment of isotopic equilibrium between ocean water and the benthonic foraminifera genus *Uvigerina*: Isotopic changes in the ocean during the last glacial. In: C.I.d. C.N.R.S. (Editor), Les méthodes quantitatives d´étude des variations du climat au cours du Pléistocène, pp. 203-209.

Shackleton, N.J., Chapman, M., Sanchez-Goni, M.F., Pailler, D. and Lancelot, Y., 2002. The classic Marine Isotope Substage 5e. Quaternary Research, 58, 14-16.

Shackleton, N.J. and Opdyke, N.D., 1973. Oxygen isotope and paleomagnetic stratigraphy of Equatorial Pacific core V28–238; Oxygen isotope temperature and ice volumes on a 10^5 year and 10^6 year scale. Quaternary Research, 3, 39–55.

Shemesh, A., Macko, S.A., Charles, C.D. and Rau, G.H., 1993. Isotopic evidence for reduced productivity in the glacial Southern Ocean. Science, 262, 407-410.

Skinner, L.C. and Shackleton, N.J., 2004. Rapid transient changes in northeast Atlantic deep water ventilation age across Termination I. Paleoceanography, 19 (2), -.

Sousa, F.M. and Bricaud, A., 1992. Satellite-Derived phytoplankton pigment structures in the Portuguese Upwelling Area. Journal of Geophysical Research, 97 (C7), 11,343-11,356.

Stein, R. and Stax, R., 1991. Late Quaternary organic carbon cycles and productivity in the Labrador Sea. Geo-Marine Letters, 11, 90-95.

Stoner, J.S., Channell, J.E.T. and HillaireMarcel, C., 1996. The magnetic signature of rapidly deposited detrital layers from the deep Labrador Sea: Relationship to North Atlantic Heinrich layers. Paleoceanography, 11 (3), 309-325.

Stuiver, M. and Grootes, P.M., 2000. GISP2 oxygen isotope ratios. Quaternary Research, 53 (3), 277-283.

Thomas, E., Booth, L., Maslin, M. and Shackleton, N.J., 1995. Northeastern Atlantic Benthic Foraminifera During the Last 45,000 Years - Changes in Productivity Seen from the Bottom Up. Paleoceanography, 10 (3), 545-562.

Thomson, J. et al., 1999. Implications for sedimentation changes on the Iberian margin over the last two glacial/interglacial transitions from (200Thexcess)0 Systematics. Earth and Planetary Science Letters, 165, 255-270.

Thunell, R. and Sautter, L.R., 1992. Planktonic foraminiferal faunal and stable isotopic indices of upwelling: a sediment trap study in the San Pedro Basin, Southern California Bight. In: C.P. Summerhayes, W.L. Prell and K.C. Emeis (Editors), Upwelling Systems: Evolution Since the Early Miocene. Geological Society Special Publication, pp. 77-91.

van Kreveld, S. et al., 2000. Potential links between surging ice sheets, circulation changes, and the Dansgaard-Oeschger cycles in the Irminger Sea, 60-18 kyr. Paleoceanography, 15 (4), 425-442.

van Kreveld, S.A., Knappertsbusch, M., Ottens, J., Ganssen, G.M. and vanHinte, J.E., 1996. Biogenic carbonate and ice-rafted debris (Heinrich layer) accumulation in deep-sea sediments from a Northeast Atlantic piston core. Marine Geology, 131 (1-2), 21-46.

Van Weering, T. and Rijk, S., 1991. Sedimentation and climate-induced sediments on Feni Ridge, Northeast Atlantic Ocean. Marine Geology, 101, 49-69.

VanAndel, T.H. and Tzedakis, P.C., 1996. Palaeolithic landscapes of Europe and environs, 150,000-25,000 years ago: An overview. Quaternary Science Reviews, 15 (5-6), 481-500.

Vidal, L. et al., 1997. Evidence for changes in the North Atlantic Deep Water linked to meltwater surges during the Heinrich events. Earth and Planetary Science Letters, 146 (1-2), 13-27.

Voelker, A.H.L. et al., 2006. Mediterranean outflow strengthening during northern hemisphere coolings: A salt source for the glacial Atlantic? Earth and Planetary Science Letters, 245, 39-55.

Wefer, G., Berger, W.H., Bijma, J. and Fischer, G., 1999. Clues to Ocean History: a Brief Overview of Proxies. In: G. Fischer and G. Wefer (Editors), Use of Proxies in Paleoceanography: Examples from the South Atlantic. Springer-Verlag, pp. 1-68.

Weinelt, M., Rosell-Mele, A., Pflaumann, U., Sarnthein, M. and Kiefer, T., 2003. Zur Rolle der Produktivitat im Nordostatlantik bei abrupten klimaanderungen in den letzten 80 000 jahren. Z.dt. geol. Ges., 154 (1), 47-66.

Wunsch, C., 2003. Determining paleoceanographic circulations, with emphasis on the Last Glacial Maximum. Quaternary Science Reviews, 22 (2-4), 371-385.

Wyputta, U. and Grieger, B., 1999. Comparison of eastern Atlantic atmospheric trajectories for present day and last glacial maximum. Palaeogeography Palaeoclimatology Palaeoecology, 146 (1-4), 53-66.

Zahn, R. et al., 1997. Thermohaline instability in the North Atlantic during meltwater events: Stable isotope and ice-rafted detritus records from core SO75-26KL, Portuguese margin. Paleoceanography, 12 (5), 696-710.

CHAPTER 5

Conclusions and Future perspectives

Planktonic foraminiferal census data preserved in surface sediments along the western Iberian margin revealed *G. bulloides* as the most abundant and widespread species and its distribution pattern shows a close relationship to the present-day spatial occurrence of coastal upwelling. Its importance in the fauna is further highlighted by the Q-mode factorial analysis that reveals the prominent factor 1, as the upwelling factor, which is defined mainly by this species. The other two factors are interpreted as representing two other important hydrographic features on the Iberian margin: the Portugal Current (factor 2) characterized by the presence of *N. pachyderma* (dextral) and *G. inflata* and the warm eastern branch of the Azores Current (factor 3) defined by *G. ruber* (white), *G. trilobus trilobus*, *and G. inflata*. Thus, the geographical relevance of these species/factors allows to deduce that the foraminiferal assemblages and distribution patterns on the Iberian margin are linked to the actual, seasonally variable hydrographic conditions, especially to the various upwelling features.

The assemblage data and satellite-derived sea surface temperature (SST) were used to calibrate, a regional SST transfer function for summer and winter, for the first time in a coastal upwelling region. By minimizing the bias associated with the absence of sufficient analogs in this particular region, better temperature reconstructions for the past became possible for North Atlantic upwelling areas, and the Iberian margin in particular.

For the regional transfer function we tested two commonly used techniques: Imbrie & Kipp´s (Imbrie and Kipp, 1971) and Pflaumann´s SIMMAX (with and without distance weighting options; Pflaumann et al., 1996; 2003). The simultaneous application of both distinct computational approaches to one database, allowed us to establish that SIMMAX (with distance weighting- dw) derived results are more consistent than the other ones, both during the calibration, and in the application to geological case-studies along the Iberian

margin. However, both techniques indicate insufficient number of modern analogs in the current data base for the Azores Current/subtropical warm water sphere. Furthermore, the analog set suffers from the lack of analogs for (sub)polar conditions on the western Iberian margin, i.e. the *N. pachyderma* left coiling caveat. So that the best approach to estimate glacial and Heinrich event SST at present was to include our regional data set into the MARGO reference data set of the North Atlantic (Kucera et al., 2005) and apply it in the study of the last 150 ky. Another possibility would be to use the past variability of species to define modern faunal assemblages (Mix et al., 1999).

For the study of the latest Holocene productivity and hydrographic conditions along the Iberian margin we applied the regional transfer function SIMMAX (dw) to estimate SST. The SST data was combined with various other proxy data including planktonic and benthic foraminifera abundances, stable isotope data and organic carbon obtained on sediment sequences recovered along an E-W transect off Sines (37˚ 50´N), and a N-S transect off Albufeira (8˚ 15´W).

Considerable temporal productivity changes in the Sines and Albufeira transects reflect the widely recognized European climate periods for the last 2500 yr: the Roman Warm Period (RWP); the Dark Ages (DA); the Medieval Warm Period (MWP); and the Little Ice Age (LIA).

Along the Sines transect, warm periods, in particular the MWP are dominated by stable upwelling conditions and increased productivity. On the other hand, cold periods, the DA and the LIA, are characterized by higher upwelling variability with an average decrease in productivity, most probably, caused by spatial and temporal variations in the Cape Roca and Espichel filaments' intensity and persistence. Along the Albufeira transect, an opposite trend is observed, with productivity indicators decreasing during the warm periods (RWP and MWP) and increasing during the cold periods (DA and LIA). The alternate intensification of the winds observed during the different North Atlantic Oscillation (NAO) phases could explain our record. If warm periods are characterized by a prevalent positive NAO phase, strong northerly winds are induced and an increase of upwelling along the southwestern margin, is likely to occur. Concurrently, a dominant negative NAO phase during the cold periods would lead to strong westerly winds and the occurrence of upwelling on the southern Iberian margin. However, the southwestern transect shows higher productivity than the southern transect through time, which is

attributed to a stronger and more persistent upwelling influence on the western Portuguese margin such as today.

No other major changes occurred in the hydrographic conditions between warm and cold climatic periods in both transects. As so, upwelling and surface water currents show patterns similar to the modern conditions throughout the last 2500 yr BP. The intermediate and deep water currents, the Mediterranean Outflow Water (MOW) and the North Atlantic Deep Water, flowed within the same water depths as at present. In addition, the sites influenced by the MOW, recorded the presence in both transects of the youngest contourite deposit identified in the Gulf of Cadiz (e.g., Faugeres et al., 1994; Voelker et al., 2006).

After the regional transfer function had been applied to Present and Late Holocene conditions, the last aim of this work was to reconstruct millennial-scale temperature and productivity variations during the last two glacial - interglacial cycles. Three high-resolution cores (SU92-03, MD95-2040, MD95-2042) located along an N-S profile (43º12´N – 37º48´N) off the West Iberian margin were used. For this study, the regional planktonic foraminifera assemblage data was incorporated into the North Atlantic modern analog file for SST leading to a total of 1020 analogs. In addition, the combined assemblage data base was used to establish a new version for the SIMMAX transfer function for export productivity (Pexp) with a total of 999 analogs.

Millennial-scale variability, related to Heinrich events (H) and Dansgaard-Oeschger cycles, is evidenced along the north - south transect by the most used proxies, $\delta^{18}O$ *G. bulloides*, IRD, summer SST (SST_{su}) and summer Pexp ($Pexp_{su}$), which show similar patterns throughout the studied interval.

The northernmost core (SU92-03) reveals the coldest conditions with values closer to the ones obtained for MD95-2040 than for MD95-2042, the later of which is, as at present, more affected by subtropical waters.

Coldest SST_{su} and lowest $Pexp_{su}$ are found during Heinrich events (H)1 – H8 and H10 - H11 at all sites. Only at the southernmost site (MD95-2042), less influenced by H, does the lowest $Pexp_{su}$ not coincide with all of these events.

The interglacial periods, Eemian and Holocene, are the most stable and warm periods at the 3 sites during the last 150 ky, with a clear north-south increase in SST_{su} (2-3ºC) and a decrease in $Pexp_{su}$ (30-40 $gC/m^2/yr$). This gradient between the 3 latitudes fully reflects the modern conditions and demonstrates the efficiency of our transfer function. During the

glacial periods all cores show high SST_{su} and $Pexp_{su}$ variability, with the H being well marked by short cold periods. The mean SST_{su}, excluding the H, also record a north-south temperature increase (3-4ºC) during the glacials, but no latitudinal variation is seen in the mean $Pexp_{su}$ (without H).

The site SU92-03 like other North Atlantic sites from mid to high latitudes, between 48º and 58ºN, reveals higher interglacial than glacial $Pexp_{su}$ through benthic foraminifera (Thomas et al., 1995), or through planktonic foraminifera AR and carbonate mass AR in core T88-9P (48º23´N, 25º06´W: van Kreveld et al., 1996), or through the organic carbon content in sediments from the Feni Drift (54º-56ºN: Stein and Stax, 1991; Van Weering and Rijk, 1991). Productivity was also higher during interglacials at high latitudes of the Southern Ocean (e.g., Berger and Wefer, 1991; Shemesh et al., 1993). Contrarily, the other two cores show higher glacial than interglacial $Pexp_{su}$ concordant with observations in low latitude regions and upwelling areas of the North Atlantic. The geographic boundary between these differences in glacial/interglacial productivity occurs between 43º12´N and 40º35´N.

The main conclusions could be summarize in four major points: (1) for the first time, the regional transfer function in an area of coastal upwelling was successfully applied; (2) this thesis contributes with a considerable amount of analogs from one upwelling region into the North Atlantic data set, (3) the widely recognized European climate periods of the last 2500 yr did not influence the behavior and position of the water masses that occur in this region. But differences in the warm/cold atmospheric circulation pattern changes the coastal upwelling intensity as well as its area of occurrence; (4) millennial scale changes reveal a north-south SST increase (2-4ºC) during the last 150 ky, with an higher range at 43º12´N (16.8ºC) than at 37º48´N (13.6ºC). During glacial periods Pexp is high (90-100 $gC/m^2/yr$) and homogeneous along the western Iberian margin, while, during interglacial periods it increases from south to north, between ~84 $gC/m^2/yr$ at 40º35´N and 108 $gC/m^2/yr$ at 43º12´N.

As our regional transfer function is doing so well in reconstructing the upwelling related SST patterns along the Iberia margin, one of my future objectives is to extend the regional coverage to the upwelling area off NW Africa, which belongs to the same upwelling system but experiences year record upwelling favorable conditions and so,

higher productivity than the Iberian margin. However, the calibration for the Pexp transfer function has shown that there is currently a lack of analogs for such high productivity areas. To overcome this situation, it is important to increase the number of analogs for upwelling features, both for a regionally restricted and the North Atlantic database in order to obtain more reliable paleo-SST and paleo-productivicty estimates in the upwelling regions of the eastern North Atlantic.

References

Berger, W.H., Wefer, G., 1991. Productivity of the oceans: Discussion of the iron hypothesis. Paleoceanography, 36: 1899-1918.

Faugeres, J.-C., Gonthier, E., Monteiro, H., Vergnaud-Grazzini, C., 1994. Sedimentary records of deep contour currents: an example, the Mediterranean Outflow in the late Quaternary. Comunicações do Instituto Geológico e Mineiro, 80: 71-88.

Imbrie, J., Kipp, N.G., 1971. A new micropaleontological method for quantitative paleoclimatology: Application to a late Pleistocene Caribbean core. In: Turekian, K.K., ed. (Eds.), The late Cenozoic glacial ages. Yale University Press, New Haven, Conneticut, pp. 71–181.

Kucera, M., Weinelt, M., Kiefer, T., Pflaumann, U., Hayes, A., Weinelt, M., Chen, M.T., Mix, A.C., Barrows, T.T., Cortijo, E., Duprat, J., Juggins, S., Waelbroeck, C., 2005. Reconstruction of sea-surface temperatures from assemblages of planktonic foraminifera: multi-technique approach based on geographically constrained calibration data sets and its application to glacial Atlantic and Pacific Oceans. Quaternary Science Reviews, 24(7-9): 951-998.

Mix, A.C., Morey, A.E., Pisias, N.G., Hostetler, S.W., 1999. Foraminiferal faunal estimates of paleotemperature: Circumventing the no-analog problem yields cool ice age tropics. Paleoceanography, 14(3): 350-359.

Pflaumann, U., Duprat, J., Pujol, C., Labeyrie, L.D., 1996. SIMMAX: A modern analog technique to deduce Atlantic sea surface temperatures from planktonic foraminifera in deep-sea sediments. Paleoceanography, 11(1): 15-35.

Pflaumann, U., Sarnthein, M., Chapman, M., d'Abreu, L., Funnell, B., Huels, M., Kiefer, T., Maslin, M., Schulz, H., Swallow, J., van Kreveld, S., Vautravers, M., Vogelsang, E., Weinelt, M., 2003. Glacial North Atlantic: Sea-surface conditions reconstructed by GLAMAP 2000. Paleoceanography, 18(3): 1065, doi: 10.1029/2002PA000774.

Shemesh, A., Macko, S.A., Charles, C.D., Rau, G.H., 1993. Isotopic evidence for reduced productivity in the glacial Southern Ocean. Science, 262: 407-410.

Stein, R., Stax, R., 1991. Late Quaternary organic carbon cycles and productivity in the Labrador Sea. Geo-Marine Letters, 11: 90-95.

Thomas, E., Booth, L., Maslin, M., Shackleton, N.J., 1995. Northeastern Atlantic Benthic Foraminifera During the Last 45,000 Years - Changes in Productivity Seen from the Bottom Up. Paleoceanography, 10(3): 545-562.

van Kreveld, S.A., Knappertsbusch, M., Ottens, J., Ganssen, G.M., vanHinte, J.E., 1996. Biogenic carbonate and ice-rafted debris (Heinrich layer) accumulation in deep-sea sediments from a Northeast Atlantic piston core. Marine Geology, 131(1-2): 21-46.

Van Weering, T., Rijk, S., 1991. Sedimentation and climate-induced sediments on Feni Ridge, Northeast Atlantic Ocean. Marine Geology, 101: 49-69.

Voelker, A.H.L., Lebreiro, S.M., Schonfeld, J., Cacho, I., Erlenkeuser, H., Abrantes, F., 2006. Mediterranean outflow strengthening during northern hemisphere coolings: A salt source for the glacial Atlantic? Earth and Planetary Science Letters, 245(1-2): 39-55.